

Synthesis and Characterization of Temperature-  
and Light-Responsive Donor–Acceptor  
Stenhouse Adduct-Polymer Conjugates

---

Dissertation

*to obtain the academic degree*

*Doctor rerum naturalium (Dr. rer. nat.)*

submitted to the University of Hamburg,  
Department of Chemistry, Faculty of Mathematics,  
Informatics and Natural Sciences

by

**Julia Steicke**

Hamburg 2024

Gutachter der Dissertation: Prof. Dr. Patrick Téato  
Prof. Dr. Gerrit Luinstra

Gutachter der Disputation: Prof. Dr. Volker Abetz  
Prof. Dr. Wolfgang Maison  
Prof. Dr. Patrick Théato

Datum der Disputation: 10.01.2025

Datum der Druckfreigabe: 30.05.2025

Alle praktischen Arbeiten für die Erstellung dieser Dissertation wurden von Februar 2016 bis Februar 2020 in der Arbeitsgruppe von Prof. Dr. Théato am Institut für Technische und Makromolekulare Chemie im Fachbereich Chemie der Universität Hamburg durchgeführt.

*Life is what happens to us while  
we are making other plans.*

*— Allen Saunders —*

# Table of Content

<b>Abbreviations</b>	<b>III</b>
<b>Variables and Constants</b>	<b>V</b>
<b>Zusammenfassung</b>	<b>VII</b>
<b>1 Introduction</b>	<b>1</b>
<b>2 Theoretical Background</b>	<b>3</b>
2.1 Polymerization techniques .....	3
2.1.1 Conventional free-radical polymerization .....	4
2.1.2 Reversible-deactivation radical polymerization .....	7
2.1.3 Step polymerization .....	9
2.2 Post-polymerization modifications .....	11
2.3 Stimuli-responsive polymers .....	13
2.3.1 Temperature-responsive polymer solutions .....	13
2.3.1.1 Turbidimetry .....	16
2.3.2 Light-responsive polymers .....	17
2.3.3 Photochromic organic compounds .....	19
2.3.3.1 Azobenzenes .....	20
2.3.3.2 Donor-Acceptor Stenhouse Adducts (DASAs) .....	21
2.3.4 Dual light- and temperature-responsive polymers .....	25
<b>3 Motivation</b>	<b>31</b>
<b>4 Results and Discussion</b>	<b>33</b>
4.1 Poly(methyl methacrylate)-DASA conjugates .....	35
4.1.1 Synthesis of PMMA-DASA-polymer conjugates .....	36
4.1.2 Temperature and light responsiveness of PMMA-DASA conjugates .....	50
4.2 Poly( <i>N</i> -isopropylarylamide)-DASA conjugates and poly( <i>N,N</i> -diethylacrylamid)- DASA conjugates .....	71
4.2.1 Synthesis of PNIPAM-DASA- and PDEA-DASA-polymer conjugates .....	72
4.2.2 Temperature and light responsiveness of DEA and NIPAM-DASA copolymers .....	89
4.3 Orthogonal photoswitching copolymer systems .....	98
4.3.1 Synthesis of PDEA-DASA-Azo polymer conjugates .....	98
4.3.2 Temperature and light responsiveness of DEA-DASA-Azobenzene conjugates .....	104

<b>5 Experimental Part</b>	<b>109</b>
5.1 Materials and Characterization .....	109
5.1.1 Chemicals and solvents .....	109
5.1.2 Characterization and Purification Methods .....	109
5.2 Synthesis .....	112
5.2.1 Monomers .....	112
5.2.2 Chromophores and Chromophore Precursors .....	114
5.2.3 Polymer synthesis .....	121
5.2.4 Post-polymerization modifications .....	125
<b>6 References</b>	<b>130</b>
<b>A Additional Supporting Informations</b>	<b>i</b>
A.1 NMR spectra .....	i
A.2 FT-IR spectra .....	iii
A.3 UV-vis linear regression analysis of DASA contents .....	viii
<b>B Safety</b>	<b>xi</b>
B.1 Chemicals.....	xi
B.2 CMR substances .....	xvii
<b>C Danksagung</b>	<b>xviii</b>
<b>D Erklärung zur Identität der digitalen und schriftlichen Fassungen</b>	<b>xix</b>
<b>E Eidesstattliche Versicherung</b>	<b>xx</b>

## Abbreviations

ABS	Acrylonitrile butadiene styrene
AIBN	2,2'-Azobis(2-methylpropionitrile)
ATR	Attenuated total reflectance
ATRP	Atom transfer radical polymerization
BHET	Bis(2-hydroxyethyl) terephthalate
CAS	Chemical abstract service
CTA	Chain Transfer Agent
CP	Cloud point
CDSTP	4-Cyano-4-[(dodecyl-sulfanylthiocarbonyl)sulfanyl]pentanoic acid
DASA	Donor-acceptor Stenhouse adduct
DCM	Dichlormethane
DEA	<i>N,N</i> -Diethylacrylamide
DMF	<i>N,N</i> -Dimethylformamide
DMSO	Dimethyl sulfoxide
EEDA	<i>N</i> -Ethylethylenediamine
EI	Electron ionization
EPS	Expanded polystyrene
eq.	Equivalent
FRP	Free-radical polymerization
FT-IR	Fourier-transform infrared
GHS	Globally Harmonized System of Classification and Labelling of Chemicals
HSQC	Heteronuclear single quantum coherence
LCST	Lower critical solution temperature
MIBK	4-Methylpentan-2-one
MIBK	Methyl isobutyl ketone
MMA	Methyl methacrylate
MS	Mass spectrometry
MWCO	Molecular weight cut-off

NHS	N-Hydroxysuccinimide
NMP	Nitroxide mediated-polymerization
NMR	Nuclear magnetic resonance
PAEK	Polyaryletherketone
PBI	Poly[2,2'-(m-phenylen)-5,5'-bisbenzimidazole
PC	Polycarbonate
PDEA	Poly( <i>N,N</i> -diethylacrylamide)
PE	Petroleum ether
PEEK	Polyether ether ketone
PET	Poly(ethylene terephthalate)
PFP	Pentafluorophenyl
PFPA	Pentafluorophenyl acrylate
PFMA	Pentafluorophenyl methacrylate
PI	Polyimide
PMMA	Poly(methyl methacrylate)
PNIPAM	Poly( <i>N</i> -isopropylacrylamide)
POM	Polyoxymethylene
PP	Polypropylene
PS	Polystyrene
PVC	Poly(vinyl chloride)
RAFT	Reversible addition fragmentation (chain) transfer
RDRP	Reversible-deactivation radical polymerization
rt	Room temperature
SEC	Size-Exclusion Chromatography
TEA	<i>N,N</i> -Diethylethanamine
THF	Tetrahydrofuran
Trp	Tryptophan
UCST	Upper critical solution temperature
UV	Ultraviolet
UV-vis	Ultraviolet-visible

## Variables and Constants

$A$	Absorbance
$c$	Molar concentration
$D$	Dispersity
$\delta$	Chemical shift
$G_m$	Gibbs free energy of a polymer solution
$h$	Planck constant
$H_m$	Enthalpie of a polymer solution
$J$	Coupling constant
$k_B$	Boltzmann constant
$l$	Wavelength of electromagnetic radiation
$m$	Mass
$M$	Molecular mass
$\bar{M}_n$	Number-average molar mass
$\bar{M}_w$	Mass-average molar mass
$R_f$	Retenion factor
$S_m$	Entropy of a polymer solution
$T$	Temperature
$T_{CP-C}$	Cloud point upon cooling
$T_{CP-H}$	Cloud point upon heating
$V$	Volume
$\nu$	Frequency
$X_i$	Amount fraction
$\tilde{\nu}$	Wavenumber



# Zusammenfassung

Materialien mit der Fähigkeit, ihre Eigenschaften als Reaktion auf äußere Reize spontan zu verändern, sind in der Polymerforschung vielversprechend und bergen den Schlüssel zu zahlreichen potenziellen Anwendungen. So ändern beispielsweise bestimmte organische Chromophore ihre chemischen/physikalischen Eigenschaften, wenn sie Licht ausgesetzt werden, wodurch sie sich für den Einsatz in Polymersystemen anbieten. In dieser Arbeit wurde eine photochrome Gruppe, das so genannte Donor–Acceptor Stenhouse Addukt (DASA), in verschiedene Reihen von Polyacrylat- und Polyacrylamid-Copolymeren eingearbeitet. Diese Copolymere wurden aufgrund ihres thermoresponsiven Verhaltens in wässrigen Lösungen ausgewählt. Dies ermöglichte weitere Untersuchungen zu der Einstellbarkeit ihres responsiven Verhaltens durch die lichtinduzierte Isomerisierung der entsprechenden chromophoren Gruppe.

In einem ersten Schritt wurde eine PMMA-DASA-Copolymer Reihe mit Chromophor-anteilen zwischen 1 und 11 Mol% hergestellt. Dazu wurde eine radikalische Copolymerisation mit Methylmethacrylat und einem aktivierten Esteracrylat durchgeführt. Das Chromophor wurde anschließend durch zwei polymeranaloge Reaktionen mit einem Amin und einem aktivierten Furan-Vorläufer hergestellt. Dieses Verfahren ermöglichte den Zugang zu definierten, responsiven Materialien mit hohem Molekulargewicht und genau abgestimmtem Chromophorgehalt. Alle Copolymere wiesen eine obere kritische Lösungstemperatur (UCST) in Ethanol-Wasser-Gemischen auf. Es war eine Korrelation zwischen der Chromophormenge und der Ethanolkonzentration (zwischen 65 und 95 Volumenprozent) zu beobachten. Im Vergleich zu PMMA zeigten die Copolymere im Allgemeinen eine Abnahme der UCST bis zu einer Ethanolkonzentration von 80%. Höhere Konzentrationen führten jedoch zu einem Anstieg der UCST. Eine Bestrahlung der Polymerlösungen mit sichtbarem Licht (520 nm), und der dadurch erfolgten Schaltung der DASA-Gruppe, bewirkte die resultierende hydrophile Struktur eine Abnahme aller UCST-Werte. Nach zwei Stunden Bestrahlung erreichte eine Probe mit 10,7 Mol% Farbstoff eine maximale UCST-Verschiebung von 20 °C. Insgesamt wurde die UCST der PMMA-DASA-Copolymere durch die lichtinduzierte Löslichkeitsänderung stark beeinflusst. Obwohl dieser Prozess in Ethanol-Wasser-Gemischen irreversibel war, konnte nachgewiesen werden, dass die Proben durch Erhitzen in Dichlormethan zu ihrer ursprünglichen UCST vor der Lichtbestrahlung zurückkehren. Die Untersuchung des UCST-Verhaltens wurde auf Polymere ausgedehnt, die beim Erhitzen eine niedrigere kritische Lösungstemperatur (LCST) aufweisen. Durch Anwendung des beschriebenen Syntheseverfahrens wurden zwei statistisch angeordnete PNIPAM- und PDEA-Copolymer-Serien mit unterschiedlichen Mengen an eingebauten DASA-Seitengruppen erfolgreich synthetisiert. Die Löslichkeit aller Polymere schien in wässriger Lösung im Vergleich zu den homogenen PNIPAM/PDEA-Proben verringert zu sein. Eine Korrelation zwischen dem Phasenübergangspunkt und der Menge der DASA-Seitengruppe wurde durch die Messung der LCST-Werte eindeutig nachgewiesen und zeigte eine nahezu lineare Abhängigkeit. Nach einer 4-stündigen Bestrahlungsdauer zeigten die Polymerlösungen eine Verschiebung zu einer höheren LCST. Im Fall von PNIPAM wurde eine maximale Verschiebung der LCST von 11,6 °C für eine Probe mit 11,5 Mol% DASA-Gehalt beobachtet. Der Einbau von 10 Mol% chromophorer Gruppen in PDEA führte zu LCST-Verschiebungen von bis zu 9,5 °C. Die thermoresponsive

Eigenschaft der Polyacrylamide wurde also wesentlich durch die Schaltbarkeit der eingebauten Seitengruppe beeinflusst. Letztendlich erfolgte die Synthese von PDEA-Proben unter Verwendung von DASA und einer Azoverbindung, die als zweite chromophore Seitengruppe fungierte. Alle Probenlösungen wurden einer Sequenz von zwei Bestrahlungen unterzogen ( $\lambda_1 = 570 \text{ nm}$ ;  $\lambda_2 = 365 \text{ nm}$ ). Das Verfahren bewies, dass es möglich ist, die Chromophore im polymeren System orthogonal zu schalten, was zu zwei unabhängigen LCST mit erhöhten Werten im Vergleich zu PDEA führt.

Zusammengefasst hat sich die chemische Beschaffenheit des DASA-Chromophors als hochwirksame Gruppe zur Einstellung der thermoresponsiven Eigenschaften verschiedener Polyacrylate und Polyacrylamide erwiesen. Die funktionelle Gruppe ist somit sehr vielversprechend für Materialien auf Polymerbasis. Bemerkenswert ist, dass das DASA-Schaltverhalten mit einem hohen Verlust an Farbintensität einhergeht. Während der praktischen Arbeit an den LCST-Verschiebungen war die höchste Polarität bei allen Messungen makroskopisch leicht durch eine Entfärbung erkennbar. Dieser Effekt verleiht dem DASA Chromophor zusätzlich ein großes Potential für verschiedene Anwendungen.

## Abstract

Materials with the remarkable ability to undergo spontaneous property changes in response to external stimuli hold great promise in the field of polymer research and hold the key to numerous potential applications. For instance, specific organic chromophores alter their chemical/physical characteristics when exposed to light, making them well-suited for use in polymer systems. This work adopted a photochromic group known as the donor–acceptor Stenhouse adduct (DASA) by effectively incorporating it into different series of polyacrylate and polyacrylamide copolymers. These copolymers were well-selected for their thermo-responsive behavior in aqueous solutions, allowing further investigations into their tunability by light-induced isomerization of the corresponding chromophoric moiety.

In a first step, a PMMA-DASA copolymer library was prepared with varying chromophore content between 1 and 11 mol%. Therefore, a free-radical copolymerization involving MMA (methyl methacrylate) and an activated ester acrylate was performed. The grafted chromophore was subsequently generated *via* two consecutive polymer analogous reactions first with an amine and then with an activated furan precursor. This designed procedure provided access to well-defined stimuli-responsive polymers with high molecular weights and precisely targeted chromophoric content. All copolymers exhibited an *upper critical solution temperature* (UCST) in ethanol-water mixtures. A notable correlation between the amount of chromophore and the concentration of ethanol (ranging from 65% to 95% by volume) was revealed. When compared to PMMA, the copolymers generally displayed a decrease in UCST up to an ethanol concentration of 80%. Higher concentrations, however, caused an increase in the UCST. By subjecting the polymer solutions to visible light (520 nm) and inducing the photoswitching of the DASA group, the resulting hydrophilic structure caused a decrease of UCST values of all copolymers. After 2 h of irradiation, a sample containing 10.7 mol% dye reached the  $\Delta\text{UCST}_{\text{max}}$  of 20 °C. Overall, the UCST of the PMMA-DASA copolymers was hardly affected by the light-induced solubility change. Despite this process being irreversible in ethanol-water mixtures, heating in dichloromethane was proven to revert the samples to their initial UCST prior to light irradiation. The investigation on UCST behavior was extended to polymers showing a *lower critical solution temperature* (LCST) upon heating. By adopting the synthetic protocol, two PNIPAM and PDEA statistically arranged copolymer series with different amounts of incorporated DASA side groups were successfully prepared. The solubility of all polymers appeared to decrease in aqueous solution compared to the homogenous PNIPAM/PDEA samples. The correlation between the phase transition point and the amount of DASA side group was clearly demonstrated by measuring the LCST values, showing a nearly linear dependency. Following a 4 h duration of irradiation (white light bulb) the copolymer solutions exhibited a shift towards higher LCST. In the case of PNIPAM, the maximum  $\Delta\text{LCST}$  of 11.6 °C was observed for a sample including 11.5 mol% DASA content. The presence of 10 mol% chromophoric group in PDEA resulted in  $\Delta\text{LCST}$  of 9.5 °C. Thus, the thermo-responsive property of the polyacrylamides was significantly influenced by the photoswitching nature of the incorporated side group. Finally, PDEA samples including DASA and azobenzene as second chromophoric side group were synthesized by RAFT polymerization. All polymer solutions underwent a sequence of light irradiation ( $\lambda_1 = 570 \text{ nm}$ ;  $\lambda_2 = 365 \text{ nm}$ ). The procedure proved that

it is possible to switch the chromophore orthogonally, resulting in two independent  $\Delta$ LCSTs to increased values as compared to PDEA.

Concluding, the chemical nature of the DASA chromophore has proven to be a highly effective stimuli-responsive group for tuning the thermo-responsive properties of various polyacrylates and polyacrylamides. The functional group have been demonstrated to be very promising for smart materials based on polymers. Noteworthy, the DASA switching behavior is accompanied by a high loss of color intensity. During the practical work on the LCST shifts, the highest polarity was easily recognizable macroscopically in all measurements by discoloration. This effect gives DASA also a great potential for several further applications.

# 1

## Introduction

---

Since the very beginning, nature in its diversity and uniqueness has always been an inspiration for mankind, and especially for scientists. Nature gives us questions and offers us possibilities, it holds previously unknown phenomena in store and reveals new mysteries in a beautiful way, but it also shows us the limits and the unembellished side of perishability. On its long journey, nature therefore created molecules that enabled it to achieve an incredible wealth of detail. Nature emerged with the idea to establish macromolecular structures as an essential element of evolution. As cellulose in plants, as gene-carrying chains of amino acids or as proteinogenic silk, biological macromolecules have become an indispensable part of processes in life. Following this model, the everyday life of many people today is accompanied and facilitated by a material that has driven technical development and innovation like no other. It is the man-made artificial correspondence to biomacromolecules. We are talking about synthetic plastics, named polymers.

Although the birth of this remarkable material is difficult to relate to a precise date from today's perspective, the chemist H. Staudinger is well-known as a polymer pioneer. His key paper<sup>1</sup> in 1920 postulated the first polymerization processes and set the date for the 100-year anniversary in 2020. Based on his chemical structure clarification and his method for determining the molecular weight of polymers, international research interest has aroused. In recognition of his revolutionary achievements, Staudinger was awarded the Nobel Prize in chemistry in 1953.<sup>2,3</sup> But what makes plastics such special and important materials for our daily lives? Due to its versatile synthesis possibilities and modifications, polymers are highly flexible and adaptable materials that can be precisely tailored to different applications. Chemical variations can cause quite different physical properties. Furthermore, synthetic plastics combine advantages over other materials. They are lighter than metals and ceramics, often cheaper and are not mined underground. In everyday life, we find polymers primarily as packaging and disposal materials (~40 % of total plastic volume in Europe 2018<sup>4</sup>, Figure 1.1, top), as components in all conceivable means of transport, as coatings or even as synthetic clothing. Finally, polymers are of great importance in medical technology, where they are required for the manufacture of medical products, but also for example as direct component in dental technology.

People's demands on their environment are constantly increasing. In addition to the commercially known bulk polymers, such as polyethylene, Nylon or poly(ethylene terephthalate) (PET), special high-performance polymers that are perfectly tailored to a specific area of application are becoming more important (Figure 1.1, bottom). In contrast to standard thermoplastics, the costs of high performance polymer increase the more specialized they are developed.<sup>5</sup>



**Figure 1.1.** Top: Distribution of European (EU28-NO/CH) plastics converters demand by segment in 2018, from left to right: Packaging, building & construction, others (appliances, mechanical engineering, furniture, medical etc.), automotive, electronic, sports, agriculture. Data were included.<sup>4</sup> Bottom: Data comparison of the Europe (EU28+NO/CH) market segment of standard thermoplastics in comparison to high performance polymers in 2015 and distribution of European (EU28+NO/CH).<sup>5</sup>

One step further leads to the so-called “smart polymers”, which respond to external influences such as changes in temperature- or pH-values.<sup>6</sup> Such smart polymers are highly versatile and show tuneable properties for several applications. Among the different available stimuli, the stimulus light has gained great interest in recent years, due to unique advantages, such as its localized use.<sup>7</sup> Upon light irradiation, specific organic chromophores are able to change their chemical or physical properties spontaneously. This concept is a multi-faceted and promising field, which deserves a continued focus in the scientific community. For this reason, a recently emerging chromophore class has been investigated in polymer science. The so-called donor–acceptor Stenhouse adducts (DASAs) are characterized by impressive changeable properties and were therefore chosen as the focus of this study.

The theoretical aspect of this study offers a basic comprehension of polymerization techniques and the characteristics of temperature-responsive polymers in aqueous solutions. A thorough understanding of the presented processes is necessary in order to fully grasp the fascinating photoswitching phenomenon, which has an impact on the behavior of polymers in this work. In addition, detailed explanations are provided on the individual chromophoric features.

### 2.1 Polymerization techniques

This section of polymerization techniques describes synthetic methods to obtain polymers. Nowadays, the possibilities for preparing polymers are highly versatile and form a powerful tool, since the polymerizability of different monomers and the chemical/physical properties of the desired polymer are given by the polymerization technique used. Therefore, synthetic methods attract widespread interest in both academic research and industry.

Polymerization techniques can be divided into two basic types (Figure 2.1).<sup>8</sup> The first one is the chain polymerization, which is characterized by an active chain end that is extended by one monomer unit at a time.<sup>9</sup> Consequently, the activity is continuously transferred to the last bound monomer and is attributed to radical or ionic functionality.<sup>10–12</sup> In addition, different coordinative processes have been published based on the use of organometallic complexes during the last few decades.<sup>13,14</sup> To overcome some disadvantages of the conventional free-radical polymerization, a number of key strategies belonging to the class of reversible deactivation radical polymerizations (RDRP, by IUPAC)<sup>15,16</sup> were investigated. During the whole process, the chain growth requires monomer presence in the reaction mixture to prevent it from coming to an end.<sup>17</sup> In contrast to this, the second polymerization technique, called step polymerization, proceeds stepwise without reactivity transfer and can take place between molecules, regardless of the degree of polymerization.<sup>18</sup> This type of polymerization technique can either be carried out with an elimination of low molecular weight compounds (polycondensation) or without (polyaddition).<sup>19</sup>

Overall, each process has its own merits and special characteristics, hence the choice of polymerization depends on the nature of the monomer(s), *i.e.*, on the selected product with its desired properties and acceptable reaction conditions. Individual processes are explained in detail in the following sections.

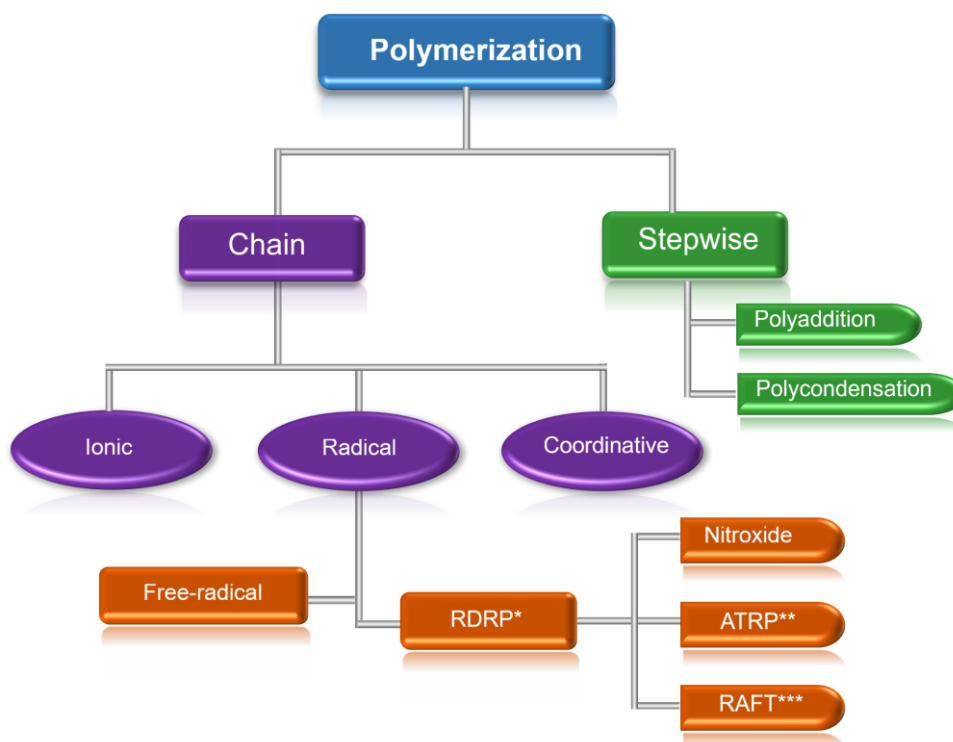


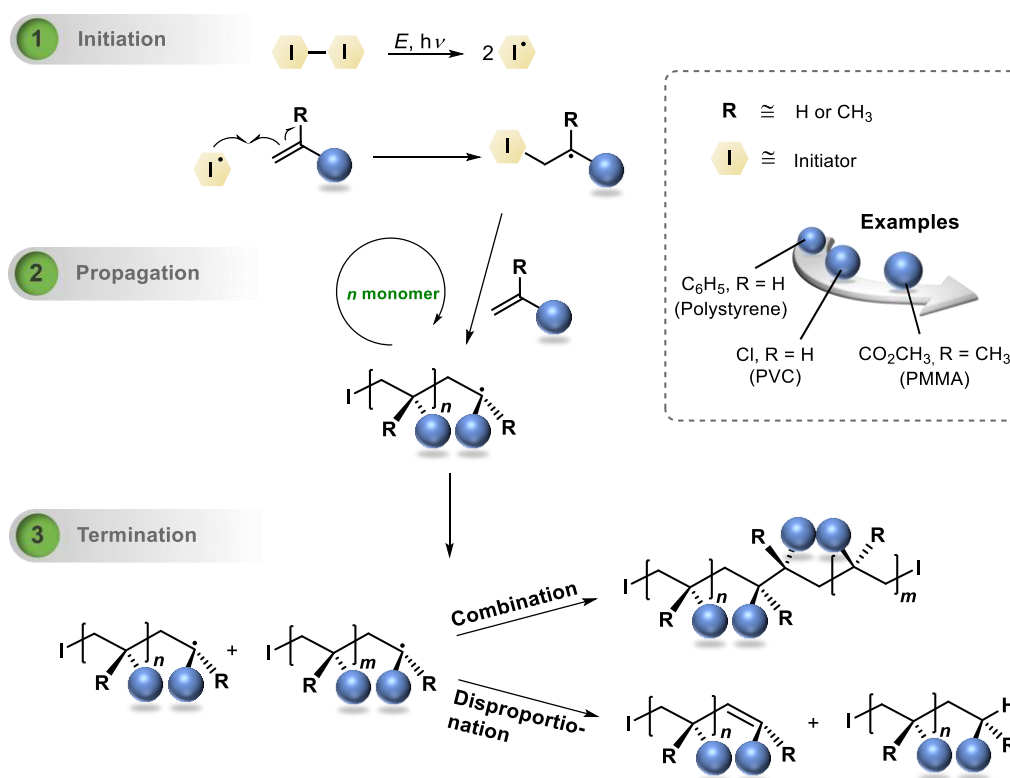
**Figure 2.1.** Basic chart flow of the investigated polymerization techniques utilized in research and industry. \**Reversible deactivation radical polymerization* \*\**Atom transfer radical polymerization* \*\*\**Reversible addition fragmentation (chain) transfer*.

### 2.1.1 Conventional free-radical polymerization

Nowadays, polymers derived from chain polymerization account for more than 80% of the total plastic consumption in our daily life.<sup>20</sup> The majority of them based on radicals, which makes free-radical polymerization the most commonly used reaction technique with respect to bulk polymers.<sup>21</sup> It is mainly known for the conversion of unsaturated monomers, which includes mono- and disubstituted ethylene compounds.<sup>20</sup> One well-known example is poly(vinyl chloride) (PVC), which is produced in an order of magnitude of around 60 million tons<sup>22</sup> per year, plays a crucial role as synthetic plastic in the world and is significant for the construction industry for the production of doors, windows and drinking water/wastewater pipes.<sup>23</sup> For products, that require transparency, such as food packaging, polystyrene (PS) is an excellent representative.<sup>24</sup> Moreover, its expanded form (EPS) is famous for being used as a material for insulating buildings and as food container.<sup>25</sup> Another well-known material is poly(methyl methacrylate) (PMMA), also called Plexiglas<sup>®</sup>, which is a widely used material for several applications in sectors like transportation, electronic and health.<sup>26,27</sup> And last but not least, ethylene itself can also be polymerized *via* free-radical polymerization technique to yield polyethylene (PE) that can be utilized as packaging materials or foils.<sup>28</sup> In principle, radical polymerization

has become a key component in global plastics production due to its various advantages. First, the reaction shows a high acceptance regarding the number of polymerizable monomer structures and often results in polymers with high number-average molar masses after comparatively short reaction times. In addition, the reaction is tolerant towards solvents and conditions, which, unlike other reaction techniques, makes syntheses easy to perform in terms of cost and equipment. Finally, free-radically polymerizable monomers and consequently the resulting polymers are often a type of thermoplastic material, that can easily be formed in melt and therefore offers many application possibilities.<sup>29</sup>

At a closer look, the commercial success of the conventional radical polymerization is directly related to the mechanism, that can be divided into three fundamental steps as follows: Initiation, propagation and termination. Additionally, chain transfer is involved.<sup>17</sup> Scheme 2.1 illustrates the reaction course utilizing a general vinyl monomer.



**Scheme 2.1.** Diagram of the fundamental reaction steps involved in the free-radical polymerization mechanism: Initiation, propagation and termination through combination or disproportionation.

During initiation, the monomer is attacked by a radical formed previously for example *via* homolytic bond cleavage. Hence, this initiator-monomer adduct forms the shortest propagation radical and starts the chain growth.<sup>30</sup> For this, the C=C-bonds of monomers are attacked by the active species and radical functionality is transferred. The process is repeated and

consequently many more monomers are successively added. At some point, this propagation is terminated through electron saturation of the radical species by combination or disproportionation. This general view can now be considered in more detail, as shown in Figure 2.2. Initiator systems are the starting material, which usually decompose into two free-radical fragments by energy absorption (*e.g.*, thermal, redox or photo reaction influences).<sup>17</sup> A well-known and probably most widely used thermal representative is 2,2'-azobis(2-methyl-propionitril) (AIBN)<sup>21</sup>, outlined in Figure 2.2a). Here, the decomposition and formation of cyanopropyl radicals takes place through nitrogen elimination, the driving force for the process.<sup>17</sup> Generally, radicals form a group of organic species characterized by unpaired electrons. This energetically unfavorable state gives radicals their typical unstable nature, which leads to an extremely high reactivity and is expressed by a short lifetime.<sup>31</sup> To compensate for this state, radicals react preferentially with functionalities that have a high electron density, such as C=C double bonds. Ideally, the initiators should be relatively stable at room temperature but should rapidly decompose under polymerization conditions. Thus, reactions initiated by AIBN ensure a practical reaction rate due to its favorable decomposition during the synthesis performed at 50-80 °C.<sup>17,22</sup>

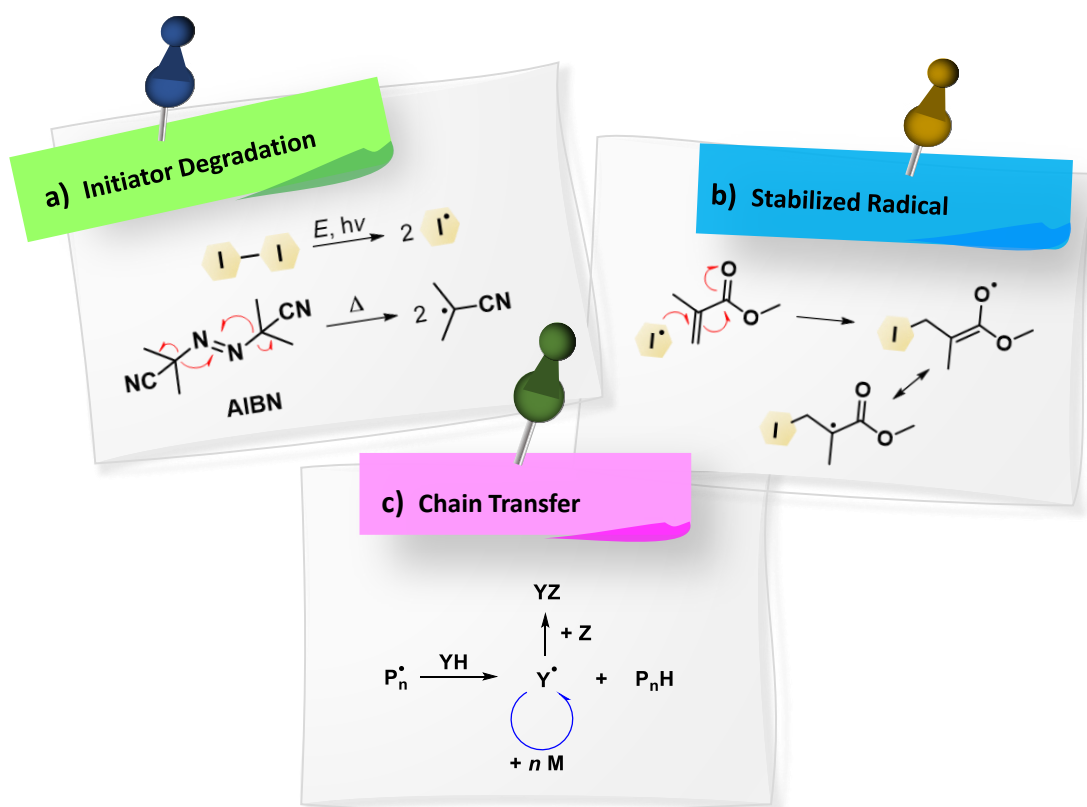


**Figure 2.2.** Information board about aspects in the free-radical polymerization technique includes **a)** initiator degradation of 2,2'-azobis(2-methylpropionitril) (AIBN) through heating, **b)** stabilized radical forming by structure resonance and **c)** possible pathways of chain transfer, with  $P_n^{\bullet}$  (active radical chain),  $YH$  (monomer, initiator, solvent or another polymer chain),  $Y^{\bullet}$  (radical recipient) and  $M$  (monomer).

After reaction with the initiator radical, the new radical functionality is favorably localized at the most stabilized carbon atom.<sup>32–34</sup> This fact has an impact in two ways. First, radical polymerization was preferred for monomers capable of stabilizing radicals by delocalization (example PMMA in Figure 2.2b) or by inductive effects. Second, the radical position determines the point of attachment for the propagation process. Due to stabilization, the type of monomer arrangement usually results in the head-to-tail linkage, which means substituents alternate along the polymer backbone.<sup>20</sup> In addition, Figure 2.2c summarizes the chain transfer reaction, a mechanism accompanying the polymerization process and it describes the consequence of transferring the radical function from the growing chain  $P_n^\bullet$  to another species  $XY$  (*i.e.*, monomer, initiator, solvent or another polymer chain). While the  $P_n^\bullet$  chain is terminated, the novel radical bearing species  $Y^\bullet$  can typically start a new propagation or lead to another dead polymer chain  $YZ$  by combination with  $Z$ . It can be either another hydrogen atom or another species with unpaired electrons. The actual radical transfer can occur for example through hydrogen abstraction, which is respectively possible as intra- or interchain reaction.<sup>35–37</sup> Within intramolecular processes, the hydrogen atom abstraction refers to backbiting, which manifests itself in branched polymer chains. All in all, chain transfer reactions lead to a decrease in the length of the growing polymer chain, *i.e.*, the degree of polymerization.<sup>17</sup>

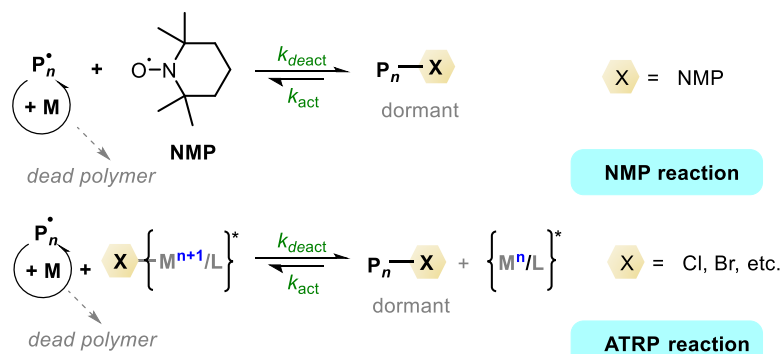
In summary, free-radical polymerization offers multiple possibilities and forms a profitable technology that has been of high economic importance for several decades. However, even this powerful tool reaches its limits, namely through poor control of molecular weight distribution and in preparing well-defined copolymer structures, *e.g.*, block copolymers or polymers with a given functionality sequence. In order to cope with these limitations, the RDRP has recently generated considerable research interest.

## 2.1.2 Reversible-deactivation radical polymerization

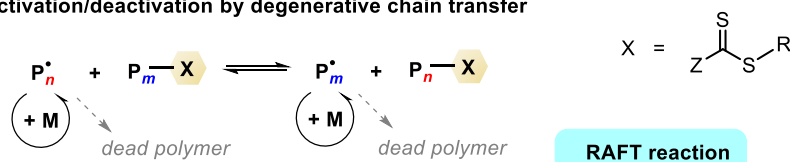
Reversible-deactivation radical polymerization (RDRP) is a useful tool to synthesize polymers that are characterized by adjusted molecular masses and narrow molecular weight distributions in contrast to FRP.<sup>38</sup> The main idea is the minimization of chain termination processes. For this, the concentration of active radical species is kept low and consequently the probability of termination through two active propagating chains is reduced. In practice, RDRP uses a reversible activation/deactivation dynamic equilibrium within propagating polymer radicals that are portioning between active and dormant states.<sup>39,40</sup> Two basic strategies for establishing equilibria have been discovered<sup>41</sup>, which are illustrated in Figure 2.3. First, free radical concentration minimization originates from a reversible trapping mechanism with activation/deactivation of the propagating radical including a species  $X$  (Figure 2.3a). For example, in the nitroxide mediated-polymerization (NMP), reversible termination occurs through nitroxide capping<sup>42</sup>, while atom transfer radical polymerization (ATRP) is based on a catalyzed redox process with a metal halide salt.<sup>43</sup> Both types have an equilibrium which strongly favors the dormant state.<sup>44</sup> The second strategy provides control *via* a degenerative chain transfer mechanism, for example the reversible addition-fragmentation (chain) transfer (RAFT) outlined in

Figure 2.3b and 2.3c. RAFT polymerizations include a chain transfer agents (RAFT-CTA) which typically consist of a thiocarbonyl group like dithiobenzoates, trithiocarbonates or dithiocarbamates.<sup>45</sup> All structures have a free-radical leaving group **R** (weak bond)<sup>46</sup>, which is responsible for a rapid equilibrium between propagating chains, giving all chains an equal chance to grow and resulting in low dispersity.<sup>44</sup> After full monomer conversion, RDRP offers the possibility to be continued upon addition of further monomer. Hence, by getting microstructure and end group control, RDRP provides access to complex polymeric architectures, *e.g.*, block copolymers<sup>47,48</sup>, star polymers<sup>49</sup> or dendrimeric structures<sup>50,51</sup>. During the last two decades, especially RAFT polymerization grew in popularity, due to a much broader range of functional monomers as compared to living systems like anionic polymerization. Moreover, RAFT is significantly less stringent towards reaction parameters, which enables the synthesis of a wide range of new polymeric materials.<sup>52,53</sup>

a) Activation/deactivation by reversible termination



b) Activation/deactivation by degenerative chain transfer



c) General reaction procedure of RAFT synthesis

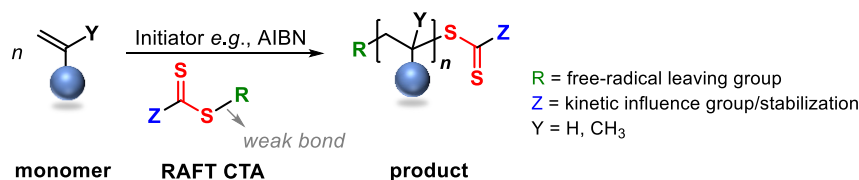


**Figure 2.3.** Types of reversible-deactivation radical polymerization with **a)** mechanism based on reversible termination/trapping (*e.g.*,  $\text{X} = \text{nitroxide/halogen}$ ) and **b)** mechanism based on degenerative chain transfer (*e.g.*, RAFT polymerization) and **c)** basic RAFT reaction including chain transfer agents (CTA) and thiocarbonyl groups.

### 2.1.3 Step polymerization

Step polymerizations are as old as synthetic macromolecules themselves. By synthesizing one of the first real synthetic polymer through reaction of phenol and formaldehyde in 1907, L. Baekeland started the history of intensive polymer use.<sup>54</sup> A few years later, Carothers formalized the step polymerization as the technique that focuses on different functional groups to form novel covalent bonds.<sup>19</sup> Today, the differences to chain polymerizations are mainly considered, and, in fact, the techniques are fundamentally dissimilar. While chain reaction activity is located at some propagating chains, each monomer in step processes can react to build extended linkages, and usually no initiator system is required.<sup>18</sup> Consequently, the mechanism consists of simple dimer formation in the first stage, which might bind another monomer or dimer in the next stage (Figure 2.4). Therefore, molecular weights increase steadily during the reaction which leads to a high conversion requirement and long reaction times to obtain polymer structures instead of oligomers. However, there are no terminations, and macromolecules bearing various functionalities in the backbone can be easily established.<sup>55</sup>

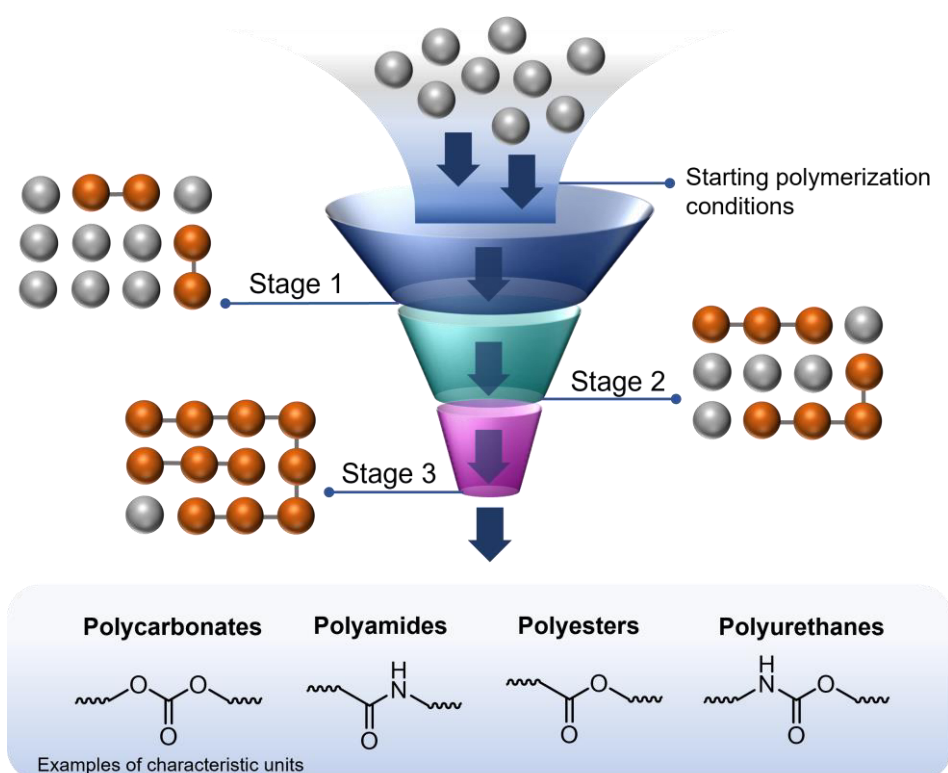


**Figure 2.4.** Model of step-growth monomer conversion over time. Dimer formations lead to monomer or dimer binding in the second stage, etc. Typically, functional backbone groups of step-growth processes lead, *e.g.*, to polyesters, polyamides, polyurethanes and polycarbonates.

Two basic types of monomers are commonly used for syntheses, which are illustrated in Figure 2.5.<sup>55</sup> AB-type monomers consist of two different functional groups, A and B, which react under polymerization conditions. For example,  $\epsilon$ -caprolactam undergoes ring opening by hydrolysis yielding  $\epsilon$ -aminocaproic acid, which serves as an AB-type monomer in the formation of polycaprolactam (nylon 6). Nowadays, nylon 6 is a well-established construction material in the industry.<sup>56,57</sup> In contrast, AA-BB-type reactions require two different monomer structures and a strict stoichiometrical equal molar ratio of 1:1. Probably the most famous example is the polyester poly(ethylene terephthalate) (PET), which can be synthesized through polycondensation of terephthalic acid and ethylene glycol accompanied by water removal as depicted Figure 2.5.<sup>58</sup> Technically, PET batches are manufactured in three steps. These are accompanied by diverse metal catalysts. The intermediate bis(2-hydroxyethyl) terephthalate (BHET) is produced through the transesterification of dimethyl terephthalate with ethylene glycol. Subsequently, this is subjected to high temperatures to undergo polycondensation.<sup>59,60</sup> In addition to linear polymer chains, branched polymer networks can easily be created by using monomers with three or more functional groups, resulting in a wide variety of thermosets.

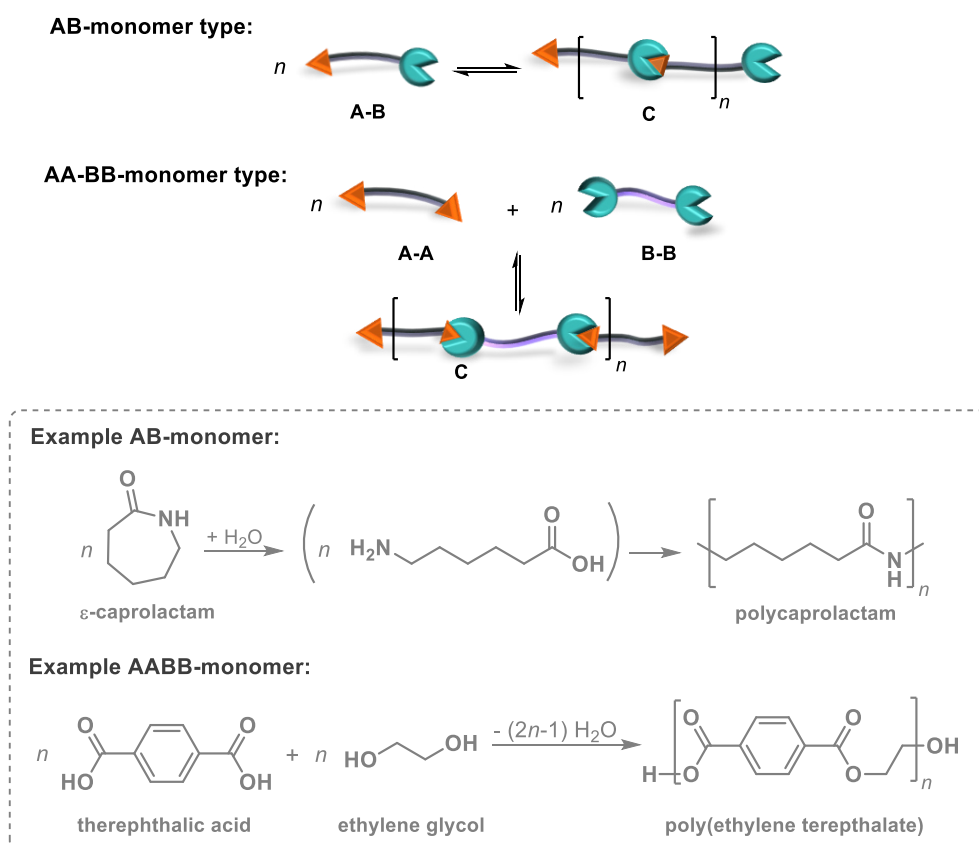


**Figure 2.5.** Monomer types for linear thermoplastic syntheses *via* step polymerization. A and B are functional groups before polymerization to form the covalent bond C.

In summary, step polymerization accounts for about 20% of worldwide plastics production and is therefore an important part of the plastics industry.<sup>61</sup> In terms of reaction times and conditions, it is inferior to the chain reaction. However, step-growth reaction owes its advantages to many different monomer structures that can be used and to the associated tolerance toward functional groups.

## 2.2 Post-polymerization modifications

In the previous sections, some of the best-known and most important polymerization techniques were discussed. However, the synthesis of polymers, including side-chain functionalities, well-defined architectures and defined compositions with specific properties, is still a challenge. On the one hand, this is due to an incompatibility of the functional groups with the required synthesis conditions, on the other hand, the occurrence of undesired side reactions is known. The situation becomes even more difficult when low dispersities are desired. Although various controlled polymerization mechanisms have been developed, the possibilities for direct polymerization of monomers containing functional groups are still limited. To overcome these limitations, post-polymerization modifications (also known as polymer-analogous reactions) have been established in the polymer community and have attracted particular interest in the last three decades.<sup>62–64</sup>

The approach of post-polymerization modification is based on the polymerization of an inert monomer type, whose side groups can be quantitatively converted into a broad range of functionalities in a subsequent step. For this, reactions have come into the focus, which are associated with the “click” chemistry introduced by Sharpless in 2001.<sup>65</sup> Today, a number of reactions, such as the Huisgen 1,3-dipolar cycloaddition<sup>66</sup> or Michael-type additions<sup>67</sup>, are popular syntheses in the field of post-modifications. Independent of this, Ferruti *et al.*<sup>68</sup> and the group of Ringsdorf<sup>69</sup> reported active ester monomers to offer a diverse library to generate polymers with different side-functionalities in 1971. Such active esters have become a popular method of post-modifications. The activated ester group can easily be cleaved by nucleophilic amines to form stable amide bonds. Figure 2.6 shows a schematic illustration of the active ester practice. Well-known monomers, such as *N*-hydroxysuccinimide (NHS) acrylate or pentafluorophenol (PFP) acrylate or their corresponding methyl acrylates, were polymerized by FRP or a controlled mechanism in order to be converted into poly(methyl)acrylamides.<sup>70–72</sup> Such reactions allow access to complex structures under mild reaction conditions (room temperature), and orthogonal functionalization with complete control of the molar ratios can be realized in one-pot syntheses. Especially PFP offers advantages. In contrast to Huisgen reactions, no environmentally harmful metal catalyst is needed, besides PFP-based polymers have a clearly higher solubility in common solvents than NHS analogues. Another useful option is to monitor complete reaction conversions (quantitative PFP exchange) *via* <sup>19</sup>F NMR spectroscopy.<sup>73</sup>

The mentioned advantages of active esters lead to their use as the means of choice in the field of temperature- and/or light-responsive polymer preparation when sensitive units are involved.

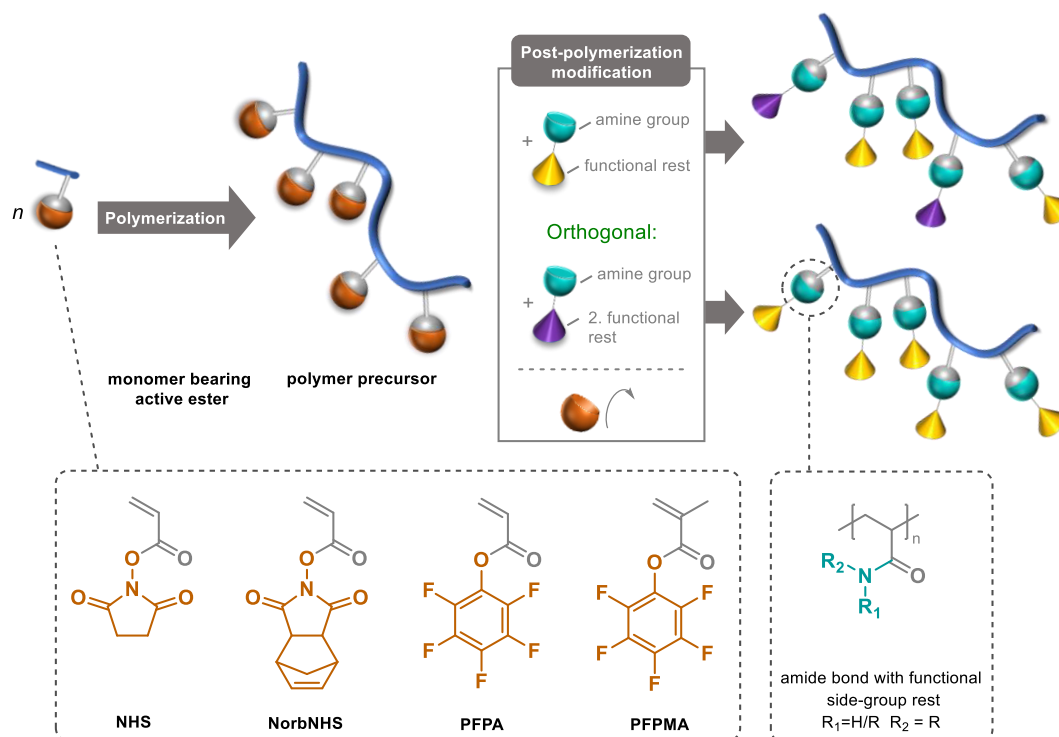


**Figure 2.6.** Model of activated ester exchange by amine groups. Various activated ester monomers are polymerized to form homogenous polymer precursor, which ester groups are converted into amid bonds *via* amidation under mild conditions. Amidations can happen using different functional amine compounds in one pot synthesis to generate orthogonal systems. R denotes any other rest than a proton.

## 2.3 Stimuli-responsive polymers

When polymers respond spontaneously in a perceptible way, *e.g.*, by shrinking, swelling or color change, their behavior is frequently associated with so-called “stimuli-responsive” systems.<sup>74</sup> In this context, the polymer response is generated by external, controlled and abrupt stimuli. Many research focus areas have been based on such “smart materials” in the last few decades. Although the nature of such materials is not limited, especially macromolecules have become a focal point of interest in many research publications.<sup>75</sup> This is due to their high functionalization and modification possibilities by designed synthetic pathways. In addition, most commercially available polymer compounds are cheaper than metals and ceramics.<sup>76</sup> The stimuli-responsive behavior can either be a consequence of the polymer structure itself or can be generated by compounds, that bind to macromolecules.<sup>77</sup>

The changes in the polymer environment can be caused by various stimuli, which are classified into biological, physical and chemical impulses.<sup>77</sup> The latter include changes in pH values, ionic strength and solvent, as well as redox-reaction initiations. Biological stimuli involve, *e.g.*, enzyme activities and receptor recognition. Responsive behavior after light irradiation, electrical/magnetic/mechanical changes are the consequence of physical stimuli, moreover, responsivity caused by temperature changes has been intensively studied. In general, polymer systems can also be stimuli-responsive to one or more stimuli. Such multi-stimuli systems show simultaneous responses to two or more stimuli.<sup>78</sup>

The noteworthy aspect is in the diversity of polymer systems, encompassing a wide range of responsivity types and a multitude of stimuli. Temperature- and light-responsive structures are particularly important since they have a wide range of uses and are compatible with living organisms. Their advantages and applications are described below.

### 2.3.1 Temperature-responsive polymer solutions

When cooking, many people find that household salt dissolves better the warmer the water is. In fact, many low molar mass compounds behave in a similar way. Surprisingly, several aqueous polymer solutions show precipitation upon heating, which can be observed macroscopically by opacity. This fascinating phenomenon has been studied intensively over the past decades. Nowadays, it is probably the most studied temperature-responsive behavior, also known as *lower critical solution temperature* (LCST).<sup>79</sup> Most LCST behaviors occur in water or water/solvent mixtures. Due to the relatively cheap, safe and biocompatible water properties, LCST plays a major role in several applications<sup>80</sup>, such as in drug delivery<sup>81,82</sup>, sensors/ labeling<sup>83</sup> and hydrogels<sup>84</sup>. Regarding the phase diagram of the binary polymer/solvent mixture (Figure 2.7a), the opacity is a result of the phase separation due to a miscibility gap. By definition, the LCST is the lowest point on such a binodal temperature *vs.* composition diagram.<sup>85,86</sup>

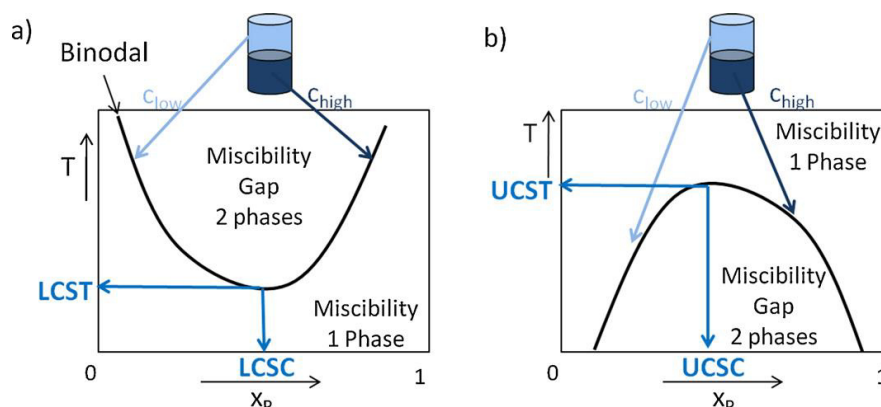


**Figure 2.7.** Temperature vs. composition phase diagram of aqueous polymer solution with a) LCST and b) UCST behavior. Reproduced with permission from Elsevier Ltd, copyright: 2011.<sup>86</sup>

In practice, LCST behavior is based on altering hydrophobicity/hydrophilicity upon temperature variation caused by different forces. First, polymers that consist of polar groups are able to form hydrogen bonds with water molecules. Second, polymer chains consist of intramolecular polar/non-polar interactions. Below LCST, hydrogen-bonds with water molecules form preferentially. Consequently, polymer chains are present as hydrated coils (Figure 2.8) and the miscibility is high, which leads to a one-phase system. In contrast, above LCST, these hydrogen bonds to water molecules are strongly weakened, and intramolecular polymer interactions increase. As a result, polymer coils collapse and aggregate in globule conformations.<sup>87,88</sup>

From a thermodynamic point of view, LCST behavior is an entropy-driven effect, which is explained in terms of the relation between the free Gibbs energy  $\Delta G_m$  of solvent/polymer mixtures, the enthalpy  $\Delta H_m$  and the entropy  $\Delta S_m$ <sup>89</sup>:

$$\Delta G_m = \Delta H_m - T\Delta S_m \quad (2.1)$$

Below LCST, hydrogen-bonds between polymer chains and water molecules lead to the favorable free energy  $\Delta G_m < 0$  for ideal miscibility. When the temperature is increased, *Brownian motion* of small water molecules are much more affected and facilitated than sterically hindered polymer chains. Due to the fact that hydrogen bonds are directional forces, polymer/water interactions are weakened and water molecules are preferentially expelled from the polymer structure.  $\Delta S_m$  decreases, thus  $\Delta H_m$  values overcome the negative  $T\Delta S_m$  term. The free energy turns to the unfavorable state  $\Delta G_m > 0$ , and phase separation occurs.<sup>90,91</sup> It is worth noting that LCST behavior is not a real phase separation. In fact, it is a two-phase system consisting of a highly concentrated polymer phase and a water phase including a very low polymer concentration. Furthermore, the LCST behavior is not limited to being present in aqueous solutions. Also, solvent mixtures with other solvents have been reported.<sup>92</sup>

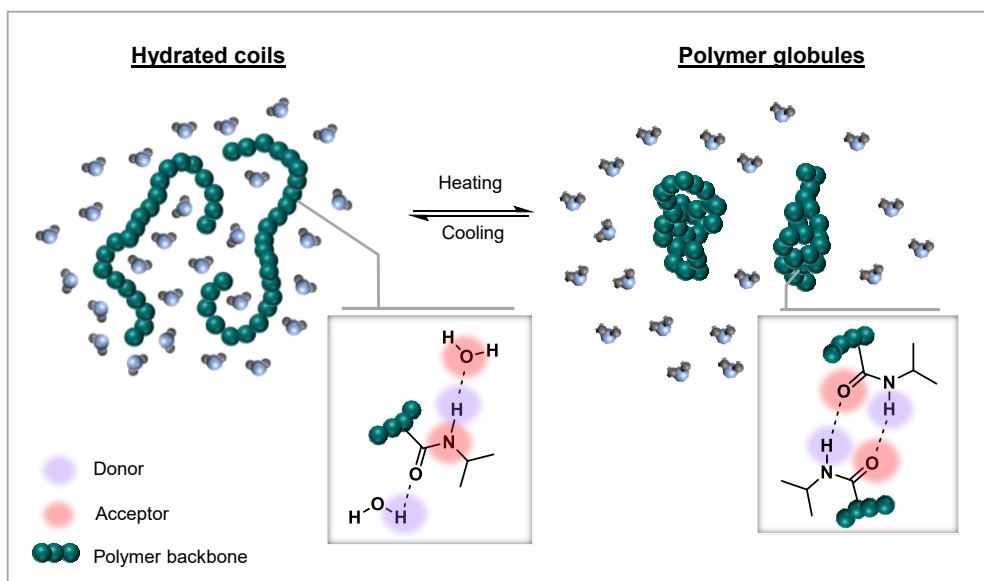


**Figure 2.8.** Classical coil-to-globule transition and *vice versa* of polymer chains in aqueous solutions. The strength of the hydrogen bonds is temperature-dependent.

Besides LCST, so-called *upper critical solution temperatures* (UCST) have also been mentioned for numerous aqueous polymer systems in recent decades. This behavior exhibits rapid miscibility with increasing temperature (Figure 2.7b). The scientific interest has been aroused in particular, since non-ionic polymer systems have been reported that may be applicable in the field of biocompatible technologies.<sup>91</sup> It is noteworthy that the UCST/LCST behavior can be found in a polymer system that is characterized by loop-shaped miscibility gaps. As a prominent example, poly(ethylene oxide) (PEO), shows LCST behavior at 107 °C<sup>93</sup>, while miscibility caused by UCST is detected at 232 °C<sup>93</sup> in a closed system. However, only a few polymers are known that exhibit UCST between 0-100 °C. One such non-ionic is the homogeneous poly(*N*-acryloyl glycinamide) (PNAGA), the UCST behavior of which was intensively investigated by Agarwal and coworkers.<sup>94,95</sup>

On the LCST side, poly(*N*-isopropylacrylamid) (PNIPAM) is probably the most studied representative, which was reported in 1956.<sup>96</sup> The LCST value of 32 °C<sup>97</sup> close to body temperature made PNIPAM an outstanding polymer system for application research in the medical field. In this context, it should be noted, that the name LCST is not used consistently in the literature. As mentioned before, the LCST defines the lowest point in binodal temperature-composition curves. However, the LCST is frequently quoted independently of composition values, and “cloud point” is probably the more appropriate term.<sup>88</sup> For consistency with original publications, the two terms will be used throughout this thesis.

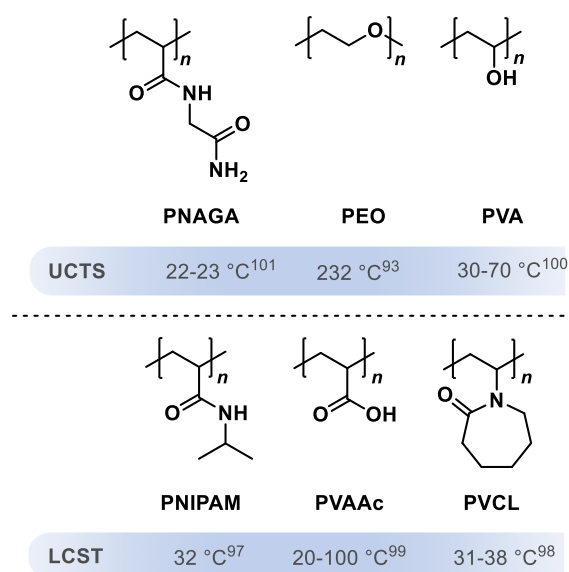


**Figure 2.9.** Structure examples of temperature-responsive polymer systems, including UCST behavior (top) and LCST behavior (bottom). The UCST and LCST (in water) values shown in this figure pertain to the measurement conditions, such as number-average molar mass and polymer concentration.<sup>93,97–101</sup>

Regarding the scope of temperature-responsive systems, values can be dramatically affected by, *e.g.*, copolymerizations. Thus, an increase in the LCST is obtained as a function of the influence of the hydrophilic comonomer. The trend is opposite when hydrophobic groups are incorporated. Ionic structures also show a remarkable influence. However, the UCST is much more affected, especially when salts are involved. Overall, the temperature-responsive behaviors are significantly influenced by the polymer concentrations, the type of solvent mixtures and the molecular masses, dispersities and salt impurities/additions.<sup>102</sup>

### 2.3.1.1 Turbidimetry

In polymer science, several methods have been developed for determining LCST and UCST values. One involves observing the cloud point. This is the temperature below which a clear solution separates into a liquid-liquid phase to form an emulsion or suspension. Macroscopically, this means that a precipitate or turbidity is visible, which can be easily measured. The cloud points themselves can be obtained *via* turbidimetry.<sup>94,103</sup> This technique has been established to determine the critical solution temperature by tracking the intensity loss of transmitted light. For this purpose, a light beam with a defined wavelength passes through a polymer/solvent solution. The transmittance intensity  $\tau$  as the ratio of  $I_0$  (intensity before passing) and  $I$  (intensity after passing) is determined while the sample is heating. Then, this raw data can be plotted as transmittance *vs.* temperature function, which is shown schematically in Figure 2.10. Below LCST, the solvent/polymer mixture appears completely transparent, hence

the transmittance is close to 100%. As the temperature increases, the hydrated polymer coils collapse, globules are formed resulting in a phase separation and hence a turbidity is observed. The transmittance decreases sharply to a minimum. In most cases, it is suggested to determine the cloud point temperature at 50% transmittance. In general, cloud point measurements depend on various parameters, including polymer concentration, stirring, cuvette type and wavelength of the incident light. The latter was found to influence the turbidimetry results only slightly.<sup>85,104,105</sup>

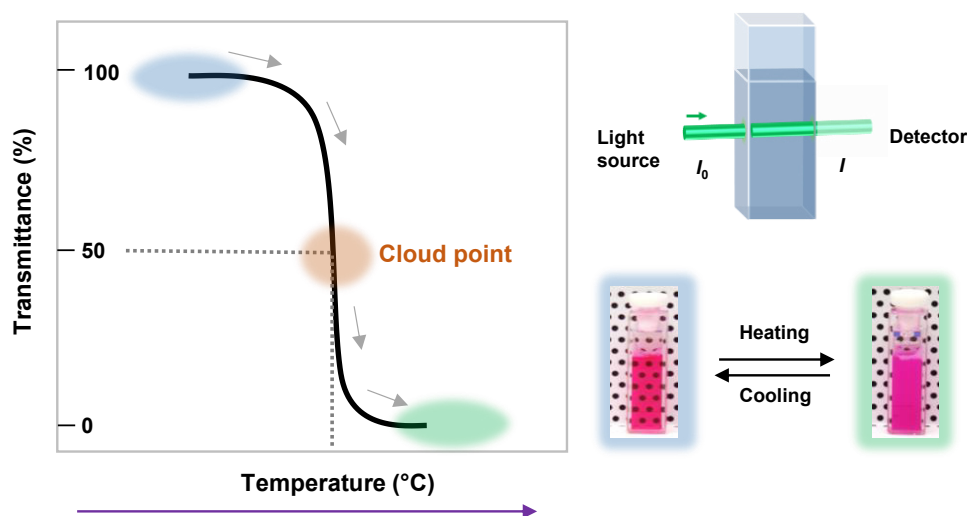


**Figure 2.10.** Example of transmission vs. temperature curve for a polymer solution that exhibits an LCST behavior.

### 2.3.2 Light-responsive polymers

From the physicist's point of view, light is a complex, fascinating phenomenon that can be described as an electromagnetic wave or as a particle. From the perspective of a plant, however, light is simply a powerful source of energy that is responsible for biochemical life processes, such as photosynthesis. Based on the role of light in nature, it can also be found as information carrier, *e.g.* phototaxis or phototropism.<sup>106</sup> With the intention of developing intelligent polymer materials that change properties spontaneously, polymer scientists were very interested in mimicking such natural systems. For this reason, from the 1980s onwards, there was a special activity in the research of light-sensitive polymers. Nowadays, those light-induced characteristic changes play a major role in polymeric solutions<sup>107,108</sup>, micelles<sup>109</sup> and core-shell particles<sup>110</sup>. Furthermore, light responsivity has attracted attention within the areas of photonics/telecommunications (optical data storage<sup>111</sup>) or biotechnology (drug delivery<sup>112,113</sup>, cell labeling<sup>114</sup>). Also hydrogel networks<sup>115</sup> and films<sup>116</sup> have been modified using light-responsive groups. The comprehensive

investigation of such materials is based on easy accessibility of light as stimulus, which is easy to control in space and time, can be applied quickly, can be controlled outside of the system, can be adjusted in intensity and is inexpensive compared to special chemicals that act as catalysts and various more.<sup>107,117,106,117</sup> In general, light-responsive behavior in polymers is achieved by incorporation of photochromic compounds into polymers. For this, various topological configurations, *e.g.*, as side groups, as crosslinkers or as backbone units, are possible.<sup>118</sup> Chromophores can cause different reversible/irreversible effects after light irradiation, which can be subdivided into four main classes:

1. **Dimerization:** A single photo-excited molecule undergoes a reaction with a second molecule of identical chemical composition but in a non-excited state, resulting in the formation of new covalent bonds (*e.g.*, anthracene dimerization<sup>119</sup>).
2. **Conjugation:** A single photo-excited molecule undergoes a reaction with a second molecule of another chemical composition but in a non-excited state, resulting in the formation of new covalent bonds (*e.g.*, Diels-Alder reaction<sup>120</sup>).
3. **Photocleavage:** Light induces a controllable cleavage within the absorbing molecule (*e.g.*, *o*-nitrobenzyl-based photolabile protecting groups<sup>121</sup>).
4. **Isomerization:** Light induces a (reversible) conjugation variation to transfer one molecule to its isomer. This can be observed macroscopically by, *e.g.*, a change in color, shape or solubility.<sup>122</sup>

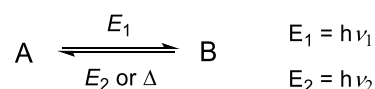
Dimerization and conjugation are useful tools for *in situ* preparation/modification of cross-linking hydrogels. Various chromophores have been published, of which coumarin and cinnamic acid derivatives are most commonly used.<sup>123</sup> In general, this process is a reversible method, which allows further reversible network formation or cleavage. In the opposite case, *o*-nitrobenzyl groups are widely used, when photo lability is required. This group is popular because of its easy handling and controllable polymer chain cleavage.<sup>124,125</sup>

Isomerization, in particular, has raised great interest in the scientific community. Here, azobenzene is probably the most studied representative. This chromophore is converted from the *trans* to the *cis* configuration upon UV light and *vice versa* upon light irradiation.<sup>126</sup> Noteworthy, the polarity is changed from non-polar to polar. Structurally, the increase in polarity is due an increase in the dipole moment from 0 (*trans*) to 3 (*cis*) Debye.<sup>127</sup> Spiropyran (SP) also undergoes a change in polarity from 14-18 Debye to 14-18 Debye<sup>128</sup> when converted to merocyanine (MC), but this responsivity is additionally accompanied by a change in color from colorless to highly colored.<sup>129</sup> Based on these properties, both chromophores have been intensively investigated in recent years. In order to achieve further progress in the field of smart materials, individual research groups have adopted a new class of chromophores, namely *donor-acceptor Stenhouse adducts* (DASA).<sup>130</sup> These colorful dyes exhibit color-, polarity-, and conformation changes upon light irradiation. DASAs, thus, promise interesting multi-responsive polymer systems. The chemical structures of the mentioned photochromophores and the light influence of light on them are explained in Section 2.3.3.

After a separate discussion of temperature and light sensitivity, some examples of stimuli combinations are described in the following. Such systems are known as dual/multi-responsive polymers. In general, dual responsiveness can consist of any kind of stimuli. However, temperature- and light-responsive polymers have gained special interest.

### 2.3.3 Photochromic organic compounds

Photochromic organic compounds undergo photochemical transformations through light absorption, as explained in Section 2.3.2. Due to the application of an external input energy, a specific property (*e.g.*, pKa, color, polarity) can be changed. The photochromism is a powerful phenomenon. Hence, there is a high motivation for designing innovative materials consisting of such smart photochromic compounds. In general, photochromic reactions are reversible and unimolecular.<sup>131</sup> The reversible process occurs between a thermodynamically stable state A and state B (Scheme 2.2), which can be reconverted to A by thermal or photochemical influence. Depending on the thermal stability, there are two classes for photochromism, which are called T- and P-type. The T-type is converted thermally induced and occurs when B is a metastable state. In the opposite case, the P-type is converted under light absorption, hence *via* photons. Each switching process requires light of specific wavelengths, due to the characteristic absorption spectra of the compound.<sup>132–134, 135</sup>

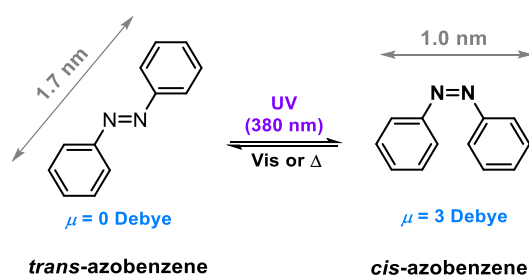


**Scheme 2.2.** Example of photochromism including reversible conversion from state A to B and *vice versa*. State A and state B show different absorption spectra.

Therefore, it is important to note that light-induced reversible conversion happens through different wavelengths ( $\lambda_1, \lambda_2$ ).<sup>136</sup> The list of interesting photoactive compounds has become longer as their role in polymer chemistry has increased. Azobenzene is probably the most studied chromophoric unit that has been successfully established in several responsive polymer systems, due to light-induced polarity changes.<sup>137</sup> A new class of responsive dyes has caught the interest of the polymer community since they have been discovered in 2014. So called Donor-Acceptor Stenhouse adducts are brightly colored compounds that show isomerization upon irradiation with light. Distinguishing itself from other azobenzene derivatives, the DASA photochromism is induced by visible light exposure, which is less energetic and thereby makes it suitable for biocompatible applications. As a result of their capacity to be synthesized in a controlled manner, DASAs have garnered a great deal of interest in the field of polymer research. The discussion in Section 2.3.3.2 provides a more in-depth understanding of the structural nature of DASA compounds as well as the potential uses of these interesting dyes.

## 2.3.3.1 Azobenzenes

Azobenzene is the structurally simplest aryl azo compound, which consists of an N=N double bond and was first prepared almost 200 years ago by Mitscherlich.<sup>106</sup> In general, this type of compound absorbs light and is well-known as a classical dye. However, azobenzene itself exhibits a fascinating photoisomerization process from *trans* to *cis* configuration under UV-light (Scheme 2.3). In general, the *trans*-isomer is by  $\sim 50 \text{ kcal mol}^{-1}$  more thermally stable. Under UV-light irradiation, the structure switches to the higher energy *cis* state. Through thermal relaxation in the dark or under visible light irradiation, the *trans*-state is reached again.<sup>138,139</sup>



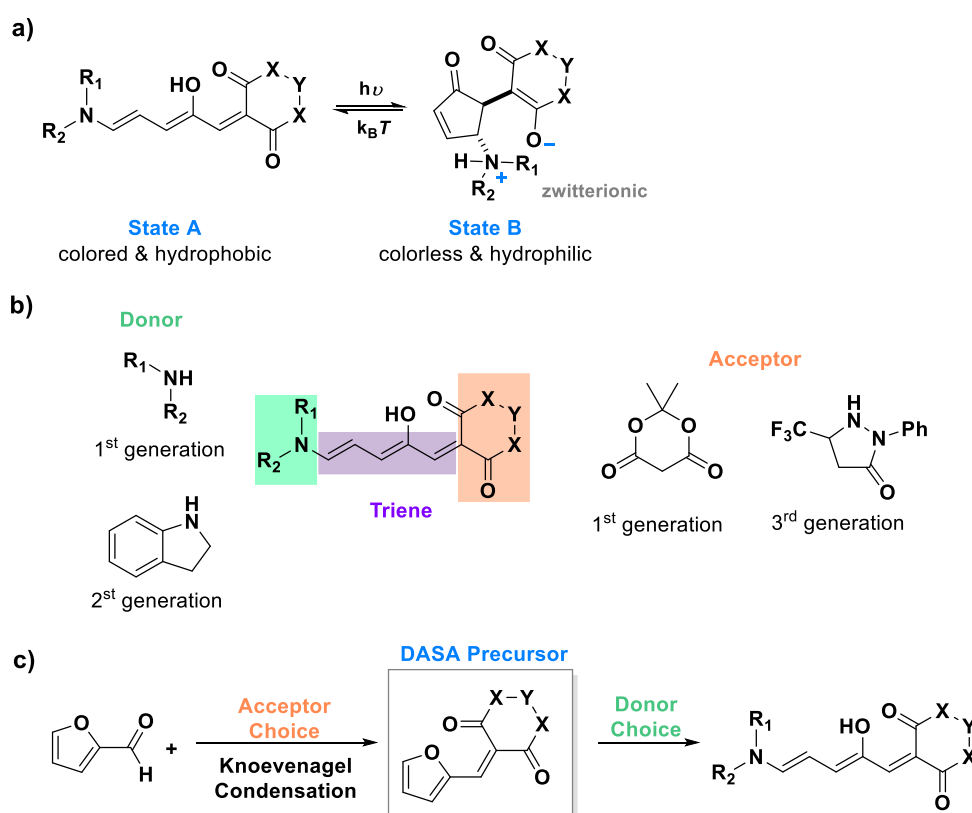
**Scheme 2.3.** UV-light-induced isomerization from *trans*- to *cis*-azobenzene and its light or thermal induced inversion.

The photoisomerization is accompanied by a dipole moment increase from 0 Debye to 3 Debye (*trans* to *cis*) as a result of geometrical modification. Consequently, the polarity is increased. While this photoisomerization happens within picoseconds, the reversal process usually takes several hours. Overall, the absorption wavelength for photoisomerization strongly depends on the substitution of the compound and its position. For the unsubstituted azobenzene, the wavelength for  $\pi \rightarrow \pi^*$  belonging to the *trans* azobenzene appears at 380 nm, however the *cis*-isomer shows a strong absorption at 440 nm for the  $n \rightarrow \pi^*$  transition.<sup>140</sup>

Derivatives of zobenzene have progressed from basic dyes to complex compounds with light-dependent properties that can be utilized to manipulate a wide range of materials, including *e.g.*, biomacromolecules<sup>141</sup>, polymers<sup>142</sup> and metal-organic frameworks<sup>143</sup>.

### 2.3.3.2 Donor-Acceptor Stenhouse Adducts (DASAs)

Based on previous works of J. Stenhouse, Read de Alaniz and coworkers presented the first generation of a highly versatile and new class of organic photochromic compounds and implemented the name donor-acceptor Stenhouse adduct (DASA) in 2014.<sup>130</sup> These photoswitches undergo a reversible transformation within two states, which have completely different photochemical and photophysical properties. Up to this point, three generations of DASAs have been identified.<sup>144</sup> Scheme 2.4a shows the general structures of DASAs before (A) and after (B) irradiation. DASA state A is strongly colored and consists of a conjugated triene system, which forms a bridge between an acceptor and donor part on opposite sides (push-pull system).<sup>145</sup> The DASA structure and typical building blocks are outlined in Scheme 2.4b. The acceptor generally consists of cyclic  $\beta$ -carbonyl acids (1<sup>st</sup> and 2<sup>nd</sup> generation) and offer optical tuning by varying the structure (*e.g.*, Meldrum's acid or 1,3- barbituric acid derivatives). The 3<sup>rd</sup> generation is based on heterocycles, *e.g.*, pyrazolone.<sup>144</sup> The donor simply consists of secondary aliphatic (1<sup>st</sup> generation) or secondary aromatic (2<sup>nd</sup> generation) amines. Photoswitching of state A leads to the colorless cyclopentenone DASA salt. This process is further accompanied by 50% loss of volume contraction as a consequence of triene removal.<sup>146,147</sup>



**Scheme 2.4.** a) Photoswitching process of DASA through visible and NIR light b) DASA structure building blocks c) General synthetic route, including furfural and various acceptor/donor compounds.

The predominant DASA synthetic pathway employs fufural as the starting material (Scheme 2.4c). After treatment with un-/modified acceptor groups, various activated furan precursors can be prepared through Knoevenagel condensation (Scheme 2.4b).<sup>145</sup> In the second step, the furan core is subsequently opened through nucleophilic secondary amines. The supposed mechanism occurs through a series of rearrangements and is quite similar to (aza-)Piancatelli reactions. Medrum's acid and 1,3-barbituric acid derivatives have proven to be suitable acceptors, while nitrogen-based nucleophiles are strong enough for ring opening initiation in contrast to oxygen and sulfur.<sup>147-149</sup> The 1<sup>st</sup> generation consists of dialkylamine donors, while syntheses of the second generation of DASA compounds employ *N*-alkyl anilines.<sup>150</sup> It is worth noting that *N*-alkyl anilines produce DASAs without zwitterionic character, due to the absence of ammonium formation. Furthermore, the usage of primary amines generally results in unstable salts.<sup>130</sup>

Upon visible light stimulation, the first DASA generation shows impressive property changes, namely negative photochromic behavior, a polarity change and volume contraction. Therefore, DASA represents an ideal candidate in the field of stimuli-responsive polymer applications. Additionally, DASAs promise to be an interesting alternative because, unlike most other chromophores, their light absorption is in the biocompatible range of visible light and NIR. Each DASA UV-spectrum exhibits a very strong absorption between 450-700 nm, which corresponds to the  $\pi-\pi^*$  transition in the triene structure (Figure 2.11, 1A, highlighted in green).<sup>147</sup>

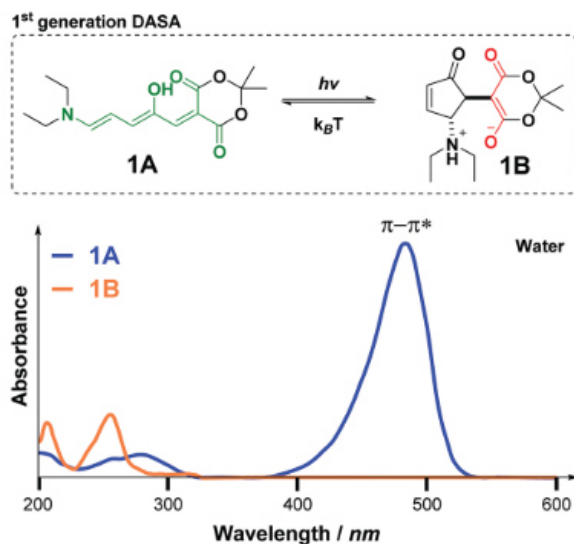


**Figure 2.11.** Absorption spectra of DASA 1A before irradiation with visible light and after 1B. Reproduced with permission from the Royal Society of Chemistry, copyright 2017.<sup>147</sup>

This push-pull conjugated electron system is responsible for the strong coloring of the DASAs.<sup>130</sup> In the case of structure 1A, the aqueous DASA solution appears in red. After

photoswitching and triene bond breaking, the visible light absorption band completely disappears and absorption in the range of 265 nm can be recognized, which is attributed to the activated dicarbonyl structure in the acceptor (Figure 2.11, 1B, highlighted in red).<sup>147</sup> In general, the maximum absorption values of DASAs can be tuned by variation of the acceptor. For example: 1,3-barbituric acid acceptors permit bathochromic shifts of approximately 35 nm as compared to Meldrum's acid acceptors. In contrast, 1<sup>st</sup> generation amine donor groups have almost no shifting influence.<sup>130</sup>

The mechanism of the photoreaction of DASAs has not been finally clarified. However, mechanistic hypotheses have been published based on NMR-, UV-vis steady state spectroscopy, ultrafast time-resolved UV-vis and mid-IR spectroscopy. Based on the theory, the mechanism is thought to follow a complicated multistage pathway. Accordingly, the photoisomerization can be divided into a visible light-driven part (so called actinic step<sup>151</sup>) and in a series of thermally-driven follow-up reactions. In particular, it was discovered that photoisomerization only occurs in the presence of the C<sub>2</sub>-hydroxy group (Figure 2.12).<sup>152</sup> Other heteroatoms are theoretically also feasible. In 2024, C. Reyes *et al.* demonstrated the utilization of an amino group and examined the impact of this backbone atom on the photoswitching.<sup>145</sup>

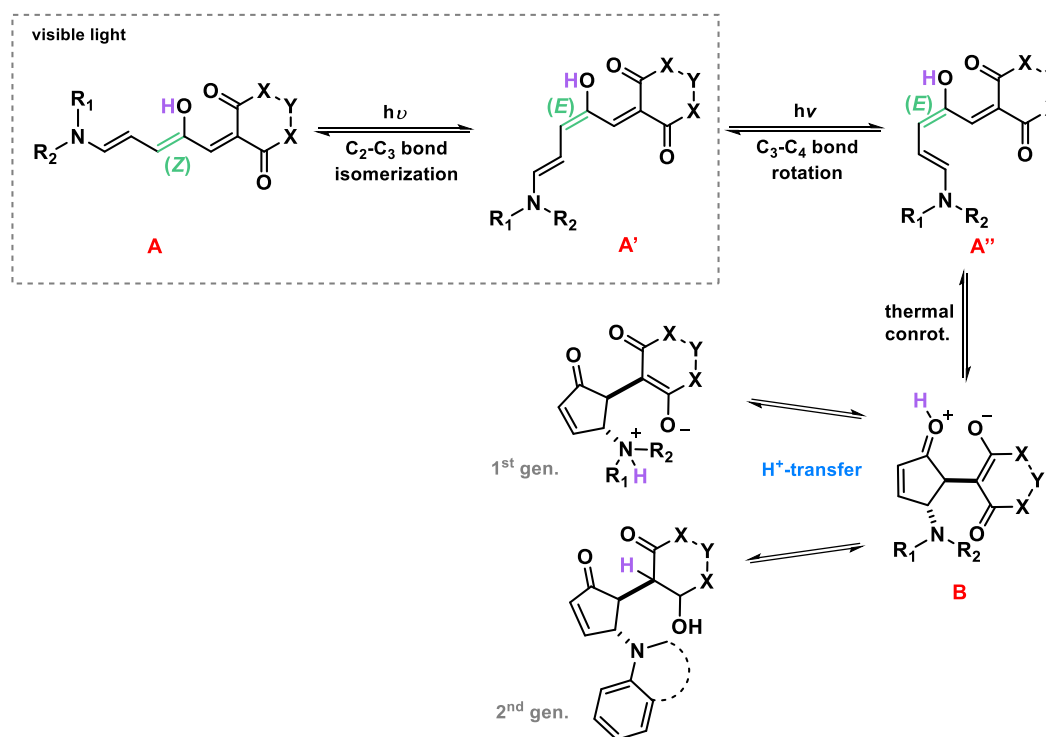


**Figure 2.12.** Proposed mechanism of the DASA switching (1<sup>st</sup> and 2<sup>nd</sup> generation) induced through visible light.<sup>147</sup>

According to the proposed mechanism, the thermodynamically most stable isomer A (EEZZ) undergoes photoisomerization along the C<sub>2</sub>-C<sub>3</sub> position with the hydroxyl group (green

bond), which leads to a favorable isomerization of this double bond and forms isomer A' (EEEZ). While compound A' was detected *via* time-resolved UV–vis measurements, A'' (EZEZ) and B could not be observed so far. The intermediate A' is supposed to be metastable and is generated within picoseconds. The ring formation is assumed to be a consequence of conrotatory  $4\pi$ -electrocyclization, followed by proton transfer to yield the colorless DASA salts. However, the proton role has not yet been clarified either.<sup>153,154</sup>

The switching behavior of the DASA compound is strongly influenced by the solvent nature and the dimensions of the side chains modifications with respect to acceptor and donor groups. For first-generation DASAs, Read de Alaniz and coworkers have impressively illustrated the solvent dependency through phase transfer experiments (Figure 2.13). Therefore, DASA solutions based on Meldrum's acid acceptors and different donor alkyl lengths were tested to transfer from toluene to water and finally to dichloromethane. The example shows that protic solvents promote DASA salt formation, while the thermal conversion to elongated trienes is carried out in halogenated solvents. In fact, colored compounds cannot be recovered in protic solvents and the latter also promote switching in the dark without light. Moreover, only aromatic environments allow for a reversible switching.<sup>130</sup>

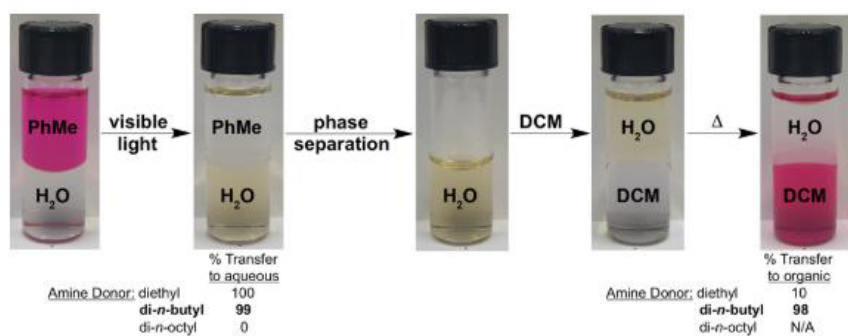


**Figure 2.13.** Phase transfer process of Meldrum's acid-based DASA first-generation. Polar solvents stabilize DASA salt formation, whereas thermal conversion requires aromatic or halogenated solvents. Reproduced with permission from the American Chemical Society, copyright 2014.<sup>130</sup>

The publication of novel DASA compounds by Read de Alaniz laid the foundation for highly interesting applications in which DASAs prove their versatility and flexibility. Thus, DASAs were, for example, designed for the rapid and selective calorimetric detection of nerve agent mimics<sup>155</sup> and as highly sensitive sensors for the detection of amines<sup>156</sup>. Furthermore, DASAs have been successfully integrated into polymer science applications. For example, a cross-linked polyurethane elastomer with modified DASAs for local temperature analysis was incubated with thermochromic molecular sensor technology.<sup>157</sup>

A further example is the successful synthesis of acryl and methacryl polymers bearing 3–4 mol% of a DASA compound, published by the groups of Boeasel and Read de Alaniz in 2017 (Figure 2.14).<sup>158</sup> Their approach involved using pentafluorophenyl ester chemistry to incorporate

different quantities of DASA side groups into the polymer structure. Hence, an amine precursor was treated with activated furans to produce the DASA side group. The authors demonstrated the effective reversible photoswitching of the first and second DASA generation by exposing the spin-coated film to white light irradiation. In addition, the study examined the impact of the polymer glass transition temperature on switching kinetics, revealing a significant acceleration in the transition from a glassy to a rubbery matrix.<sup>158</sup>

a) General synthesis of R. de Alaniz and coworkers

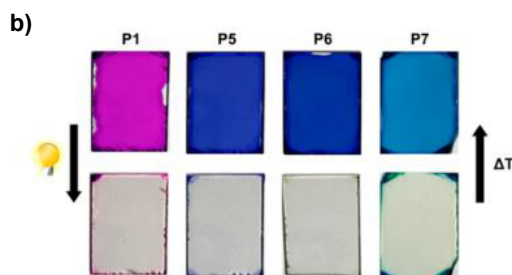
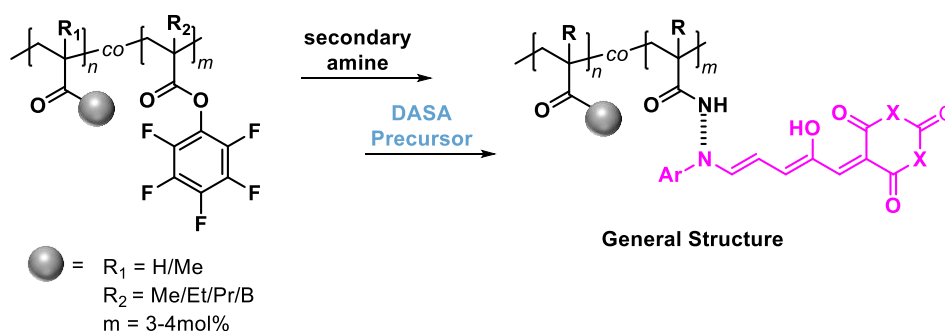


**Figure 2.14.** The general synthesis of DASA polymer conjugates a) published by Alaniz and coworkers and b) their prepared thin films before and after irradiation with visible light and thermal conversion. Reproduced with permission from the American Chemical Society, 2017.<sup>158</sup>

### 2.3.4 Dual light- and temperature-responsive polymers

Reports have been published of several applications using either temperature or light as stimulus. In the next step, dual responsive systems were developed in which both stimuli are combined. Such systems have attracted considerable interest for the preparation of biomedical applications. This results from the fact, that some important thermo-responsive polymers (*e.g.*, PNIPAM, PDMHEMA) that exhibit LCST/UCST behavior, are water-soluble and biocompatible. In addition, their cloud points are in the range of human body temperature, which makes them suitable for use as drug-carriers. To generate even more powerful tools, such systems can be further modulated by light-responsive chromophore units which lead to cloud point shifts after light irradiation. Well-known dual thermo- and light-responsive polymers consist of

azobenzenes as chromophores. The first successful report was published in 1987 by Kungwachakun and Irie, who used a copolymer of NIPAAm and *N*-(4-phenylazophenyl)-acrylamide to study the effect of photoisomerization on LCST values.<sup>159</sup> The general idea of such aqueous polymer systems is explained in Figure 2.15. First, the LCST of the considered copolymer is measured (black curve). The azobenzene derivative is in state A, which means the non-polar *trans* configuration. In the next step, the sample is irradiated with UV-light. As a result, the azobenzene state A is converted into the *cis* isomer state B. Due to the change from non-polar to polar, the phase separation now takes place.

As mentioned in Section 2.3.1, the LCST values depend on a balance between the formation of hydrogen bonds formation and the intermolecular hydrophobic forces of the polymer to precipitate.

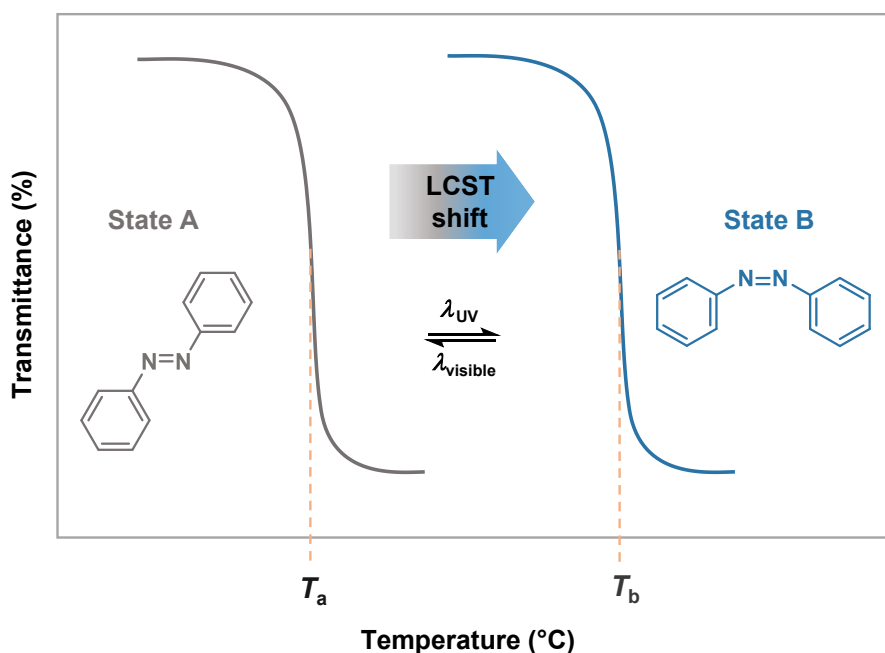


**Figure 2.15:** Schematic illustration of the light-responsive chromophore effect on the LCST values before ( $T_a$ ) and after irradiation ( $T_b$ ).

By introducing a higher polarity, the tendency towards the formation of hydrogen bonds is higher. Consequently, the polymer solubility increases and the LCST is shifted from  $T_a$  to  $T_b$  (blue curve). Overall, the gap between the irradiated and the non-irradiated state can be calculated as the  $\Delta$ LCST value.

In the case of Kungwachakun and Irie, after irradiation with UV-light and a 2.7 mol% azobenzene compound in the copolymer, they showed a temperature shift from 21.0 to 26.0 °C. They further postulated that 2.7 mol% was the best ratio that most affected the cloud point.<sup>160</sup> Shortly before reaching the LCST, such systems are in an unstable state, which leads to a dramatic effect on the properties in that only a few photons are absorbed. This dramatic effect becomes

even clearer if one considers a publication by Menzel and coworkers from 1992. They reported an impressive LCST shift up to 20 °C for 7.3 mol% azobenzene groups in a temperature-responsive polymer based on *N,N*-dimethylacrylamide.<sup>161</sup> While their system was synthesized by direct free radical polymerization of *N,N*-dimethylacrylamide and 4-phenylazophenyl acrylate, Jochum and Theato investigated an excellent tool for preparing dual temperature- and light-responsive copolymers in 2009 by using the activated ester chemistry.<sup>75,162</sup>

By using PPFPA (Figure 2.16), they demonstrated the high applicability of such a synthesis route. This resulted in several temperature-responsive polymers containing different amounts of azobenzene side-groups.<sup>75, 162</sup>

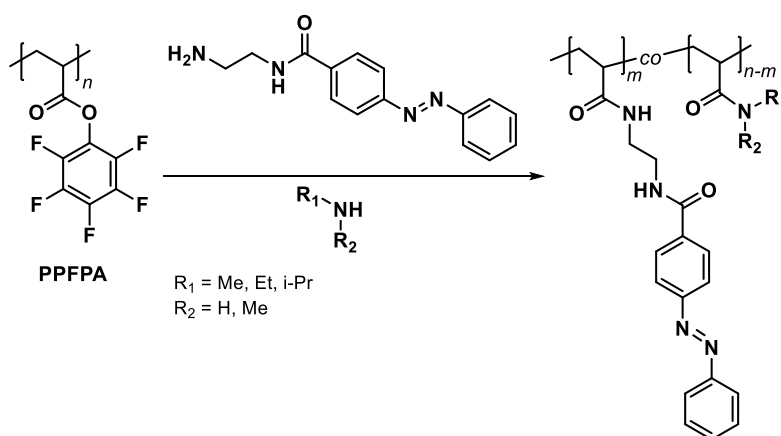
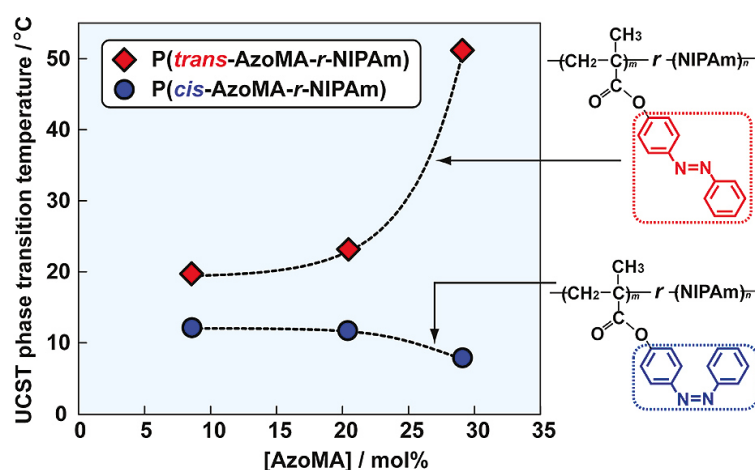


**Figure 2.16.** Schematic model of the use of polymer-analogous reactions to produce functional polymers. The treatment of PPFPA with an azobenzene amine precursor and isopropylamine for the preparation of dual temperature- and light-responsive copolymers as utilized by Jochum *et al.*<sup>162</sup>

As mentioned before in Section 2.2, especially PFP-based post-polymerization modifications exhibit particular advantages. In contrast to Menzel, all polymer samples consist of the same dispersity, due to a polymer precursor which is used as the starting material for a series of azobenzene contents. By examining the light-controlling effect of azobenzene, they found a maximum temperature shift of 7 °C, attributed to poly(*N,N*-dimethylacrylamide) containing 8.5 mol% of azobenzene groups.<sup>162</sup>

Furthermore, Jochum and Theato published a report on the preparation of dual temperature- and light-responsive copolymers by double polymer-analogous reaction using PPFPA as polymer precursor. Here, salicylidene aniline was incorporated as a side-group and light-responsive chromophore. The highest temperature shift was observed for copolymers based on poly(*N*-cyclopropyl-acrylamide) with 15.0 mol% salicylidene aniline. This system allows a maximum cloud point difference of 13 °C upon irradiation, which also clearly shows the efficient control of temperature-responsive polymers by light.<sup>163</sup>

In addition to the LCST values, also the UCST behavior is tunable upon irradiation of an incorporated light-responsive group. However, the direction of UCST shifts is opposite to that of LCST. Higher polarities as consequence of chromophore switching increase the polymer solubility, hence the UCST values decrease. The classical LCST polymer PNIPAM shows an impressive UCST shift from 50.9 °C to 7.9 °C in an ionic liquid of 1-ethyl-3-methylimidazolium bis(trifluoromethane sulfone)amide. Therefore, Ueki and coworkers prepared random p(AzoMA-*co*-NIPAM) copolymers containing different azobenzene groups. The maximum shift is noted for 30 mol% azobenzene (Figure 2.17).<sup>164</sup> Consequently, the example demonstrated the high influence of ionic liquids, in which the UCST is influenced before the irradiation (poorer solubility as compared to pure NIPAM) and during the irradiation due to the better solubility of *cis*-azobenzene in ionic environments.

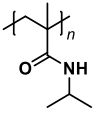
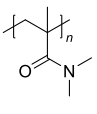
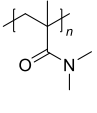
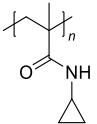
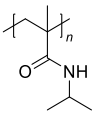
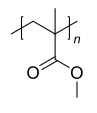


**Figure 2.17.** Light-controlled UCST shifts of P(AzoMA-*co*-NIPAM) as a function of azobenzene group content. All samples were measured in an ionic liquid of 1-ethyl-3-methylimidazolium bis(trifluoromethane sulfone)amide. Reproduced with permission from American Chemical Society, copyright 2011.<sup>164</sup>

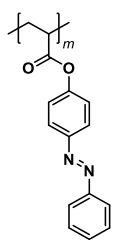
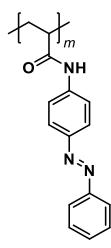
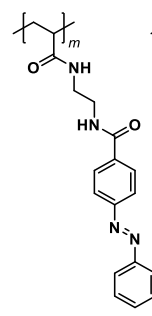
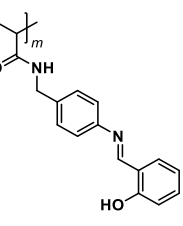
Temperature responsivity control through light can further be influenced by solvent compositions. Zhang and Theato prepared a series of PMMA copolymers containing 6-8% azobenzene side groups and also 6-8% isopropylamine or ethanolamine. All samples were measured in ethanol/water mixtures containing 60 to 100% ethanol. The group found a linear correlation of increasing  $\Delta$ UCST values and increasing water content in the solvent mixture with a maximum shift of 6 °C, resulting from 6% azobenzene and 6% ethanolamine as polymer side-groups.<sup>165</sup>

Overall, the light-controlled phase separation is a powerful tool, which has attracted considerable interest. Especially in the field of biocompatible materials, smart dual responsive polymers offer the possibility for future successful inventions. All the systems mentioned are summarized in Table 2.1 to give an overview.

**Table 2.1.** List of mentioned  $\Delta$ LCST/UCST shifts due to dual temperature- and light responsive polymer systems.

Temperature-responsive polymer matrix	Light-responsive unit	solvent	Amount of chromophore (mol%)	$\Delta$ LCST (°C)	$\Delta$ UCST (°C)	Ref.
	Azobenzene derivative <b>A</b>	water	2.7	5	–	160
	Azobenzene derivative <b>B</b>	water	7.3	20	–	161
	Azobenzene derivative <b>C</b>	water	8.5	7	–	162
	Salicylidene aniline <b>D</b>	water	15	13	–	163
	Azobenzene derivative <b>B</b>	Ionic liquid	30	–	40	164
	Azobenzene derivate <b>C</b>	ethanol/ water (60:40)	6	–	6	165

<b>A</b>	<b>B</b>	<b>C</b>	<b>D</b>
			

In addition to chromophore structures, dispersities and, in particular, the type of temperature-responsive compounds, the range of shift values is influenced by solvent compositions and chemical environments.

The present work focuses on the subject of tuning thermo-responsive polymers by the use of non-thermal radiation. Hence, the subsequent chapters elucidate the motivation and outcomes of the actual work, while also examining the impact of light-switchability. DASA

compounds are the primary subject of investigation as light-switchable chromophores. In an extended synthesis, an azobenzene derivative was also employed.

# 3 Chapter 3

## Motivation

Stimuli-responsive polymers, sometimes also referred to as “smart” polymers, have garnered great attention as they are able to change their physical or chemical properties spontaneously in response to external stimuli (*e.g.*, light, temperature). Usually, slight changes in the environment are sufficient to trigger significant modifications in the characteristics of the polymeric material. In light of this context, polymeric materials that respond to several external stimuli at once present substantial opportunities for applications in the future. Hence, the fundamental concept of this study focuses on examining thermo-responsive polymer systems that also possess light-switching chromophores, enabling them to respond to both temperature and light stimuli. An ideal chromophoric group for this purpose is known as the *donor–acceptor Stenhouse adduct* (DASA). These DASA dyes undergo isomerization when stimulated by visible light. Their photoswitching not only results in a remarkable transition from a highly colored state to a colorless state but also involves a chemical change from being hydrophobic to becoming hydrophilic (Figure 3.1).

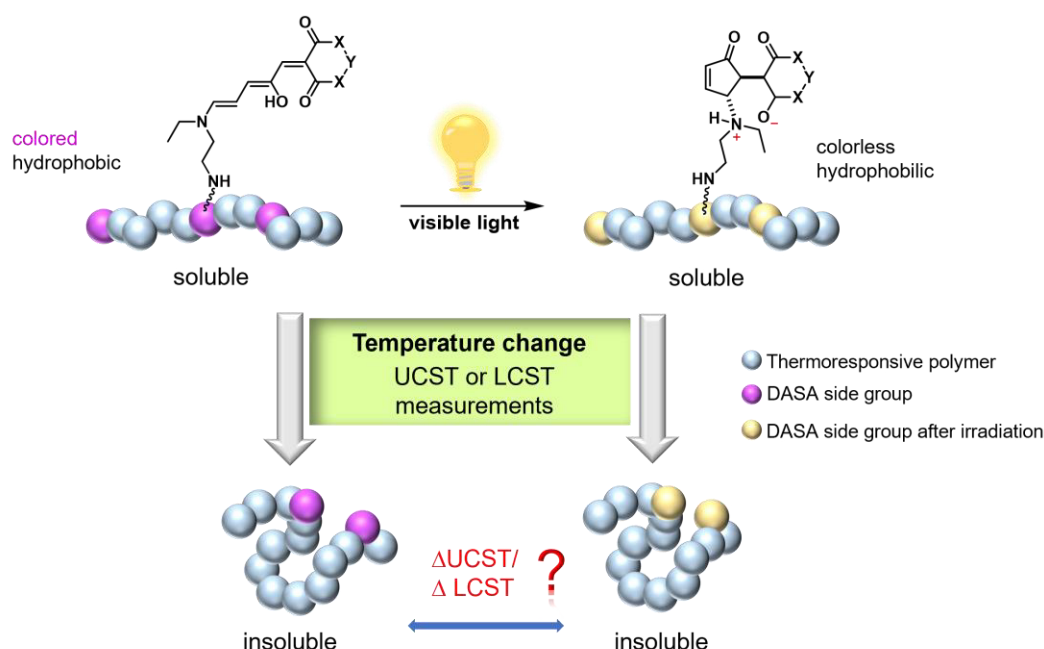


**Figure 3.1.** Schematic overview of thermo- and light-responsive copolymers with donor–acceptor Stenhouse adducts as chromophoric side groups. The copolymers showed a tunable LCST or UCST behavior (based on the main monomer system), depending on the DASA content and irradiation conditions.

The local increase in polarity caused by light is able to shift the phase-transition temperatures of the overall polymer. Thus, the objective of this work is the preparation of various temperature- and light-responsive copolymers that consist of statistically arranged DASA side groups. In order to successfully impact the behavior of phase transition, this thesis investigates materials with the following properties:

The copolymers should either demonstrate an *upper critical solution temperature* (UCST) or a *lower critical solution temperature* (LCST) in aqueous solutions, which can be measured prior to and after exposure to visible light. This enables the determination of the  $\Delta\text{UCST}/\Delta\text{LCST}$  values, allowing for conclusions to be generated on the specific influence of the chromophore in the polymer system. The isomerization of the chromophore should result in a maximum difference between the phase transition temperatures of the non-irradiated and the irradiated species. Therefore, the synthetic protocol should provide access to systematic copolymer libraries containing varying amounts of incorporated DASA side groups, allowing for comparison of DASA content across a certain temperature range. The polymer and phase transition conditions should be chosen so that the DASA structure's isomerization is only affected by light of a specific wavelength and not by other physical or chemical stimuli, such as temperature. Investigating these polymers is a challenge, as it is necessary to demonstrate the stability of the DASA structure in the presence of aqueous solutions. Given the expected preference for stabilization in polymers with a high molar mass, it is necessary to employ polymerization techniques that fulfill this criterion, *e.g.*, free-radical polymerization. Under the specified conditions, PMMA-based (poly(methyl methacrylate)) polymers that undergo phase transitions in ethanol-water mixtures are appropriate for conducting UCST investigations. These solvent mixtures offer the potential to stabilize the DASA chromophore. LCST studies, on the other hand, might benefit from the use of PNIPAM (poly(*N*-isopropylacrylamide)) copolymers due to their phase transition occurring near human body temperature. This implies that there is no need to heat the polymer solution to a high temperature, resulting in reduced stress on the DASA structure.

Once having analyzed the properties of thermo- and lightresponsive copolymers consisting of DASA side groups, an expansion of the current study would involve the incorporation of a second chromophoric unit. Given that previous research on non-polymeric systems has demonstrated the independent, *i.e.*, orthogonal, switching potential of azobenzenes with DASA, this chromophoric group is highly appropriate. When integrated into a polymeric system with a LCST like PDEA (poly(*N,N*-diethylacrylamide)), the chromophores ideally demonstrate independent switching behavior at distinct wavelengths. The resulting isomerization of each chromophore should lead to a change in polarity, which can be verified by measuring the shifted phase transition temperatures.

## 4 Chapter 4

---

# 4 Results and Discussion

Due to their multifunctional responsiveness, DASA promised highly interesting application possibilities. Their light-responsive nature with an external on-demand control over the change in polarity was particularly attractive in combination with materials that display LCST/UCST behavior. Here, the characteristics of Stenhouse adducts were perfectly suited to provide influences of polymers on their cloud point. Consequently, the first decision entailed the selection of a temperature-responsive polymer matrix, which was then accompanied by the implementation of a comprehensive synthesis technique that integrates DASA onto the polymer's side chains. The detailed results are presented in the following three sections, which differ in terms of polymer matrix and stimuli response. The description begins with an intensive study of PMMA-DASA-polymer conjugates and their UCST behavior, which lays the foundation for the second part. By adapting the procedure of PMMA for PNIPAM and PDEA, the focus was then on investigations of the widely known LCST phenomenon. The third part summarizes the results of orthogonal photo-isomerization systems, where the polymer side groups carried two different chromophoric units. All projects have one thing in common: The significance of the light-induced switchable DASA system, which produced drastic changes in the polymer properties and thus had a lasting influence on the temperature-responsive behavior and even made it controllable.

Figure 4.1a represents the general synthetic pathway. Notably, it was based on investigations by Ulrich *et al.*<sup>158</sup> The group successfully prepared polymer conjugates consisting of max. 4% DASA and made use of amidation as described in more detail in Section 2.3.3. The preparation described in this work involved two sequential post-polymerization modifications in which, first, PFP ester groups were substituted by *N*-ethylethylenediamine (EEDA) as an amine linker and, secondly, DASA formation was achieved by treatment with an activated furan precursor. The employed methodology offered favorable reaction conditions and facilitated effective regulation of the desirable mole ratios of DASA attached to the polymer chains. This work primarily aimed to investigate the furan precursor of Meldrum's acid and the 1,3-disubstituted barbituric acid in order to obtain the appropriate colored Stenhouse structures (Figure 4.1b). The research conducted by Ulrich and colleagues concentrated mainly on investigating the impact of various modifications of DASA on glass transitions, particularly in relation to the second generation of DASA. However, the present study aimed to examine the changes in cloud point temperatures upon light irradiation. This study exclusively concentrated on 1<sup>st</sup> generation Stenhouse adducts due to their capability to undergo zwitterionic production upon absorption of visible light, as changes in polarity were crucial for inducing cloud point alterations (Figure 4.1c)

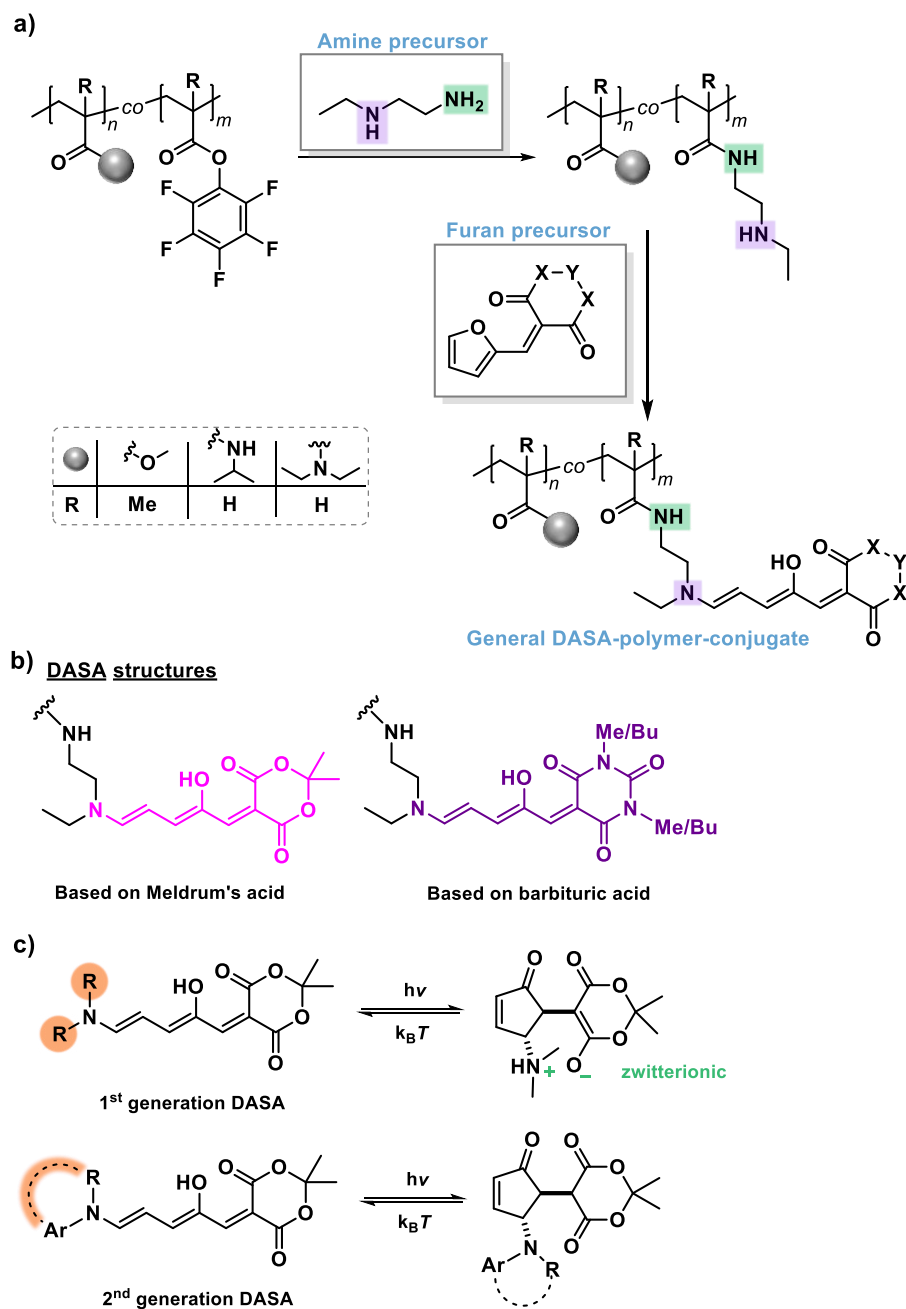


**Figure 4.1.** DASA-polymer conjugates overview. **a)** General synthesis route of this work to obtain temperature-responsive copolymers bearing DASA side groups. **b)** DASA structures based on Meldrum's acid and barbituric acid furan precursors. **c)** Photoswitching processes of the 1<sup>st</sup> and 2<sup>nd</sup> generation DASA.

For the purpose to acquire a comprehensive understanding of the impact of DASA on cloud points, the objective was to generate polymer conjugates containing a DASA concentration exceeding 4 mol%. Hence, the main challenge addressed was the successful synthesis of a copolymer library with a range of 2 to 12 mol% DASA moiety content. In order to prevent the

concurrent formation of the colorless cyclopentenone, it was imperative to conduct preparatory procedures and analyses under conditions devoid of illumination.

## 4.1 Poly(methyl methacrylate)-DASA conjugates

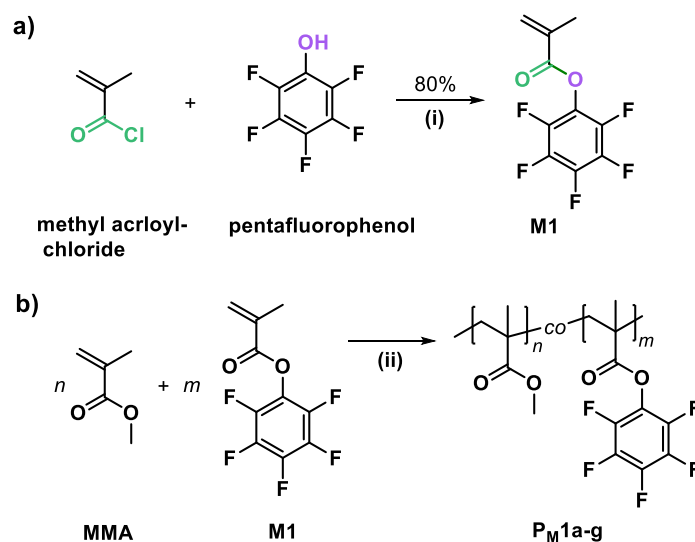
Poly(methyl methacrylate) (PMMA) is one of the well-known synthetic polymers, discovered in the early 1930s by Rowald Hill and John Crawford.<sup>166</sup> The first application followed 1933, when Otto Röhm recognized PMMA as interesting safety glass. Nowadays, the resulting PLEXIGLAS® brand is world-renowned and PMMA has long been established in a wide range of applications. The reason for this success is directly related to its physical properties. PMMA is an amorphous thermoplastic polymer characterized by high impact strength, shatter and weather resistance, high resistance to sunshine exposure and good thermal stability. Nicely, it exhibits outstanding processing conditions. Besides the utilization as electrically conductive filler<sup>167</sup>, as polymer electrolyte membrane for batteries<sup>168,169</sup> or as nanomaterial in plastic chips<sup>170</sup>, PMMA is further highly attractive in the field of biomedical applications. For example, Nien *et al.* described bone cements for drug delivery/release<sup>171</sup> using PMMA as non-toxic polymer. Furthermore, PMMA shows an interesting solution behavior. Although the polymer is not soluble in water, clear solubility in ethanol at ~86 °C<sup>172</sup> can be observed including a sharp phase transition. As the number of reports dealing with non-toxic and non-zwitterionic UCST systems (especially upon 100 °C) is severely limited, PMMA offers a great opportunity for UCST tuning studies.<sup>172</sup> This has been proven by introducing different functional groups into the polymer side chain, as example fluorescent dyes<sup>173</sup> or active ester amidation reactions with a series of amines published by Theato and Hoogenboom<sup>174</sup> in 2012. They demonstrated impressively the controllability of phase transition temperatures by varying side groups and their content within polymer side chains. As explained in Section 2.3.4, Theato and Hoogenboom further developed their study in 2015 by azobenzene incorporation to the PMMA side chain and presented the existing of UCST shifts ( $\Delta$ UCST) after UV-light irradiation.<sup>165</sup> The influence and control of such cloud point temperatures could potentially offer a novel application route towards drug delivery/release.

In light of these findings, PMMA was strategically chosen as the polymeric substrate for tuning the UCST in the present work. Hence, it was hypothesized that the modulation of PMMA cloud points in different aqueous ethanol mixes might be achieved through the utilization of Stenhouse adducts as chromophores, exhibiting a range of polarity spanning from hydrophobic to hydrophilic. In contrast to the dipole moment change of azobenzene, the polarity change of DASA compounds is caused by formation of zwitterions. Hence, the observation of higher  $\Delta$ UCST values was assumed. Further, Stenhouse dyes provided the advantage of photo-switching with visible light, which is much more biocompatible compared to energy-rich UV-light. Last but not least, their negative photochromic tendency from highly colored to colorless is an attractive side effect.

The results of the synthesis and characterisation of PMMA-DASA-polymer conjugates are described in the following sections. Following that, measurements of the UCST prior to and after light irradiation are shown and discussed.

#### 4.1.1 Synthesis of PMMA-DASA-polymer conjugates

To commence, a poly(methyl methacrylate-*co*-pentafluorophenyl methacrylate) (p(MMA-*co*-PFPMA), **P<sub>M1</sub>**) library was prepared, varying in the active ester content carefully by targeting different monomer mole ratios. For this purpose, the monomer pentafluorophenyl methacrylate (PFPMA, **M1**) was first synthesized through a nucleophilic addition of pentafluorophenol to methylacryloyl chloride, according to the literature.<sup>175</sup> While TEA was used as an auxiliary base to increase the reactivity of pentafluorophenol<sup>176</sup>, a routinely obtainable yield of 80% was achieved (Scheme 4.1a). Since free-radical polymerization techniques provide access to polymers with a high average molecular mass, 2,2'-azobis(2-methylpropionitril) (AIBN) initiated the direct copolymerization of MMA and **M1** (Scheme 4.1b). This process followed the published description of Theato and Hoogenboom.<sup>174</sup> In order to achieve PMMA-DASA polymer conjugates consisting of different chromophore contents, the amount of monomer **M1** was varied between 2 mol% and 14 mol% (**P<sub>M1a</sub>** – **P<sub>M1g</sub>**).



**Scheme 4.1.** a) Reaction between methylacryloyl chloride and pentafluorophenol to perform pentafluorophenyl methacrylate (**M1**) adopted from ref.<sup>175</sup>. Reaction conditions: (i) Dry Et<sub>2</sub>O, TEA, rt, 19 h. b) Free-radical polymerization of MMA and **M1** with AIBN as initiator. Synthesis conditions (ii) were adopted from ref.<sup>174</sup>: Dry 1,4-dioxane, AIBN, 6 h.

All **P<sub>M1</sub>** copolymer syntheses resulted in practically quantitative conversions and yields (Appendix A.1). Thus, the polymerization conditions used allowed for precise control of the appropriate **M1** content inside the polymer chains. Table 4.1 summarizes the analytical data for the size-exclusion chromatography (SEC) determination. To facilitate the conclusions of the characterization methods, the corresponding PMMA homopolymer was also successfully synthesized under the same reaction conditions.

**Table 4.1.** SEC measurement results of the **P<sub>M1</sub>** copolymer series.

Sample	M1 expected (mol%)	$\bar{M}_n$ (g mol <sup>-1</sup> ) <sup>a</sup>	$\bar{M}_w$ (g mol <sup>-1</sup> ) <sup>a</sup>	$\mathcal{D}^a$
PMMA	—	4.79·10 <sup>4</sup>	1.04·10 <sup>5</sup>	2.18
<b>P<sub>M1a</sub></b>	2	6.22·10 <sup>4</sup>	1.31·10 <sup>5</sup>	2.11
<b>P<sub>M1b</sub></b>	4	5.40·10 <sup>4</sup>	1.21·10 <sup>5</sup>	2.24
<b>P<sub>M1c</sub></b>	6	6.18·10 <sup>4</sup>	1.35·10 <sup>5</sup>	2.18
<b>P<sub>M1d</sub></b>	8	5.59·10 <sup>4</sup>	1.22·10 <sup>5</sup>	2.18
<b>P<sub>M1e</sub></b>	10	5.84·10 <sup>4</sup>	1.29·10 <sup>5</sup>	2.21
<b>P<sub>M1f</sub></b>	12	5.49·10 <sup>4</sup>	1.20·10 <sup>5</sup>	2.18
<b>P<sub>M1g</sub></b>	14	5.46·10 <sup>4</sup>	1.28·10 <sup>5</sup>	2.35

<sup>a</sup>determined by SEC

The SEC measurements were carried out using THF as the solvent, and the molecular masses were calculated using a PMMA standard. The observation of unimodal curve progressions indicated successful statistical copolymerizations (Figure 4.2a). The average molecular masses  $\bar{M}_n$  of all **P<sub>M1</sub>** samples were in the same range of 60,000 g mol<sup>-1</sup>, whereas PMMA had an average molecular mass of approximately 10,000 g mol<sup>-1</sup> lower as compared to the copolymers. All dispersities were in the range of  $\mathcal{D}$ = 2.2. Since the copolymers only differed slightly in terms of molecular weight and dispersity values, they represent excellent parent materials by allowing an accurate comparison of the cloud point measurement results.

The amount of incorporated **M1** was determined *via* <sup>1</sup>H NMR spectroscopy, respectively. Peaks originating from the methoxy protons H<sub>c</sub> (Figure 4.2b) were compared to the corresponding methyl backbone protons H<sub>d</sub>. This calculation method was verified by using hetero nuclear single coherence (HSQC) NMR to confirm the clear separation of methyl backbone protons (H<sub>a</sub>+H<sub>d</sub>) and methylene backbone protons (H<sub>b</sub>+H<sub>e</sub>). Thus, the mol% ratio of **P<sub>M1</sub>** was calculated through Equation 4.1.

$$X_{\text{PPF}} = 1 - \frac{\int_{\text{H}_c}}{3} \quad (4.1)$$

As example, calculation of **P<sub>M</sub>1d** with the integral  $H_c$  (2.77) resulted in approximately 7.7% of PFP ester moiety. By adopting the calculation for each **P<sub>M</sub>1** sample, Table 4.2 reveals that the determined values nicely correspond to the expected calculated amounts (*i.e.*, feeding ratio). This high control over the incorporated monomer ratios was a consequence of the quantitative conversion due to the free-radical polymerization technique. However, small inaccuracies of  $\pm 10\%$  could be caused by phase corrections during NMR spectra analysis.

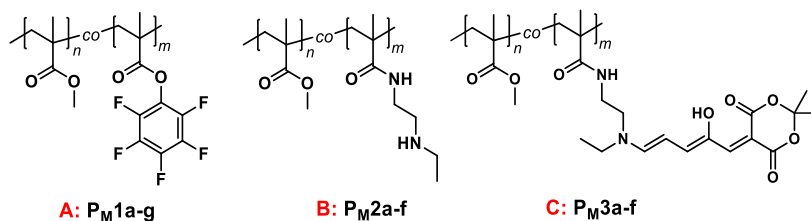
**Table 4.2.** Expected and measured mol ratios of the activated PFP ester group and conversion to functionalized amine and DASA group of the PMMA-DASA copolymers.

Sample	expected (mol%) <sup>a</sup>	<sup>A</sup> $X_{\text{PFP}}$ (mol%) (Y = 1)	<sup>B</sup> $X_{\text{amine}}$ (mol%) (Y = 2)	<sup>C</sup> $X_{\text{DASA}}$ <sup>b</sup> (mol%) (Y = 3)	<sup>C</sup> $X_{\text{DASA}}$ <sup>c</sup> (mol%) (Y = 3)
<b>P<sub>M</sub>Ya</b>	2	2.0	2.1	1.0*	1.1
<b>P<sub>M</sub>Yb</b>	4	3.9	4.2	3.8*	2.6
<b>P<sub>M</sub>Yc</b>	6	7.1	6.5	5.7*	5.1
<b>P<sub>M</sub>Yd</b>	8	7.7	8.5	7.4*	6.6
<b>P<sub>M</sub>Ye</b>	10	10.4	10.3	10.7**	7.8
<b>P<sub>M</sub>Yf</b>	12	12.6	12.0	12.2**	10.6
<b>P<sub>M</sub>Yg</b>	14	14.5	—	—	—

<sup>a</sup>theoretical PFP ester content with respect to the used mol ratios of **M1**.

<sup>b</sup>determined by <sup>1</sup>H NMR integration with \*Measured in CDCl<sub>3</sub> and \*\* Measured in DMF-*d*<sub>7</sub>

<sup>c</sup>determined by UV-vis absorption measurement through calibration.



In addition, the <sup>1</sup>H NMR spectra depicted in Figure 4.2c highlight the successful copolymerization between MMA and **M1** instead of two concurrent homo-polymerizations. The observed broadening of the peak at 3.66 ppm ( $H_c$ ) was attributed to changes in the chemical environment of  $-\text{CH}_3$  resulting from the integration of a second monomer species, as the **M1** concentration exhibited a linear increase.

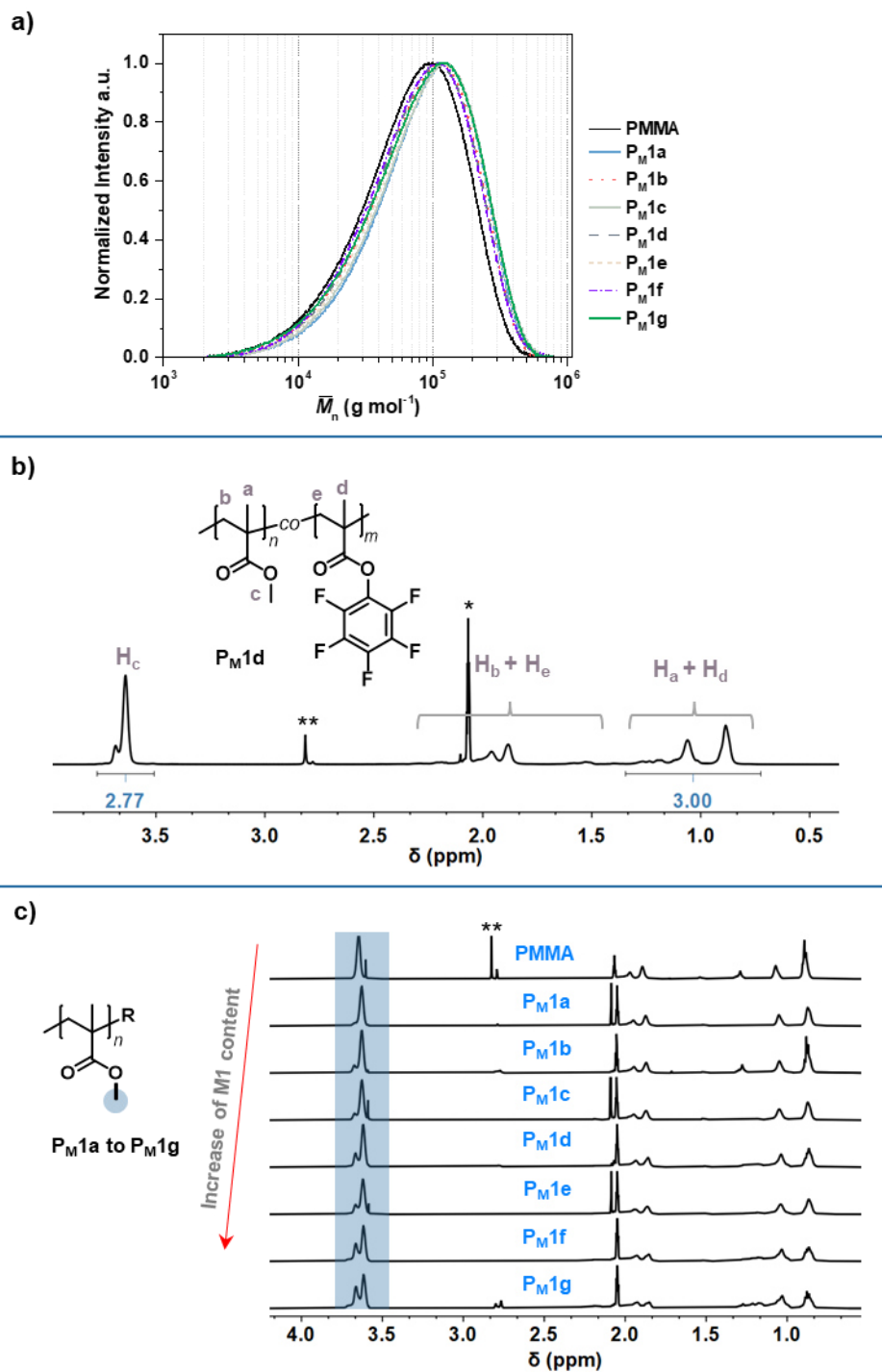
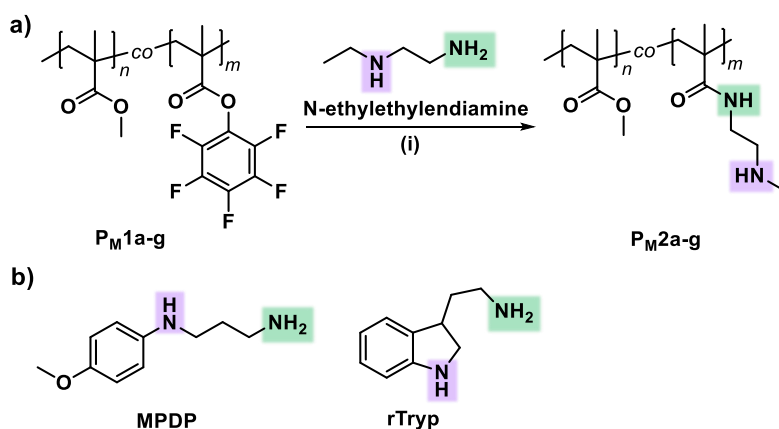


**Figure 4.2.** a) SEC curves of the synthesized PMMA and the  $P_{M1}$  series measured in THF. All data were determined relative to linear PMMA standards. b)  $^1\text{H}$  NMR spectrum ( $^*\text{acetone-}d_6$ ) of  $P_{M1d}$  with integrals of the PMMA methoxy group  $H_c$  and  $H_a/H_d$  polymer backbone for **M1** content determination. c)  $^1\text{H}$  NMR spectra (chloroform- $d$ ) of the  $P_{M1}$  copolymers for methoxy peak (3.63 ppm) monitoring. \*\*residue solvent

While the PFP ester exchange by primary amines is generally advantageous and the DASA formation requires a secondary amine functionality, *N*-ethylethyldiamine (EEDA) was chosen as linker due to its commercial availability, ease of handling and low steric hindrance (Scheme 4.2a). The aminolysis of the **P<sub>M1</sub>** series to form poly(*N*-(2-(ethylamino)ethyl)-methacrylamide-*co*-MMA) (p(EEDA-*co*-MMA), **P<sub>M2</sub>**) copolymers was adapted from a general procedure of Zhang *et al.*<sup>165</sup>



**Scheme 4.2.** a) Reaction scheme of the first post-polymerization process including *N*-ethylethyldiamine (EEDA) as amine linker and reaction conditions (i): TEA, THF/acetone (80:20), 45 °C, 5d. b) Aromatic amine linker used by Ulrich *et al.*<sup>158</sup>

Following the described synthetic protocol, all **P<sub>M1</sub>** polymers were dissolved in a mixture of THF/acetone (80:20), respectively, and converted by using an excess (4 eq.) of EEDA and TEA as an auxiliary base. Compared to pentafluorophenyl acrylate, the PFP ester amidation of **M1** with its methyl group exhibits less reactivity and requires longer reaction times. Hence, the progress of this polymer analogous reaction was monitored by following the disappearance of the carbonyl band signature (C=O<sub>stretch</sub>-vibration) of the PFP ester at 1775 cm<sup>-1</sup> utilizing Fourier transform infrared spectroscopy (FT-IR) (Figure 4.3a). Accordingly, a complete vanishing of the carbonyl band was assumed to be equivalent to a 100% conversion. For the newly formed **P<sub>M2</sub>** copolymers, purification issues had to be resolved, especially for the samples with higher PFPMA moiety contents (**P<sub>M2d-f</sub>**). Purification through repetitive precipitation/solving procedures left impurities of EEDA that could cause undesirable side reactions in the next step. In addition, pentafluorophenolate residues were detected, causing problems in coincidence with the colored DASA state due to the high salt polarity. To address these issues, the crude products were purified by dialysis against acetone for at least 5 days using a membrane with a molecular weight cut-off (MWCO) of 6000 Da, which proved to be highly efficient. Furthermore, the disappearance of <sup>19</sup>F atom signals in the <sup>19</sup>F NMR spectra of the pure products corroborated the successful quantitative substitution of the PFP ester (Figure 4.3b). Noteworthy, the detected

number of peaks belonging to PFP fluorine atoms is unusual due to a splitting effect concerning the *ortho*-fluorine atoms. This phenomenon might be a result of the change in the chemical environment caused by the tacticity of the methyl group in the polymer backbone.

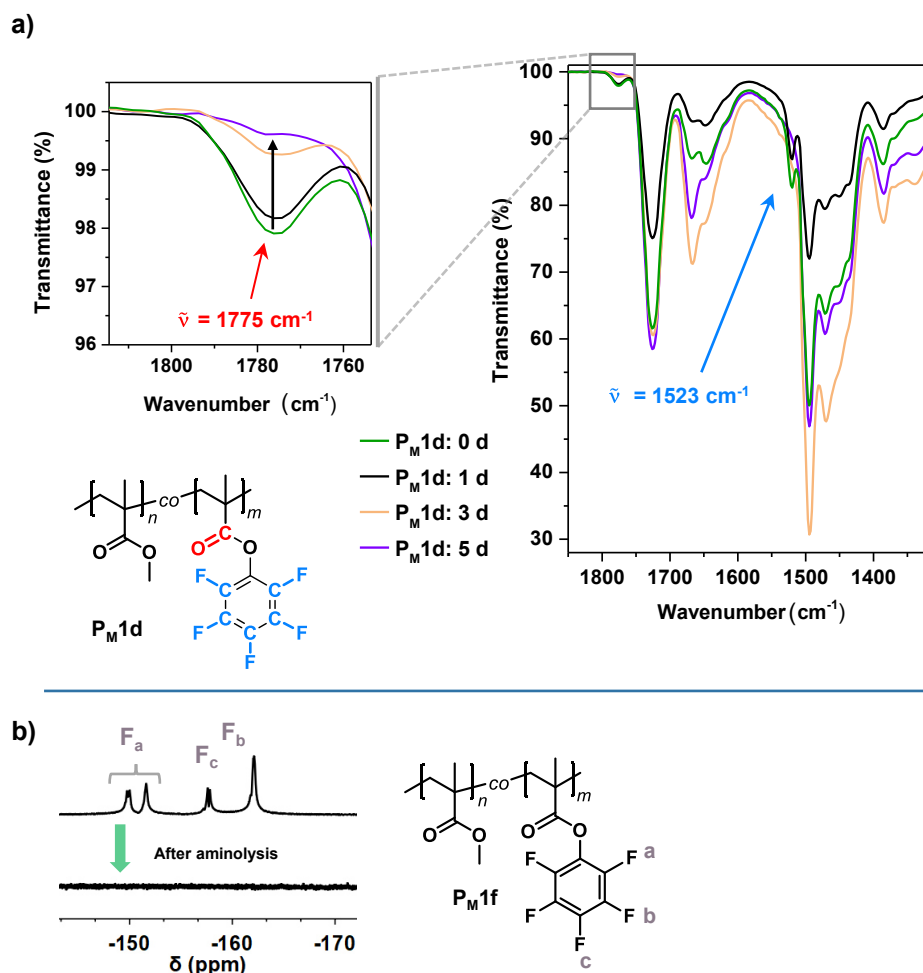
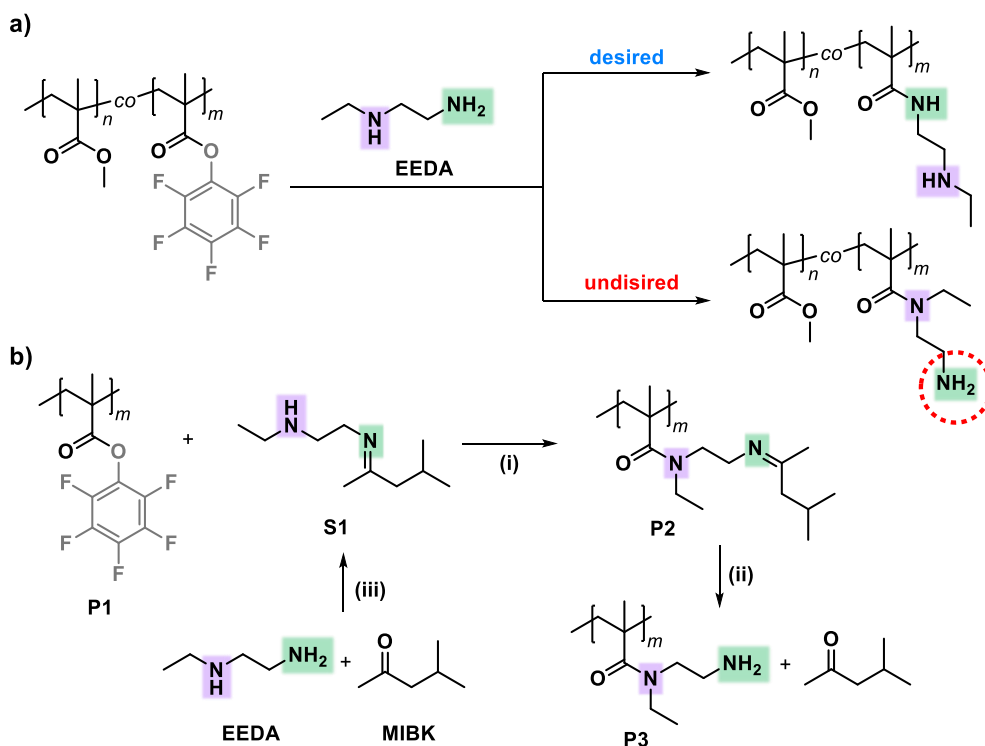


**Figure 4.3.** a) Conversion monitoring *via* FT-IR spectra (selected region) of  $P_{M1d}$  before (0 d) and during aminolysis with EEDA. b)  $^{19}F$  NMR spectra of  $P_{M1f}$  before (top) and after 5 d of aminolysis (bottom) and sample purification.

The preceding discussion presumed the prioritized substitution of the PFP ester moiety with the primary amine functionality of EEDA, rather than its secondary amine group. The current state of research provides substantial evidence supporting the feasibility of amidation reactions involving secondary amines through the utilization of the PFPMA/PFPA ester moiety.<sup>175</sup> In the present methodology by Ulrich and coworkers, an aromatic-bonded amine linker was utilized (Scheme 4.2b).<sup>158</sup> Since electron-rich aromatic neighboring groups markedly reduced the reactivity of the secondary amine, no side reactions were observed. In contrast, the secondary amine functionality of EEDA showed more reactivity. Scheme 4.3 summarizes possible synthetic pathways for the PFP ester aminolysis through EEDA.



**Scheme 4.3.** a) Desired and possible undesired (side) reaction of the **P<sub>M1</sub>** copolymer series during aminolysis with EEDA. b) Protecting process of **S1** including imine formation. Reaction conditions: (i) MIBK, MgSO<sub>4</sub>, argon, reflux, 21 h; (ii) MIBK, TEA, argon, reflux, 48 h; (iii) water, 2-propanol, 50 °C, 21 h.

Given the study's goal of achieving higher DASA content ratios in the polymer backbone relative to Ulrich's previous work, it was statistically probable that side reactions would occur. This presented two complications: First, the amount of secondary amine precursor for DASA formation would be lower than expected. Secondly, the side reaction created the free primary amine (Scheme 4.3b, red dotted line), which would form an unstable salt in the second post-polymerization reaction. Since <sup>15</sup>N NMR spectra of the **P<sub>M2</sub>** series suffered from resolution issues and <sup>1</sup>H NMR spectra showed overlaps, a protective reaction cycle involving poly(pentafluorophenyl methacrylate) (**P1**) as a homopolymer (Scheme 4.3b) was performed. The general mechanism was based on the achievements of Laduron *et al.*<sup>177</sup>, with an imine playing a crucial role as protecting group. For an equivalent emulsion, EEDA was selectively protected by an imine condensation with 4-methylpentan-2-one (MIBK) giving **S1**, which was further employed for the polymer analogous reaction of **P1**, yielding in the intermediate **P2**. By hydrolysis, the polyacrylamide **P3** was obtained, having solely primary amine functionalities. Hence, **P3** was the homopolymer representant of the possible undesired reaction shown in Scheme 4.3a. Owing to significant differences in the <sup>1</sup>H spectra and 2D HSQC spectra, the comparison of the appropriate analytical data enlightened the absence of the primary amines in the chemical structure of the **P<sub>M2</sub>** series (Figure 4.4).

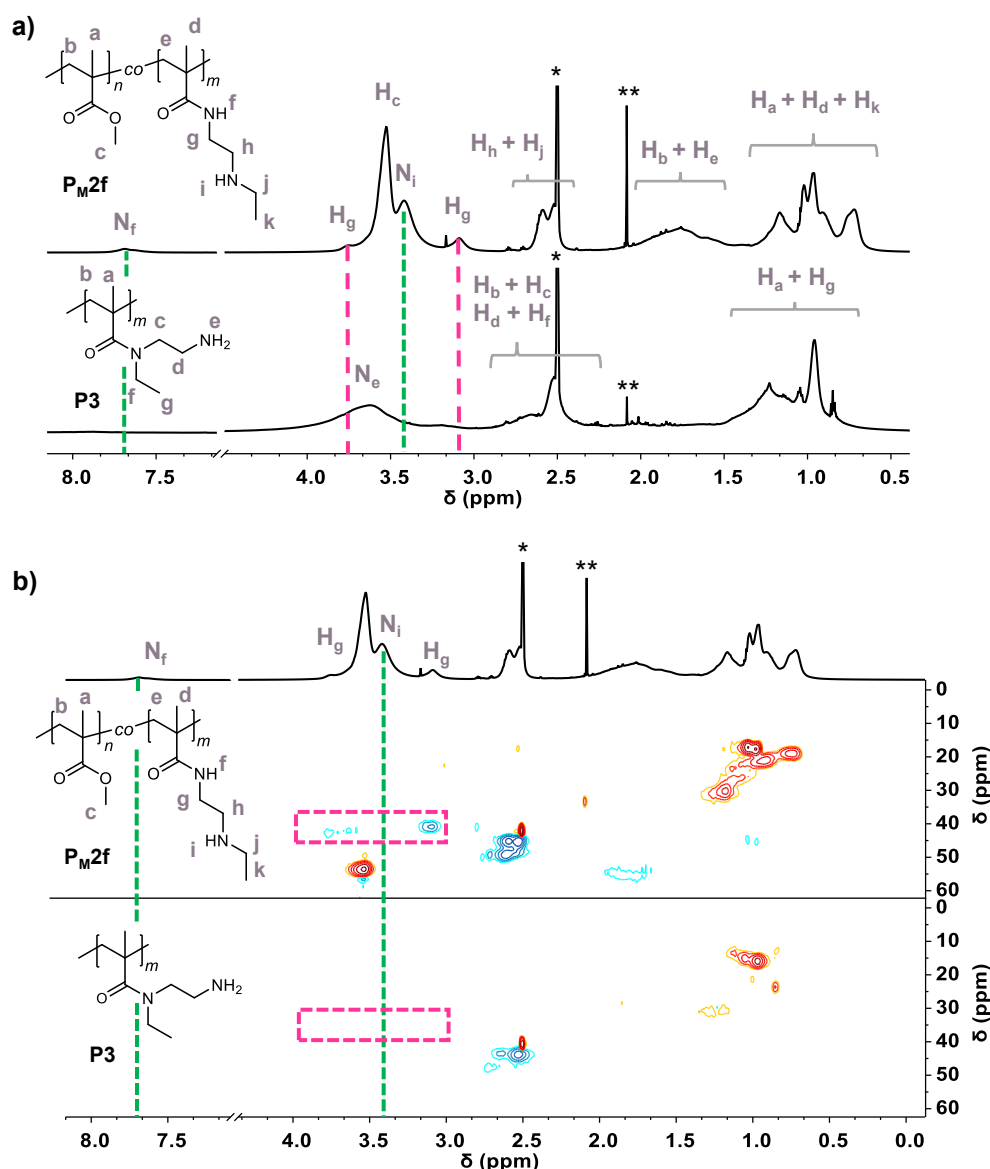


**Figure 4.4.** a)  $^1\text{H}$  NMR spectra of  $\text{P}_{\text{M}2\text{f}}$  (top) and  $\text{P}3$  (bottom) measured in  $\text{DMSO-}d_6$ . b) 2D HSQC spectra of  $\text{P}_{\text{M}2\text{f}}$  (top) and  $\text{P}3$  (bottom) measured in  $\text{DMSO-}d_6$ .

Determining of the  $-\text{NH}$  atoms  $\text{N}_f$  ( $\delta = 7.68$  ppm) and  $\text{N}_i$  ( $\delta = 3.47$  ppm) in the  $^1\text{H}$  NMR spectrum of  $\text{P}_{\text{M}2\text{f}}$  (Figure 4.4a) did not reveal a corresponding signal in the spectrum of  $\text{P}3$  (green dotted lines). Moreover, while the signals of  $\text{H}_g$  (protons next to amide) were clearly identified at  $\delta = 3.77$  and  $3.09$  ppm, a corresponding signal was not located in the 2D HSQC spectrum of  $\text{P}3$  (pink dotted boxes). Overall, there was a prevalent assumption that the desired reaction occurred with a higher preference. This might be attributed to the utilization of a lower reaction temperature and an excess amount of EEDA in the polymer equivalent process. Incidentally, the presented  $^1\text{H}$  NMR spectra of  $\text{P}_{\text{M}2\text{f}}$  revealed the unexpectedly splitting of the  $\text{H}_g$  signal. This phenomenon was hypothesized to be a consequence of the conformational equilibrium of acrylamides<sup>165</sup>, as depicted in Figure 4.5. As for PNIPAM, the acrylamide equilibrium usually

displays one broad averaged peak. However, splitting can be observed due to sterically hindrance or probably influence of the polymer backbone methyl group.

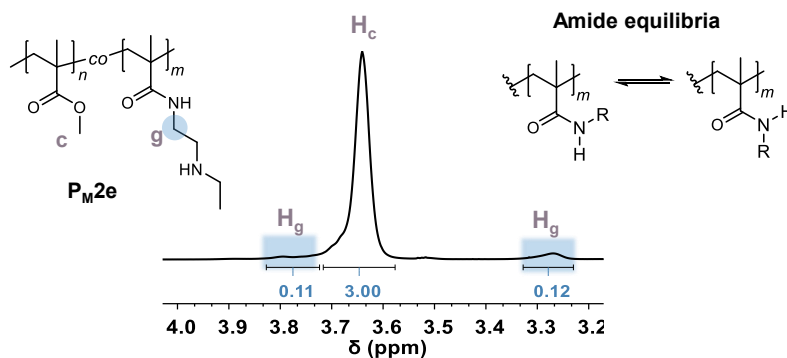


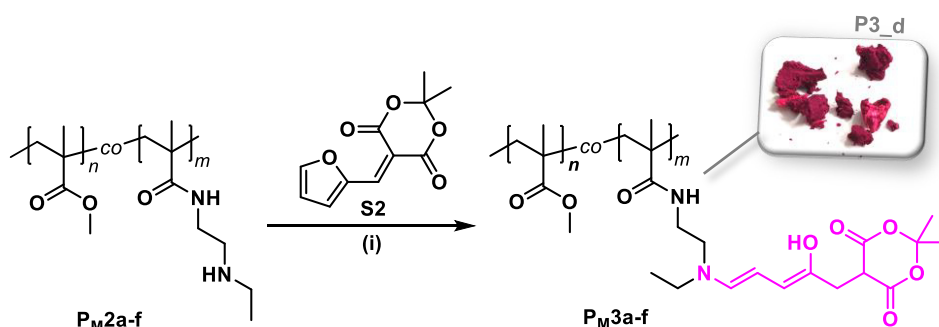
**Figure 4.5.**  $^1\text{H}$  NMR spectrum (selected region) of **P<sub>M2e</sub>** measured in acetone- $d_6$  for the amide content estimation and the methyl acrylamide equilibrium as presumed cause for the  $\text{H}_g$  signal splitting.

The **P<sub>M2</sub>** copolymer compositions were determined by  $^1\text{H}$  NMR signal integration as depicted in Figure 4.5. The algebraic sum of  $\text{H}_g$  was used as integral area  $A_{\text{amide}}$  and was inserted into Equation 4.2:

$$X_{\text{amine}} = \frac{\int \text{H}_g \cdot \frac{1}{2}}{\int \text{H}_g \cdot \frac{1}{2} + 1} \quad (4.2)$$

The factor one as the denominator resulted from three MMA methoxy protons multiplied by one third. Hence, Equation 4.2 leads to a 10.3% of acrylamide content in **P<sub>M2e</sub>**. Equivalently, all mol% fractions of  $X_{\text{amine}}$  of the **P<sub>M2</sub>** series were calculated and listed in Table 4.2. As expected, these confirmed adequately the p(MMA-*co*-PFPMA) amounts by exhibiting minor differences, that might arise from phase tolerances. The synthetic procedure involving the facile and selective post-polymerization modification of **P<sub>M1</sub>** through EEDA amidation presented a straightforward method for developing an initial library of substances for DASA binding in the subsequent step.

The second polymer analogous reaction was performed *via* ring opening addition of an activated furan precursor, as generally described by Helmy *et al.*<sup>69,130</sup> Noteworthy, they impressively demonstrated the selective formation of the colored open Stenhouse structure instead of the concomitant generation of the colorless cyclopentanone (Section 2.3.3) by using THF as reaction solvent. Accordingly, furylidene-Medrum'acid (**S2**) was selected to obtain the strongly pink colored p(MMA-EEDA-DASA) (**P<sub>M3</sub>** series) copolymers as illustrated in Scheme 4.4. The synthesis of **S2** was adopted from the literature.<sup>178</sup>



**Scheme 4.4.** Second post-polymerization modification process. Stenhouse adduct formation by ring opening addition of the fuylidene-Meldrum's acid precursor (S2). Reaction conditions (i): Dry THF, rt, 5 d.

An excess (4 eq.) of the furylidene precursor **S2** was added to the **P<sub>M</sub>2** series dissolved in dry THF under an argon atmosphere, respectively, and stirred at room temperature. Upon furan addition, the colorless solution turned immediately pink. The progress of the DASA formation was monitored by UV–vis measurements of the reaction solution (Figure 4.6a) to indicate complete conversion. For example, the successful conversion of **P<sub>M</sub>3d** was evident from the increase of the absorption band at  $\lambda = 540$  nm, which corresponded to green light. The majority of DASA formation progress was seen on the initial day (Figure 4.6b). Subsequently, the reaction exhibited a decreased rate, ultimately reaching a saturation point where there was no further increase in absorption values after 5.5 days, suggesting the conclusion of the conversion process. The purification process involved dialysis in dichloromethane for 5 days at room temperature, using a membrane with a MWCO of 6000 Da. Dichloromethane was used for its advantageous property of preventing the undesired switching behavior to the colorless cyclopentenone (Section 2.3.3).

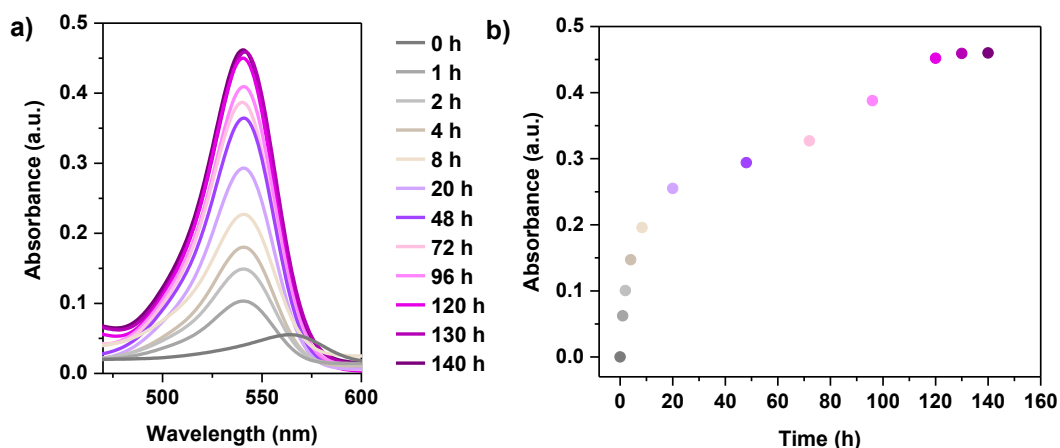


**Figure 4.6.** a) DASA formation monitoring *via* UV–vis absorption measurements. b) Absorption maxima change depended on time scale.

The pure product was analyzed by  $^1\text{H}$  NMR spectroscopy, UV-vis spectroscopy and FT-IR (ATR) spectroscopy.

The  $^1\text{H}$  NMR spectra comparison between  $\text{P}_M\text{2d}$  and  $\text{P}_M\text{3d}$  confirmed the successful attachment of DASA chromophores within the polymer side chains (Figure 4.7a). This was clearly denoted by the appearance of the characteristic conjugated double bond protons (pink dots) and the obvious appearance of the signal corresponding to  $\text{H}_e$  (11.4 ppm), belonging to the DASA hydroxyl group. Furthermore, the signals of  $\text{H}_b$  (3.46 ppm) and  $\text{H}_c/\text{H}_d$  (2.73 ppm) shifted down-field, due to the deshielding effect of the double bond protons (green dotted lines). The DASA moiety content was estimated from the  $^1\text{H}$  NMR spectrum by comparing the integral areas of the double bond protons and the methoxy proton  $\text{H}_c$ , as shown in the selected  $^1\text{H}$  NMR region in Figure 4.7b.

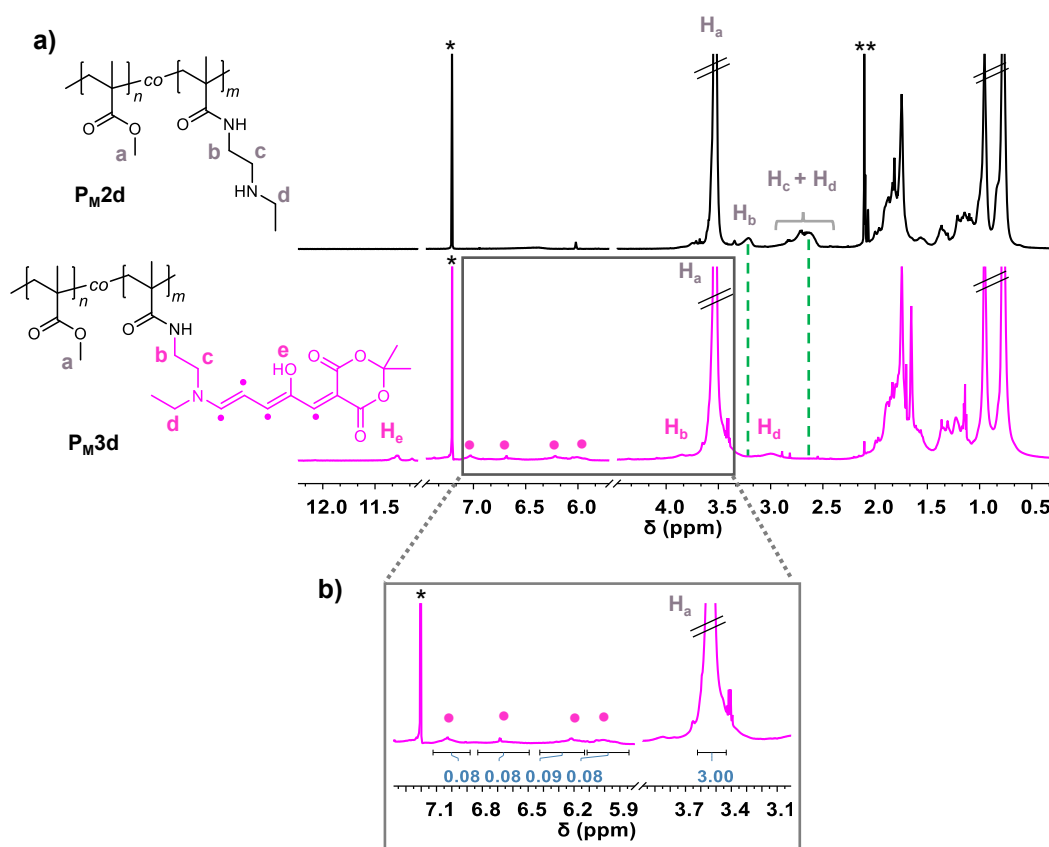


**Figure 4.7.**  $^1\text{H}$  NMR spectroscopy characterization of  $\text{P}_M\text{3d}$ . **a)** Comparison to sample  $\text{P}_M\text{2d}$  corroborated the shift of the peaks  $\text{H}_b/\text{H}_d$  and appearance of  $\text{H}_e$ . Due to overlapping,  $\text{H}_c$  is not visible (bottom). **b)** Selected NMR region of **a)**: Integral areas of the conjugated double bond systems in relation to  $\text{H}_a$ . \* $\text{CDCl}_3$  solvent signal \*\*solvent residue

Therefore, the double bound proton integral value  $H_{DB}$  of 0.08 was used in Equation 4.3.

$$X_{DASA} = \frac{\int H_{DB}}{\int H_{DB} + 1} \quad (4.3)$$

The DASA content calculation of sample **P<sub>M</sub>3d**, for instance, yielded a chromophore proportion of 7.4% (Table 4.2).

Following the explained general calculation, the amount of incorporated DASA for the **P<sub>M</sub>3** series was determined by integrating the associated <sup>1</sup>H NMR double bound protons and methoxy protons, respectively (Appendix A.1). The calculated values are summarized in Table 4.2 compared with the theoretical DASA amounts (based on MMA and **M1** weights) and the estimated amine linker contents. As a whole, **P<sub>M</sub>3a-d** samples were measured in CDCl<sub>3</sub> and exhibit lower calculated DASA values as compared to the determined amine linker. In contrast, **P<sub>M</sub>3e+f** samples were measured in deuterated dimethyl sulfoxide due to poor solubility and show slightly higher DASA values. Altogether, the double bond peaks are much lower in intensity as compared to the methoxy peak. Such an intense methoxy protons signal could affect the signal/noise ratio of the double bond peaks. This might be a suitable explanation for the divergence of 1% DASA content determined for **P<sub>M</sub>3a**. Interestingly, **P<sub>M</sub>3e** and **P<sub>M</sub>3f** displayed slightly higher  $X_{DASA}$  values as expected. This indicated a different influence of the solvents.

Besides <sup>1</sup>H NMR spectroscopy, the dye contents were also estimated *via* UV-vis absorption measurements. Due to the linear correlation between absorbance intensity and DASA content, a linear regression offered access to chromophoric content calculations. Therefore, a quantified stock solution was required. The homopolymeric **P1** sample was used for a treatment with EEDA and subsequently treated with Meldrum's acid furan precursor to synthesized 100 mol% DASA side chain groups. The obtained polymer was not soluble in conventionally used solvents. Moreover, full conversion to DASA homopolymer could not be confirmed, presumably caused by steric hindrance.

In order to address this issue, compound **S3** was synthesized, as described in the literature (Figure 4.8a).<sup>146</sup> To confirm its absorption maximum alignment with the **P<sub>M</sub>3** series, a comparative UV-vis absorption measurement was conducted in chloroform (Figure 4.8b). The copolymers exhibited an absorption maximum at  $\lambda_{max} = 542$  nm, whereas the **S3** maximum appears at  $\lambda_{max} = 540$  nm. Due to the minor variance, a concentration *vs.* absorbance plot of **S3** was targeted by measuring the UV-vis spectra of different sample concentrations (Figure 4.8c). The resulting curve maxima (left side) and the corresponding concentrations were plotted (right side) and a linear regression fit represent the dependency between the absorbance  $A$  and the concentration  $c_{S3}$  of **S3**

$$A = 0.0083 + 0.11956 \cdot c_{S3} \quad (4.4)$$

when the sample was dissolved in chloroform. Table A.1 displays the concentrations of the samples and their matching absorbance values.

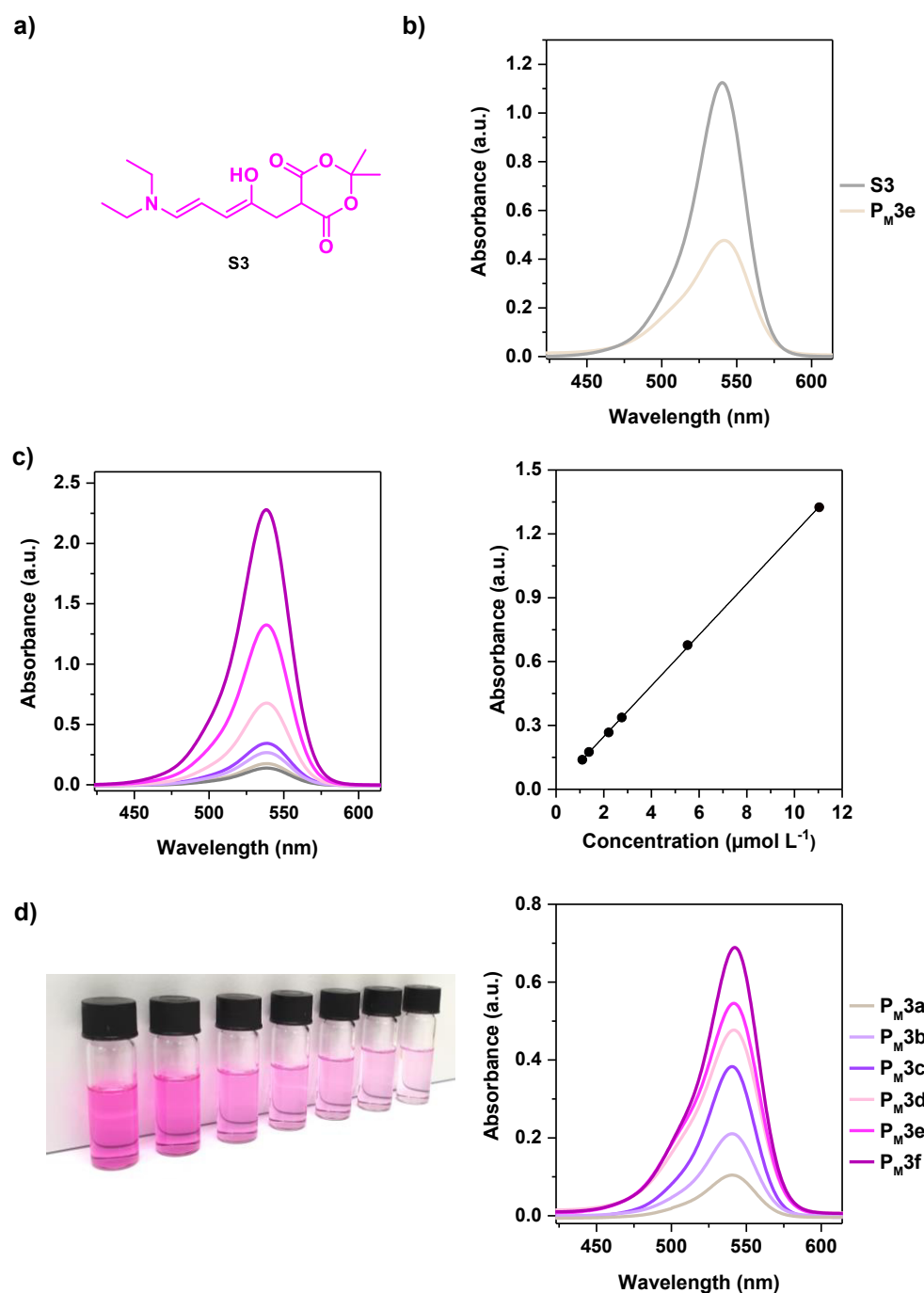


**Figure 4.8.** UV-vis calibration board. a) Structure of **S3**. b) Absorbance maxima comparison of **S3** and **P<sub>M</sub>3d** ( $\lambda = 540$  nm), measured in chloroform. c) Measured UV-vis spectra of calibration series (left) and resulting linear regression fit with  $R^2 = 0.999$ . d) Calibration series of **S3** from the concentration  $c = 1.37$  mmol mL<sup>-1</sup> to 11.0 mmol mL<sup>-1</sup> dissolved in dichloromethane (left) and corresponding UV-vis absorbance measurements (right).

It was further assumed that the intensities of absorbance from **S3** and the DASA content in the **P<sub>M3</sub>** series were the same. As a result, the content of  $X_{\text{DASA}}$  in the **P<sub>M3</sub>** series was determined by calculating the molar concentration of  $c_{\text{DASA}}$  and MMA  $c_{\text{MMA}}$  with

$$X_{\text{DASA}} = \frac{c_{\text{DASA}}}{c_{\text{DASA}} + c_{\text{MMA}}} \quad (4.5)$$

for the corresponding **P<sub>M3</sub>** samples. Another assumption used was the relationship between the concentration of MMA  $c_{\text{MMA}}$  and the mass concentration of  $c_{\text{PM3}}$ , as well as their respective molar mass, as demonstrated in Equation 4.6:

$$c_{\text{PM3}} = M_{\text{MMA}} \cdot c_{\text{MMA}} + M_{\text{DASA}} \cdot c_{\text{DASA}} \quad (4.6)$$

By insertion of Equation 4.4 and 4.6 in 4.5, the DASA content  $X_{\text{DASA}}$  was calculated using Equation 4.7

$$X_{\text{DASA}} = \frac{\frac{A - 0.0083}{0.11956}}{\frac{A - 0.0083}{0.11956} + \frac{c_{\text{PM3}} - M_{\text{DASA}} \cdot \frac{A - 0.0083}{0.11956}}{M_{\text{MMA}}}} \quad (4.7)$$

and the following term was summarized to the concentration  $c_{\text{DASA}}$

$$c_{\text{DASA}} = \frac{A - 0.0083}{0.11956} \quad (4.8)$$

which led to a simplification of Equation 4.8 to

$$X_{\text{DASA}} = \frac{c_{\text{DASA}}}{c_{\text{DASA}} + \frac{c_{\text{PM3}} - M_{\text{DASA}} \cdot c_{\text{DASA}}}{M_{\text{MMA}}}} \quad (4.9)$$

Finally, Equation 4.9 was used to calculate the DASA mol% fractions  $X_{\text{DASA}}$  in the **P<sub>M3</sub>** series from the UV–vis spectra in Figure 4.8d. All molar masses and concentrations, as the calculated  $c_{\text{DASA}}$  values, are listed in Table A.2. The obtained  $X_{\text{DASA}}$  values derived from the corresponding UV–vis spectra of the dissolved **P<sub>M3</sub>** sample are summarized in Table 4.2. In comparison with the calculated **P<sub>M2</sub>** methacrylamide contents, the **P<sub>M3</sub>** values were lower. One reason for the variance might be the usage of **S3** and the resulting low difference in molecular weight.

Overall, the ring opening mechanism of Meldrum's acid furan derivatives and secondary amines is highly favorable, due to its easy handle conversion monitoring. Moreover, the reaction occurs selective and almost quantitative, which makes it particularly suitable for such post-polymerization modifications under mild reaction conditions. Minor divergences in the DASA content determination *via*  $^1\text{H}$  NMR might be caused by phase corrections. Nevertheless, our synthetic protocol works efficiently and yielded an MMA-DASA-copolymer series from almost 1% to 12% chromophoric amount.

#### 4.1.2 Temperature and light responsiveness of PMMA-DASA conjugates

Following the successful synthesis of the PMMA-DASA conjugate series, a subsequent examination of its light-responsive properties was carried out. Unlike, *e.g.*, azobenzene, Stenhouse adducts of low molar masses show reduced stability when dissolved in polar protic solvents. The inability to control switching behavior was a barrier to achieving light-induced UCST changes. Therefore, it was necessary to evaluate the **P<sub>M</sub>3** samples' resistance to water and combinations of ethanol in an aqueous solution. An initial estimation of the **P<sub>M</sub>3** stability in various solvents was made by conducting solubility tests and comparing the results with sample **S3**. Due to the resulting red colored alcoholic solution, **S3** was indicated as a red dye. When dissolved in water, however, the solution immediately changed to yellow after a few seconds without the influence of light (Figure 4.9). The rapid change from the colored hydrophobic triene structure to the colorless zwitterionic state in water generated this optical phenomenon since it was energetically more favorable. The macroscopic observation of the DASA-bearing copolymer **P<sub>M</sub>3d** yielded acceptable findings. The copolymer exhibited delayed dissolving behavior in water, and interestingly, the solution turned red instead of yellow. This indicated the significant impact of the polymer environment on the DASA nature. As a result, the polymer matrix provided stability to the colored structure.

A direct comparison between **S3** and **P<sub>M</sub>3d** in aqueous ethanol revealed the PMMA matrix to be the predominant part of the solution characteristics. The non-polymeric **S2** sample dissolved rapidly. However, the PMMA matrix in **P<sub>M</sub>3d** reduced the dissolution behavior. Furthermore, a color dependence on the sample concentration, *i.e.*, a pink solution turning red at higher concentrations, was observed.

Besides water stability, the light responsiveness was a supplementary condition for successful UCST tuning studies. The UV-vis absorption of the sample **P<sub>M</sub>3b** dissolved in water ( $2\text{ mg mL}^{-1}$ ,  $30\text{ }^\circ\text{C}$ ) before and after irradiation was compared (Figure 4.10, red curves). The strong absorbance peak at 520 nm corresponding to the  $\pi$ - $\pi^*$  transition, decreased apparently after 90 min of irradiation (green arrow) due to the bond breaking of the conjugated DASA structure. On the opposite, the absorbance peak corresponding to the activated dicarbonyl of the cyclopentenone (red structure) increased.

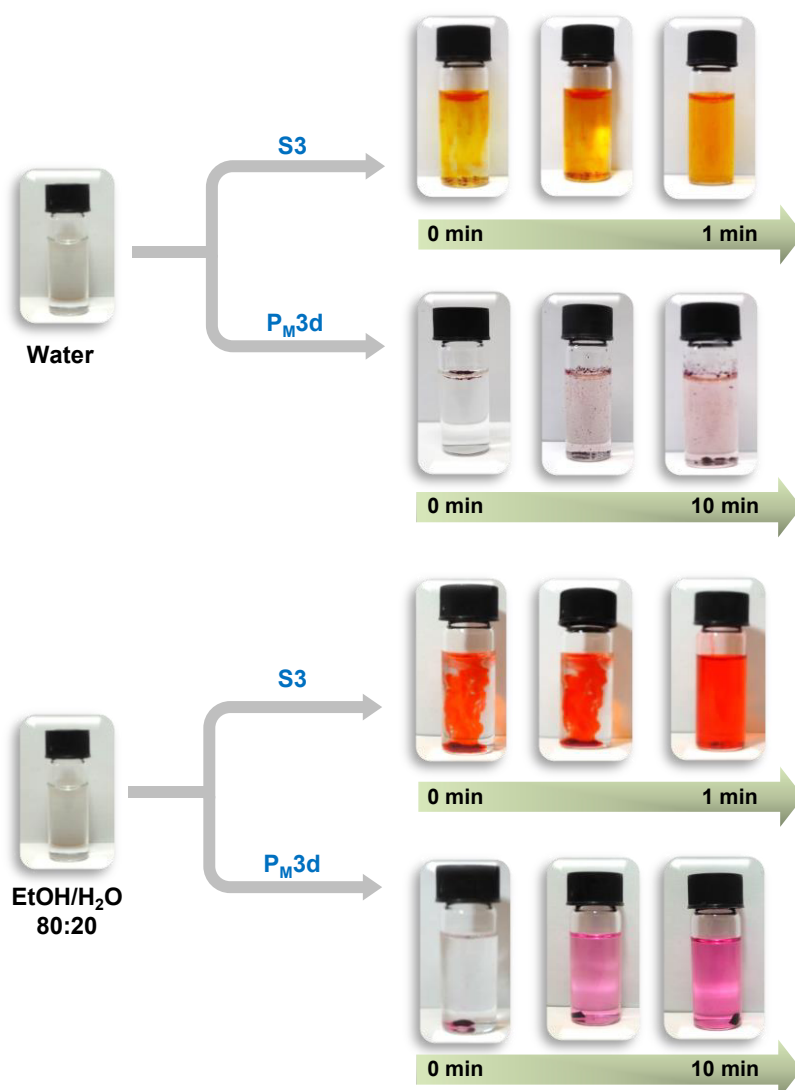


**Figure 4.9.** Solubility investigations of S3 and P<sub>M</sub>3d in water and an ethanol/water mixture (80:20), respectively.

The process was accompanied by the optical loss of the red color intensity and revealed Stenhouse dyes as negative photoswitching chromophores. It shall be noted, absorption in the region of green light led to complementary visual red polymers. While the reversible transformation from the colorless state back to the triene did not occur in polar protic solvents (for 1<sup>st</sup> generation DASA), thermal conversion proceeds in halogenated environment. Thus, 30 min heating at 30 °C of P<sub>M</sub>3b dissolved in DCM (2 mg mL<sup>-1</sup>) led to a higher color intensity (pink curves) at 545 nm and 360 nm (blue arrows) as compared to the absorption behavior in water. Notably, the acceptor of the triene exhibited absorption as well, which was shifted to the UV region at approximately 220 nm as a consequence of solvent influence. The thermal conversion yielded the complete disappearance of the bond at 360 nm. Furthermore, the solvent effect resulted in a bathochromical shift of 25 nm in the visible region from red to pink color.

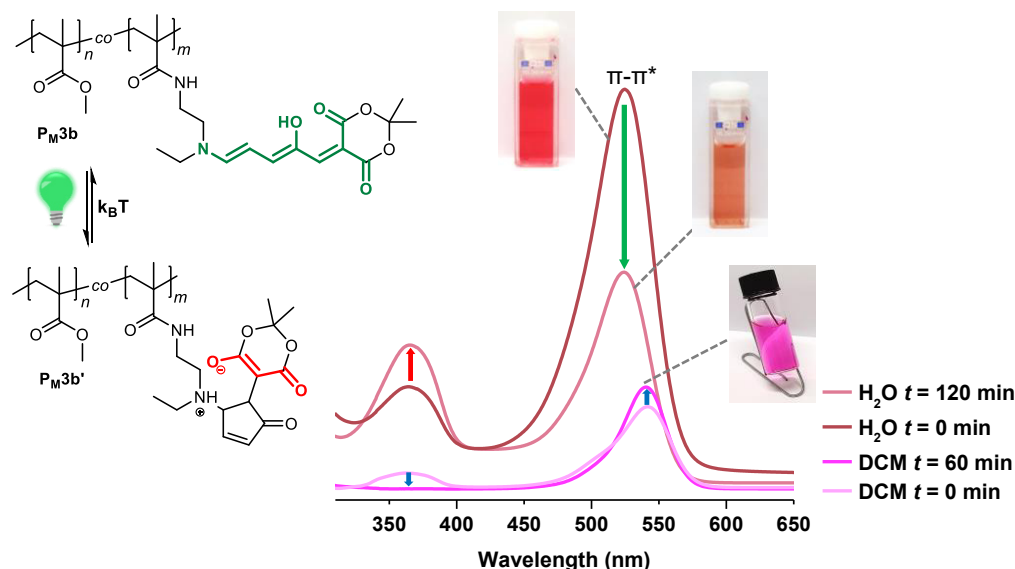


**Figure 4.10.** Absorption efforts of sample  $P_{M3b}$  in water (red lines) before and after irradiation with green light and in DCM (pink lines) before and after heating. In water: The characteristic triene absorption bond decrease after 90 min of light irradiation (green arrow), while the bond corresponding to the 1,3-dicarbonyl structure increase (red arrow). In DCM: Heating for 30 min at 35 °C produces the opposite effect.

As a point of reference, Helmy *et al.* introduced the complete conversion of the barbituric acid analogous Stenhouse substance over a course of 35 min in methanol by monitoring the characteristic triene absorption disappearance.<sup>130</sup> In comparison, the colored DASA proportion in sample  $P_{M3b}$  was reduced by half within 120 min and significantly differed from the non-polymeric sample, which confirmed the efficient regulation of the photoswitching effect by using PMMA as polymer matrix. The effect was probably caused by hydrophobic interactions of PMMA and sterically hindrance of the cyclopentenone formation due to the polymer backbone. Overall, the UV-vis results give access to successful UCST investigations in the next step, since increased stability towards aqueous ethanol has been proven.

There has been significant interest in studying alcohol-water mixtures for a number of years, particularly due to their relevance in biological processes such as protein extraction.<sup>179</sup> Within the liquid phase, the structures have the capability to form complex connectivities of hydrogen bonds, which are referred to as clusters.<sup>180</sup> The characteristics of these assemblies vary from those of the individual solvents and exhibit an immense dependence on the volume ratio. Consequently, alcohol-water solutions have garnered interest in this field of UCST research.

To broaden the scope of this work, the investigations conducted by Zhang *et al.*<sup>174</sup> were adopted and involved in the utilization of a range of ethanol/water mixtures for the  $P_{M3}$  samples. Typically, the ability of a polymer to dissolve is influenced by the development of

hydrogen bonds between its structure and the binary solvent. This competes with the process of solvation, which occurs when the polarity of the solvent changes due to heating. Hence, Zhang and colleagues convincingly illustrated the correlation between the composition of the solvent (ranging from 60 to 95 vol% ethanol) and the associated UCST values during both heating ( $T_{CP-H}$ ) and cooling ( $T_{CP-C}$ ), commonly referred to as hysteresis.<sup>174</sup>

To proceed further into this investigation, the cloud points  $T_{CP-C}$  of the synthesized PMMA sample were initially identified (Figure 4.11). The UCST values were determined by turbidimetry, which involved monitoring the transmittance as the temperature was changed.

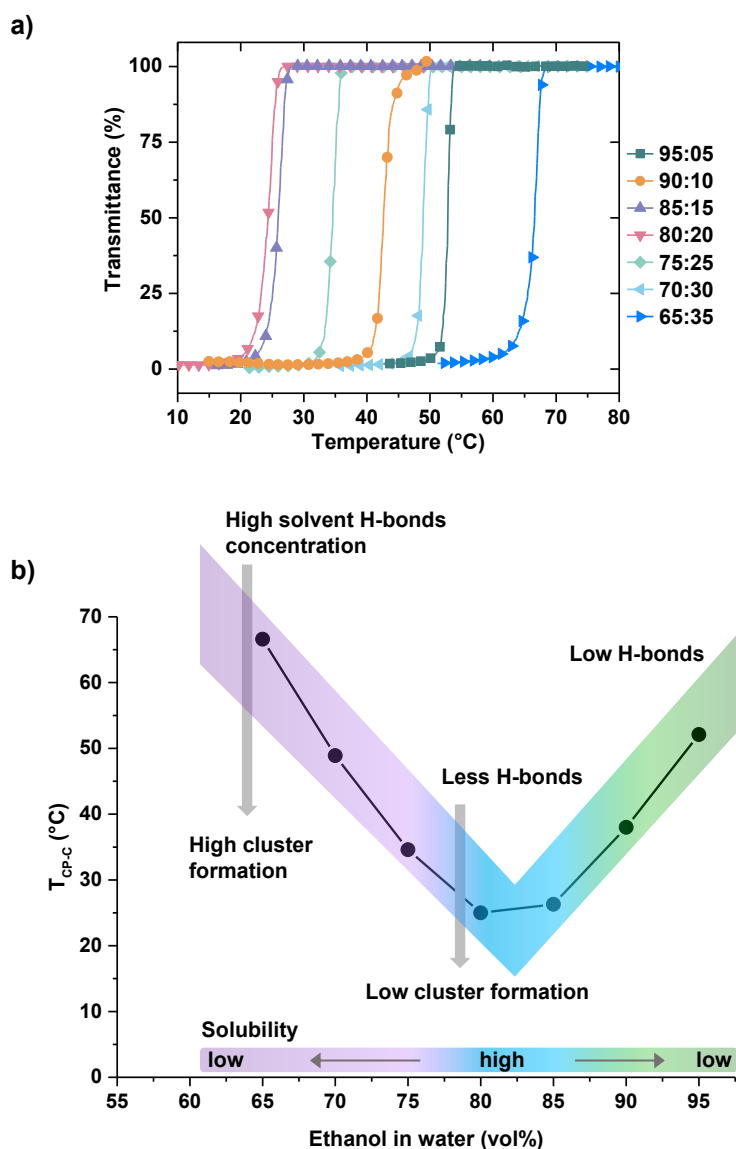


**Figure 4.11.** PMMA UCST investigation. **a)** Transmittance vs. temperature plot of PMMA in various ethanol-water mixtures polymer solution concentration  $4 \text{ mg mL}^{-1}$ ; PMMA ( $M_n = 4.79 \cdot 10^4 \text{ g mol}^{-1}$ ). **b)** Resulting cloud points  $T_{CP}$  vs. ethanol content plot and dependency of water cluster formation.

A laser beam with a wavelength of 700 nm was transmitted through a silica cuvette located in the sample cell of a spectrometer. The sample preparation was done by heating (under exclusion of light) to a suitable temperature in order to obtain clear solutions. Afterwards the transmission was recorded continuously (starting from 100%) while the temperature was lowered. Due to aggregation of the polymer, each sample exhibited a transition from the one-phase solution to an opaque two-phase system upon cooling. The resulting UCSTs were defined as the temperature belonging to the 50% transmission value. The curves obtained in this way are represented in Figure 4.11a, from which  $T_{CP-C}$  are then determined and plotted (black dots) as a function of the ethanol vol% as shown in Figure 4.11b.

In comparison to Zhang *et al.*, the phase separation temperatures of PMMA described in this study were slightly higher, probably because of the larger molar mass. However, the phase transition values exhibited similar characteristics and demonstrated identical binary solution behavior within the specified range. The solubility and transition, which were dependent on the water content, can be described by referring to Figure 4.11b. The aforementioned cluster formation of the solvent molecules through hydrogen bonds was related to the content of water, whereby cluster formation was preferred by increasing water availability. However, the polymer solvation through hydration shells suffered from a low content of single state water molecules. Since the concentration of clusters lowered with decreased water presence, more single state water molecules (not clustered) formed hydrated shells and the polymer solubility within the range of 80 vol% ethanol increased significantly. When taking into account the presence of a high concentration of ethanol, the number of hydrogen bonds was significantly reduced, and the solubility behavior depended on the solvent's ability to dissolve substances.

The cloud points of the **P<sub>M</sub>3** samples were determined using the same method. As expected, the series exhibited a hysteresis pattern similar to that of sample **P<sub>M</sub>3d**, which was dissolved in 95-vol% ethanol, as illustrated (Figure 4.12a). While the cloud point  $T_{CP-C}$  was reached at 49.5 °C, the clearance point  $T_{CP-H}$  upon heating was approximately 5 °C lower. However, by increasing the amount of water, the hydrated coil-to-globule transition  $T_{CP-C}$  occurred at lower temperatures compared to  $T_{CP-H}$ . This effect resulted from the capability of water molecules to induce hydrogen bonding, including the ester and amid moieties of the polymer side chains which energetically favored the hydrated polymer state. In contrast, the hydration in ethanol-water composition including low water contents was overlaid by solvation processes as a consequence of change in the solvent polarity upon heating and resulted in lower  $T_{CP-H}$  than  $T_{CP-C}$  values. These observations were in good agreement with the results of Zhang and coworkers for PMMA containing several amid side groups (max. 6 mol%). In contrast, this study further focused on the comparison of the cooling curves instead of investigations into hysteresis. Besides the solvent mixture, the polymer concentration had an impact on the cloud points as well. The addition of 1 mg mL<sup>-1</sup> of polymer to a sample containing 4 mg mL<sup>-1</sup> of **P<sub>M</sub>3** dissolved in 80 vol% ethanol resulted in an increase in the polymer phase transition temperature of about 6 °C.

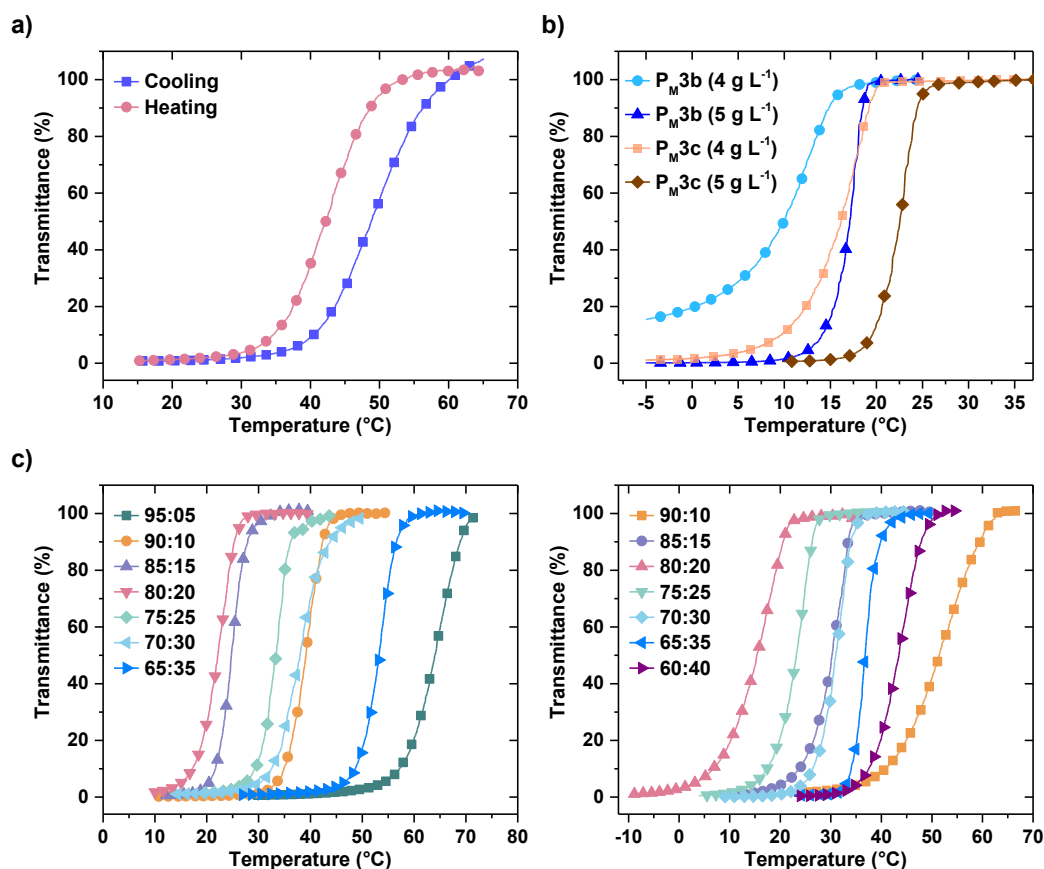


**Figure 4.12.** a) Hysteresis pattern of  $P_{M3d}$ . b) Influence of sample concentration on the UCST behavior. c) Turbidity curves of  $P_{M3b}$  (left) and  $P_{M3d}$  (right) measured in different ethanol-water solvent mixtures ranging from 95 vol% ethanol to 65 vol%. Legend: *e.g.*, 95:05 (ethanol:water (v.v)) denote 95 vol% ethanol.

For  $P_{M3b}$ , when 4 mg mL<sup>-1</sup> of polymer was dissolved in the same solvent mixture, a curve with a minimum of 15% transmittance was obtained (Figure 4.12b). The concentration comparison demonstrated that a concentration of 5 mg mL<sup>-1</sup> of  $P_{M3}$  polymer was necessary to achieve precise tuning of the UCST. The curves obtained from the transmittance monitoring prior to exposure to visible light exhibited a distinct and sharp change in phase, which was highly influenced by the composition of the solvent. As an example, the transmission *vs.* temperature curves of the samples  $P_{M3b}$  and  $P_{M3d}$  are illustrated in Figure 4.12c. By varying the ethanol content around 15 vol% higher, the  $T_{CP-C}$  of  $P_{M3b}$  increased impressively from 21 °C to 44 °C. An analysis of the cloud points of  $P_{M3b}$  and  $P_{M3d}$  revealed a correlation with the quantity of DASA chromophore, particularly noticeable in the curves related to 80 vol% ethanol. While the lowest phase transition point for  $P_{M3b}$  was indicated as 20 °C, a slight increase of the DASA content ( $P_{M3d}$ ) enabled the controllable addressing to a minimum UCST value of 14 °C. Significantly, the determination of  $T_{CP-C}$  of  $P_{M3d}$  dissolved in a 95-vol% solution was not possible due to incomplete solubility before the solvent mixture reached its boiling point.

The turbidity curves of the  $P_M3$  were applied to determine the associated  $T_{CP-C}$  values, which are presented in Figure 4.13 together with the corresponding solvent composition. A review revealed slight variation in the cloud points of PMMA and the polymer-conjugates with 2 and 4 mol% DASA side chain groups.

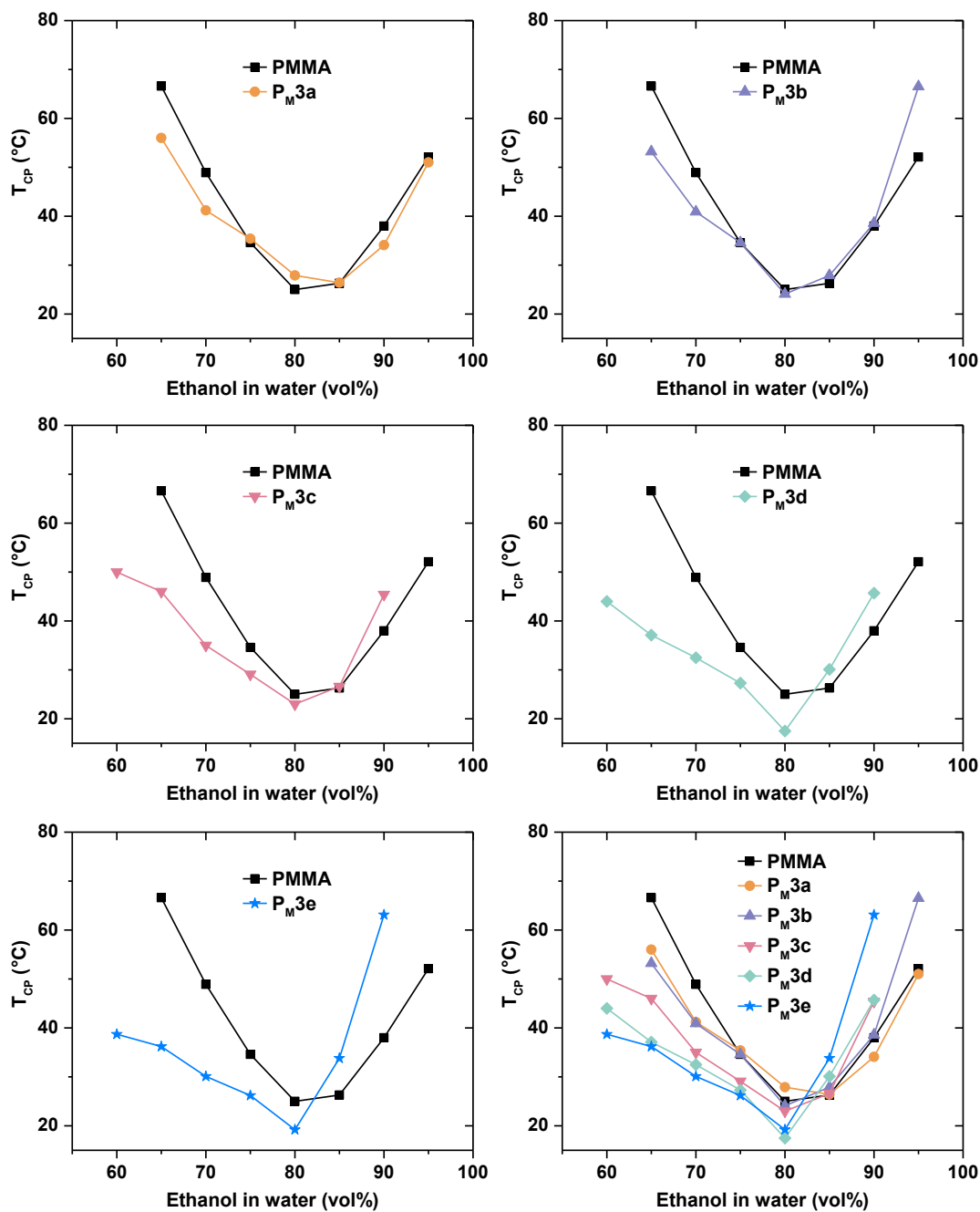


**Figure 4.13.** Determined cloud points  $T_{CP}$  of the samples  $P_{M3a}$ - $P_{M3e}$  in comparison to PMMA using different ethanol-water mixtures.

However, the impact of the chromophore became increasingly evident as the ratio increased, as demonstrated by the contrasting behavior of **P<sub>M</sub>3c**, **P<sub>M</sub>3d** and **P<sub>M</sub>3e** compared to PMMA. In addition, all samples except **P<sub>M</sub>3a** exhibited the lowest phase separation temperatures when dissolved in a solution containing 80 vol% ethanol. This suggested that the solvent composition with the highest solubility was achieved by using this ethanol concentration.

The cloud point gap between PMMA and the polymer conjugates noticeably increased, particularly in the ethanol range of 60 to 80 vol%, depending on the concentration of DASA. On the one hand, a suitable explanation was the additional formation of hydrogen bonds between the water molecules and the amide, as well as the carbonyl-functionalities within the Stenhouse structure. By enhancing the hydration shell, lower  $T_{CP}$  values were observed. On the other hand, the assumption was that ionic interactions due to light background switched from the neutral DASA state to the zwitterionic structure without light irradiation. This assumption was consistent with the observation of the **S3** switching behavior in the dark without light insertion. Conversely, ethanol mixtures with 5-15 vol% water result in less solubility of the polymer conjugates compared to PMMA.

By simultaneous consideration of the phase transition temperature measured in the range of 60 to 80 vol% ethanol and also 85 to 95 vol%, the correlations became more evident (Figure 4.14). Increasing water concentrations resulted in an almost linear decrease in cloud points as the DASA content increased (red dots, left). In contrast, reducing the number of water molecules led to an increase in UCST values relative to PMMA (blue dots, right). For instance, measurements of PMMA and **P<sub>M</sub>3e** in 90 vol% ethanol resulted in  $T_{CP}$ , which exhibited a value distance of 25 °C. In addition, although the turbidity curve of PMMA in 95 vol% ethanol was examined, the **P<sub>M</sub>3c-e** copolymers did not dissolve below the boiling point of the solvent mixture. The assumption was that ionic interactions, evoked from the unaffected cyclopentenone formation, interfered with the solvation at high ethanol content due to ionic polarity.

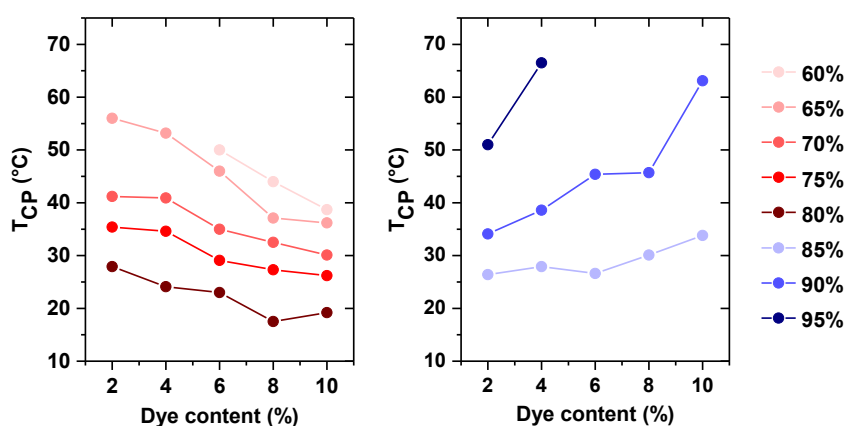


**Figure 4.14.** Cloud points  $T_{CP}$  of **P<sub>M</sub>3a-e** in correlation to the ethanol content in the ethanol-water mixtures.

In conclusion, higher concentrations of DASA side chain groups had a significant impact on the UCST prior to light irradiation. Compared to unmodified PMMA, the phase transitions occurred at lower temperatures when using ethanol volume concentrations ranging from 60 to 80%. However, higher proportions of ethanol increased the polymer-conjugates  $T_{CP-C}$  over that of PMMA. The cloud point measurements were plotted to establish a correlation between the ethanol volume percentage and dye concentration. This resulted in the creation of the area diagram shown in Figure 4.15. Each point of the plot represents a  $T_{CP}$  value, depending on the corresponding dye and ethanol content.

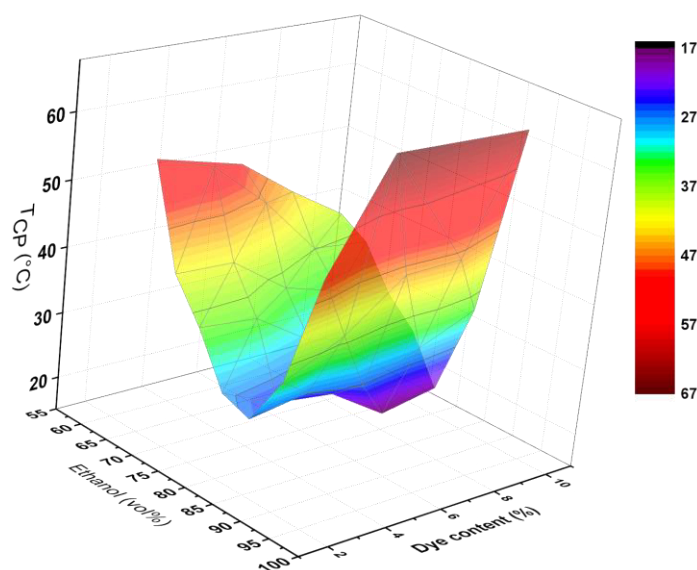


**Figure 4.15.** Area plot type of  $T_{CP}$  in correlation to dye content (2% to 10% dye content, **P<sub>M3a-e</sub>**) and ethanol vol% in ethanol-water mixture.

Hence, the incorporation of the DASA side group moiety in PMMA provides a very broad spectrum for precisely determining cloud points, encompassing temperatures ranging from 17.4 °C to 66.6 °C. A direct and straightforward method for regulating the UCST using visible light exposure has been successfully developed, enabling a wide range of potential uses. The cloud points of several PMMA-DASA-polymer conjugates dissolved in ethanol-water mixtures were further adjusted using the light-induced isomerization of the chromophore unit.

Therefore, each sample was dissolved by heating the solution over the corresponding UCST. As illustrated in the schematic overview (Figure 4.16), this temperature is denoted as  $T$ . The corresponding cloud points were measured by cooling the sample solution under the UCST, which is denoted as  $T_1$ . After reheating above  $T$  and irradiation for 30 min with green light, the remeasured cloud point  $T_2$  exhibited lower values as compared to  $T_1$  (before irradiation). The irradiation process was repeated to yield cloud point  $T_3$ , which was even lower than  $T_2$  and  $T_1$ . The observed phenomenon can be attributed to a substantial shift in polarity of the Stenhouse adduct, switching from an unpolar to a polar state. This change ultimately led to an increase in solubility.

Remarkably, the macroscopic observation of negative photochromism revealed a decrease in color intensity over time. The UCST study was conducted in accordance with the following procedure: Each **P<sub>M</sub>3** sample was heated in a number of ethanol-water mixtures ( $5 \text{ mg mL}^{-1}$ ) until complete dis-solution was seen. Following the turbidity measurement prior to irradiation ( $t = 0$ ), each sample was subjected to visible light ( $\lambda = 520 \text{ nm}$ , green) for a duration of 120 min, during which opacity observations were taken at 30-minute intervals by tracking transmittance. All irradiation processes were performed at the required temperature for full dissolution of the respective sample.

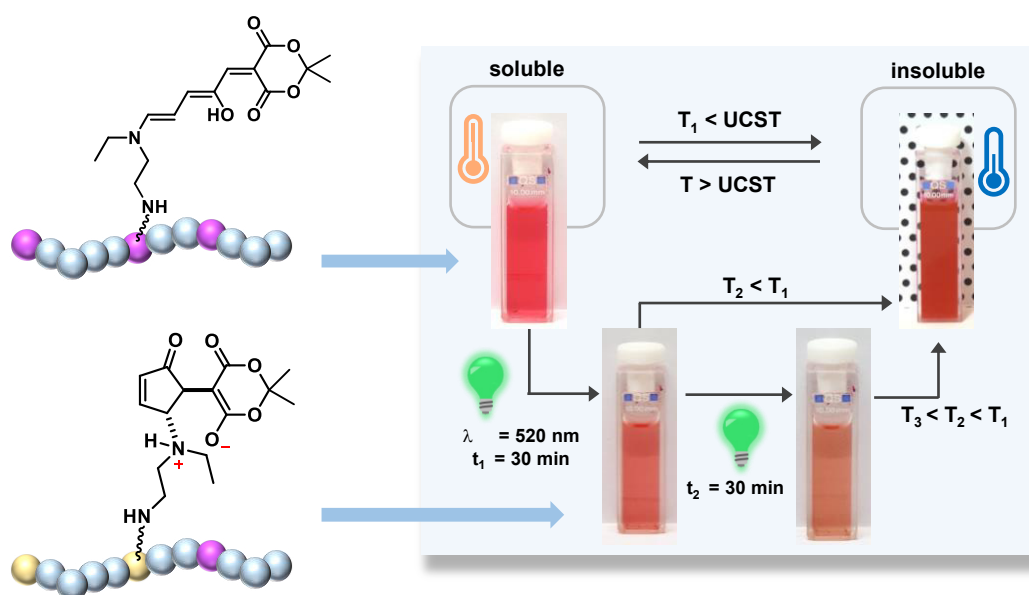


**Figure 4.16.** Schematic overview of the visible light ( $\lambda = 520 \text{ nm}$ ) induced upper critical solution temperature shift of PMMA-DASA-conjugates solved in ethanol-water solutions ( $5 \text{ mg mL}^{-1}$ ). The structural property changes are caused by the photoswitching process of the chromophoric unit. The temperatures are specified as follows:  $T$ : Temperature over UCST, which means the copolymer sample is fully dissolved.  $T_1$ : Cloud point before sample irradiation with visible light.  $T_2$ : Cloud point after sample irradiation for 30 min.  $T_3$ : Cloud point after sample irradiation for further 30 min.

Several turbidity curves are plotted in Figure 4.17, as examples. Due to enhanced polarity, each curve resulting from polymer solutions following light exposure ( $t_1 = 30$ ,  $t_2 = 60$ ,  $t_3 = 90$ , and  $t_4 = 120 \text{ min}$ ) displayed a downward shift in temperature relative to the matching initial polymer solution. It was obvious that the gaps between the UCST curves increased as the DASA side chain content (**P<sub>M</sub>3a-d**) expanded, indicating a positive UCST tuning. In some cases, the transmittance curves do not end at  $T = 0\%$ , especially in those measured after 120 min irradiation time. Besides, these curves became even broader in comparison to  $t = 0 \text{ min}$  due to increased polarity, leading to a deviating precipitation behavior.

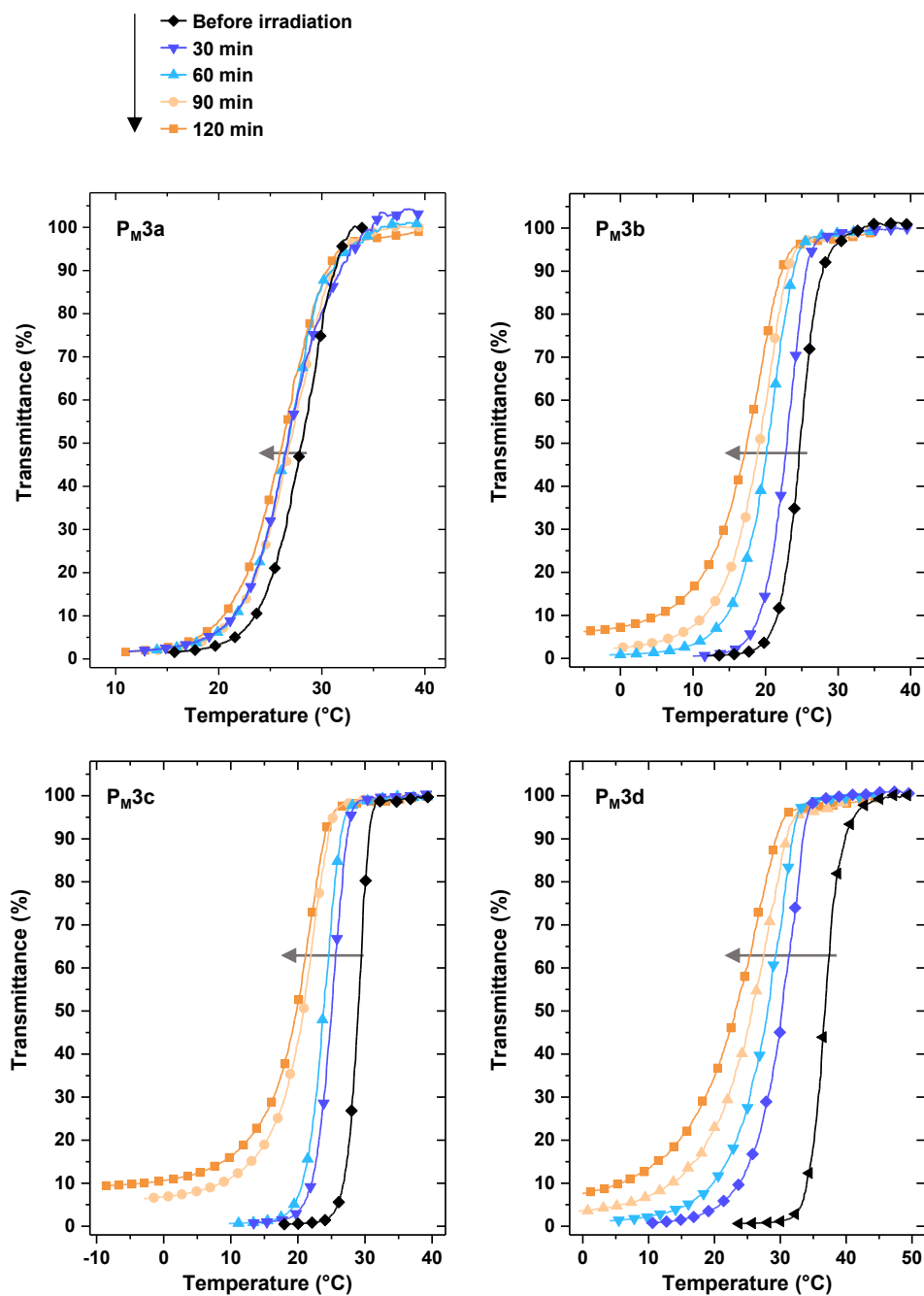


**Figure 4.17.** Examples of turbidity curves of the P<sub>M</sub>3 series. Each sample were performed with a concentration of 5 mg mL<sup>-1</sup> and a heating rate of 1 °C min utilizing a quartz cuvette. The transmission was detected using a light beam of  $\lambda = 700$  nm. Solvents: P<sub>M</sub>3a (ethanol:water, 80:20 v/v); P<sub>M</sub>3b (ethanol:water, 85:15 v/v); P<sub>M</sub>3c (ethanol:water, 75:25 v/v); P<sub>M</sub>3d (ethanol:water, 65:35 v/v);

Based on the turbidity curves, all cloud points belonging to P<sub>M</sub>3 were calculated as  $T = 50\%$  transmittance value and summarized in Table 4.3.

**Table 4.3.** Determined UCST for the **P<sub>M</sub>3** series values before and after light induces DASA photoswitching in dependency of the ethanol-water ratio.

Sample	Ethanol content (vol%)	UCST before irradiation <sup>2</sup> (°C)	UCST after irradiation <sup>2,3</sup> (°C)	$\Delta$ UCST (°C)
<b>P<sub>M</sub>3a</b> (1.0 mol% DASA) <sup>1</sup>	95	50.4	47.8	2.6
	90	34.1	30.8	3.3
	85	26.4	24.2	2.2
	80	28.1	25.9	2.2
	75	36.8	31.5	5.3
	70	41.2	35.9	5.3
	65	56.4	53.6	2.8
	60	—	—	—
<b>P<sub>M</sub>3b</b> (3.8 mol% DASA) <sup>1</sup>	95	66.5	60.8	5.7
	90	38.6	32.5	6.1
	85	27.9	19.1	8.8
	80	24.1	17.9	6.2
	75	34.6	28.1	6.5
	70	41.0	32.8	8.2
	65	53.2	45.7	7.5
	60	—	—	—
<b>P<sub>M</sub>3c</b> (5.7 mol% DASA) <sup>1</sup>	95	61.3	56.1	5.1
	90	45.4	40.3	5.1
	85	26.6	17.8	8.8
	80	23.9	9.7	14.2
	75	29.1	19.8	9.3
	70	38.8	29.9	9.2
	65	50.2	41.6	8.7
	60	—	—	—
<b>P<sub>M</sub>3d</b> (7.4 mol% DASA) <sup>1</sup>	95	—	—	—
	90	54.2	42.1	12.1
	85	30.1	17.5	12.6
	80	21.1	9.1	12.0
	75	28.3	11.5	16.8
	70	34.3	21.6	12.6
	65	36.8	23.2	13.6
	60	43.5	24.2	19.3
<b>P<sub>M</sub>3e</b> (10.7 mol% DASA) <sup>1</sup>	95	—	—	—
	90	63.2	41.8	21.4
	85	33.8	23.4	10.4
	80	19.2	6.3	12.8

Sample	Ethanol content (vol%)	UCST before irradiation <sup>2</sup> (°C)	UCST after irradiation <sup>2,3</sup> (°C)	$\Delta$ UCST (°C)
	75	26.2	5.5	20.7
	70	30.1	11.2	18.9
	65	36.2	15.9	20.3
	60	38.0	29.7	8.3

<sup>1</sup>DASA content calculated by <sup>1</sup>H NMR spectroscopy as listed in Table 4.2

<sup>2</sup>Measured by turbidimetry

<sup>3</sup>P<sub>M3a</sub>, P<sub>M3b</sub>, P<sub>M3c</sub> and P<sub>M3d</sub> UCST values after 120 min irradiation in total, for P<sub>M3e</sub>: After 90 min of irradiation.

The observed UCST shifts demonstrated the complete spectrum of the impact of the DASA concentration and the ethanol-water mixture. Remarkably, the addition of a modest amount (1 mol%) of DASA (**P<sub>M3a</sub>**) resulted in a significant increase in UCST by 5.3 °C when 75 vol% ethanol was used. Typically, the experiments conducted in 70-80 vol% ethanol had the greatest  $\Delta$ UCST values, except for **P<sub>M3d</sub>**, which showed a preference for 85 vol% ethanol. The finding was consistent with the previously demonstrated correlation between the composition of aqueous alcohol and the presence of individual water molecules that are not part of a cluster. It was assumed that mixtures with low cluster concentrations would energetically promote the light-induced switching process by enhancing the solvation of the cyclopentenone state. Interestingly, sample **P<sub>M3e</sub>** deviated from this consideration by additionally achieving high  $\Delta$ UCSTs when 90 and 65 vol% ethanol are utilized. A suitable explanation was the facilitated bond breaking of hydrogen-hydrogen and ethanol-ethanol interactions by the zwitterionic Stenhouse structure. Furthermore, in contrast to sample **P<sub>M3d</sub>** where a 60 vol% ethanol portion generated an almost 20 °C difference between prior and after irradiation, while **P<sub>M3e</sub>** exhibited a significantly lower value of 8.3 °C.

It was plausible to assume that non-light-induced switching processes occurred immediately following the dissolution of **P<sub>M3e</sub>**, with a reduced probability of polarity change through photoswitching. In order to enhance clarity, all cloud points were graphed with their respective ethanol-water compositions (Figure 4.18). Among them, **P<sub>M3e</sub>** at  $t_4 = 120$  min was not calculated due to an extremely high solubility with more than 40% transmission at a temperature of 0 °C in each solvent mixture. The cloud points vs. ethanol-water composition plots clearly identified **P<sub>M3e</sub>** to yield the highest temperature shift.

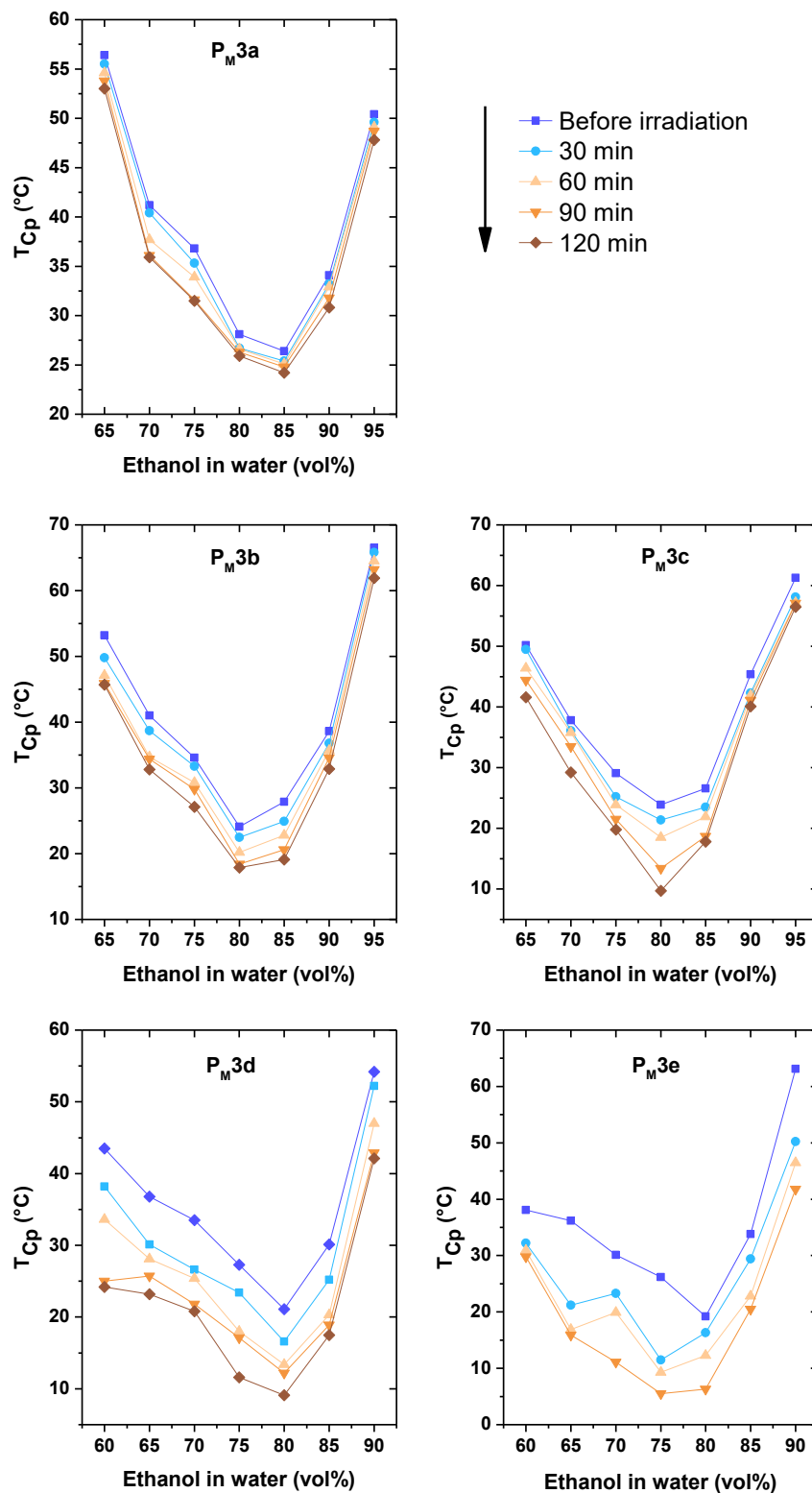
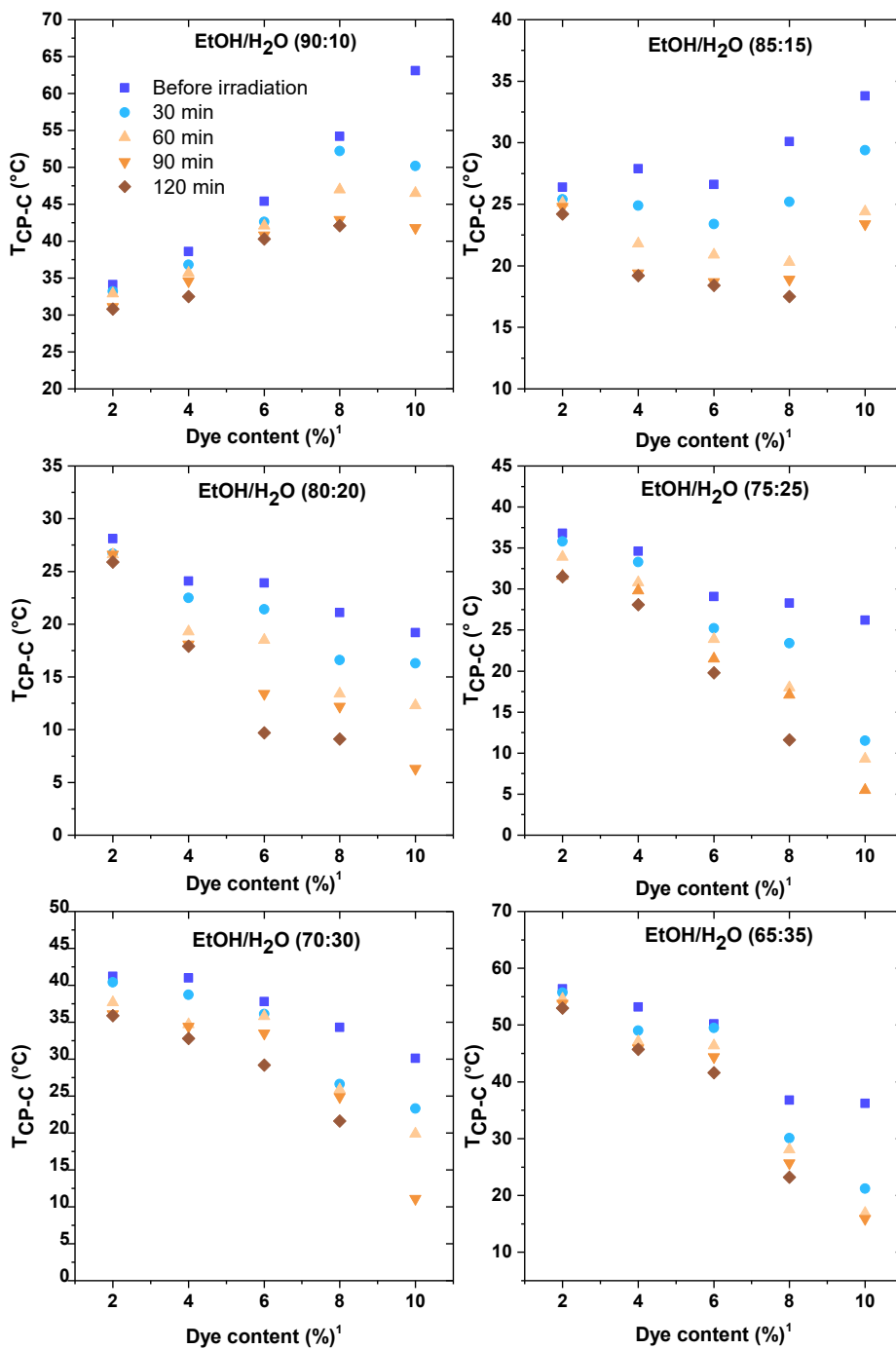


Figure 4.18. Cloud points vs ethanol-water composition plot for  $P_{M2a-e}$  before irradiation ( $t=0$ ) and after 30 min steps.

The influence of the solvent mixture on the cloud point gaps was apparent for the analyzed data (Figure 4.19).



**Figure 4.19.**  $T_{cp-c}$  vs. DASA content plot for the  $P_{M3}$  copolymer series before ( $t = 0$  min) and after irradiation, measured in 30 min intervals over a course of 120 min (except for  $P_{M3e}$  (10% DASA)).

In this case, the presence of increased water amounts, ranging from 40 to 15%, significantly affected the DASA switching behavior. This distinction was most evident when comparing the cloud point differences of **P<sub>M3d</sub>** and **P<sub>M3e</sub>** at ethanol concentrations below 85 vol% with those at higher concentrations. Consequently, increased water levels resulted in the anticipated preference for the energetically favorable zwitterionic cyclopentenone structure, leading to an improved transition from the colored to the uncolored state. On the contrary, the presence of high amounts of ethanol decreased the switching process, as seen by the smaller differences in cloud point between 95% ethanol and 60% ethanol in all instances.

The polymer aggregations of the samples **P<sub>M3a</sub>** to **P<sub>M3c</sub>** created almost symmetrical cloud points *vs.* composition plots, however, slight variations were observed for **P<sub>M3d</sub>** and **P<sub>M3e</sub>** (especially for 70 vol% ethanol). This was accompanied by non-uniform cloud point shifts from  $t = 0$  min to  $t = 120$  min. Based on the DASA switching behavior, it was seen that the colored form exhibited an exponential fall when exposed to visible light and measured by UV-vis spectroscopy.<sup>144</sup> It was assumed that the difference in UCST would decrease as the duration of irradiation increased. The increased influence of chromophores can be attributed to the neighboring-effect of the polymer side groups, which becomes more pronounced with higher levels of DASA content. The increased occurrence of steric hindrance can lead to a higher risk of irregular switching behavior due to the statistical distribution of side chains.

Further, the aggregation behavior after 150 min and 180 min was studied. However, for **P<sub>M3a</sub>** to **P<sub>M3d</sub>**, there was no noticeable alteration in the cloud point when compared to an irradiation duration of 120 min. As previously noted, subjecting sample **P<sub>M3e</sub>** to 120 minutes of visible light exposure resulted in the formation of highly soluble molecules.

The successful UCST tuning of a PMMA-DASA-polymer conjugate series by biocompatible visible light irradiation ( $\lambda = 520$  nm) over a course of max. 120 min was presented, resulting in impressively outstanding  $\Delta$ UCST values of more than 20 °C belonging to polymers with 7.4 and 10.4 mol% of chromophore content. The total UCST shifts of each **P<sub>M3</sub>** sample after a duration time of 120 min are outlined in Figure 4.20 as a function of the dye content (rounded) and ethanol-water ratio. The figure graphically demonstrates the correlation between the increasing DASA concentration in the related polymer sample and the corresponding rise in the temperature shifts.

In general, due to the irreversible switching behavior of DASA compounds (1<sup>st</sup> generation) in polar protic solvents, the initial UCST values cannot be re-obtained by thermal conversion after exposure to visible light. In order to address this limitation, a solvent-exchange cycle was utilized to successfully achieve "healing". Sample **P<sub>M3d</sub>** serves as a representative example (Figure 4.21a).

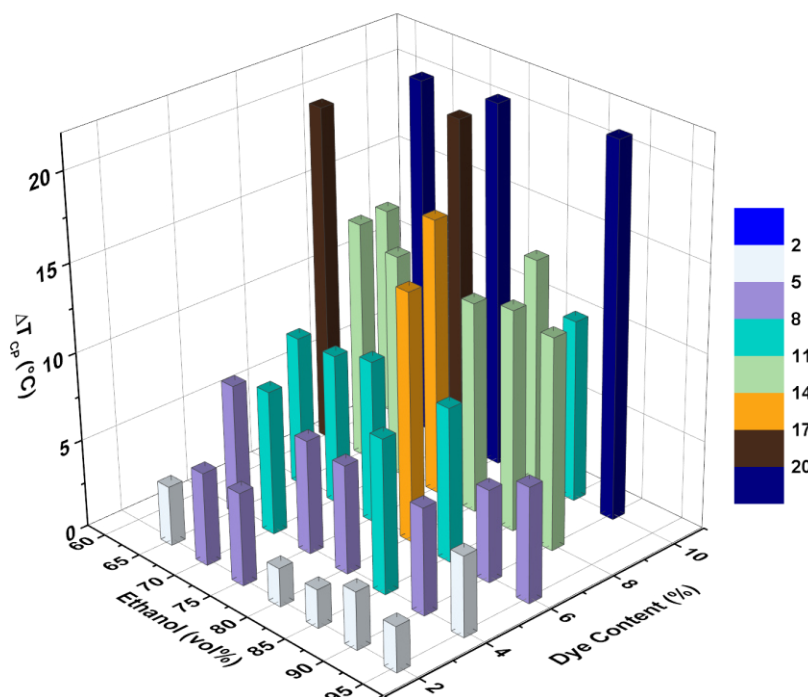


**Figure 4.20.** Total UCST shifts of the  $P_M3$  series as function of Stenhouse content and ethanol vol% content in the ethanol-water mixture.

After complete dissolution in an ethanol-water mixture (85:15) at 40 °C (1), the transmittance was followed as a function of time and the cloud point was determined at  $T_{CP} = 30.1$  °C (2). Light irradiation ( $\lambda = 520$  nm) over a course of 40 °C yielded a UCST shift of 12.6 °C (3). The selective regeneration of the colored unpolar DASA state was performed in chloroform after evaporation of the aqueous ethanol under reduced pressure, as halogenated solvents enabled thermal conversion processes<sup>146</sup> (4, 5). The increased triene amount was macroscopically observed by color intensification (6). A second solvent evaporation (7) and renewed dissolution in aqueous ethanol resulted in the successful recovery of the initial cloud point.

The corresponding turbidimetry measurements are outlined in Figure 4.21b. While this reactivation method was successful for the majority of samples, it was ineffective for  $P_M3e$  (except for EtOH/H<sub>2</sub>O (80:20)) and also for  $P_M3d$  when performed with 60 and 90 vol% ethanol content. Subsequently, the impact of temperature on the switching behavior and stability of the Stenhouse structure was examined.

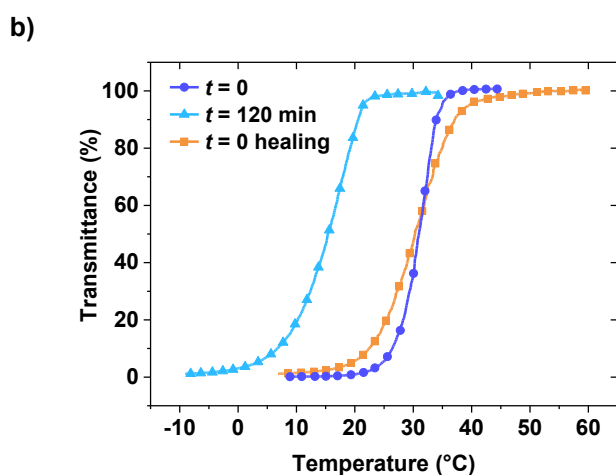
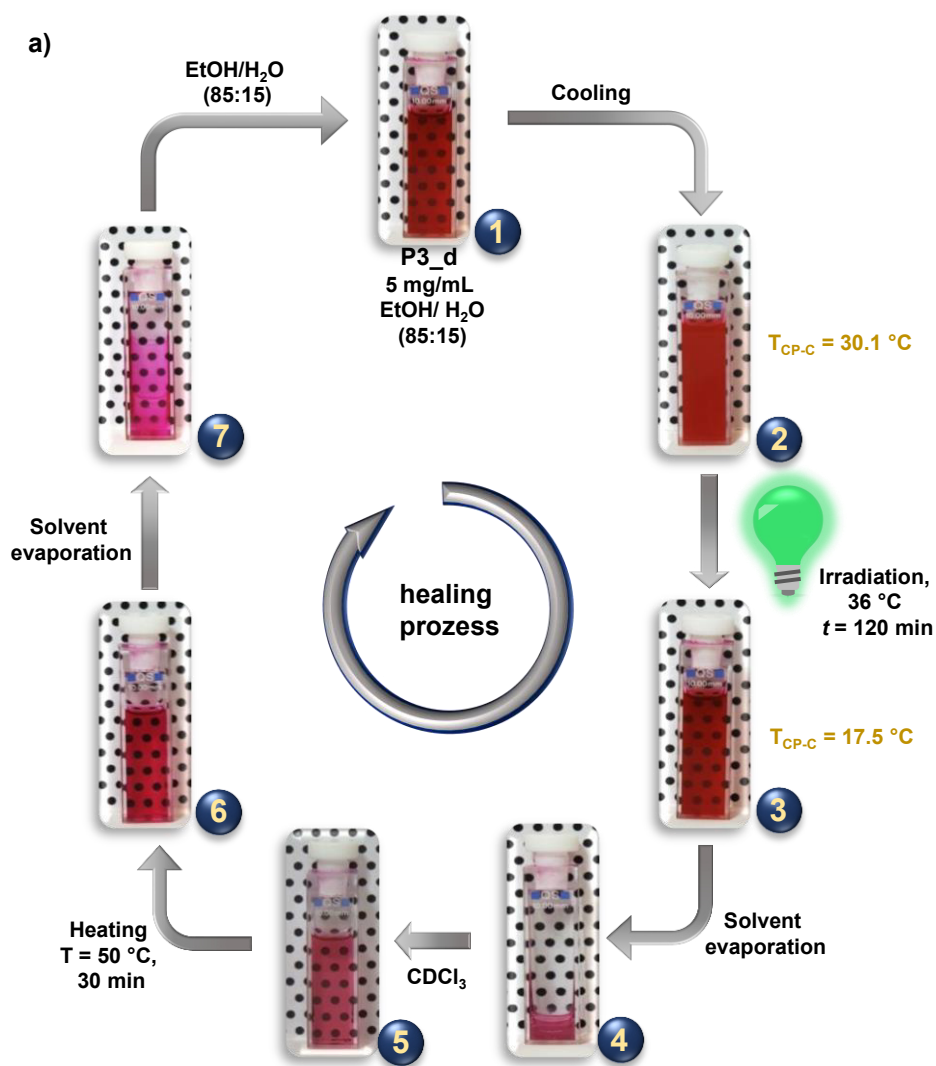


**Figure 4.21.** Healing process of the P<sub>M</sub>3 copolymer series. **a)** Sample P<sub>M</sub>3d dissolved in EtOH/H<sub>2</sub>O (85:15) was recovered. The unpolar colored DASA structure can be re-obtained through sample solvation in chloroform and heating at 50 °C for 30 min (6). **b)** Measured turbidity curves before irradiation ( $t = 0$  min), after irradiation ( $t = 120$  min) and after generation cycle ( $t = 0$ , healing).

When exposed to visible light at 30 °C, a comparison of the UV–vis absorption maxima of **P<sub>M</sub>3b** and **P<sub>M</sub>3e** (0.2 mg mL<sup>-1</sup>) at three-minute intervals revealed that the reduction in color intensity was more pronounced in the case of **P<sub>M</sub>3e** during the initial 10 minutes (Figure 4.22a). When comparing the initial cloud point difference between  $t = 0$  and  $t = 0$  of **P<sub>M</sub>3d** and **P<sub>M</sub>3e**, the change in UCST was larger than in the following measurements. Notice that the UV–vis measurements necessitated a significantly lower sample concentration compared to that utilized for UCST determination. Hence, the reason for the extra fast decline in the switching behavior of **P<sub>M</sub>de** might be attributed to the statistically larger likelihood of a photon stimulating DASA electrons to transition to a higher energy state.

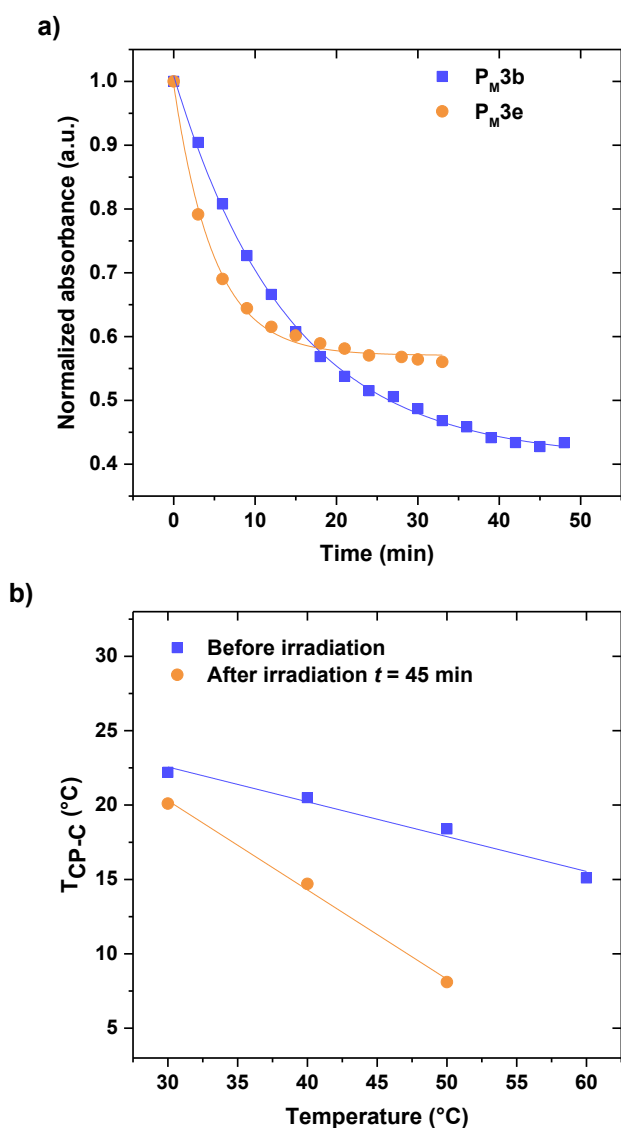


**Figure 4.22.** Temperature influence on PMMA-DASA-polymer conjugates in solution. **a)** UV–vis absorption maxima vs. time plot (normalized) of **P<sub>M</sub>3b** and **P<sub>M</sub>3d** performed in EtOH/H<sub>2</sub>O (80:20) at 30 °C. **b)** Cloud point results in dependence of different temperature values of **P<sub>M</sub>3d** (5 mg mL<sup>-1</sup>) before and after irradiation with visible light over a course of 45 min and solved in EtOH/H<sub>2</sub>O (80:20).

In order to evaluate the influence of temperature during dissolution and switching, sample **P<sub>M</sub>3d** was irradiated at 30, 40, 50 and 60 °C, respectively, and the corresponding  $T_{CP-C}$  values were compared (Figure 4.22b). The procedure revealed a dramatic increase in the  $\Delta UCST$  that was almost linearly dependent on the temperature rise. The cloud points before irradiation decreased with increasing dissolution temperatures. Since the dissolution occurred under the exclusion of light, only background switching can be responsible, which was also more distinct the faster the molecules migrated. In the case of light irradiation at 60 °C, no  $T_{CP-C}$  value was received. For further investigation of the temperature dependency, a time resolved UV-vis tracking at 18 °C and 55 °C, respectively, was carried out to study the characteristic absorption intensity at  $\lambda = 525$  nm (Figure 4.23).

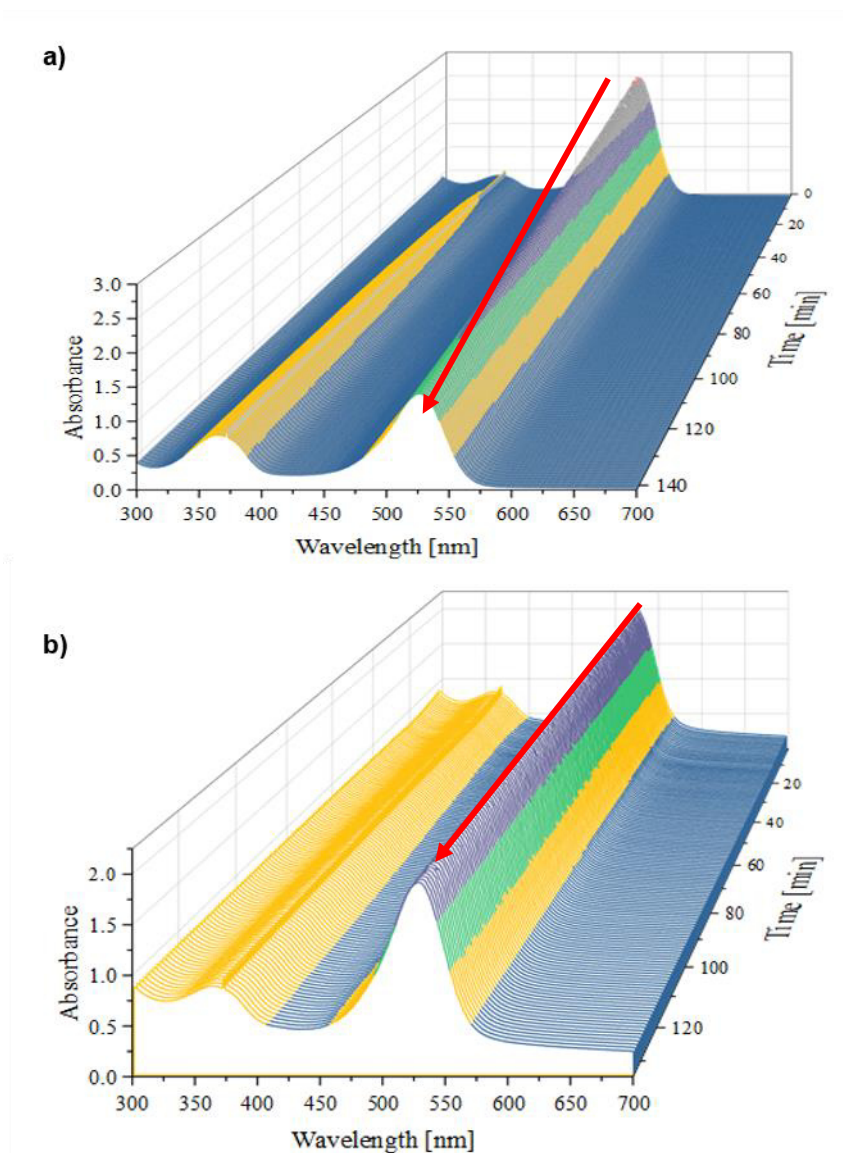


**Figure 4.23.** Time resolved UV-vis tracking (every minute) of a PMMA-DASA-polymer conjugate (6.5 mol% DASA) performed in EtOH/H<sub>2</sub>O (0.25 mg mL<sup>-1</sup>) at a) 55 °C and b) at 18 °C over a course of more than 120 min.

Therefore, the sample containing 6.5 mol% DASA was dissolved in 80 vol% ethanol and the change of the color intensity was observed by monitoring the UV-vis spectra at 60 s intervals. A temperature of 55 °C was more efficient to induce the non-irradiated switching behavior of the chromophoric unit, since the characteristic triene absorption (at 525 nm) stronger decreased as compared to measurements at 18 °C (red arrows). However, a slight intensity loss (background switching) was observed at lower temperatures. This phenomenon might arise either due to the impact of temperature and the polarity of the solvent combination or as a result of the necessary illumination during the measurement process.

Overall, a temperature- and light-responsive PMMA series including Stenhouse adducts as chromophoric moieties with concentrations ranging from 1 mol% to 10.7 mol% was successfully synthesized. The straightforward synthetic route relied on a subsequent polymer analogous reaction, which employed the activated ester pentafluorophenyl methyl acrylate (PFMA) as the starting material for an easy incorporation of DASA side chains. Through the utilization of these copolymers in UCST experiments using ethanol-water mixtures (with ethanol concentrations ranging from 65% to 95% by volume), a significant correlation between the quantity of the integrated chromophore and the analysis of cloud points was discovered. Encouragingly, the deployment of biocompatible green light triggered isomerization processes that resulted in a decrease in the cloud point in all instances. The UCST changes were observed to be the highest, reaching 20 °C, after 2 hours of exposure, notably for DASA concentrations of 7.4/10.7 mol%. In addition, the original cloud points of the majority of the samples have been repaired using a healing process that involved changing the solvent and thermally converting them from the colorless state to the colorful DASA condition. In summary, the PMMA polymer matrix was effectively modified to stabilize the unstable DASA compounds (1<sup>st</sup> generation) against protic polar solvents. Additionally, the negative photoisomerization of these compounds was applied to achieve excellent control over the cloud point.

## 4.2 Poly(*N*-isopropylacrylamide)-DASA conjugates and poly(*N,N*-diethylacrylamid)-DASA conjugates

Inspired by the promising results obtained from the investigation of poly(methyl methacrylate)-DASA conjugates with adjustable UCST behavior, the synthetic approach was subsequently advanced. For this reason, the focus of this work was broadened to encompass polymers that demonstrate phase separation upon heating in an aqueous solution. The point of lowest solubility in the cloud-point curve is referred to as the precipitation threshold, also known as the *lower critical solution temperature* (LCST)  $T_{CP}$  (Section 2.3.1).<sup>181</sup> In recent decades, the scientific community has shown an intense fascination in such an inverse solubility phenomenon. This interest has mostly been motivated by the potential applications in the field of water exploration.<sup>75</sup> One of the most widely recognized examples is poly(*N*-isopropylacrylamide) (PNIPAM), which exhibits a cloud point in water that falls within the temperature range of  $T_{CP} \cong 31\text{--}35\text{ }^{\circ}\text{C}$ .<sup>96,182</sup> The observed variations are related to the detailed microstructure of the macromolecule and the polymer concentration.<sup>163,183</sup> Since Heskins and Guillet originally reported the solution properties of PNIPAM in 1968<sup>184</sup>, the list of applications has grown to include, *e.g.*, microgels<sup>185,186</sup>, drug-delivery systems<sup>187</sup>, sensors<sup>188</sup>, thin films<sup>189</sup> and biomedical engineering<sup>190,191</sup>. In part, the high level of academic interest can be attributed to the favorable condition of the globule-to-coil transition occurring around the human body temperature.<sup>163</sup> Additionally, the monomer *N*-isopropylacrylamide can be readily exposed to several polymerization processes, including free radical polymerizations as well as controlled methods, which also allow for copolymerizations using a significant array of distinct comonomers.<sup>192–194</sup> With respect to this work, the numerous advantages associated with PNIPAM have resulted in being highly motivated for its adoption as the primary framework for further studies on the LCST behavior, particularly in conjunction with DASA side groups. Due to their reduced stability in hydrophilic solutions/chemical environments, Stenhouse adducts are prone to undesired switching processes. To investigate this influence, the strategic decision was made to include a second primary monomer moiety, namely *N,N*-diethylacrylamide (DEA). While PDEA meets the PNIPAM criteria on the one hand ( $T_{CP} \cong 33\text{ }^{\circ}\text{C}$ , water solution<sup>195</sup>), its ethyl groups contribute to its higher hydrophobicity than PNIPAM on the other (Figure 4.24).

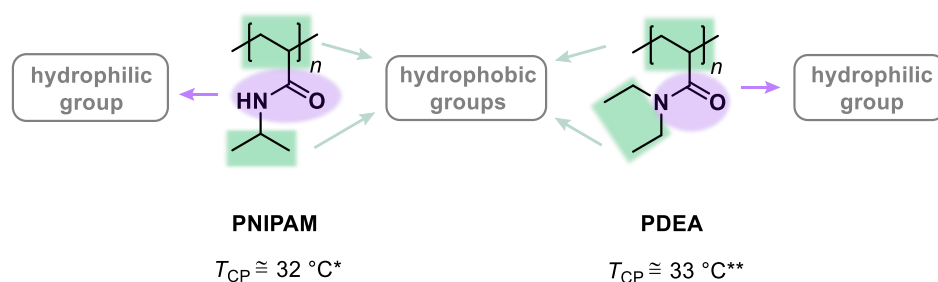


**Figure 4.24.** Structure comparison of poly(*N*-isopropylacrylamide) (\*PNIPAM)<sup>182</sup> and poly(*N,N*-diethylacrylamide) (\*\*PDEA)<sup>195</sup>.

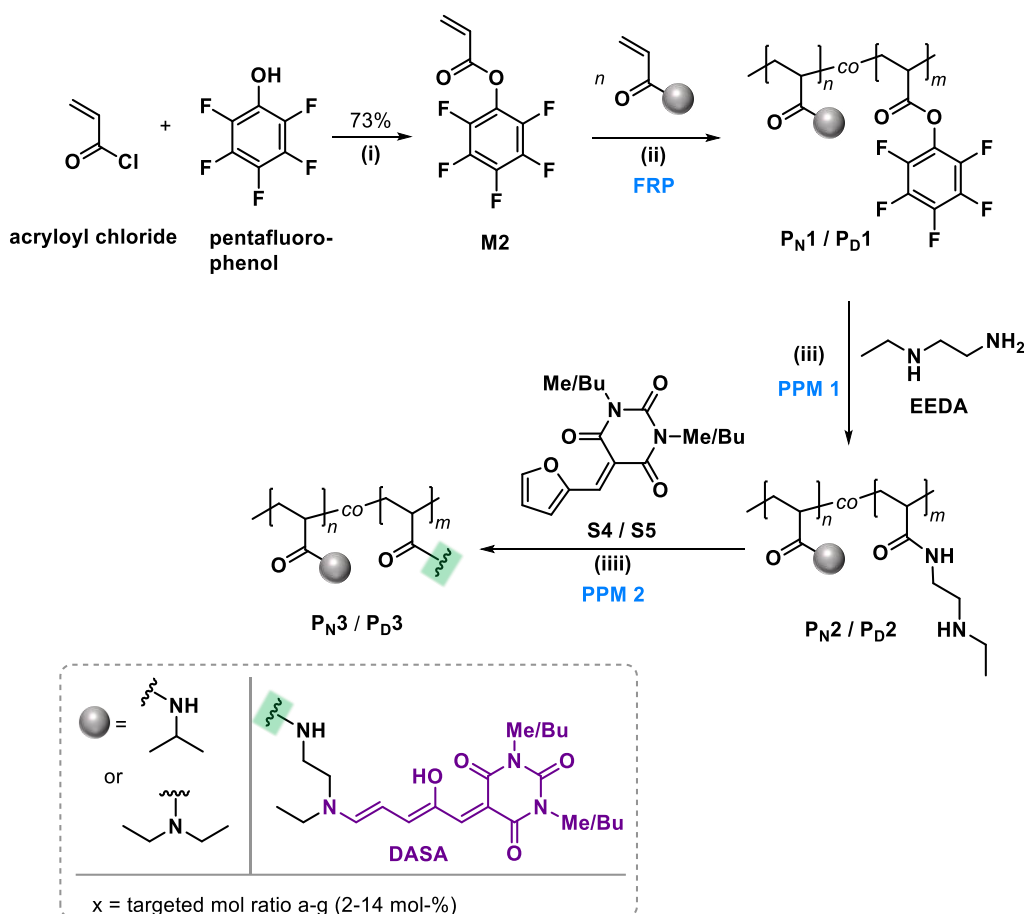
The slightly enhanced hydrophobic character is attained without significantly augmenting the likelihood of steric hindrance for the DASA side chains, as could be found for cyclic monomers. The sections that follow discuss the results of the synthetic strategy employed to acquire access to a PNIPAM-DASA and PDEA-DASA conjugate library, respectively. The primary emphasis lies in the examination of the LCST phenomenon both prior to and subsequent to the activation of the chromophore through illumination.

#### 4.2.1 Synthesis of PNIPAM-DASA- and PDEA-DASA-polymer conjugates

The utilization of activated ester chemistry, specifically incorporating the pentafluorophenyl (PFP) side group, has demonstrated its efficacy in providing a convenient synthetic approach to obtain polymer precursors for temperature-responsive polymer materials. These materials readily undergo subsequent reactions, resulting in the synthesis of tailor-made copolymer libraries containing DASA moieties (Section 4.1.1).

Hence, the previously described method for PMMA copolymers was applied and slightly modified. Scheme 4.5 illustrates the process overview. The activated PFP ester group was incorporated into the polymer matrix through the utilization of the monomer pentafluorophenyl acrylate (PFPA, **M2**). The selection to approve of this alternative over pentafluorophenyl methyl acrylate (**M1**), as used for PMMA conjugates, was based on its more advantageous copolymerization conditions with DEA and NIPAM. Hence, **M2** was routinely synthesized through the reaction of pentafluorophenol (1.0 eq.) with acryloyl chloride (1.1 eq.) in anhydrous THF. The reaction solution was stirred for 20 h at room temperature in an argon atmosphere, while TEA was added as an auxiliary base. In accordance with the literature, the desired product was isolated with a 73% yield after purification using column chromatography.<sup>163,163</sup> For the preparation of the copolymer libraries poly(*N*-isopropylacrylamid-*co*-pentafluorophenyl acrylate) (p(NIPAM-*co*-PFPA), **P<sub>N1</sub>**) and poly(*N,N*-diethylacrylamid-*co*-pentafluorophenyl methacrylate) (p(DEA-*co*-PFPA) **P<sub>D1</sub>**) as starting material, **M2** was further subjected to a statistical FRP (Scheme 4.5) method, which was previously reported and slightly modified.

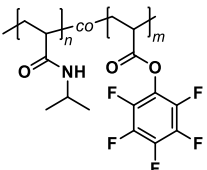
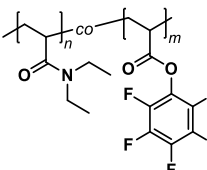
The monomer quantities were systematically altered, leading to samples ranging from 2 mol% to 14 mol% of the PFP side group. In order to confirm sample identification in context with this study, the index *x* is utilized to denote the theoretical amount of PFPA monomer included. The corresponding values for *x* are as follows: *a* = 2%, *b* = 4%, *c* = 6%, *d* = 8%, *e* = 10% and *f* = 12%. The crude samples were obtained after treating either NIPAM/**M2** or DEA/**M2** in anhydrous dioxane with AIBN as initiator and heating at 75 °C overnight.



**Scheme 4.5.** Synthesis steps for NIPAM/DEA-DASA-polymer conjugates. (i) **M2** synthesis adopted from ref.<sup>196</sup> Reaction conditions: Dry THF, TEA, rt, 19 h; (ii) FRP polymerization. Reaction conditions (adopted from ref.<sup>174</sup>): Dry 1,4-dioxane, AIBN, 6 h; (iii) Treatment with *N*-ethylethyldiamine (EEDA). Reaction conditions: TEA, THF/acetone (60:40, v/v), 45 °C, 3 h); (iii) Treatment with furan precursor (**S4/S5**). Reaction conditions: THF, rt, 4 d, light exclusion.

All copolymers were obtained in quantitative conversions (<sup>1</sup>H NMR monitoring of the reaction solution, appendix A.1) and yields. The full characterization of both copolymer libraries was conducted *via* <sup>1</sup>H NMR, <sup>13</sup>C NMR, FT IR spectroscopy and SEC chromatography. The results of the SEC analyses are displayed in Table 4.4 and discussed below. The number-average molar mass  $\bar{M}_n$  and mass-average molar mass  $\bar{M}_w$  were determined from an analysis of the SEC traces illustrated in Figure 4.25a and 4.25b. These SEC traces exhibited unimodal curves, indicating the successful occurrence of statistical copolymerization. All measurements were conducted in DMF as the eluent, with a polystyrene standard serving as a reference. For the **P<sub>N1</sub>** series, values of  $\bar{M}_n$  varied from 88.000 to 110.000 g mol<sup>-1</sup>, including standard dispersities  $\mathcal{D}$  of the free-radical polymerization process.

**Table 4.4.** Analytical data of SEC of of p(NIPAM-*co*-PFPA) (**P<sub>N</sub>1a-g**) and p(DEA-*co*-PFPA) (**P<sub>D</sub>1a-g**) copolymers.

Structure	Sample	M2 expected (mol%)	$X_{M2}$ (mol%) <sup>a</sup>	$\bar{M}_n$ (g mol <sup>-1</sup> ) <sup>b</sup>	$\bar{M}_w$ (g mol <sup>-1</sup> ) <sup>b</sup>	$\mathcal{D}^b$
	<b>P<sub>N</sub>1a</b>	2.0	2.1	1.08·10 <sup>5</sup>	3.53·10 <sup>5</sup>	3.24
	<b>P<sub>N</sub>1b</b>	4.0	3.8	1.10·10 <sup>5</sup>	3.33·10 <sup>5</sup>	3.33
	<b>P<sub>N</sub>1c</b>	6.0	6.2	9.90·10 <sup>4</sup>	3.57·10 <sup>5</sup>	3.60
	<b>P<sub>N</sub>1d</b>	8.0	8.3	9.32·10 <sup>4</sup>	2.87·10 <sup>5</sup>	3.03
	<b>P<sub>N</sub>1e</b>	10	9.8	9.57·10 <sup>4</sup>	3.18·10 <sup>5</sup>	3.32
	<b>P<sub>N</sub>1f</b>	12.0	11.6	8.75·10 <sup>4</sup>	2.60·10 <sup>5</sup>	2.96
	<b>P<sub>N</sub>1g</b>	14.0	13.7	9.00·10 <sup>4</sup>	2.61·10 <sup>5</sup>	2.80
	<b>P<sub>D</sub>1a</b>	2.0	1.50	4.49·10 <sup>4</sup>	1.17·10 <sup>5</sup>	2.60
	<b>P<sub>D</sub>1b</b>	4.0	3.50	2.04·10 <sup>4</sup>	5.59·10 <sup>4</sup>	2.68
	<b>P<sub>D</sub>1c</b>	6.0	6.70	5.58·10 <sup>4</sup>	1.33·10 <sup>5</sup>	2.39
	<b>P<sub>D</sub>1d</b>	8.0	8.30	5.57·10 <sup>4</sup>	1.33·10 <sup>5</sup>	2.40
	<b>P<sub>D</sub>1e</b>	10.0	10.1	7.30·10 <sup>4</sup>	1.72·10 <sup>5</sup>	2.36
	<b>P<sub>D</sub>1f</b>	12.0	12.1	5.05·10 <sup>4</sup>	1.35·10 <sup>5</sup>	2.67
	<b>P<sub>D</sub>1g</b>	14.0	13.0	5.76·10 <sup>4</sup>	1.21·10 <sup>5</sup>	2.20

<sup>a</sup>determined by <sup>1</sup>H NMR-spectroscopy<sup>b</sup>determined by SEC

The latter was also displayed for the **P<sub>D</sub>1** copolymers. In comparison, the **P<sub>D</sub>1** library showed  $\bar{M}_n$  values ranging from 50.000 to 70.000 g mol<sup>-1</sup>. By comparing the relative peak intensities of the -CH< (H<sub>e</sub>) NIPAM proton signal and the methyl backbone protons of the **M2** moiety -CH<sub>2</sub>- (H<sub>b</sub>) in the <sup>1</sup>H NMR (in acetone-*d*<sub>6</sub>;  $\delta$ /ppm: 2.7, 4.0), an incorporation ratio of PFP side groups in **P<sub>N</sub>1** (Figure 4.26a) was revealed. The sharp separation of the H<sub>b</sub> signal from other backbone peaks was validated by applying heteronuclear single coherence (HSQC) NMR. The calculation occurred through Equation 4.10.

$$X_{M2} = \frac{\int H_b}{0.09 + 1} \quad (4.10)$$

Using sample **P<sub>N</sub>1d** as an example, the calculation with the peak of H<sub>b</sub> (0.09) yielded about 8.3% **M2** moiety content. For each p(NIPAM-*co*-PFPA) copolymer, a similar calculation was employed. Gratifyingly, the obtained values closely matched the expected amounts (Table 4.4), with minor discrepancies due to phase corrections during NMR analysis.

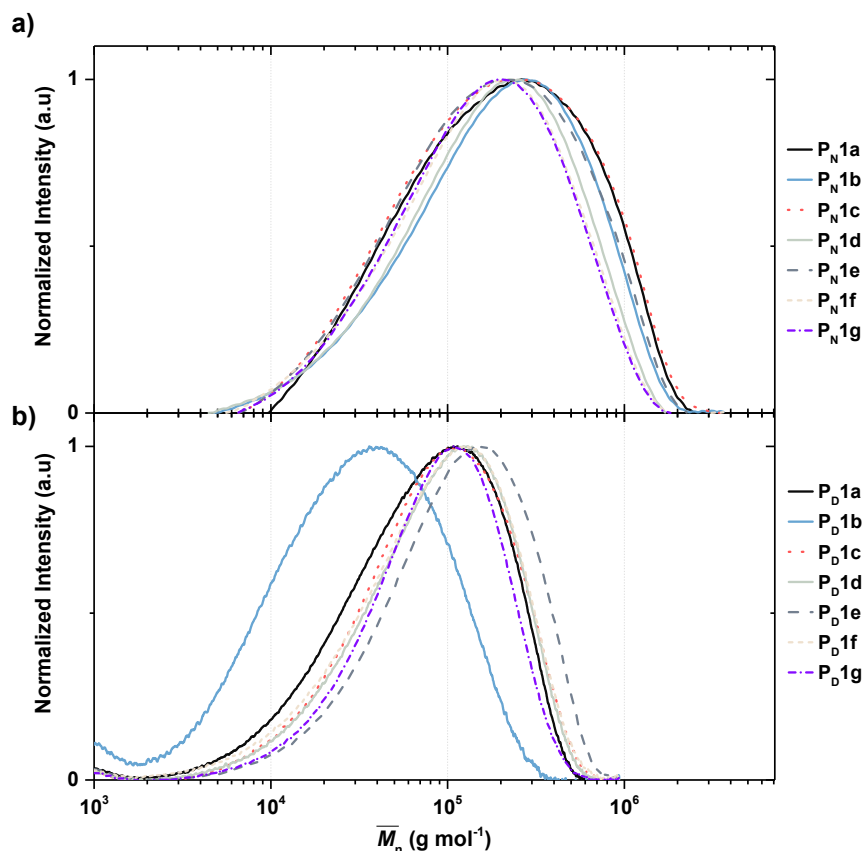


**Figure 4.25.** SEC traces of **a)**  $P_{N1}$  series and **b)**  $P_{D1}$  series measured in DMF. All data were determined relative to linear PS standards.

While the proton signal  $H_c$  emerged at the  $^1\text{H}$  NMR (in acetone- $d_6$ ), the spectrum of  $P_{D1g}$  confirmed successful integration of the PFP ester group, however the computation of incorporated **M2** monomer was not achievable due to signal overlapping (Figure 4.26b). Therefore, the quantitative PFP ester substitution through amidation using an excess of benzylamine in anhydrous THF at ambient temperature and stirring for 1 h revealed the broad peak in the aromatic region (in  $\text{CDCl}_3$ ;  $\delta/\text{ppm}$ : 7.0-7.5), attributed to benzene protons (Figure 4.26c). In conjunction with the benzylamine architecture, the peak corresponding to the methylene protons  $H_g$  ( $\delta/\text{ppm}$ : 4.25) displayed a downfield shift. The relative integration of the separated peaks  $H_g/H_a$  and subsequent estimation with Equation 4.11

$$X_{\text{BA}} = \frac{\int H_g \cdot \frac{1}{2}}{\int H_g \cdot \frac{1}{2} + 1} \quad (4.11)$$

yielded a quantification of the benzylamine side group  $X_{\text{BA}}$ , expressed as a percentage (6.7 mol%), for  $P_{D1c}$ . Assuming that  $X_{\text{BA}}$  is equivalent to  $X_{\text{PFP}}$ , the procedure was applied to all  $P_{D1}$

samples. This assumption was derived from the convenience of verifying the quantitative conversion of the PFP ester through the utilization of highly sensitive  $^{19}\text{F}$  NMR analysis.

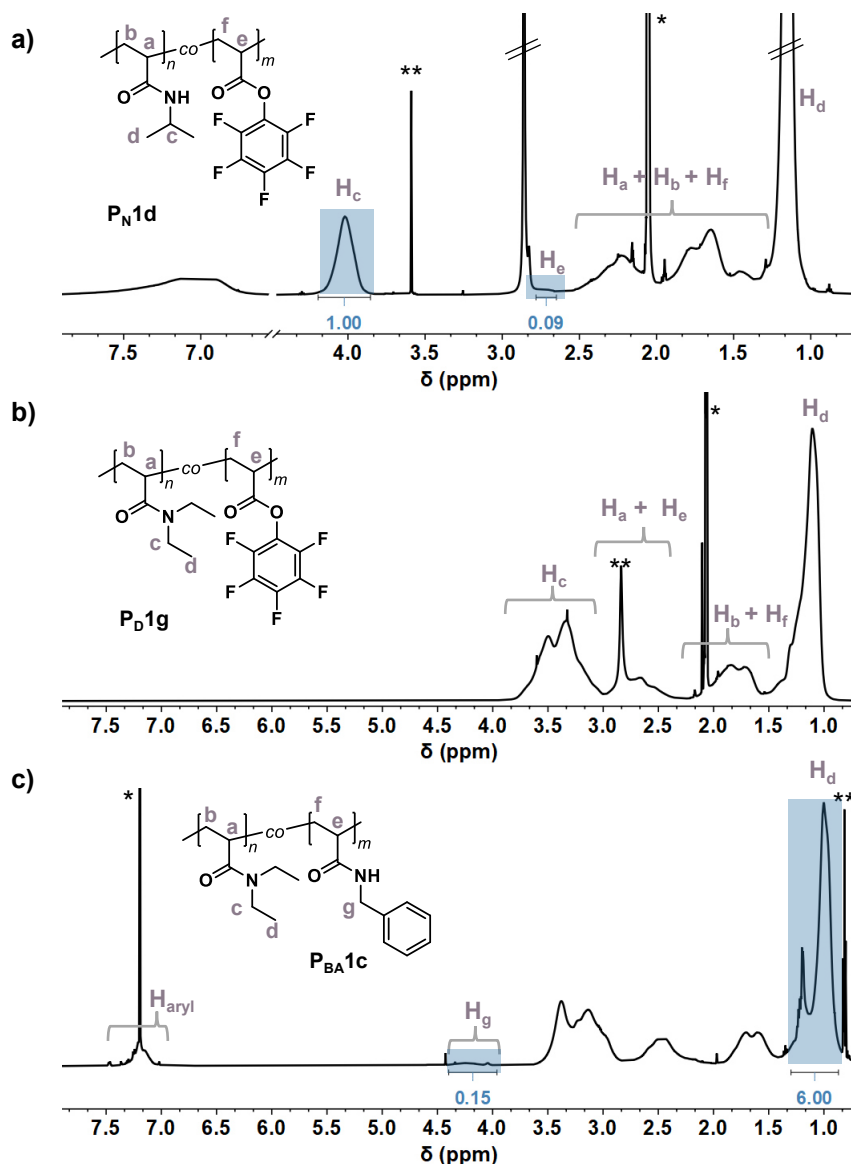


**Figure 4.26.**  $^1\text{H}$  NMR spectrum of a) sample  $\text{P}_{\text{N}1\text{d}}$  measured in acetone- $d_6$ . b) sample  $\text{P}_{\text{D}1\text{g}}$  measured in acetone- $d_6$ . c) sample  $\text{P}_{\text{D}1\text{g}}$  after quantitative substitution of the PFP ester side group by benzylamine measured in chloroform- $d_3$ . \*Reference solvent \*\*solvent residue

FT-IR spectroscopy was employed to conduct further characterization of the  $\text{P}_{\text{N}1}$  and  $\text{P}_{\text{D}1}$  copolymer libraries. The PFP ester showed a prominent peak corresponding to the  $\text{C}-\text{F}_{\text{stretch}}$ -vibration at wavenumbers  $\bar{\nu} = 1516 \text{ cm}^{-1}$  (Figure 4.27a,  $\text{P}_{\text{N}1}$ ) and  $\bar{\nu} = 1519 \text{ cm}^{-1}$  (Figure 4.27b,  $\text{P}_{\text{D}1}$ ). Furthermore, the PFP ester and amide  $\text{C}=\text{O}_{\text{stretch}}$ -vibration bands were clearly separated. The linear absorption increase observed in the selected regions of the PFP ester  $\text{C}=\text{O}_{\text{stretch}}$ -vibration

band at  $\bar{\nu} = 1728 \text{ cm}^{-1}$  (**P<sub>N</sub>1**) and  $1780 \text{ cm}^{-1}$  (**P<sub>D</sub>1**) demonstrated an increase in the PFP ester content within both copolymer series. This observation was concomitant with a concurrent reduction in the absorption of the respective amide bands at  $1642 \text{ cm}^{-1}$  (**P<sub>D</sub>1**) and  $1625 \text{ cm}^{-1}$  (**P<sub>N</sub>1**).

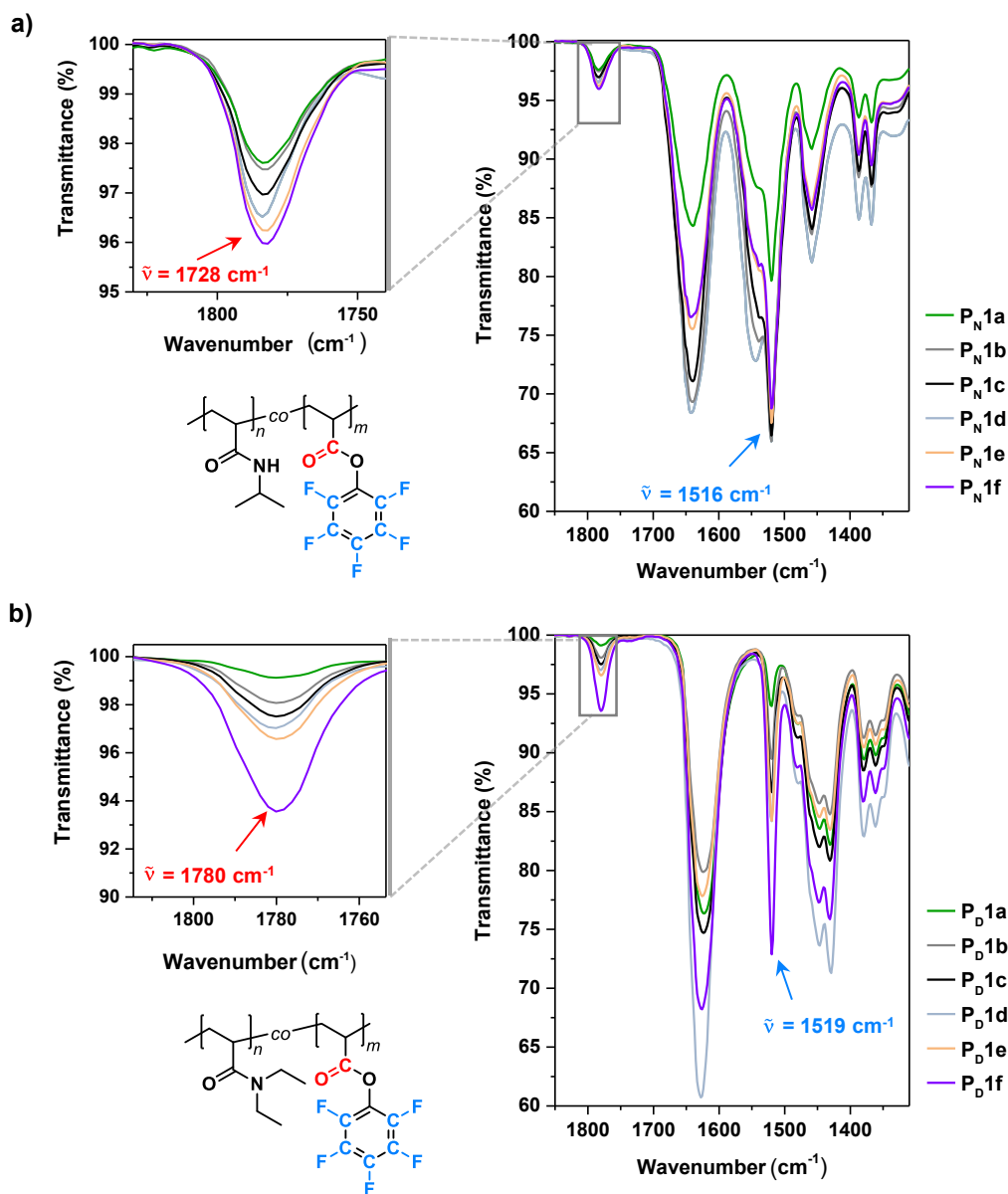


**Figure 4.27.** a) FT-IR spectra of **P<sub>N</sub>1a-g** with the selected region of the **M2** ester band at  $1728 \text{ cm}^{-1}$ . b) FT-IR spectra of **P<sub>D</sub>1a-g** with the selected region of the **M2** ester band at  $1780 \text{ cm}^{-1}$ .

The next step involved the initial post-polymerization modification PPM 1, specifically the integration of EEDA to form amine linker side groups (Scheme 4.5). The copolymer samples were dissolved in acetone at room temperature and subjected to an excess of EEDA and TEA as

an auxiliary base. After 1.5 h of reaction time, the quantitative conversion was confirmed by FT-IR spectroscopy due to the full disappearance of the C=O<sub>stretch</sub>-vibration band at 1728 cm<sup>-1</sup> and 1780 cm<sup>-1</sup> (Figure 4.28a). The newly modified polymers were purified by dialysis from methanol for at least 5 d using a membrane with MWCO of 8000 Da.

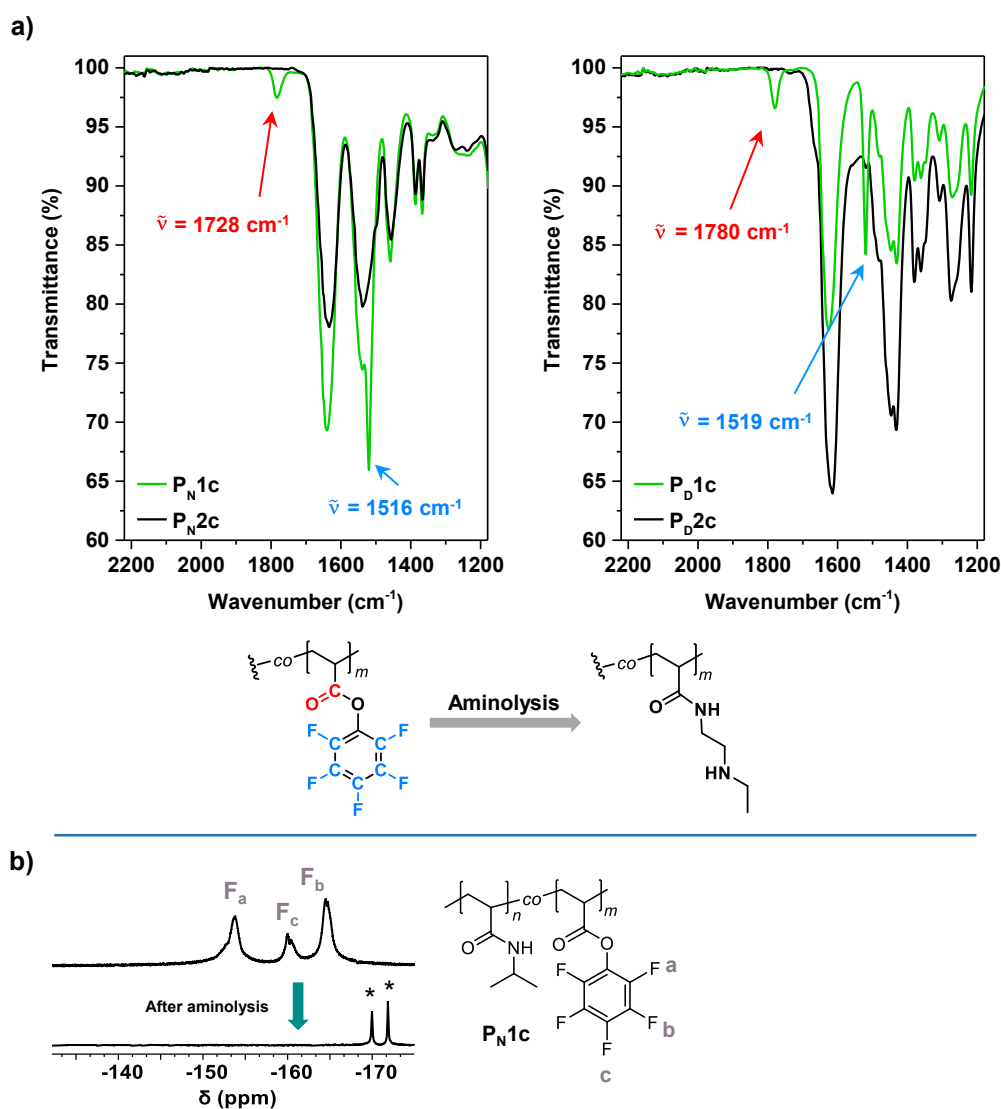
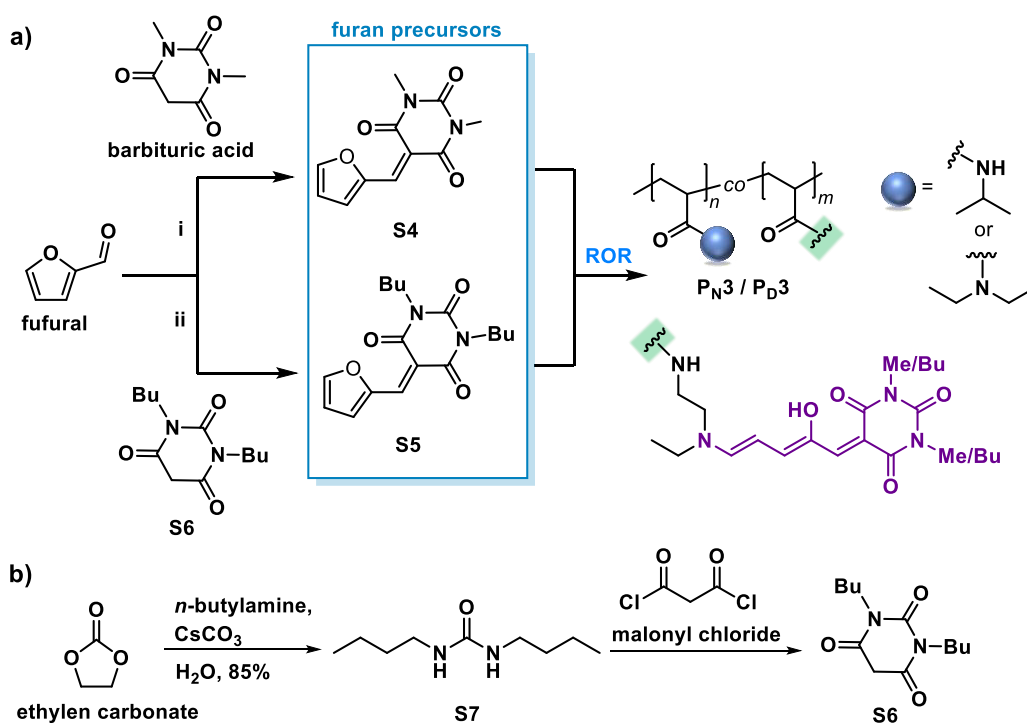


**Figure 4.28.** a) Conversion monitoring *via* IR spectra (selected region) of **P<sub>N</sub>1c** and **P<sub>D</sub>1d** before and after aminolysis with *N*-ethylethylenediamine (EEDA). b) <sup>19</sup>F NMR spectra of **P<sub>N</sub>1c** before (top) and after aminolysis (bottom). \*Signals resulted from PFP-salt residue.

The validity of the quantitative PFP ester substitution was further proven by the absence of <sup>19</sup>F atom signals in the <sup>19</sup>F NMR spectra of all samples, together with the presence of residual pentafluorophenolate peaks (Figure 4.28b). As a result, it was assumed that the side group ratio of EDDA and either NIPAM or DEA equated  $X_{\text{EDDA}} = X_{\text{M}2}$  for all copolymers. Hence, the polymer

analogous synthetic pathway facilitated a highly efficient method for obtaining primary amine groups. The approach guaranteed complete yields and ensured the quantitative substitution of PFP groups.

In the subsequent synthetic procedure, the colored copolymers of interest were generated by subjecting the reactive parent polymer libraries **P<sub>N</sub>2** and **P<sub>D</sub>2** to a secondary post-polymerization reaction (PPM 2, Scheme 4.5) involving furan precursors (Scheme 4.6a). The precursors are typically synthesized by an environmentally sustainable, non-catalyzed condensation reaction involving activated methylene compounds and aldehydes in an aqueous medium.<sup>178</sup> Illustrative examples of such compounds include Meldrum's acid, as previously discussed in Section 2.1.1, and derivatives of 1,3-disubstituted barbituric acid. Notably, for the following investigations, the acceptor moiety present in the DASA architecture was derived from barbituric acid derivatives rather than Meldrum's acid. As shown in Scheme 4.6a, 5-(furan-2-ylmethylene)-1,3-dimethyl-pyrimidine-2,4,6(1H,3H,5H)-trione (**S4**) and 5-(furan-2-ylmethylene)-1,3-dibutyl-pyrimidine-2,4,6(1H,3H,5H)-trione (**S5**) were isolated through filtering from the aqueous reaction mixture containing 1,3-dimethyl-barbituric/1,3-dibutyl-barbituric acid (**S6**) (1.1 eq.) and furfural (1.0 eq.) following a 2-hour stirring period at a temperature of 75 °C. In accordance with the literature, a yield of 90% (**S4**)<sup>146</sup> and 85% (**S5**)<sup>130</sup> was obtained.



**Scheme 4.6.** a) Schematic overview of the furan precursor synthesis with furfural and (i) barbituric acid or (ii) *N,N*-diebutylbarbituric acid followed by DASA formation. b) Two step synthesis of *N,N*-diebutylbarbituric acid (**S6**).

The synthesis of sample **S6** was accomplished by means of a two-step process. Initially, the use of ethylene carbonate (1.0 eq.) was implemented in a symmetrical CsCO<sub>3</sub>-catalyzed (0.1 eq.) transamination process, wherein *n*-butylamine (1.0 eq.) was employed as the reactant to produce 1,3-dibutylurea (**S7**).<sup>197</sup> Notably, this reaction was conducted in the absence of any solvent resulting in an 85% yield after filtration as purification. The findings were consistent with those published in the literature.<sup>197</sup> The urea derivative (**S7**) underwent a cyclic addition reaction with malonyl chloride, resulting in the formation of **S5**.<sup>198</sup> Generally, corresponding DASA publications frequently involves the utilization of isocyanates as a primary chemical for the synthesis of 1,3-disubstituted intermediates.<sup>199,200</sup>

This study introduces a fresh strategy employing the mild ethylene carbonate pathway as an alternative to address the significant concerns associated with the toxicity and respiratory dangers posed by isocyanates. Furthermore, no disadvantages pertaining to reaction time, purity, and yield were noticed. The furan precursors were then exposed to a ring opening reaction (ROR, Scheme 4.6a) adapted from Helmy and coworkers.<sup>146</sup> The elaboration of DASA side groups in the **P<sub>N</sub>2** series occurred with **S5**, which led to the formation of p(NIPAM-*co*-EEDA-Barb-Bu) (**P<sub>N</sub>3**) copolymers with a distinct purple color. Besides an implementation of the same procedure for **P<sub>D</sub>2** to perform p(DEA-*co*-EEDA-Barb-Bu) (**P<sub>DBu</sub>3**), the **P<sub>D</sub>2** was undergone further Stenhouse synthesis (**P<sub>DMe</sub>3**) by using **S4**. The general reaction procedure included dissolving of all **P<sub>N</sub>2** and **P<sub>D</sub>2** samples in anhydrous THF, respectively, followed by treatment with an excess of **S3** or **S4** under an argon atmosphere and stirring at room temperature. UV–visible light measurements were employed to monitor the purple solutions, ensuring their complete conversion within a period of 6 days, as described in Section 4.1.1.

The comparative analysis of the effects of various acceptor groups in the furylidene precursors on the ring formation was additionally conducted by tracking the reaction conversion of furylidene-Medrum'acid (**S2**) with p(MMA-*co*-EEDA) (**P<sub>M</sub>2c**) and **S6** with copolymer **P<sub>D</sub>2c** *via* UV-vis spectroscopy. The UV–vis absorbance spectra (THF; 0.40 mL;  $c \approx 3.9 \times 10^{-5}$  M) depicted in Figure 4.29a and 4.29b exhibit a maximum absorbance wavelength  $\lambda_{\text{max}}$  centered at 545 nm (**P<sub>M</sub>3c**) and at 565 nm (**P<sub>DBu</sub>3c**). Upon carrying out a direct comparison of the normalized absorption maxima during a reaction period of 250 min, the rate of DASA formation including **S5** was comparatively slower. The potential factors contributing to this phenomenon may be attributed to the inherent characteristics of the acceptor structures, as already discussed in the literature for non-polymeric systems.<sup>147</sup> Additionally, the structural configuration of DEA may potentially result in an increased steric hindrance.

All NIPAM/DEA based DASA copolymers (**P<sub>N</sub>3**, **P<sub>DBu</sub>3**, **P<sub>DMe</sub>3**) were purified employing dialysis in dichloromethane (5 d, rt, MWCO = 8000 Da), an appropriate method owing to the advantageous non-switching property of DASA compounds when dissolved in halogenated solvents. The pure substances underwent additional analysis through <sup>1</sup>H NMR, UV–vis, and FT-IR spectroscopic techniques.

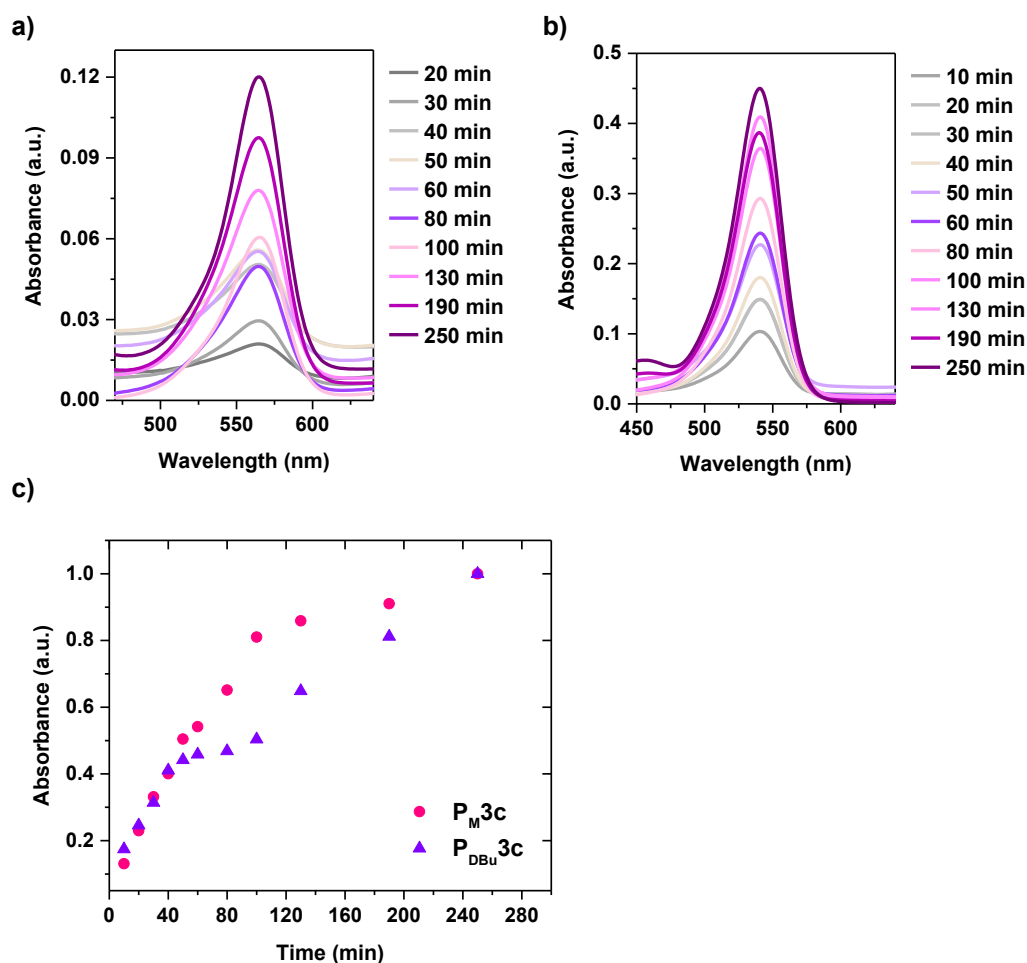


**Figure 4.29.** DASA formation monitoring via UV-vis absorption measurements in THF including a) the PMMA-polymer conjugate  $P_M2c$  and the furylidene Medrum'acid ( $S1$ ) precursor to yield  $P_M3c$ . b) DEA based  $P_D2c$  sample treated with furylidene barbituric acid ( $S5$ ) to give  $P_{DBU}3c$ . c) Normalized absorbance maxima comparison of UV traces a) and b).

A comparison between the parent copolymers  $P_D2f$  and  $P_{DBU}3f$  revealed the appearance of  $C=O_{stretch}$  vibration bands at  $1721\text{ cm}^{-1}$  and  $1711\text{ cm}^{-1}$  in the FT-IR spectrum (Figure 4.30a). The observed bands were found to correspond precisely to the  $C=O_{stretch}$  vibration band at  $1721\text{ cm}^{-1}$ , which is characteristic of the non-polymeric compound  $S8$  (Figure 4.30b). Sample  $S8$  was synthesized using the standard protocol for DASA synthesis as described in the publication by Helmy *et al.*<sup>130</sup> Also, the FT-IR spectroscopy investigation of  $P_N3c$  revealed differences in direct comparison with the diamine precursor sample  $P_N2c$ . The carbonyl  $C=O$  band at  $1728\text{ cm}^{-1}$  was slightly shifted to a higher wavelength.

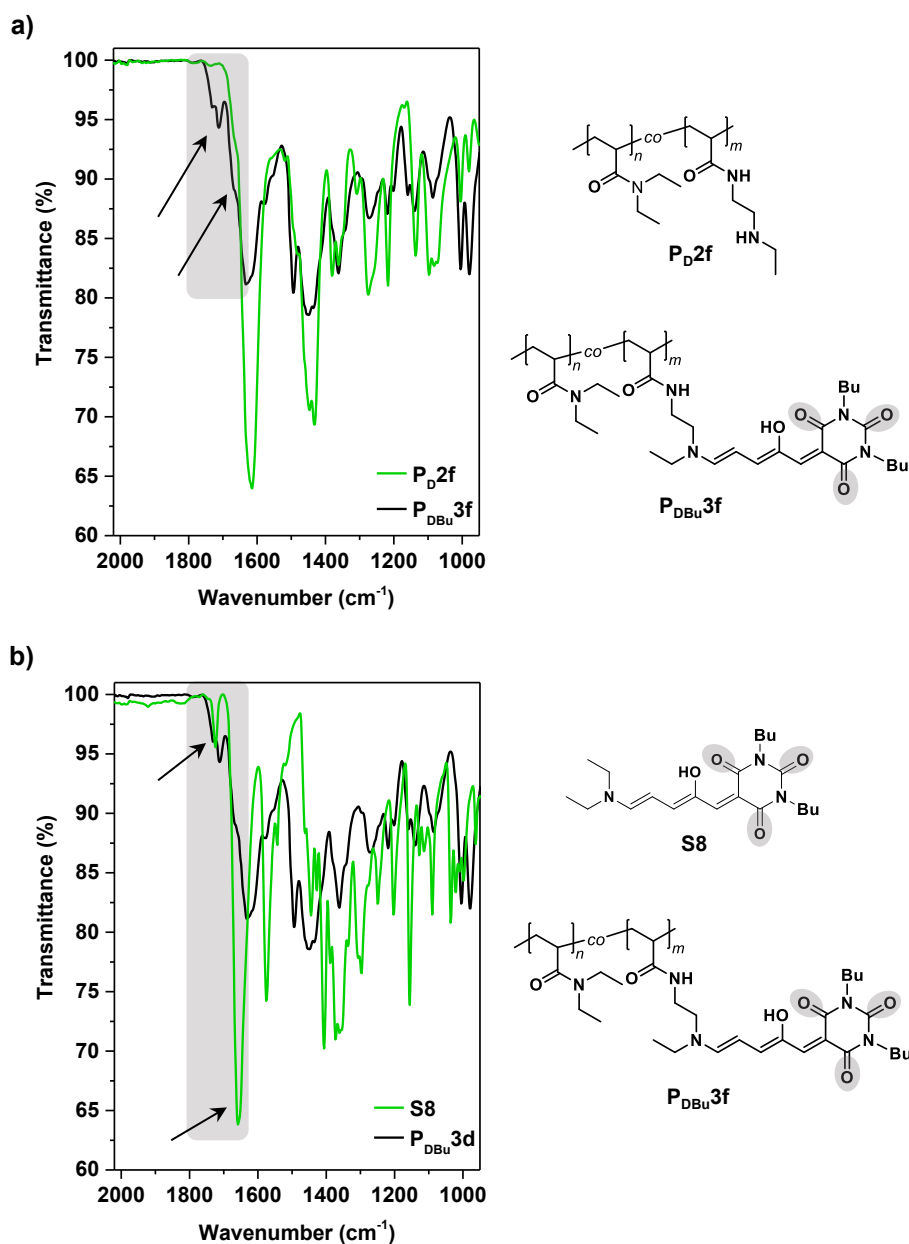


**Figure 4.30.** a) FT-IR spectra of  $P_{D2f}$  and  $P_{DBu3f}$  (selected region). b) FT-IR spectra comparison of  $P_{DBu3f}$  and the non-polymeric compound 1,3-Dibutyl-5-((2Z,4E)-5-(diethyl-amino)-2-hydroxypenta-2,4-dien-1-ylidene)pyrimidine-2,4,6(1H,3H,5H)-trione (S8).

Furthermore, additional bands appeared in the spectrum region at  $1780\text{ cm}^{-1}$  (grey), which correspond to the  $\text{C}=\text{O}_{\text{stretch}}$ -vibration of the DASA structure. The presence of the DASA unit in the polymer side chains was further substantiated by the detection of the distinctive conjugated double bond protons (Figure 4.32b; indicated purple dots) in the  $^1\text{H}$  NMR spectrum of  $P_{N3d}$ , in contrast to the parent polymer  $P_{N2d}$  (Figure 4.32a).

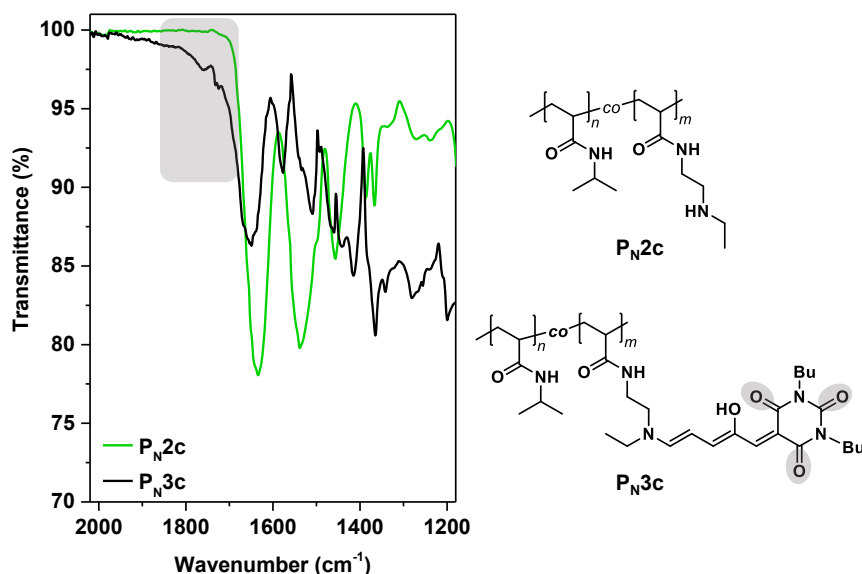


**Figure 4.31.** FT-IR spectra comparison of the C=O<sub>stretch</sub>-vibration region of sample **P<sub>N</sub>2c** and **P<sub>N</sub>3c**.

The signal downfield shift of H<sub>b</sub> (2.73 ppm) can be attributed to the deshielding impact of the double bond protons (indicated by the green dotted lines). Note, the <sup>1</sup>H NMR corresponds to DMSO-*d*<sub>6</sub> solution due to the poor solubility of the highly polar P<sub>N</sub>2 series, whereas **P<sub>N</sub>3c** was evaluated while dissolved in chloroform-*d*, because halogenated solvents stabilize the colored DASA structure. However, it was assumed that the occurrence of a methylene shift was not attributable to the solvent.

The determination of the DASA content  $X_{\text{DASA}}$  was achieved by establishing the ratio between the integral of the methylene protons H<sub>C</sub> and the integral of the amide proton of NIPAM, as defined by Equation 4.12.

$$X_{\text{DASA}} = \frac{\int H_{\text{C}} \cdot \frac{1}{2}}{\int H_{\text{C}} \cdot \frac{1}{2} + 1} \quad (4.12)$$

The calculation of DASA content for **P<sub>N</sub>3c**, as an illustrative example, yielded a chromophore proportion of 3.9 mol%. The observed deviation from the expected value of 6 mol% can be attributed to the insufficient solubility of **P<sub>N</sub>3** in chloroform, leading to an unfavorable signal-to-noise ratio. Hence, it was solely practicable to ascertain the DASA composition of **P<sub>N</sub>3a-b** using <sup>1</sup>H NMR, which, incidentally, were found to be lower than the anticipated values as indicated in Table 4.5. The DASA fraction for the samples **P<sub>N</sub>3d-e** was estimated using a linear regression analysis of the chromophore measured by UV-vis spectroscopy.

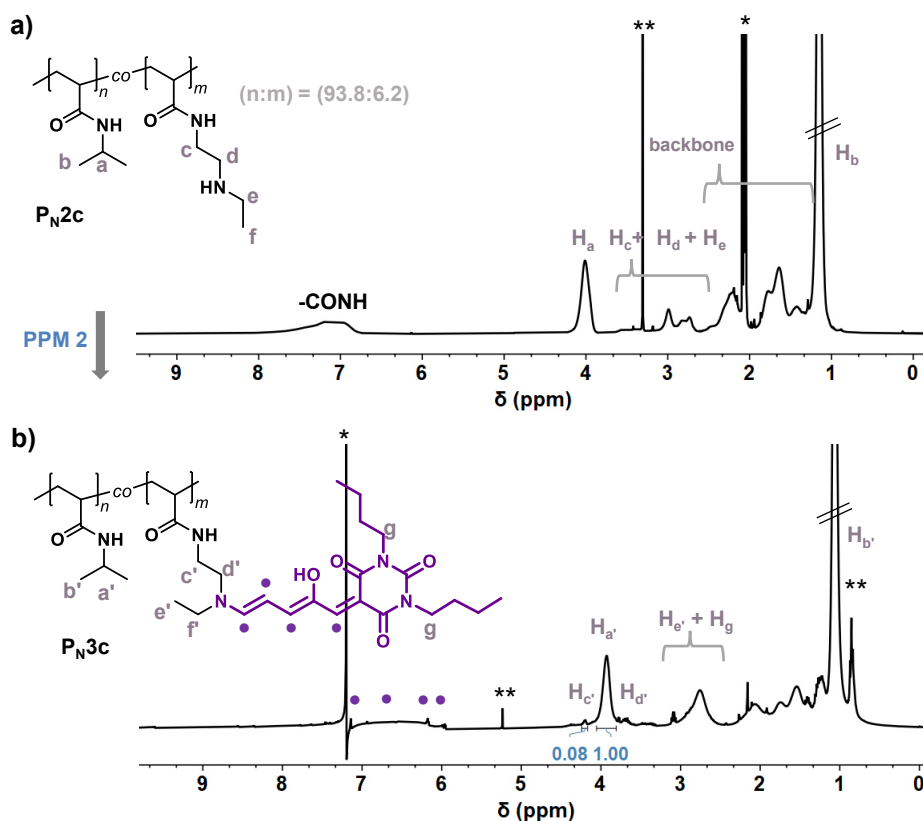
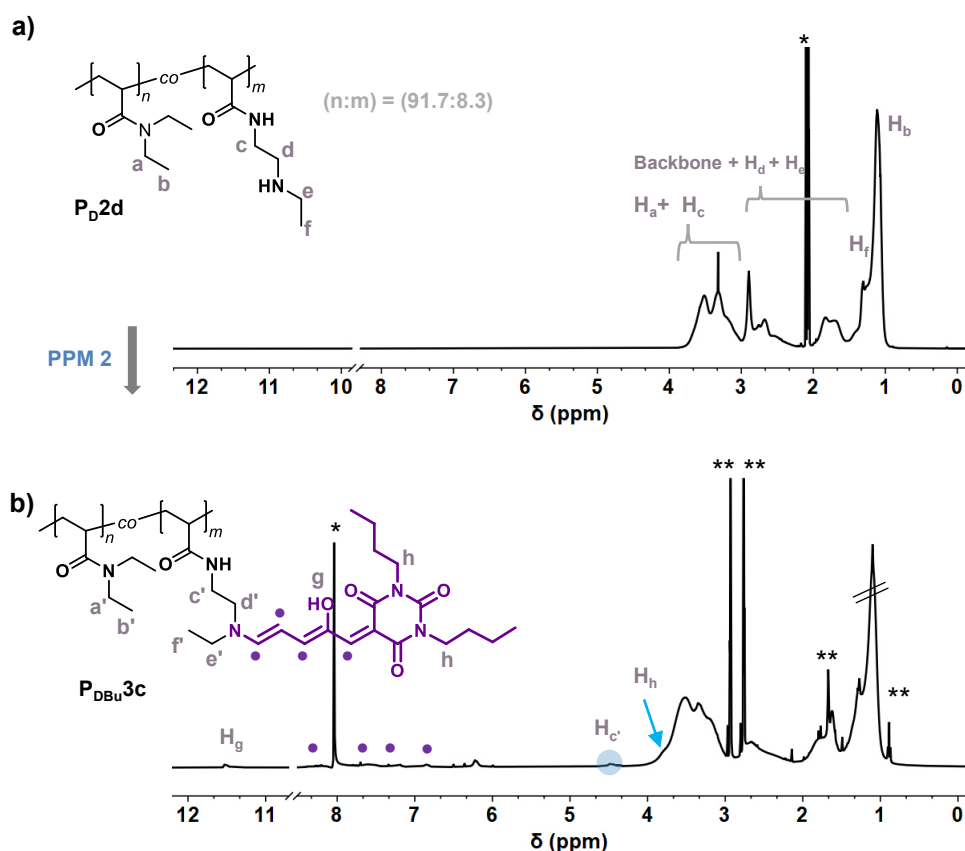


Figure 4.32.  $^1\text{H}$  NMR spectroscopy characterization of a)  $\text{P}_{\text{N}2\text{c}}$  dissolved in  $\text{DMSO-}d_6$  in comparison to b) sample  $\text{P}_{\text{N}3\text{d}}$  dissolved in chloroform- $d$  after DASA formation. \*calibration solvent \*\*solvent residue signal

Along with the NIPAM-based copolymer series  $\text{P}_{\text{N}3}$ , the corresponding  $\text{P}_{\text{D}3}$  library was also subjected to characterization using  $^1\text{H}$  NMR spectroscopy, as depicted in Figure 4.33. The successful formation of DASA was denoted by the presence of signals matching to the conjugated double bond system in the chemical shift region of 6.7–8.4 ppm, as well as the signal of the DASA hydroxyl group ( $\text{H}_{\text{g}}$ ) at 11.5 ppm. Additionally, the identification of a distinct peak at 4.5 ppm, belonging to the amine linker methylene protons ( $\text{H}_{\text{c}}$ ), was readily observable. However, the signal of  $\text{H}_{\text{h}}$  (DASA acceptor) was already overlapping. Note, that the proton NMR spectroscopy measurements were performed on samples that were dissolved in  $\text{DMF-}d_6$  due to the limited solubility of the  $\text{P}_{\text{DBu}3}$  series.

The inability to distinguish and integrate signals from the backbone and side groups in the DEA structure was attributed to their closely matched chemical shifts in NMR spectra. The quantification of the chromophore content by NMR was not achievable, thus requiring its evaluation through UV–vis spectroscopy. This observation was similar to the  $\text{P}_{\text{DMc}3}$  series, where NMR spectra entirely varied in the position of  $\text{H}_{\text{h}}$ , which exhibited total overlap.

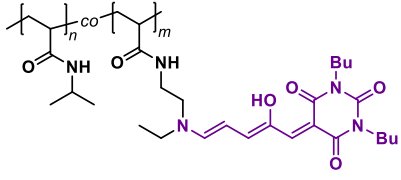
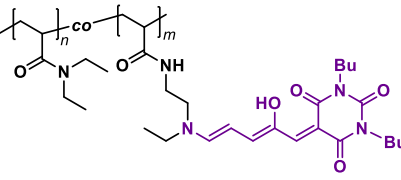
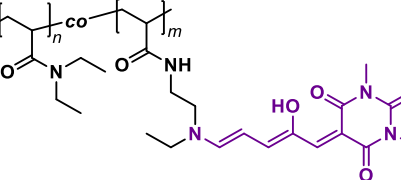


**Figure 4.33.**  $^1\text{H}$  NMR spectroscopy characterization of **a)**  $\text{P}_{\text{D}2\text{c}}$  solved in acetone- $d_6$  in comparison to **b)**  $\text{P}_{\text{DBu}3\text{c}}$  dissolved in  $\text{DMF}-d_6$  after DASA formation and sample purification. \*calibration solvent \*\*solvent residue signal

To sum up, the successful treatment of the DEA and NIPAM amine side groups with barbituric precursors was proved by using  $^1\text{H}$  NMR spectroscopy. Following the explained general calculation, the amount of incorporated DASA was determined for  $\text{P}_{\text{N}3\text{b}}$  and  $\text{P}_{\text{N}3\text{c}}$  by integration of one methylene proton signal corresponding to the amine linker group and the NIPAM amide proton (Table 4.5). Additionally, the expected DASA amounts  $X_{ij}$  (based on DEA/NIPAM and **M2** weights) and the estimated amine linker contents  $X_{\text{EDA}}$  are summarized. For the DASA mol% estimation  $X_{\text{DASA}}$ , a linear regression of DASA content *vs.* UV-vis absorption took place, which is explained below.

The dye contents were also estimated *via* UV-vis absorption measurements. Using a linear correlation between absorbance intensity and DASA content, a linear regression offers access to chromophoric content calculations. Therefore, the absorbance maxima of the non-polymeric DASA sample **S8** and the copolymers  $\text{P}_{\text{N}3\text{d}}/\text{P}_{\text{DBu}3\text{d}}$  in dry THF were compared, and they were found to be closely aligned with  $\lambda_{\text{max}} = 570$  nm. The UV-vis spectra of various sample concentrations of **S8** were measured to generate a concentration *vs.* absorbance plot (Figure 4.34c, left).

**Table 4.5.** Comparison between theoretical DASA amount, amine linker content and estimated DASA mol% moiety via  $^1\text{H}$  NMR and quantitative UV-vis analysis for the **P<sub>N</sub>3**, **P<sub>DBu</sub>3** and **P<sub>DMe</sub>3**.

Structure	Sample	$X_{ij}^1$ (mol%)	$X_{EEDA}^2$ (mol%)	$X_{DASA}^3$ (mol%)	$X_{DASA}^4$ (mol%)
	<b>P<sub>N</sub>3a</b>	2	2.1	—	1.3
	<b>P<sub>N</sub>3b</b>	4	4.2	2.3*	3.1
	<b>P<sub>N</sub>3c</b>	6	6.5	3.9*	4.9
	<b>P<sub>N</sub>3d</b>	8	8.5	—	7.7
	<b>P<sub>N</sub>3e</b>	10	10.3	—	11.3
	<b>P<sub>N</sub>3f</b>	12	12.0	—	12.5
	<b>P<sub>DBu</sub>3a</b>	2	1.8	—	1.5
	<b>P<sub>DBu</sub>3b</b>	4	3.9	—	3.2
	<b>P<sub>DBu</sub>3c</b>	6	6.5	—	6.3
	<b>P<sub>DBu</sub>3d</b>	8	9.1	—	8.3
	<b>P<sub>DBu</sub>3e</b>	10	10.2	—	9.5
	<b>P<sub>DBu</sub>3f</b>	12	12.1	—	12.6
	<b>P<sub>DMe</sub>3a</b>	2	2.3	—	1.3
	<b>P<sub>DMe</sub>3b</b>	4	4.2	—	3.7
	<b>P<sub>DMe</sub>3c</b>	6	6.5	—	5.8
	<b>P<sub>DMe</sub>3d</b>	8	8.1	—	7.3
	<b>P<sub>DMe</sub>3e</b>	10	9.9	—	10.2
	<b>P<sub>DMe</sub>3f</b>	12	11.6	—	11.8

<sup>1</sup>theoretical DASA content with respect to the used mol ratios of DEA/NIPAM and M2 monomers for the free-radical polymerization.

<sup>2</sup>determined amine linker amount by  $^1\text{H}$  NMR with the assumption  $X_{M2} = X_{EEDA}$ . The calculated values of  $X_{M2}$  were taken from Table 4.4.

<sup>3</sup>determined by  $^1\text{H}$  NMR integration with \*Measured in  $\text{CDCl}_3$ .

<sup>4</sup>determined by UV-vis measurement through calibration.

A linear regression analysis was performed to determine the relationship

$$A = 0.0432 + 0.1074 \cdot c_{S8} \quad (4.13)$$

between the absorbance  $A$  and the concentration  $c_{S8}$  of **S8**.

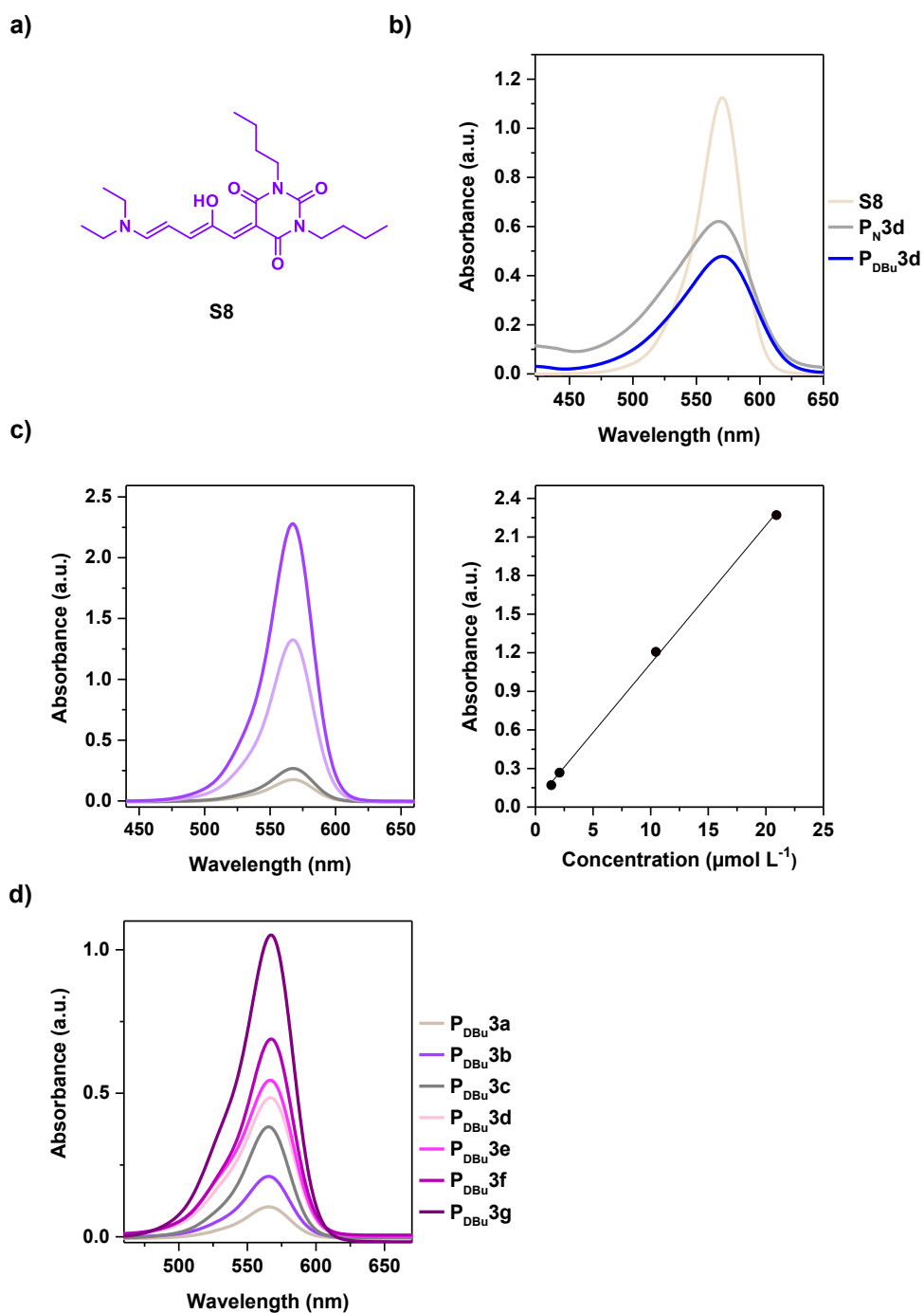


**Figure 4.34.** UV-vis calibration board. **a)** Sample **S8** structure. **b)** Absorbance maxima comparison of **S8**, **P<sub>N</sub>3d** and **P<sub>DBu</sub>3d** ( $\lambda = 570$  nm), measured in dry chloroform. **c)** Measured UV-vis spectra of **S8** (left) and corresponding linear regression fit with  $R^2 = 0.999$  (right). **d)** UV-vis absorbance measurements of the **P<sub>DBu</sub>3** series.

With the assumption that the intensities of the absorbance from **S8** and the DASA content in **P<sub>N3</sub>/P<sub>DBU3</sub>** and **P<sub>DMe3</sub>** were the same, the DASA content  $X_{\text{DASA}}$  of the copolymers were calculated using Equation 4.14.

$$X_{\text{DASA}} = \frac{C_{\text{DASA}}}{C_{\text{DASA}} + \frac{C_{\text{PN3/PDBU3/PDME3}} - M_{\text{DASA}} \cdot C_{\text{DASA}}}{M_{\text{DEA/NIPAAm}}}} \quad (4.14)$$

The Equation (4.14) resulted from the same assumptions and variables as already explained in detail in Section 4.1.1 for the PMMA-based copolymer series. The obtained  $X_{\text{DASA}}$  values derived from the corresponding UV-vis spectra of the dissolved copolymer sample as illustrated for the **P<sub>DBU3</sub>** series as an example in Figure 4.34d. The calculated  $X_{\text{DASA}}$  mol% fractions are summarized in Table 4.5. Supplementary data, such as maximum absorbance values, can be found in appendix A.3.

The ring-opening mechanism of barbituric acid furan derivatives with secondary amines proved favorable due to the ease of monitoring and conversion. In addition, the reaction displayed selectivity and achieved almost full conversion, making it very suitable for post-polymerization modifications under mild reaction conditions. To summarize, the synthetic strategy presented a method to create three different copolymer libraries that demonstrate temperature responsiveness and include varying quantities of the DASA chromophore in the polymer side chain.

#### 4.2.2 Temperature and light responsiveness of DEA and NIPAM-DASA copolymers

Following the successful synthesis of the PDEA/PNIPAM-based copolymers including DASA side groups, a subsequent examination of the light-responsive properties was carried out. Effective adjustment of the LCST necessitated the consideration of the light-dependent characteristics of the DASA chromophore. Consequently, the UV-vis absorption of sample **P<sub>D</sub>3b** dissolved in water ( $6.0 \mu\text{mol L}^{-1}$ ) before and after irradiation was compared (Figure 4.35, blue arrow). The significant absorbance peak at 560 nm, which corresponded to the  $\pi$ - $\pi^*$  transition, decreased markedly after 40 min of irradiation (white bulb). This decrease was attributed to the bond breaking of the conjugated triene DASA structure (green) and simultaneous formation of the cyclopentenone (red) structure. Upon macroscopic observation, a decrease in the intensity of the solution color was noted, transitioning from a highly pink hue to a shade of rose. Besides the UV-vis absorption of sample **P<sub>D</sub>3b** dissolved in DCM (purple curved;  $0.5 \text{ mg ml}^{-1}$ ) revealed a bathochromical shift of the absorption maxima by 10 nm. The **P<sub>N</sub>3** and **P<sub>D</sub>3** copolymer series were further subjected to LCST investigations before and after visible light irradiation. In general, the zwitterionic cyclopentenone, as compared to the brightly colored triene DASA nature, exhibited an increase in the polymer solubility after light exposure.

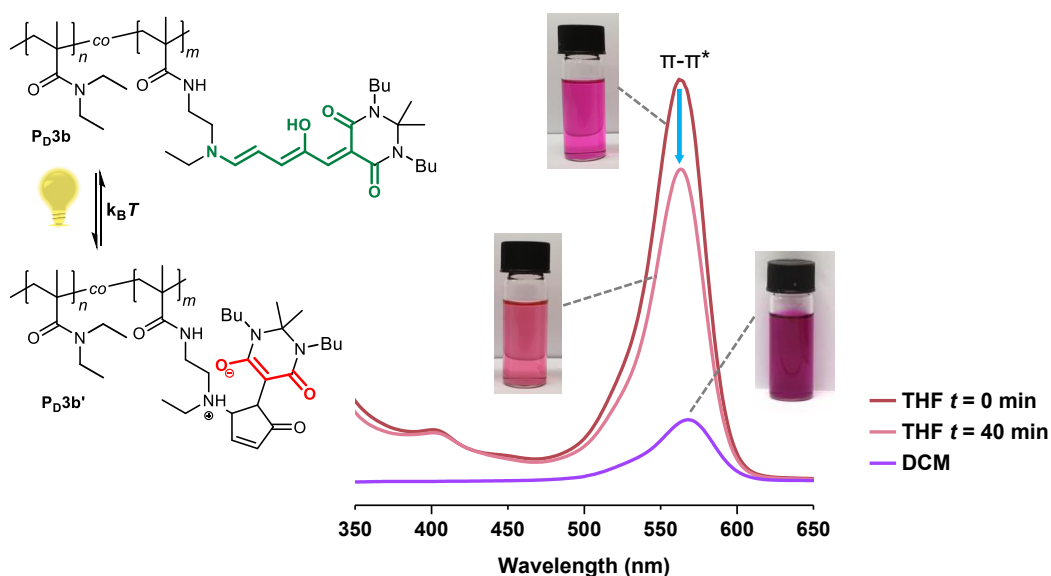


**Figure 4.35.** Absorption efforts of sample **P<sub>D</sub>3b** (butyl-Barbituric acid based) dissolved in DCM and THF before and after 40 min light-irradiation.

Consequently, the LCSTs of all copolymers displayed a noticeable upward shift, with  $T_2 > T_1$  (Figure 4.36). All LCST were determined by turbidimetry as the cloud point temperature  $T_{CP}$ . Thus, the optical transmittance of a light beam with a wavelength of  $\lambda = 700 \text{ nm}$  through the

sample cell of the photospectrometer was detected as a function of temperature. The copolymer solutions were prepared with a concentration of  $1.5 \text{ mg mL}^{-1}$  in Millipore water containing  $1 \text{ M NaCl}$ . The observed cloud points were not influenced by the relatively modest proportion of salt.

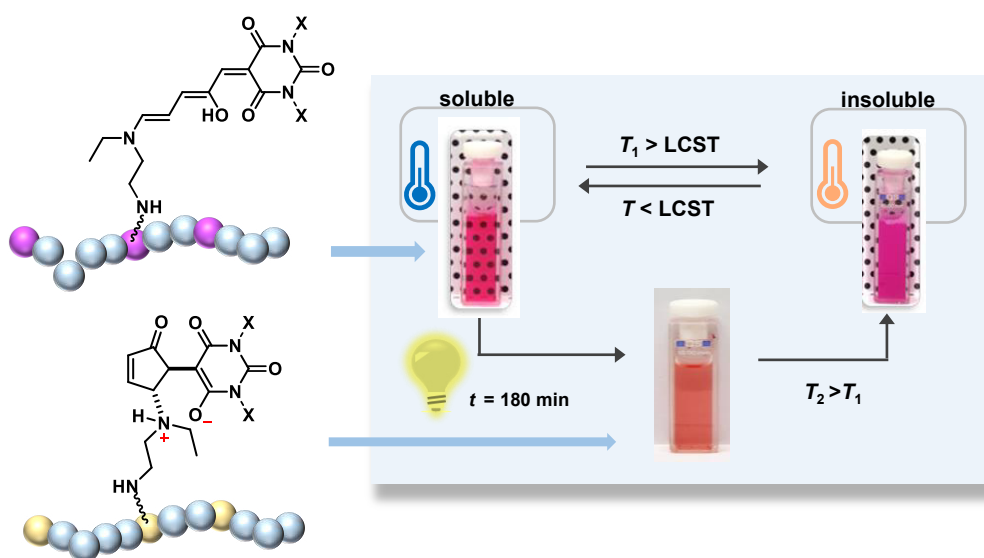


**Figure 4.36.** Schematic overview of the visible light ( $\lambda = 520 \text{ nm}$ ) induced LCST shift of PNIPAM/PDEA-DASA polymer conjugates dissolved in aqueous solution ( $1 \text{ mg mL}^{-1}$ ). The photoswitching phenomenon shown by the DASA chromophore led to the formation of a zwitterionic structure. The solubility of the polymer exhibited a rise, leading to the occurrence of a phase transition at temperature  $T_2$  that surpassed  $T_1$ .

The cloud point was operationally defined as the temperature at which a transmittance of 50% was recorded. Initially, a comparative analysis took place on the phase transition behavior of the NIPAM based **P<sub>N</sub>3** series prior to light exposure (Figure 4.37a). Likewise, a homogenous PNIPAM solution ( $M_n = 40500 \text{ g mol}^{-1}$ ;  $D = 2.7$ ) was measured under identical experimental conditions. While the latter demonstrated a phase transition of  $T_{CP} = 35.6 \text{ }^\circ\text{C}$ , all **P<sub>N</sub>3** samples displayed even lower values (Figure 4.37b-d). The LCSTs exhibited a significant reliance upon the content of incorporated DASA chromophore. In broad terms, an increase in the mole fraction of DASA side groups within the copolymer was seen to result in a decrease of  $T_{CP}$ . The observed phenomenon was related to the inherent property of the colored Stenhouse compounds, which possessed a nonpolar structure leading to lower solubility in an aqueous medium. **P<sub>N</sub>3f** revealed a temperature that was approximately  $10 \text{ }^\circ\text{C}$  lower compared to the PNIPAM sample. Furthermore, the transmittance-temperature curves displayed a broadening course rather than a distinct phase change with increasing DASA content.

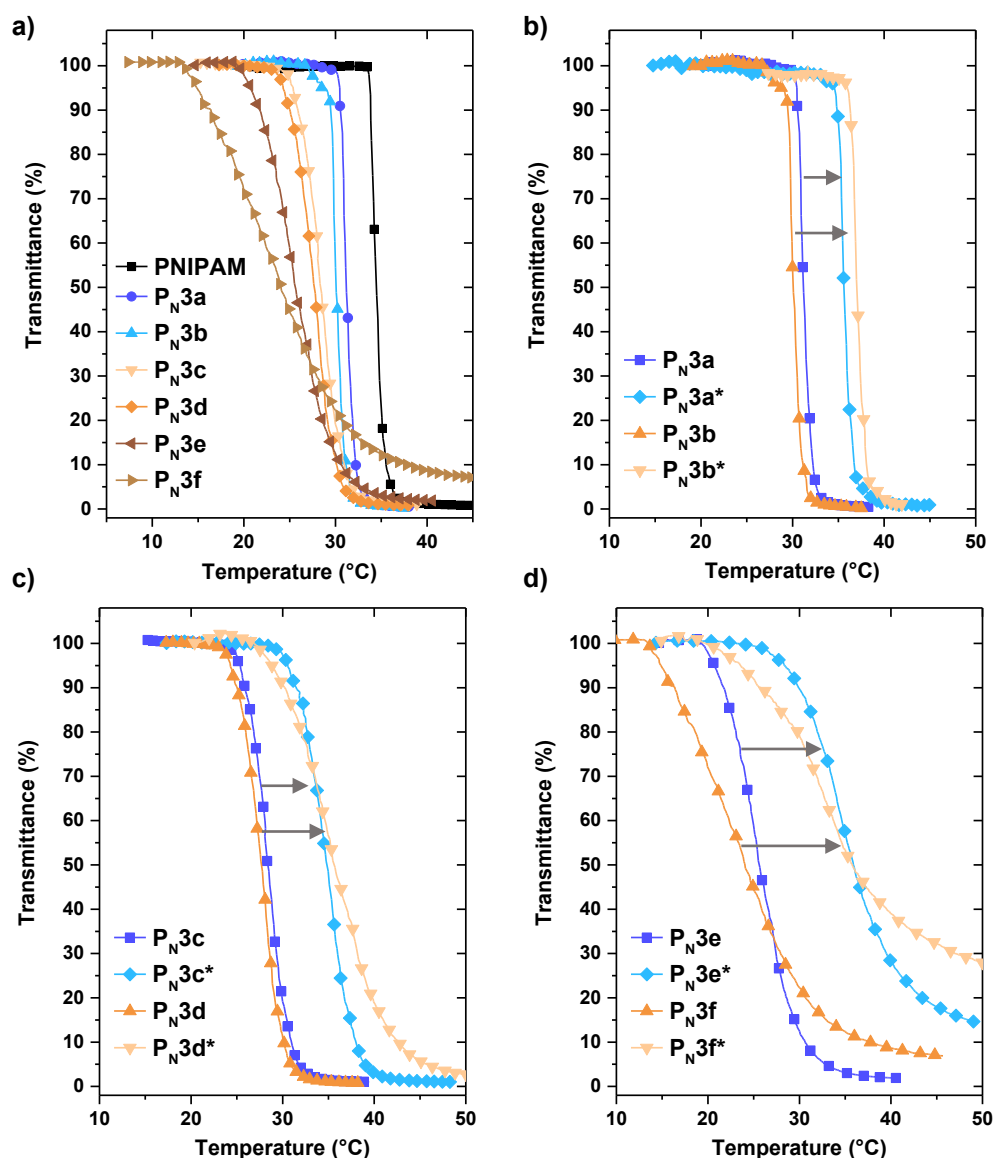


Figure 4.37. **a)** Turbidity curves of PNIPAM and  $P_{N3}a-f$  before light exposure. **b)**  $P_{N3}a+b$ , **c)**  $P_{N3}c+d$ , **d)**  $P_{N3}e+f$  after light exposure. All samples were measured while dissolved in an aqueous NaCl solution (1 M). \*After light exposure for at least 4 h by a clean 40 W light bulb.

Following the first turbidity measurements, the  $P_{N3}$  solutions were subsequently exposed to visible light emitted by a white light bulb for a minimum duration of 4 h. Afterwards, additional turbidity measurements were conducted before and after irradiation (Figure 4.37b-d) and the results of  $T_{CP}$  were compared (Table 4.6). The observed temperature shifts  $\Delta T_{CP}$  towards higher values were attributed to the polar nature of the cyclopentenone compound. Therefore, the presence of the DASA side group exerted an influence on the solubility of the copolymer, whereby an increase in the amount of integrated chromophore caused elevated  $\Delta T_{CP}$ . In the context of sample  $P_{N3}e$  and  $P_{N3}f$ , the phase transition curves demonstrated a partial full

solubility with a noted end transmission of 18/29%. This phenomenon was additionally observed for **P<sub>N</sub>3f** prior to exposure to light, which led to the assumption of uncontrolled switching mechanisms during the turbidity measurement for this particular sample.

**Table 4.6.** Determined  $T_{CP}$  for the PNIPAM-based **P<sub>N</sub>3** series before and after light induced DASA photoswitching.

Sample	$X_{DASA}$ (mol%) <sup>a</sup>	LCST before irradiation (°C)	LCST after irradiation (°C)	$\Delta$ LCST (°C)
<b>P<sub>N</sub>3a</b>	1.3	31.2	35.6	4.4
<b>P<sub>N</sub>3b</b>	3.1	29.9	35.9	5.9
<b>P<sub>N</sub>3c</b>	4.9	28.3	34.8	6.5
<b>P<sub>N</sub>3d</b>	7.7	27.1	35.8	8.7
<b>P<sub>N</sub>3e</b>	11.3	25.6	35.2	9.6
<b>P<sub>N</sub>3f</b>	12.5	24.1	35.7	11.6

<sup>a</sup>determined by UV-vis spectroscopy (Table 4.5)

Examining Figure 4.38 provided a more profound understanding of the impact of DASA incorporated side groups onto NIPAM based polymers. Prior to light irradiation, all **P<sub>N</sub>3** samples displayed an almost linear correlation, as illustrated by the grey dotted line. Hence, the incorporation of each expected 2 mol% DASA component led to a reduction of approximately 1.7 °C in the  $T_{CP}$  values.

Upon the transition from the colored structure to the non-colored DASA molecule, it was observed that all samples presented a LCST ( $T_{CP} \cong 35.5$  °C) similar to that of pure PNIPAM. The irradiation of light effectively nullified the impact of the side chain on LCST value, resulting in a binary-like system with an on-off behavior. However, in relation to the bar diagram (Figure 4.38b), the  $\Delta T_{CP}$  values were not consistently linearly dependent on the DASA content. As an example, the presence of 1.3% chromophore in sample **P<sub>N</sub>3a** caused a temperature shift of 4.4 °C, whereas sample **P<sub>N</sub>3c** exhibited  $\Delta T_{CP} \cong 6.5$  °C despite containing a higher concentration of 4.9% chromophore.

The polymer conjugates based on DEA were subjected to LCST examinations in a similar manner, consistent with the procedure previously reported for the **P<sub>N</sub>3** series. In contrast, the methyl-barbituric structure (**P<sub>DMe</sub>3**) was additionally studied alongside the buthyl-copolymers (**P<sub>DBu</sub>3**).

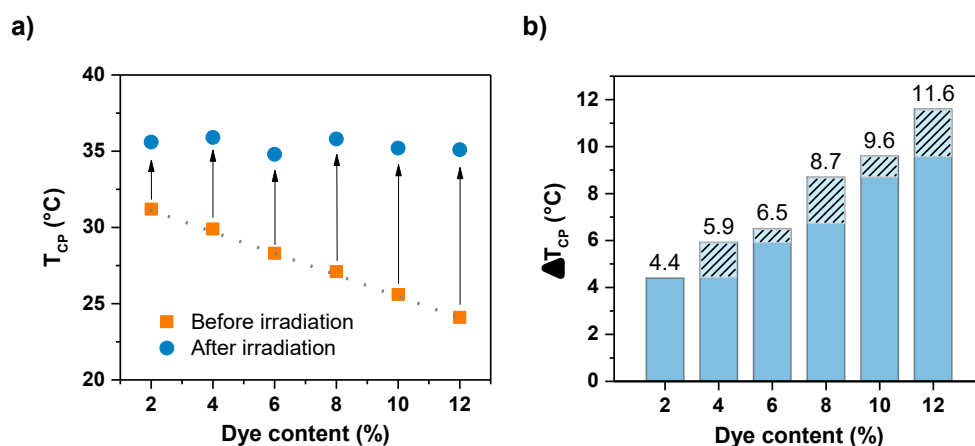


**Figure 4.38.** a) Cloud point temperatures of  $P_N3$  series before and after irradiation. The grey dotted line demonstrates the linear relationship of all  $T_{cp}$  before irradiation. b) Bar diagram of  $\Delta LCST$  ( $^{\circ}C$ ) and temperature difference from one  $T_{cp}$  to the next higher DASA content (dashed lines).

The turbidity curves of the  $P_{DMe}3$  series before irradiation with visible light are illustrated in Figure 4.39a. For the  $P_{DBu}3$  series, all turbidity curves are shown in Figure 4.40a. Overall, the copolymer conjugates exhibited similarities to the PNIPAM based series. In relation to the homogeneous PDEA ( $M_n = 42700 \text{ g mol}^{-1}$ ;  $D = 2.3$ ), each sample revealed a decrease in the cloud point as the concentration of the dye moiety increased.

For instance, the PDEA solution demonstrated a distinct phase transition at a temperature of  $37 \text{ }^{\circ}C$  when heated. Conversely, the samples of  $P_{DMe}3a$  (Figure 4.39a) and  $P_{DBu}3a$  (Figure 4.40a) displayed lower LCST values, specifically at temperatures of  $32.4 \text{ }^{\circ}C$  and  $30.3 \text{ }^{\circ}C$ , respectively. The  $P_{DBu}3$  series, characterized by the presence of a butyl group, showed a relatively less polar nature, resulting in lower LCST values when compared to the sample containing the methyl barbituric acid compound. Additionally, differences appeared in the curve shapes. The course of the curves pertaining to  $P_{DMe}3$  exhibited a higher degree of broadening. Furthermore, for the  $P_{DBu}3$  series, no end transmittance  $>0\%$  was observed. It is worth mentioning that the sample  $P_{DBu}3f$  (12.6 mol% DASA) displayed insolubility in water. Therefore, the turbidity curve was not recorded.

After conducting the turbidity measurements as specified, the  $P_D3$  solutions were next subjected to visible light exposure for a duration of 4 h. The resulting curves are depicted in Figure 4.39b-d ( $P_{DMe}3$ ) Figure 4.40b-d ( $P_{DBu}3$ ).

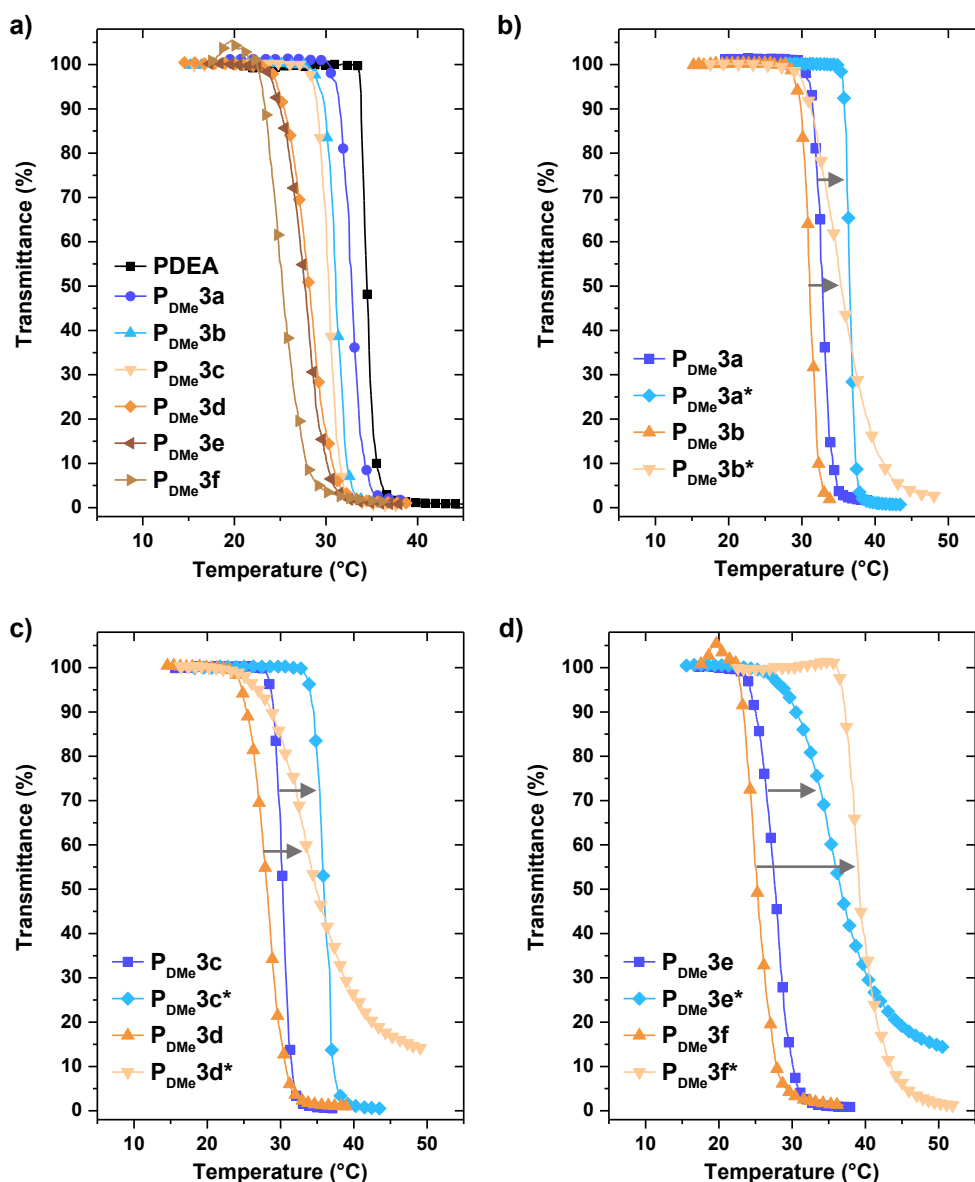


**Figure 4.39.** Turbidity curves of a) PDEA and  $P_{DMe}3$  series before irradiation. Turbidity curves of the samples b)  $P_{DMe}3a+b$ , c)  $P_{DMe}3c+d$ , d)  $P_{DMe}3e+f$  after light exposure. All samples were measured while dissolved in an aqueous NaCl solution. \*After light exposure for at least 4 h by a clean 40 W light bulb.

The LCST values obtained at a transmission of 50% and the calculated  $\Delta$ LCST are summarized in Table 4.7. In general, the  $\Delta$ LCST values of  $P_{DMe}3$  and  $P_{DBu}3$  exhibited similarity when considering the incorporation ratio of the DASA moiety. In the case of  $P_{DMe}3f$ , a significant temperature shift of 14.0 °C was recorded, providing evidence for the substantial impact of DASA isomerization mechanism on the behavior of the temperature-responsive polymer material.

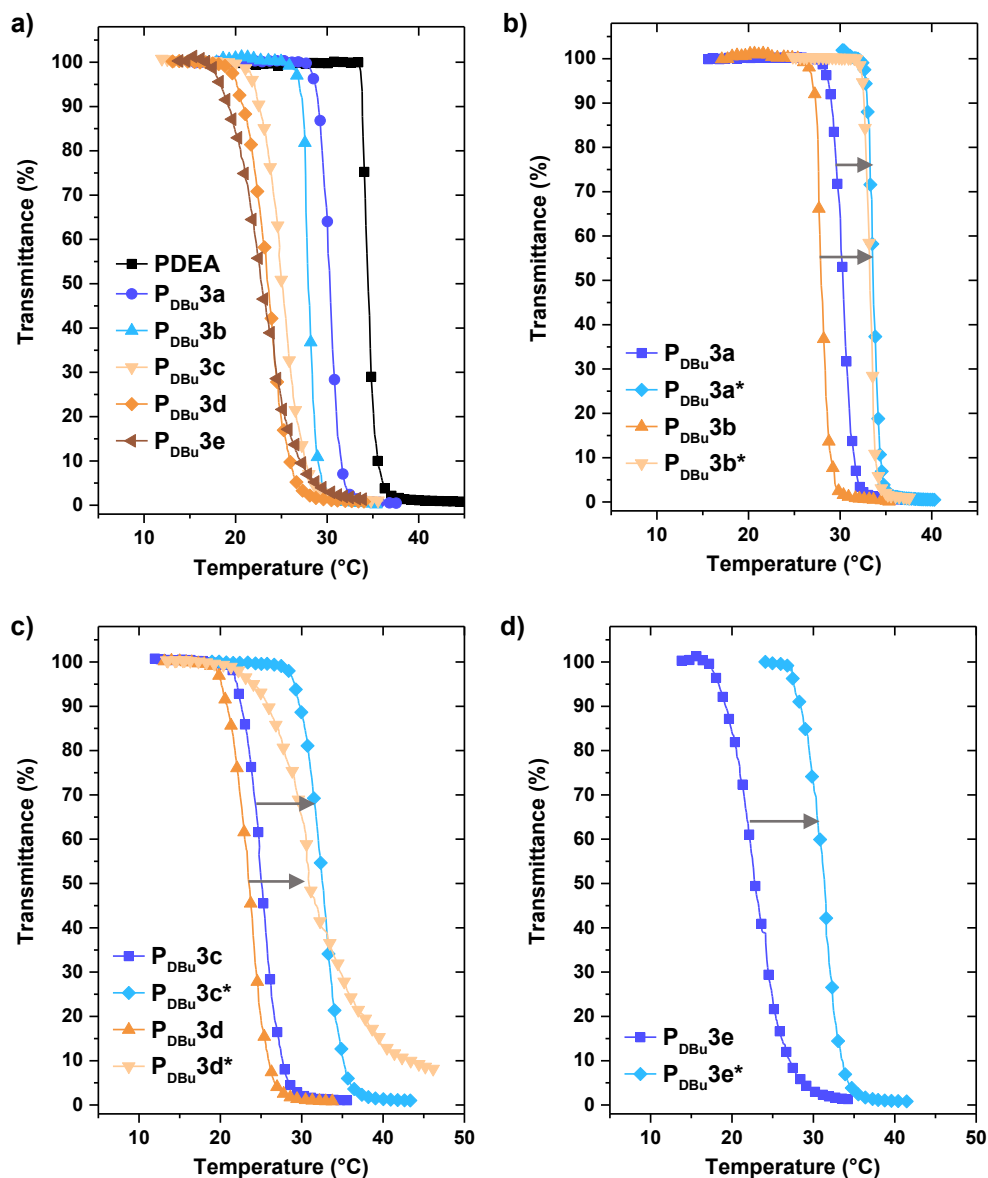


**Figure 4.40.** Turbidity curves of a) PDEA and P<sub>DBU</sub>3 series before irradiation. Turbidity curves of the samples b) P<sub>DBU</sub>3a+b, c) P<sub>DBU</sub>3c+d, d) P<sub>DBU</sub>3e after light exposure. All samples were measured while dissolved in an aqueous NaCl solution. \*After light exposure for at least 4 h by a clean 40 W light bulb.

The initial temperatures of P<sub>DMe</sub>3 indicated a nearly linear decline with increasing DASA content. In contrast to the PNIPAM based conjugates, which exhibited a consistent lower LCST of approximately 36 °C following irradiation, the cloud point of PDEA family displayed variation. The methyl series had an inclination towards increasing lower critical solution temperature (LCST) values following irradiation. In the butyl series, there is a modest drop in values observed as the dye concentration increases from sample P<sub>DBU</sub>3a (1.5%) to sample P<sub>DBU</sub>3e (9.5%).

**Table 4.7.** Determined LCST for the **P<sub>DBu</sub>3** and **P<sub>DMe</sub>3** series before and after light induced DASA photoswitching.

Polymer	$X_{\text{DASA}}$ (mol%) <sup>a</sup>	LCST before irradiation (°C)	LCST after irradiation (°C)	$\Delta$ LCST (°C)
<b>P<sub>DBu</sub>3a</b>	1.5	32.7	36.5	3.80
<b>P<sub>DBu</sub>3b</b>	3.2	31.0	35.8	4.80
<b>P<sub>DBu</sub>3c</b>	6.3	30.2	36.1	5.90
<b>P<sub>DBu</sub>3d</b>	8.3	28.3	36.9	8.60
<b>P<sub>DBu</sub>3e</b>	9.5	27.4	36.8	9.40
<b>P<sub>DBu</sub>3f</b>	12.6	25.2	39.2	14.0
<b>P<sub>DMe</sub>3a</b>	1.3	30.3	33.5	3.20
<b>P<sub>DMe</sub>3b</b>	3.7	27.9	33.9	6.00
<b>P<sub>DMe</sub>3c</b>	5.8	25.0	32.6	7.60
<b>P<sub>DMe</sub>3d</b>	7.3	23.3	31.9	8.60
<b>P<sub>DMe</sub>3e</b>	10.2	22.6	31.8	9.20

<sup>a</sup>determined by UV-vis spectroscopy (Table 4.5)

Figure 4.41 depicts a bar diagram that visually represents the similarity between the shifts in  $\Delta$ LCST seen in the methyl and butyl samples. Furthermore, it was evident that the progression from lower dye level to higher dye content is non-linear, as indicated by the uneven heights of the bars. In brief, the manipulation of acceptor side groups presents an opportunity to expand the spectrum of lower critical solution temperature (LCST) values, hence enabling a broader range of control over  $\Delta$ LCST changes.

To summary, all temperature-responsive copolymers exhibited a LCST behavior, which was significantly influenced by the incorporation of DASA side groups. The samples demonstrated a nearly linear dependency between the quantity of incorporated DASA and the LCST change following exposure to visible light (white bulb) for a duration of 4 h. Therefore, the phase-transitions were shifted towards higher values as a result of the increased solubility generated by the zwitterionic DASA structure. The sample, which consisted of a copolymer based on NIPAM and contained 10 mol% DASA, exhibited the greatest increase in  $\Delta$ LCST of 9.2 °C. The largest recorded increase in  $\Delta$ LCST for DEA-based copolymers was 14 °C, seen in a sample **P<sub>DBu</sub>f** containing 12.6 mol% of DASA.

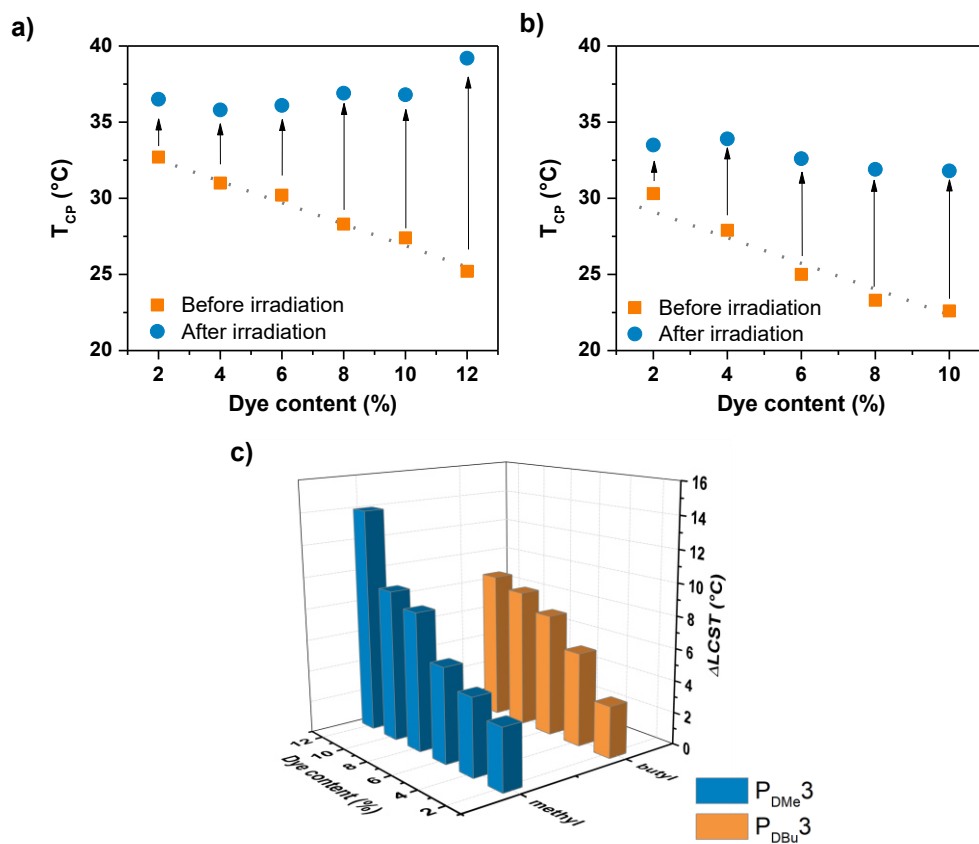


**Figure 4.41.** The linear correlation between the LCST values before and after irradiation is examined for a) P<sub>DME3</sub> series and b) P<sub>DBu3</sub> series and c) comparison of the  $\Delta LCST$ .

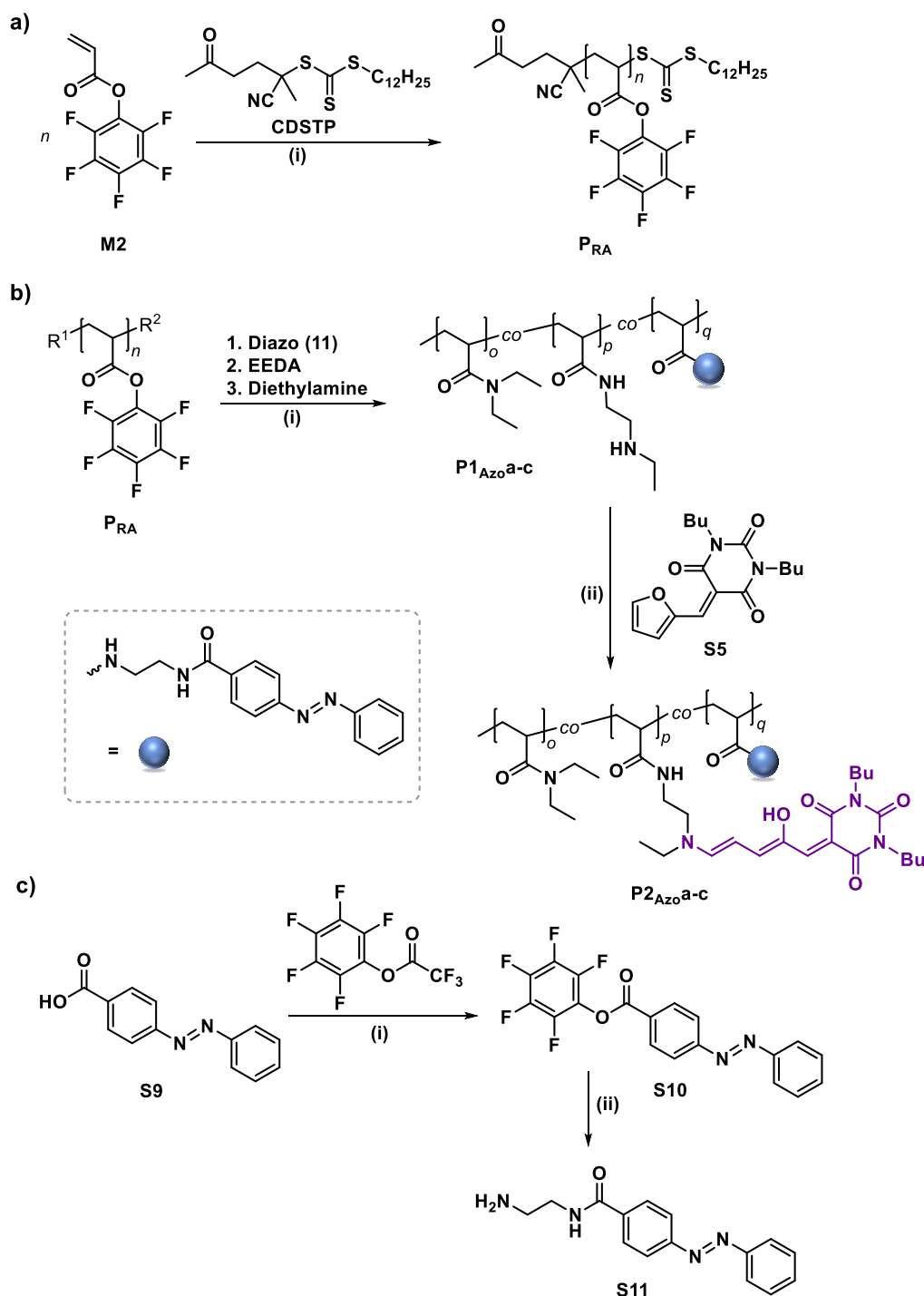
### 4.3 Orthogonal photoswitching copolymer systems

The preceding sections offer a comprehensive examination of the successful studies committed on dual temperature and light responsiveness. To broaden the scope of this work, more attention was dedicated to the photoswitching potential. This feature garnered significant interest due to its capacity of providing orthogonal light addressing. In the present context, orthogonality refers to the property of a polymer network exhibiting LCST behavior and being composed of at least two chromophoric units. The latter facilitated the ability of their simultaneous and independent activation at distinct wavelengths. In 2018, Lerch *et al.* impressively highlighted separate absorption peaks in a low molecular weight system utilizing DASA and azobenzene chromophores, as observed through UV-vis monitoring (Section 2.3.3).<sup>201</sup> Motivated by these results, the scope of the current work was widened to encompass a polymer matrix based on PDEA, incorporating DASA and azobenzene side chains.

The subsequent sections present a comprehensive account of the outcomes obtained from the synthesis of PDEA-DASA-Azo polymer conjugates, encompassing a thorough characterization of the materials. Subsequently, the cloud points prior to and after to light exposure are presented and discussed.

#### 4.3.1 Synthesis of PDEA-DASA-Azo polymer conjugates

To improve a comparative analysis of stimuli-responsive polymer systems featuring two distinct chromophores, the decision was made to synthesize the respective materials by a sequential post-polymerization process of a precursor polymer  $\mathbf{P}_{\text{RA}}$  (Scheme 4.7a). Such procedure facilitated the introduction of functional groups, while preserving the unaltered degree of polymerization and molecular masses distribution. Consequently, monomer  $\mathbf{M2}$  was exposed to a RAFT polymerization using AIBN as radical initiator and 4-cyano-4-[(dodecyl-sulfanylthiocarbonyl)sulfanyl]pentanoic acid (CDSTP) as chain transfer agent (CTA) with a feed ratio of [PFPA]:[CDSTP]:[AIBN] = 100:1:0.1. The reaction was proceeded in anhydrous THF for a duration time of 19 h at a constant temperature of 70 °C. Analysis of the reaction mixture *via*  $^1\text{H}$  NMR spectroscopy revealed a quantitative conversion. The pure product was isolated through participation in methanol and full characterized by  $^1\text{H}$  NMR and FT-IR spectroscopy which was in close agreement with the literature.<sup>202</sup> The precursor  $\mathbf{P}_{\text{RA}}$  was further subjected to a first polymer analogous reaction (PPM 1) in a one-pot synthesis with different amounts of the amino functionalized (*E*)-*N*-(2-aminoethyl)-4-(phenyldiazenyl)benzamide ( $\mathbf{S11}$ ), EEDA and TEA (Scheme 4.7b). The synthesis of  $\mathbf{S11}$  was adapted from existing literature and successfully carried out by a three-step process (Scheme 4.7c).<sup>162</sup>



**Scheme 4.7.** Synthesis pathway of **P2<sub>Azo a-c</sub>**. **a)** RAFT polymerization of monomer **M2**. Reaction conditions: **(i)** 1,4-dioxane, 75 °C, 19 h. **b)** PPM 1: Treatment of **P<sub>RA</sub>** with **S11**, EEDA and TEA; PPM 2: DASA formation through PPM 2 with barbituric acid precursor **S5**. Reaction conditions: **(i)** THF, rt, 7d; **(ii)** THF, 5d. **c)** Synthesis of (*E*)-*N*-(2-aminoethyl)-4-(phenyldiazenyl)benzamide (**S11**). Reaction conditions: **(i)** Dry THF, rt, 2.4 h; **(ii)** Ethan-1,2-diamin, dry THF, 2.5 h.

The initial step involved the addition of nitrobenzene and 4-aminobenzoic acid to yield the diazo compound (*E*)-4-(phenyldiazenyl)benzoic acid (**S9**) as described in the literature<sup>203</sup>. Subsequently, **S9** underwent esterification using pentafluorophenyl trifluoroacetate to produce pentafluorophenyl (*E*)-4-(phenyldiazenyl)-benzoate (**S10**). In the last step, an amidation reaction of **S10** occurred, using ethan-1,2-diamine, resulting in an overall yield of 31% after three steps. Using the diazo **S11** substance, the PPM 1 reaction proceeded. Due to the higher reactivity of primary amines in relation to secondary amines, a mixture of **S11** and the amine precursor EEDA were added first to a solution of **P<sub>RA</sub>** dissolved in THF, respectively. After a reaction time of 6 h at room temperature, the remaining PFP ester groups were converted with an excess of diethylamine to yield the **P1<sub>Azo</sub>** series with different amounts of DASA and azo side groups. All **P1<sub>Azo</sub>** samples were purified by dialysis in acetone for 15 d using a membrane with a MWCO of 1000 g mol<sup>-1</sup> and analyzed by FT-IR, NMR, UV-vis spectroscopy and SEC measurements. A notable change in the molecular masses was seen in the SEC traces (Figure 4.42) of the samples **P<sub>RA</sub>** (before first post-polymerization modification) and **P1<sub>Azo</sub>a** (after PPM 1) following pentafluorophenol substitution using DEA, EEDA, and **S11**. Therefore, the theoretical Number-average molar mass  $\bar{M}_n$  was determined to be around 24,000 g mol<sup>-1</sup>. Specifically,  $\bar{M}_n$  decreased from = 24800 g mol<sup>-1</sup> ( $\mathcal{D}$  = 1.5) to  $\bar{M}_n$  = 12100 g mol<sup>-1</sup> ( $\mathcal{D}$  = 2.0).

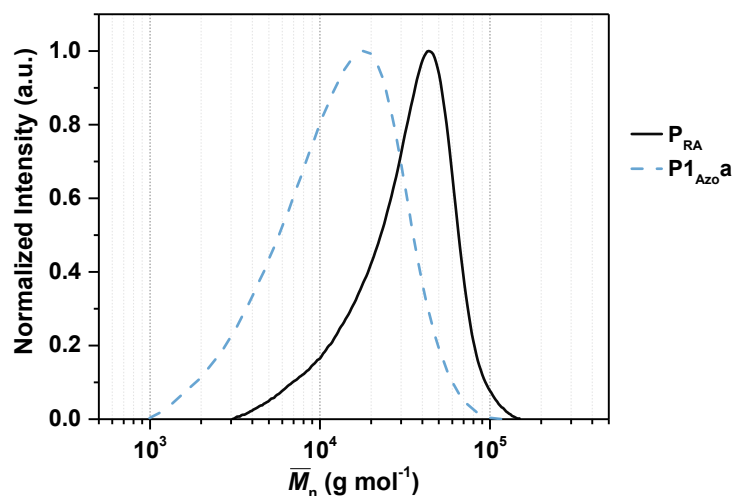


**Figure 4.42.** SEC traces of **P<sub>RA</sub>** and **P1<sub>Azo</sub>a** measured in DMF. All data were determined relative to a linear PS standard.

Complete conversion was quantified by monitoring the full disappearance of the PFP ester C=O<sub>stretch</sub>-vibration band at  $\bar{\nu}$  = 1780 cm<sup>-1</sup> and 1800 cm<sup>-1</sup> in the FT-IR spectrum of **P1<sub>Azo</sub>c** as an example (Figure 4.43). Additionally, the appearance of N-H<sub>stretch</sub>-vibration at 3400 cm<sup>-1</sup> and C=O<sub>stretch</sub>-vibration of the amides at 1650 cm<sup>-1</sup> confirmed the successful formation of amino and amide side group. Moreover, the <sup>1</sup>H NMR spectrum revealed the corresponding aromatic protons for signal integration and estimation of the aovenzene content (Figure 4.44b).

In order to achieve the copolymer series **P2<sub>Azo</sub>a-c**, which consisted of Azo and DASA moieties, the furan precursor **S5** was employed to convert the remaining EEDA amine linker by the

PPM 2 reaction. Consequently, all  $\mathbf{P1}_{\text{Azo}}$  samples were dissolved in anhydrous THF, respectively, and subjected to continuous stirring for a duration of 5 d at a constant room temperature. The complete transformation was monitored utilizing UV-vis spectroscopy, as previously detailed in the prior chapters. The purple-colored products were isolated after dialysis for 4 d in dichloromethane using a membrane with a MWCO of 1500 g mol<sup>-1</sup>.

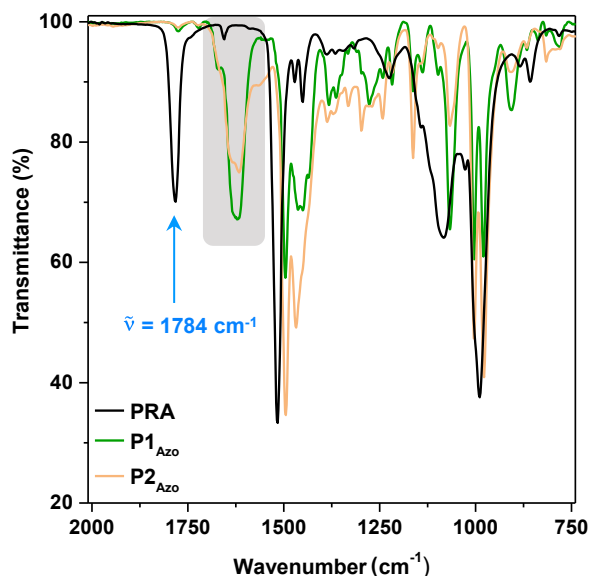


**Figure 4.43.** FT-IR spectra of the precursor polymer  $\mathbf{P}_{\text{RA}}$  in comparison to the sample after the first post-polymerization reaction  $\mathbf{P1}_{\text{Azo}}$  and the second post-polymerization sample  $\mathbf{P2}_{\text{Azo}}$ .

The evidence of the synthesis of  $\mathbf{P2}_{\text{Azo}}$  samples was verified through the allocation of <sup>1</sup>H NMR spectra signals, as illustrated in Figure 4.44c.

For example, the <sup>1</sup>H NMR spectrum of the copolymer  $\mathbf{P2}_{\text{Azo}}$  showed the characteristic signals attributed to the PDEA backbone (in acetone-d:  $\delta/\text{ppm}$ : 1.50-3.50), as well as signals originating from the side group at 1.05 ppm ( $H_b$ ) and 3.28 ppm ( $H_a$ ). Moreover, the presence of the azobenzene group was established based on the detection of signals from  $H_g/H_h$  within the chemical shift range of 7.20-8.15 ppm. The determination of the degree of substitution for the azobenzene chromophore was conducted by integrating the signals of  $H_a$  and  $H_f$ . The successful synthesis of the DASA side group was demonstrated through the identification of the double bond protons (in CDCl<sub>3</sub>:  $\delta/\text{ppm}$ : 6.58-7.60; purple dots). In addition, a downfield shifted signal of the methylene protons  $H_{c'}$  at 4.48 ppm was found. The DASA content was estimated by comparing its integrated double bond with the aromatic signals of the azobenzene group (Figure 4.44c). The computed copolymer compositions are provided in Table 4.8.

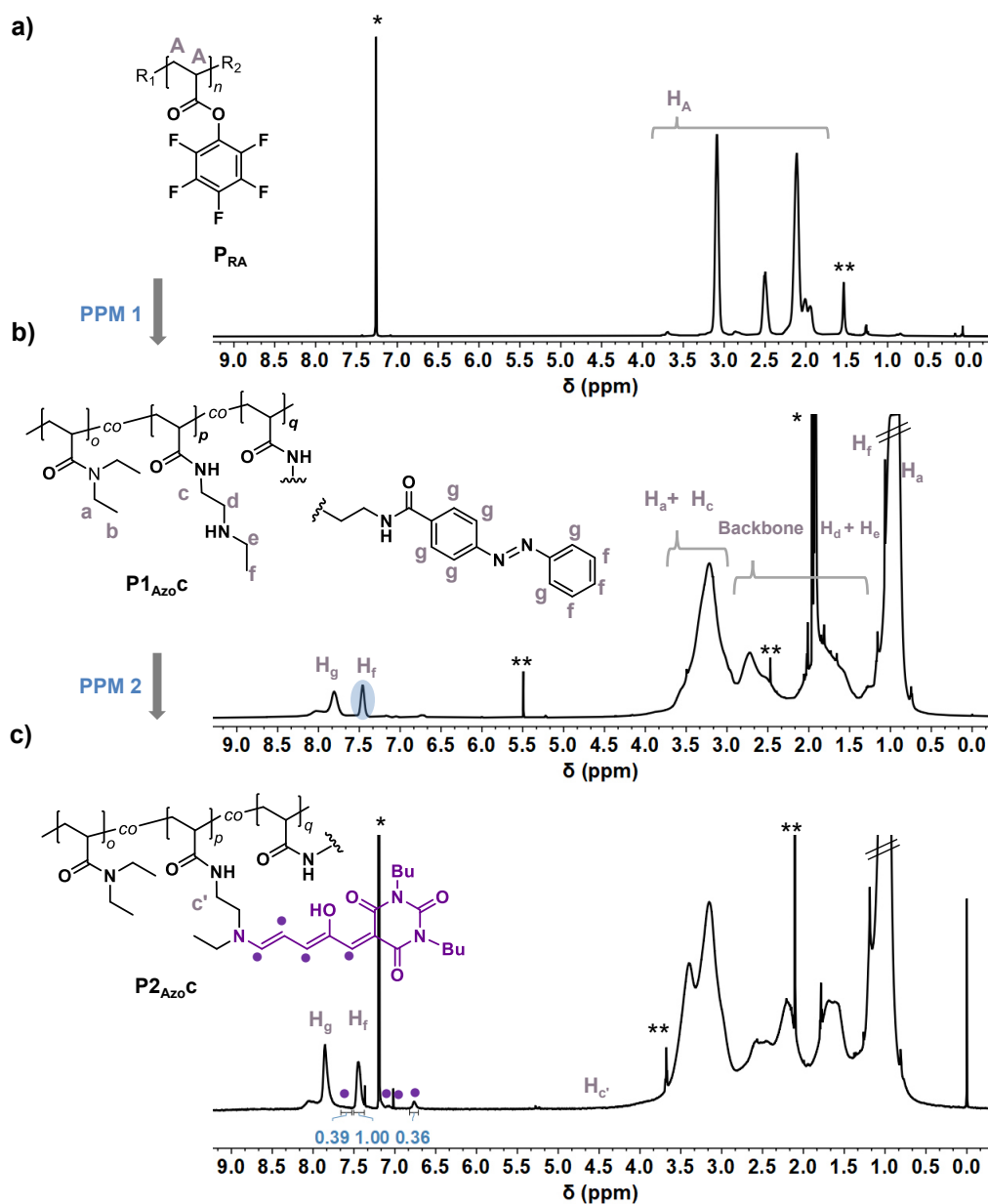


**Figure 4.44.**  $^1\text{H}$  NMR spectroscopy characterization of a)  $\text{P}_{\text{RA}}$  dissolved in  $\text{DMSO}-d_6$  b) Sample  $\text{P1}_{\text{AzoC}}$  after first post-polymerization modification dissolved in  $\text{acetone}-d_6$  and c) Sample  $\text{P2}_{\text{AzoC}}$  after second post-polymerization modification dissolved in  $\text{chloroform}-d$  with two chromophoric structures:  $\text{DASA}$  and  $\text{S11}$ . \*\*signals originating from reaction solvent residue

As an illustration, the signal integration of the double bond protons (purple dots) and  $\text{H}_f$  revealed a  $\text{DASA}$  content of 4.5 mol% for the sample  $\text{P2}_{\text{AzoC}}$ . Noteworthy, the ratio of chromophores was mutually defined. The estimate did not consider the polymer backbone.



### 4.3.2 Temperature and light responsiveness of DEA-DASA-Azobenzene conjugates

The synthesized **P2<sub>Azo</sub>** series was employed to examine its responsive behavior to temperature and light. Lerch *et al.* demonstrated the successful reversible orthogonality of DASA and azobenzene components in a low molecular mass inter- and intramolecular system. The great photoswitching efficiency observed in this system was owing to spectral areas characterized by substantial disparities. The present investigation involved the intentional choice of the azobenzene molecule **S11** and a barbituric acid based Stenhouse adduct as side groups in a PDEA-based polymer system for the purpose of irradiating them at different wavelengths.

Upon analyzing the absorbance curves of the chromophores in the UV-vis spectra before any exposure to light, the following observation was made: The DASA compound **S8** showed limited absorption characteristics between the wavelengths of 200 to 500 nm (Figure 4.45a), with the solvent utilized affecting the degree of absorption.

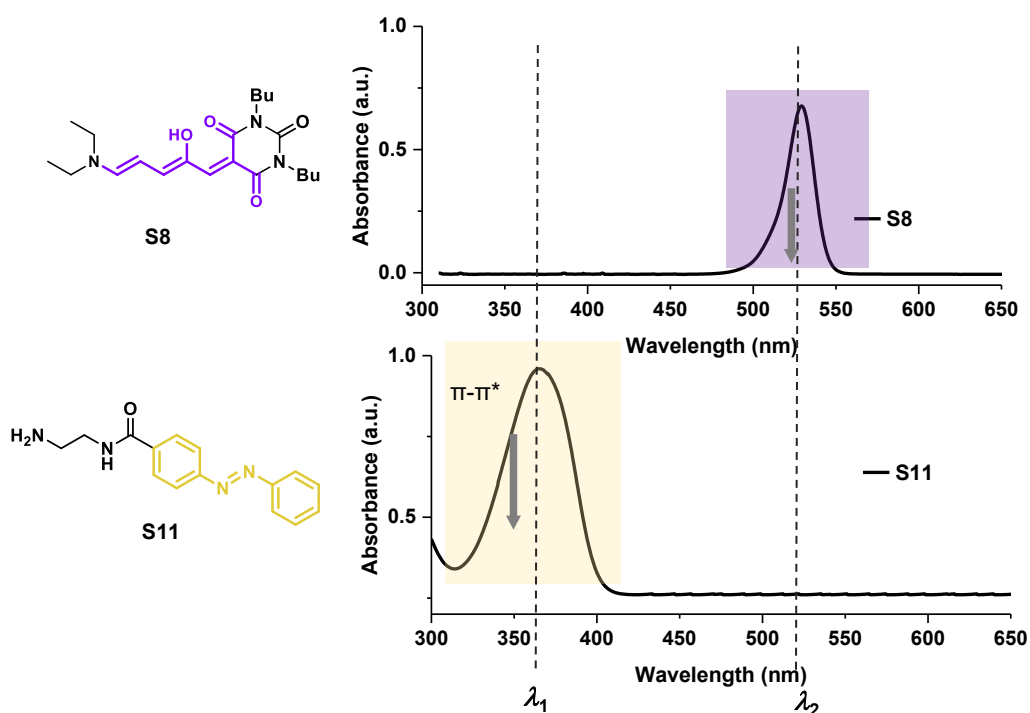


**Figure 4.45.** Comparison of the UV-vis spectra of a) barbituric acid based DASA **S8** and b) azobenzene derivative **S11**.

The most significant amount of absorbance was recorded in the visible light region at  $\lambda_2 = 545$  nm. The highest level of absorbance for **S11** was seen at  $\lambda_1 = 360$  nm, which corresponded to the  $\pi$ - $\pi^*$  transition of the *trans*-configuration (Figure 4.45b). Hence, the chosen chromophores

had the potential to serve as a complimentary class. In relation to this study, it was hypothesized that the key feature of the chromophores, which undergo a transition from nonpolar to polar polarity, would cause a shift in the LCST value towards greater magnitudes.

Subsequently, the  $\mathbf{P3}_{\text{Azo}}$  samples underwent phase separation investigations both before and after exposure to light, as depicted in Figure 4.46. The copolymers were individually dissolved in Millipore water at a concentration of  $2 \text{ mg mL}^{-1}$ . Further, the LCSTs ( $T_{\text{CP}}$ ) of each sample was ascertained by measuring the optical transmittance of a light beam ( $\lambda = 700 \text{ nm}$ ) as it passed through the sample cell of the photospectrometer. The process of phase separation occurred concurrently with the insertion of a heating rate of  $1 \text{ }^\circ\text{C min}^{-1}$  into the sample holder. The LCSTs ( $T_{\text{CP1}} - T_{\text{CP3}}$ ) were consistently defined as the temperature at which a transmission of 50% was recorded in the corresponding transmission *vs.* temperature curve. Consequently, the cloud point was utilized for optical observation of the LCST.

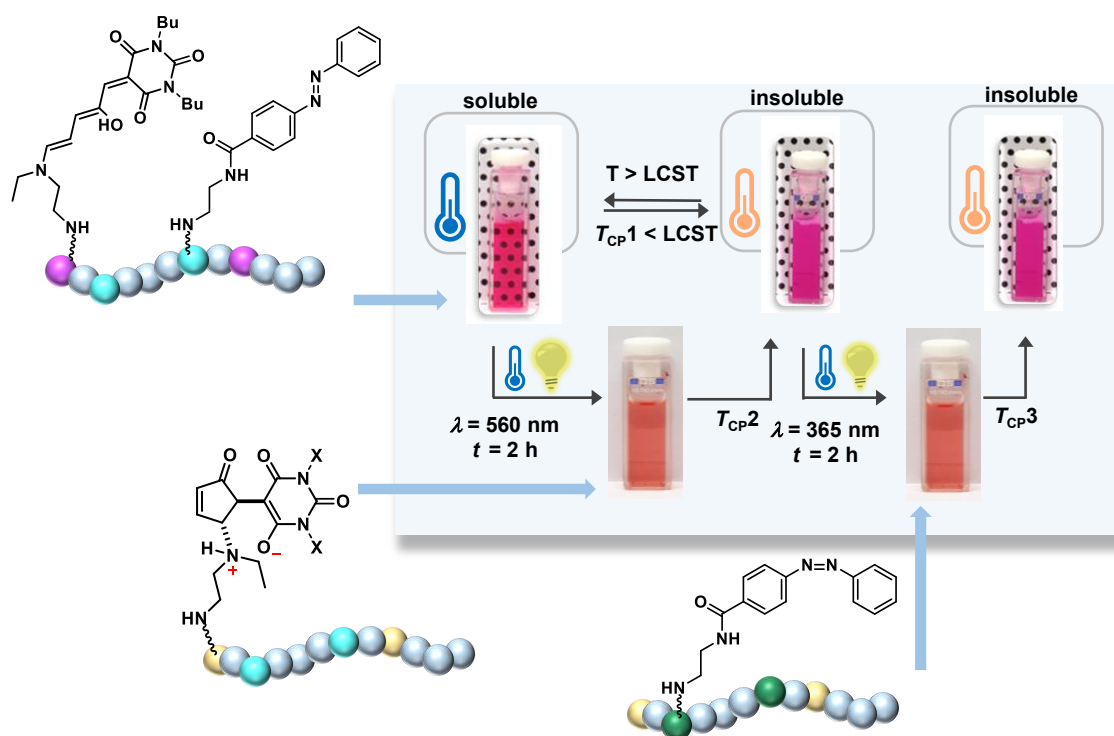


**Figure 4.46.** Schematic overview of the LCST investigations on copolymer samples  $\mathbf{P2}_{\text{Azo}}$  with DASA and azobenzene as chromophoric side groups. The material was dissolved in an aqueous solution ( $15 \text{ mg mL}^{-1}$ ). Prior to light irradiation, the copolymers displayed a LCST  $T_{\text{CP1}}$ . Following exposure to visible light ( $\lambda = 560 \text{ nm}$ ) and DASA photoswitching,  $T_1$  was increased to  $T_2$ . Following the second exposure to light ( $\lambda = 365 \text{ nm}$ ), the LCST was shifted to  $T_{\text{CP3}}$ . The correlation between the cloud points was as follows:  $T_{\text{CP1}} > T_{\text{CP2}} > T_{\text{CP3}}$ .

After being cooled to a temperature of  $T < T_{CP1}$ , each material received treatment with visible light ( $\lambda_1 = 560$  nm) for a duration of 2 h. The observed discoloration was attributed to the selective photoisomerization of the DASA chromophore from the colored triene species to the colorless zwitterionic cyclopentenone. The azobenzene structure remained unaffected during the switching process due to the presence of distinct wavelength areas that were utilized as stimuli. Based on the described procedure for cloud point determination, the value of  $T_{CP2}$  was obtained. Further, the solutions were cooled to a temperature of  $T < T_{CP2}$ . At this point, the samples were subjected to irradiation using UV light ( $\lambda_2 = 365$  nm) for 2 h, which induced the isomerization of the azobenzene group. This process of isomerization is invariably accompanied by a concomitant alteration in the dipole moment of the molecular configuration.

The sequencing of irradiation involving the wavelengths  $\lambda_1 = 565$  nm and  $\lambda_2 = 365$  nm was not arbitrary. DASA compounds exhibit a high degree of sensitivity to spontaneous switching phenomena in aqueous solutions as a consequence of their isomerization into the salt form. To prevent any additional increase in milieu polarity, the isomerization of DASA was carried out prior to that of azobenzene. Basically, Stenhouse adducts and azobenzenes are chromophores that demonstrate reversible switching properties. Nevertheless, the aspect of thermal-induced reversibility was deemed insignificant for this study in both scenarios. DASAs exhibit recyclability in aromatic and halogenated solvents through thermal means, while this process is not observed in aqueous solvents. The *cis-trans* isomerization of azobenzenes in aqueous conditions is potentially plausible. However, the prolonged half-time of 12 h rendered the undesired switching processes inconsequential within these particular settings.

Figure 4.47 depicts the recorded correlation between transmission and temperature for the **P2<sub>Azo</sub>** series in aqueous solution. In contrast to the curve shape observed for PDEA, the copolymer curves displayed a wider shape that became more noticeable with increased amounts of chromophore incorporation. Table 4.9 presents the LCST values obtained at a transmission level of 50%, together with the corresponding LCST shifts following the light exposures. Thus, the LCSTs of the aqueous solutions of the **P2<sub>Azo</sub>** series showed a dependence upon the content of incorporated chromophore.

**Table 4.9.** LCST values before and after light irradiation.

Sample	$X_{Azo}$ (mol%) <sup>a</sup>	$X_{DASA}$ (mol%) <sup>a</sup>	$T_{CP1}$ (°C)	$T_{CP2}$ (°C)	$T_{CP3}$ (°C)	$\Delta_{T1}^{T2}cp$ (°C)	$\Delta_{T2}^{T3}cp$ (°C)	$\Delta_{T1}^{T3}cp$ (°C)
PDEA	-	-	34.5	-	-	-	-	-
<b>P3<sub>Azoa</sub></b>	1.7	2.1	32.7	33.0	33.4	0.3	0.4	0.7
<b>P3<sub>Azob</sub></b>	3.1	3.4	31.6	33.0	34.6	2.3	0.7	3.0
<b>P3<sub>Azoc</sub></b>	4.7	5.1	28.7	34.7	36.1	6.0	1.4	7.4

<sup>a</sup>determined by <sup>1</sup>H NMR-spectroscopy

In general, the LCST of all copolymers decreased with increasing dye amount. In accordance with the hydrophobic character of the colored DASA structure and *trans*-azobenzene

before light irradiation, the samples exhibited  $T_{CP1}$  values that are lower in comparison to the cloud point of PDEA ( $T_{CP1} = 34.5$  °C).

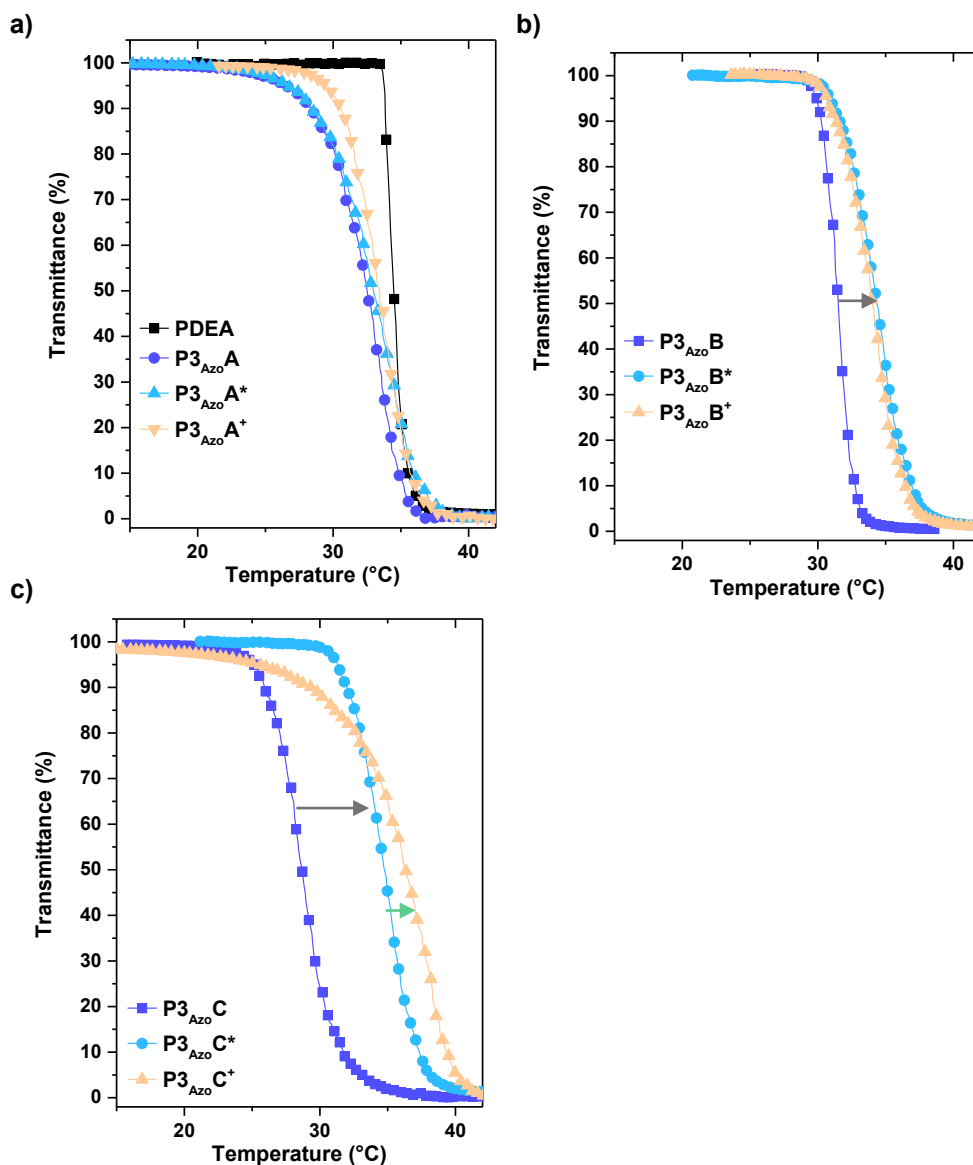


**Figure 4.47.** a) Turbidity curves of PDEA and **P2<sub>Azo</sub>a** prior to after sample exposure to light. b) Turbidity curves of **P2<sub>Azo</sub>b** prior to after sample exposure to light. c) Turbidity curves of **P2<sub>Azo</sub>c** prior to after sample exposure to light. All samples were measured while dissolved in an aqueous NaCl solution (1 M). \*After light exposure for at least 2 h with  $\lambda_1 = 560$  nm. \*\*After light exposure for at least 2 h with  $\lambda_2 = 365$  nm.

$T_{CP1}$  of the copolymer P3Azoc as example, was estimated to be 6.0 °C lower (28.7 °C) as measured for PDEA. The previous investigations on the LCST behavior of DASA bearing PDEA copolymers, as comparison, outlined  $\approx 5$  °C in difference regarding similar side group incorporation.

Hence, it was assumed that the DASA molecule has the dominant influence on the polymer solution behavior. This observation was confirmed by the results after the first and second light irradiation. The LCST shift ( $\Delta_{T_1}^{T_2}CP$ ) was particularly pronounced for P3Azo b (2.3 °C) and P3Azo c (6.0 °C), while the most intense shift resulting from the influence of *trans-cis* configuration was 1.4 °C. Nevertheless, the finding of measurable LCST modifications ( $\Delta_{T_2}^{T_3}CP$ ) following the second exposure to a 365 nm wavelength revealed the independent light-activation of the chromophores.

In total, the highest LCST shift ( $\Delta_{T_1}^{T_3}cp$ ) was calculated at 7.2 °C with an amount of 4.7 mol% azobenzene and 4.5 mol% DASA side group within the sample P3<sub>Azo</sub>c. Normally, a linear increase of the LCST shift would be predicted as the number of chromophoric units elevated. In fact, no linear correlation was seen because the influence on the copolymers P3Azoa and P3Azob was lower than expected in terms of the incorporated side group quantities. A potential explanation could be the statistical incorporation of the DASA and azobenzene moieties in the polymer, which could have resulted in a neighborhood effect caused by the included photoswitchable units. In contrast, the previously discussed results of tunable LCST values of PDEA- and PNIPAM-DASA exhibited linear correlations between the amount of chromophore units and LCST shifts. The neighboring effect appeared to be highly affected by the molecular weight. While the statistical distribution of the side chains claimed to be meaningless for very high molecular masses ( $M_n > 60,000 \text{ g mol}^{-1}$ ), it had a significant impact on polymer chains in the  $10,000 \text{ g mol}^{-1}$  molecular weight area.

# 5

## Experimental Part

---

### 5.1 Materials and Characterization

The following sections provide a concise overview of the materials and conditions used in the synthesis and characterization of the compounds in this study.

#### 5.1.1 Chemicals and solvents

Unless otherwise stated, all chemicals and solvents were commercially available and utilized as received. Azobisisobutyronitrile (AIBN; *Merck*, 98%) was purified by recrystallization from diethyl ether and stored at -7 °C. *N*-Ethylethanamine (TEA, *Merck*, 99%) was dried with activated 4 Å molecular sieve and stored under an argon atmosphere. Methyl methacrylate (MMA, *fisher scientific*, 99%) was filtered through basic alumina immediately before used to remove the stabilizer. *N,N*-Diethylacrylamide (DEA, *Merck*, 99%) was filtered through alumina immediately before used to remove the inhibitor 4-methoxyphenol. *N*-Isopropylacrylamide (NIPAM, *Merck*, 97%) was purified by recrystallization from isopropyl alcohol. Acetone, dichloromethane, ethyl acetate and petrol ether (technical grade) were distilled prior use as solvents for the column chromatography/dialysis. Tetrahydrofuran (THF) and 1,4-dioxane were distilled over sodium.

#### 5.1.2 Characterization and Purification Methods

##### Column Chromatography

The purification by column chromatography was carried out using silica gel 60 (70-230 mesh ASTM, 60 Å) obtained from *Merck*. The thin-layer chromatography was conducted with commercially available ALUGRAM® Xtra SIL G/UV<sub>254</sub> (SiO<sub>2</sub>) aluminum panels manufactured by *Macherey-Nagel*.

## Dialysis

The polymer samples were subjected to dialysis utilizing Spectra/Por<sup>®</sup> 1 and Spectra/Por<sup>®</sup> 7 membranes, which had molecular weight cut-offs of 6000 g·mol<sup>-1</sup> and 1000 g·mol<sup>-1</sup>, respectively. The specific solvent employed in each case is specified in the synthesis conditions within Section 5.2. The solvent was refilled continuously after a maximum term of 18 hours.

## FT IR spectroscopy

FT IR spectroscopy was measured on an iTR-Nicolet iS10 from *Thermo Scientific* with an attenuated total reflectance (ATR) attachment. The spectra were analyzed using Omnic 8.5.

## Irradiation systems

The light irradiations were conducted by subjecting the dissolved samples to light emitting diodes (LEDs) for the **P<sub>M</sub>3** series. To enhance efficiency and minimize irradiation duration, the LED utilized possesses a wavenumber of  $\lambda = 515$  nm, corresponding closely to the peak of the red dye's spectral curve ( $\lambda = 525$  nm) during UV measurement. All other copolymer samples were exposed to a white lamp (40 W).

## Mass spectrometrie

The ESI MS spectra were measured in positive mode using an Agilent 6224 TOF spectrometer from *Agilent Technologies*.

## NMR Spectroscopy

The NMR spectra (<sup>1</sup>H, <sup>13</sup>C, <sup>19</sup>F) were conducted using the Bruker spectrometers Avance III HD 600 MHz, Bruker Avance I 500 MHz, Bruker Avance III HD 400 MHz and Bruker Avance I 400 MHz. Tetramethylsilane served as internal standard. The denoted solvent was utilized to calibrate the chemical signal shift. When possible, the assignment of the <sup>1</sup>H and <sup>13</sup>C signals was facilitated by two-dimensional spectra (H,H COSY, HSQC, HMCB). The data were analyzed using MestReNova software version 14.1.0.

## Size Exclusion Chromatography

SEC was performed in either dimethylformamide with 0.01 mol L<sup>-1</sup> LiBr using a P1000 isocratic pump and RI detector L-7490 on MZ-Gel SD-plus 5  $\mu$ m linear column or in tetrahydrofuran using a JASCO PU-980 pump, RI detector and MZ-Gel SD. The data were analysed *via* Chromatographica V1.0.20.

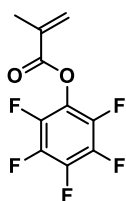
### UV-vis spectroscopy and turbidimetry

UV-vis and turbidity measurements were conducted using a *JASCO* V-630 spectrometer equipped with a silicon photodiode (S1337). The device utilized a dual-beam optical system comprising a deuterium lamp with a wavelength range of 190 to 350 nm and a halogen lamp with a wavelength range of 330 to 1100 nm. The spectrometer included an ETCS-761 thermostat for the purpose of temperature regulation. The samples were dissolved in the designated solvent and transferred (as mentioned concentrations) into a quartz glass cuvettes with a thickness of 10 mm. The UV-vis spectra were obtained within the wavelength range of 300 to 700 nm, while turbidity measurements were conducted specifically at a wavelength of 700 nm. The samples were measured with a cooling/heating rate of  $2.5\text{ }^{\circ}\text{C}\cdot\text{min}^{-1}$  or  $1.0\text{ }^{\circ}\text{C}\cdot\text{min}^{-1}$ , unless otherwise stated.

## 5.2 Synthesis

### 5.2.1 Monomers

#### Pentafluorophenyl methylacrylate (M1)



**Chemical formula:** C<sub>10</sub>H<sub>5</sub>F<sub>5</sub>O<sub>2</sub>  
**Molar mass:** 252.14 g mol<sup>-1</sup>  
**TLC:** R<sub>f</sub> = 0.35 (petrol ether)

The synthesis of pentafluorophenyl methylacrylate was carried out using the procedure provided in the literature.<sup>175</sup> Under an argon atmosphere, pentafluorophenol (45 g, 244 mmol) and trimethylamine (29.7 g, 293 mmol, 1.2 eq.) were dissolved in 400 mL dry diethylether. The solution was cooled with an ice bath and stirred. Methylacryloyl chloride (28.4 mL, 30.7 g, 293 mmol) was added dropwise through a dropping funnel over a time course of 30 min. The reaction mixture was stirred 19 h at room temperature. The precipitated salt was removed by filtration. The solvent was evaporated under reduced pressure and the crude product was isolated using column chromatography (column: silica gel, solvent: petrol ether). The title compound was obtained as a colorless liquid (49.3 g, 80% yield) and stored at 8 °C under argon atmosphere.

**<sup>1</sup>H NMR** (400 MHz, CDCl<sub>3</sub>): δ (ppm) = 6.42 (t, *J* = 17.8 Hz, 1H, CH<sub>2</sub>=C-), 5.81 (t, *J* = 17.6 Hz, 1H, CH<sub>2</sub>=C-), 2.00 (s, *J* = 10.3 Hz, 3H, CH<sub>3</sub>C-).

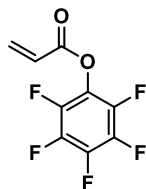
**<sup>13</sup>C NMR** (100 MHz, CDCl<sub>3</sub>): δ (ppm) = 163.1 (1C, C=O); 142.6, 140.1, 138.1, 136.9, 136.2, 135.7 (6C, C<sub>Ar</sub>); 135.4 (1H, CH<sub>2</sub>=CH-), 125.3 (1H, CH<sub>2</sub>=CH-), 19.8 (-CH<sub>3</sub>).

**<sup>19</sup>F NMR** (600 MHz, CDCl<sub>3</sub>): δ (ppm) = -162,7 (2F), -156,3 (1F), -150,5 (2F).

**FT-IR (ATR)**  $\tilde{\nu}$  (cm<sup>-1</sup>) = 1752, 1511, 1290, 1083, 989, 849, 781.

**MS (EI):** *m/z* = 69.07 (100%) [C<sub>4</sub>H<sub>5</sub>O], 41.06 (72%) [C<sub>3</sub>H<sub>5</sub>], 183.99 (29%) [C<sub>6</sub>F<sub>5</sub>HO].

## Pentafluorophenyl acrylate (M2)



**Chemical formula:** C<sub>9</sub>H<sub>3</sub>F<sub>5</sub>O<sub>2</sub>  
**Molar mass:** 238.11 g mol<sup>-1</sup>  
**TLC:** R<sub>f</sub> = 0.46 (petroleum ether)

The synthesis of pentafluorophenyl acrylate was carried out using the procedure provided in the literature.<sup>163</sup> Pentafluorophenol (50.0 g, 210 mmol) and triethylamine (25.5 g, 250 mmol, 1.2 eq.) were dissolved in 350 mL of dry diethylether and stirred under an argon atmosphere. The reaction mixture was cooled with an ice bath, and acryloyl chloride (22.8 g, 250 mmol, 1.2 eq.) was added dropwise for 30 min using a dropping funnel. Following the removal of the ice bath, the reaction was continued at ambient temperature overnight. The precipitated salt was removed by filtration. The filtrate was washed twice with 50 mL of water and dried over MgSO<sub>4</sub>. After the evaporation of the solvent under reduced pressure, the residue was purified by column chromatography (column: silica gel, solvent: petroleum ether). The title compound was obtained as a colorless liquid (46.6 g, 196 mmol, 72% yield) and stored at 8 °C under an argon atmosphere.

<sup>1</sup>H NMR (400 MHz, CDCl<sub>3</sub>): δ (ppm) = 6.72 (dd, *J* = 17.8 Hz, 1H, CH<sub>2</sub>=CH-), 6.37 (dd, *J* = 17.6 Hz, 1H, CH<sub>2</sub>=CH-), 6.18 (dd, *J* = 10.3 Hz, 1H, CH<sub>2</sub>=CH-).

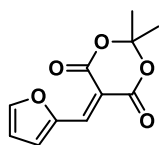
<sup>13</sup>C NMR (100 MHz, CDCl<sub>3</sub>): δ (ppm) = 161.6 (1C, C=O); 142.4, 140.7, 139.9, 138.2, 136.7, 136.1 (6C, C<sub>Ar</sub>); 135.4 (1H, CH<sub>2</sub>=CH-), 125.3 (1H, CH<sub>2</sub>=CH-).

<sup>19</sup>F NMR (600 MHz, CDCl<sub>3</sub>): δ (ppm) = -163,7 (2F), -158,3 (1F), -153,5 (2F).

FT-IR (ATR)  $\tilde{\nu}$  (cm<sup>-1</sup>) = 1769, 1513, 1388, 1214, 1109, 985, 852, 783.

MS (EI) (*m/z*) = 57.07 (100%) [C<sub>3</sub>H<sub>4</sub>O], 71.08 (82%) [C<sub>3</sub>H<sub>5</sub>O<sub>2</sub>], 55.05 (65%) [C<sub>3</sub>H<sub>3</sub>O].

## 5.2.2 Chromophores and Chromophore Precursors

5-(2-Furanylmethylene)-2,2-dimethyl-1,3-dioxane-4,6-dione (**S2**)

**Chemical formula:** C<sub>11</sub>H<sub>10</sub>O<sub>5</sub>  
**Molar mass:** 222.20 g mol<sup>-1</sup>

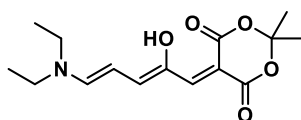
The synthesis of 5-(furan-2-ylmethylene)-2,2-dimethyl-1,3-dioxane-4,6-dione was carried out using the procedure provided in the literature.<sup>178</sup> Meldrum's acid (5.01 g, 34.7 mmol) was dissolved in 100 mL distilled water and 2-fufuraldehyde (3.00 g, 31.2 mmol, 0.9 eq.) was added dropwise. The reaction mixture was stirred for 2 h at 80 °C. Following the cooling process toward an ambient temperature, the precipitate was filtered and washed three times with 60 mL distilled water. The purification was performed by recrystallization using isopropyl alcohol. The title compound was obtained as a yellow powder (5.88 g, 26.4 mmol, 85% yield).

<sup>1</sup>H NMR (500 MHz, CDCl<sub>3</sub>): δ (ppm) = 7.17 (d, 1H, 5'-H<sub>furan</sub>), 7.00 (s, 1H, C=CH-), 6.65 (dd, 1H, 3'-H<sub>furan</sub>), 6.74 (m, 1H, 4'-H<sub>furan</sub>), 1.76 (s, 6H, CH<sub>3</sub>).

<sup>13</sup>C NMR (500 MHz, CDCl<sub>3</sub>): δ (ppm) = 163.4 (C=O), 160.4 (C=O), 151.6 (C=C), 150.1 (C=C), 141.2 (C=C), 128.5 (C=C), 115.7 (-C=OCC=O-), 108.0 (-CCH<sub>3</sub>), 27.1 (-CH<sub>3</sub>)

FT-IR (ATR)  $\tilde{\nu}$  (cm<sup>-1</sup>) = 2980, 1640, 1371, 1000, 780.

HRMS (ESI+)  $m/z$  = 222.0528 [M+H]<sup>+</sup> (calcd) / 222.0521 [M+H]<sup>+</sup> (found).

5-((2Z,4E)-5-(Diethylamino)-2-hydroxypenta-2,4-dien-1-ylidene)-2,2-dimethyl-1,3-dioxane-4,6-dione (**S3**)

**Chemical formula:** C<sub>15</sub>H<sub>21</sub>NO<sub>5</sub>  
**Molar mass:** 295.34 g mol<sup>-1</sup>

The synthesis of 5-((2Z,4E)-5-(diethylamino)-2-hydroxypenta-2,4-dien-1-ylidene)-2,2-dimethyl-1,3-dioxane-4,6-dione (**S3**) was carried out using the procedure provided in the literature.<sup>146</sup> Compound **S2** (1.24 g, 5.58 mmol) was dissolved in 20 mL THF and stirred at ambient

temperature. Triethylamine (0.564 g, 5.53 mmol (1.0 eq.) was added dropwise and the reaction mixture was stirred for 30 min followed by cooling with an ice bath for 30 min. The precipitate was filtered and washed with cold diethyl ether (three times). The title compound was isolated after solvent evaporation under reduced pressure as a red solid (1.48 g, 5.02 mmol, 90%).

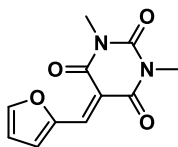
**<sup>1</sup>H NMR** (500 MHz, CDCl<sub>3</sub>):  $\delta$  (ppm) = 11.42 (s, 1H, COH), 7.20 (d,  $J$  = 12.1 Hz, 1H, -NCH=CH-), 7.06 (s, 1H, -C=CH-), 6.74 (dd,  $J$  = 12.2, 1H, -C=CHCOH-), 6.05 (t,  $J$  = 12.3 Hz, 1H, -NCH=CH=CH-), 3.46 (q, 4H, -CH<sub>2</sub>CH<sub>3</sub>) 1.76 (s, 6H, -CH<sub>3</sub>), 1.30 (dt, 6H, -CH<sub>2</sub>CH<sub>3</sub>).

**<sup>13</sup>C NMR** (500 MHz, CDCl<sub>3</sub>):  $\delta$  (ppm) = 167.7 (C=O), 164.1 (C=O), 156.2 (C=C), 151.2 (C=C), 144.2 (COH), 139.1 (C=C), 103.0 (C=C), 102.9 (-C=OCC=O-), 90.1 (-C(CH<sub>3</sub>)<sub>2</sub>), 52.1(-CH<sub>2</sub>CH<sub>3</sub>), 44.1 (-CH<sub>2</sub>CH<sub>3</sub>), 28.0 (CH<sub>3</sub>), 14.5 (-CH<sub>2</sub>CH<sub>3</sub>), 12.2 (-CH<sub>2</sub>CH<sub>3</sub>).

**FT-IR (ATR)**  $\tilde{\nu}$  (cm<sup>-1</sup>) = 3090, 2991, 2939, 1703, 1605, 1500, 1370, 1147, 918, 768, 657, 493.

**HRMS (ESI+)**  $m/z$  = 613.2732 [2M+Na]<sup>+</sup> (calcd) / 613.2750 [2M+Na]<sup>+</sup> (found).

#### 5-(Furan-2-ylmethylene)-1,3-dimethylpyrimidine-2,4,6(1H,3H,5H)-trione (S4)



**Chemical formula:** C<sub>11</sub>H<sub>10</sub>N<sub>2</sub>O<sub>4</sub>  
**Molar mass:** 234.21 g·mol<sup>-1</sup>

The synthesis of 5-(Furan-2-ylmethylene)-1,3-dimethylpyrimidine-2,4,6(1H,3H,5H)-trione (S4) was carried out using the procedure provided in the literature.<sup>146</sup> 1,3-Dimethylbarbituric acid (2.03 g, 12.9 mmol) was dissolved in 80 mL distilled water and 2-fufuraldehyde (1.21 g, 12.5 mmol, 0.95 eq.) was added dropwise. The reaction mixture was stirred for 2 h at 80 °C. Following the cooling process toward an ambient temperature, the precipitate was filtered and washed three times with 60 mL distilled water. The purification was performed by recrystallization using isopropyl alcohol. The title compound was obtained as a yellow powder (2.65g, 11.3 mmol, 90% yield).

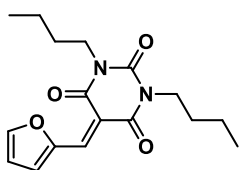
**<sup>1</sup>H NMR** (500 MHz, CDCl<sub>3</sub>):  $\delta$  (ppm) = 7.17 (d, 1H, 5'-H<sub>furan</sub>), 7.00 (s, 1H, C=CH-), 6.65 (dd, 1H, 3'-H<sub>furan</sub>), 6.74 (m, 1H, 4'-H<sub>furan</sub>), 1.76 (s, 6H, CH<sub>3</sub>).

**<sup>13</sup>C NMR** (500 MHz, CDCl<sub>3</sub>):  $\delta$  (ppm) = 162.2 (C=O), 160.6 (C=O), 150.6 (C=C), 150.3 (C=O), 149.1 (C=C), 139.1 (C=C), 127.6 (C=C), 114.0 (C=C), 111.1 (-C=OCC=O-), 28.8 (-CH<sub>3</sub>), 28.0 (-CH<sub>3</sub>).

**FT IR (ATR)**  $\tilde{\nu}$  (cm<sup>-1</sup>) = 2980, 1640, 1371, 1000, 780.

**HRMS (ESI+)**  $m/z$  = 235.0713 [M+H]<sup>+</sup> (calcd) / 235.0690 [M+H]<sup>+</sup> (found).

**5-(Furan-2-ylmethylene)-1,3-dibutylpyrimidine-2,4,6(1H,3H,5H)-trione (S5)**



**Chemical formula:** C<sub>17</sub>H<sub>22</sub>N<sub>2</sub>O<sub>4</sub>  
**Molar mass:** 318.37 g·mol<sup>-1</sup>

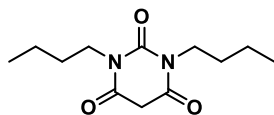
The synthesis of 5-(Furan-2-ylmethylene)-1,3-dibutylpyrimidine-2,4,6(1H,3H,5H)-trione (**S5**) was conducted to the general procedure described in the literature for 1,3-disubstituted barbituric acid furan precursors.<sup>146</sup> To a suspension of 1,3-dibutylpyrimidine-2,4,6(1H,3H,5H)-trione (**S6**) (19.7 g, 81.9 mmol) and 200 mL distilled water, fufuraldehyde (7.86 g, 81.2 mmol, 1.0 eq.) was added dropwise. The reaction mixture was stirred for 2 h at 70 °C. Following the cooling process toward an ambient temperature, the precipitate was filtered and washed three times with 60 mL distilled water. The residue was dried under reduced pressure. The purification of the crude product was performed by recrystallization (twice) using petroleum ether/EtOAc (8:2 v/v). The title compound was obtained as a yellow powder (21.7 g, 68.2 mmol, 83% yield).

**<sup>1</sup>H NMR** (500 MHz, CDCl<sub>3</sub>):  $\delta$  (ppm) = 8.61 (d, 1H, 5'-H<sub>furan</sub>), 8.41 (s, 1H, C=C), 7.83 (dd, 1H, 3'-H<sub>furan</sub>), 6.72 (m, 1H, 4'-H<sub>furan</sub>), 3.97 (dt, 4H, N-CH<sub>2</sub>-), 1.63 (m, 4H, -CH<sub>2</sub>-), 1.38 (m, 4H, -CH<sub>2</sub>-), 0.97 (td, 6H, -CH<sub>3</sub>).

**<sup>13</sup>C NMR** (500 MHz, CDCl<sub>3</sub>):  $\delta$  (ppm) = 162.2 (C=O), 160.3 (C=O), 151.2 (C=C-O), 150.9 (C=O), 150.1 (C=C), 140.2 (C=C), 128.3 (C=C), 115.0 (C=C), 111.0 (-C=OCC=O-), 42.2 (-CH<sub>2</sub>), 41.5 (-CH<sub>2</sub>), 30.5 (-CH<sub>2</sub>), 20.2 (-CH<sub>2</sub>), 13.7 (-CH<sub>3</sub>).

**FT-IR (ATR)**  $\tilde{\nu}$  (cm<sup>-1</sup>) = 2925, 2854, 1653, 1577, 1404, 1365, 1157, 788, 549, 428.

**HRMS (ESI+)**  $m/z$  = 319.1652 [M+H]<sup>+</sup> (calcd) / 319.1651 [M+H]<sup>+</sup> (found).

**1,3-dibutylpyrimidine-2,4,6(1H,3H,5H)-trione (S6)**

**Chemical formula:** C<sub>12</sub>H<sub>20</sub>N<sub>2</sub>O<sub>3</sub>  
**Molar mass:** 240.30 g·mol<sup>-1</sup>  
**TLC:** R<sub>f</sub> = 0.35 (petroleum ether/EtOAc, 2:1 v/v)

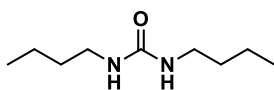
The synthesis of 1,3-dibutylpyrimidine-2,4,6(1H,3H,5H)-trione (**S6**) was conducted to the general procedure described in the literature for 1,3-disubstituted pyrimidine structures.<sup>146</sup> 1,3-Butylurea (**S7**) (5.02 g, 29.1 mmol) was dissolved in 150 mL dry dichloromethane and stirred under an argon atmosphere. Malonyl chloride (4.12 g, 29.1 mmol, 1.0 eq.) was added dropwise through a dropping funnel and the reaction mixture was subsequently heated at 55 °C for 2 h. Following the cooling process toward an ambient temperature, the reaction was quenched with 1 N HCl (100 mL). The crude product was extracted with dichloromethane (three times) and the combined organic phases were dried over MgSO<sub>4</sub> and filtered. The solvent was removed under reduced pressure. After purification using column chromatography (petroleum ether/EtOAc, 2:1 v/v), the title compound was isolated as a colorless solid (5.06 g, 21.1 mmol, 72% yield).

<sup>1</sup>H NMR (500 MHz, CDCl<sub>3</sub>): δ (ppm) = 4.01-3.92 (m, 4H, -CH<sub>2</sub>-), 3.70 (s, 2H, -C=OCH<sub>2</sub>C=O-), 1.75-1.58 (m, 4H, -CH<sub>2</sub>-), 1.42-1.32 (m, 4H, -CH<sub>2</sub>-), 0.93-0.82 (m, 6H, -CH<sub>3</sub>).

<sup>13</sup>C NMR (500 MHz, CDCl<sub>3</sub>): δ (ppm) = 163.7 (C=O), 160.3 (C=O), 150.2 (C=O), 43.1 (-CH<sub>2</sub>-), 29.1.5 (-CH<sub>2</sub>-), 20.3 (-CH<sub>2</sub>-), 13.7 (-CH<sub>3</sub>).

FT-IR (ATR)  $\tilde{\nu}$  (cm<sup>-1</sup>) = 1605, 1471, 1220, 543, 321.

HRMS (ESI+)  $m/z$  = 281.0534 [M+K]<sup>+</sup> (calcd) / 281.0528 [M+K]<sup>+</sup> (found).

**1,3-Dibutylurea (S7)**

**Chemical formula:** C<sub>9</sub>H<sub>20</sub>N<sub>2</sub>O  
**Molar mass:** 172.27 g·mol<sup>-1</sup>

The synthesis of 1,3-Dibutylurea (**S7**) was carried out using the procedure provided in the literature.<sup>197</sup> Ethylene carbonate (4.01 g, 45.5 mmol), *n*-butylamine (6.75 g, 91.5 mmol, 2.0 eq.) and Cs<sub>2</sub>CO<sub>3</sub> (0.296 g, 0.91 mmol, 0.02 eq.) were combined, stirred and heated at 100 °C for 2 h. Following the cooling process toward an ambient temperature, the colorless precipitate was filtered and washed three times with 60 mL distilled water. The title compound was isolated after solvent evaporation under reduced pressure as a colorless solid (3.21 g, 18.6 mmol, 41%).

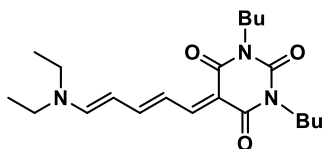
<sup>1</sup>H NMR (500 MHz, CDCl<sub>3</sub>):  $\delta$  (ppm) = 4.18 (b, 2H, NH), 3.14 (m, 4H, N-CH<sub>2</sub>CH<sub>2</sub>CH<sub>2</sub>CH<sub>3</sub>), 1.46-1.34 (m, 8H, N-CH<sub>2</sub>CH<sub>2</sub>CH<sub>2</sub>CH<sub>3</sub>), 0.90 (m, 6H, -CH<sub>3</sub>).

<sup>13</sup>C NMR (500 MHz, CDCl<sub>3</sub>):  $\delta$  (ppm) = 159.2 (C=O), 39.7 (N-CH<sub>2</sub>CH<sub>2</sub>CH<sub>2</sub>CH<sub>3</sub>), 31.9 (N-CH<sub>2</sub>CH<sub>2</sub>CH<sub>2</sub>CH<sub>3</sub>), 20.3 (N-CH<sub>2</sub>CH<sub>2</sub>CH<sub>2</sub>CH<sub>3</sub>), 13.5 (-CH<sub>3</sub>).

FT-IR (ATR)  $\tilde{\nu}$  (cm<sup>-1</sup>) = 3328, 2958, 2858, 1610, 1575, 1224, 582.

MS (EI):  $m/z$  = 173.2 (3%) / 172.2 (23%) [M], 58.1 (40%) [C<sub>4</sub>H<sub>10</sub>], 43.1 (100%) [C<sub>3</sub>H<sub>7</sub>].

**5-((2Z,4E)-5-(diethylamino)-2-hydroxypenta-2,4-dien-1-ylidene)-1,3-dibutyl-pyrimidine-2,4,6 (1H,3H,5H)-trione (S8)**



**Chemical formula:** C<sub>21</sub>H<sub>33</sub>N<sub>3</sub>O<sub>3</sub>  
**Molar mass:** 375.51 g·mol<sup>-1</sup>

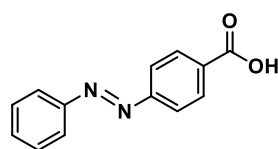
The synthesis of **S8** was conducted to the procedure described in the literature.<sup>130</sup> Barb-Bu (0.978 g, 3.07 mmol) was dissolved in 3 mL THF and stirred at ambient temperature. Diethylamine (0.225 g, 3.06 mmol, 1.0 eq.) was added dropwise and the reaction mixture was stirred for 30 min followed by cooling with an ice bath for 30 min. The precipitate was filtered and washed with cold diethyl ether (three times). The title compound was isolated after solvent evaporation under reduced pressure as a purple solid (0.877 g, 2.33 mmol, 87%).

<sup>1</sup>H NMR (500 MHz, CDCl<sub>3</sub>):  $\delta$  (ppm) = 12.5 (s, 1H, COH), 7.18 (d,  $J$  = 12.2 Hz, 1H, -NCH=CH-), 7.05 (s, 1H, -C=CH-), 6.67 (dd,  $J$  = 12.4, 1H, -C=CHCOH-), 6.01 (t,  $J$  = 12.3 Hz, 1H, -NCH=CH=CH-), 3.46 (q, 4H, -CH<sub>2</sub>CH<sub>3</sub>), 3.13 (m, 4H, H-6, -CH<sub>2</sub>-), 1.70 (s, 6H, -CH<sub>3</sub>), 1.45-1.31 (m, 8H, -CH<sub>2</sub>-), 1.34 (dt, 6H, -CH<sub>2</sub>CH<sub>3</sub>), 0.91 (m, 6H, -CH<sub>3</sub>(butyl)).

$^{13}\text{C}$  NMR (500 MHz,  $\text{CDCl}_3$ ):  $\delta$  (ppm) = 164.7 (C=O), 160.6 (C=O), 158.6 (C=C), 154.3 (C=O), 142.1 (C-OH), 128.5 (C=C), 115.7 (C=C), 108.0 (C=C), 104.9 (C=C), 52.1 ( $-\text{CH}_2-$ ), 51.7 ( $-\text{CH}_2-$ ), 28.3 ( $-\text{CH}_2-$ ), 27.2 ( $-\text{CH}_2-$ ), 26.0 ( $-\text{CH}_3$ ), 10.7 ( $-\text{CH}_3$ ).

FT-IR (ATR)  $\tilde{\nu}$  ( $\text{cm}^{-1}$ ) = 2983, 1680, 1560, 1416, 1126, 772, 507.

### (*E*)-4-(Phenyldiazenyl)benzoic acid (S9)



Chemical formula:  $\text{C}_{13}\text{H}_{10}\text{N}_2\text{O}_2$

Molar mass:  $226.24 \text{ g}\cdot\text{mol}^{-1}$

The synthesis of (*E*)-4-(Phenyldiazenyl)benzoic acid (**S9**) was carried out using the procedure provided in the literature.<sup>203</sup> Nitrobenzene (10.0 g, 81.2 mmol) and 4-aminobenzoic acid (13.41 g, 97.8 mmol, 1.2 eq.) were dissolved in 120 mL acetic acid. The pale-yellow solution was stirred at ambient temperature for 24 h. The precipitate was filtered and washed with cold water (three times) and dried under reduced pressure. The purification of the crude product was performed by recrystallization (twice) using ethyl acetate. The title compound was isolated after solvent evaporation under reduced pressure as a colorless solid (13.9 g, 61.4 mmol, 75%).

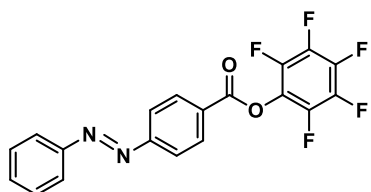
$^1\text{H}$  NMR (500 MHz,  $\text{DMSO}-d_6$ ):  $\delta$  (ppm) = 13.2 (s, brs, 1H,  $-\text{COOH}$ ), 8.15-8.12 (m, 2H, ArH), 7.95-7.88 (m, 4H, ArH), 7.61-7.56 (m, 3H, ArH).

$^{13}\text{C}$  NMR (500 MHz,  $\text{CDCl}_3$ ):  $\delta$  (ppm) = 175.6 (C=O), 152.8, 152.6, 144.1, 129.5, 129.2, 122.3, 121.3.

FT-IR (ATR)  $\tilde{\nu}$  ( $\text{cm}^{-1}$ ) = 2809, 2528, 1677, 1429, 1286, 939, 867, 775, 685, 541.

HRMS (ESI+)  $m/z$  = 269.1396  $[\text{M}+\text{H}]^+$  (calc) / 269.1270  $[\text{M}+\text{H}]^+$  (found).

### Pentafluorophenyl (*E*)-4-(phenyldiazenyl)benzoate (S10)



Chemical formula:  $\text{C}_{19}\text{H}_9\text{F}_5\text{N}_2\text{O}_2$

Molar mass:  $392.29 \text{ g}\cdot\text{mol}^{-1}$

The synthesis of pentafluorophenyl (*E*)-4-(phenyldiazenyl)benzoate (**S10**) was carried out using the procedure provided in the literature.<sup>162</sup> Under an argon atmosphere, pentafluorophenyl trifluoroacetate (14.6 g, 55.2 mmol) dissolved in 50 mL dry THF was added to a solution of **S9** (5.00 g, 22.1 mmol, 0.4 eq.) in 50 mL dry THF through a dropping funnel. The reaction mixture was stirred at ambient temperature for 2.5 h followed by quenching using 80 mL distilled water and 150 mL dichloromethane. The phases were separated, and the organic layer was dried over Na<sub>2</sub>SO<sub>4</sub>. After solvent evaporation under reduced pressure, the residue was precipitated in hexane. The title compound was isolated after solvent evaporation as a red solid (4.33 g, 11.1 mmol, 51% yield).

<sup>1</sup>H NMR (500 MHz, CDCl<sub>3</sub>): δ (ppm) = 8.35 (d, 2H, ArH), 8.05 (d, 2H, ArH), 7.98 (m, 2H, ArH), 7.59-7.53 (m, 3H, ArH).

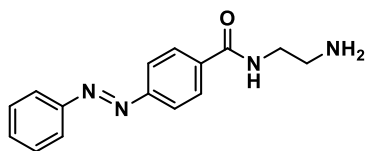
<sup>19</sup>F NMR (600 MHz, CDCl<sub>3</sub>): δ (ppm) = -152.3 (ArF), -157.7 (ArF), -162.2 (ArF).

<sup>13</sup>C NMR (500 MHz, CDCl<sub>3</sub>): δ (ppm) = 161.1, 156.2, 151.8, 132.1, 131.6, 134.9, 127.8, 123.3.

FT-IR (ATR)  $\tilde{\nu}$  (cm<sup>-1</sup>) = 1679, 1513, 1291, 1429, 1290, 949, 915, 650, 511.

HRMS (ESI+)  $m/z$  = 240.3103 [M+H]<sup>+</sup> (calc) / 240.3200 [M+H]<sup>+</sup> (found).

#### (*E*)-*N*-(2-aminoethyl)-4-(phenyldiazenyl)benzamide (**S11**)



**Chemical formula:** C<sub>15</sub>H<sub>16</sub>N<sub>4</sub>O  
**Molar mass:** 268.32 g·mol<sup>-1</sup>

The synthesis of (*E*)-*N*-(2-aminoethyl)-4-(phenyldiazenyl)benzamide (**S11**) was carried out using the procedure provided in the literature.<sup>162</sup> A solution of **S10** (5.02 g, 12.8 mmol) in 100 mL dry THF was stirred under an argon atmosphere at ambient temperature. Through a dropping funnel, ethan-1,2-diamine (6.13 g, 101 mmol, 8 eq.) dissolved in 50 mL dry THF was added slowly. The reaction mixture was stirred for 2.5 h and subsequently quenched with 120 mL dichloromethane and 100 mL distilled water. The phases were separated, and the organic layer was washed with distilled water (3 times) and dried over MgSO<sub>4</sub>. The solvent was evaporated under reduced pressure. The title compound was obtained as an orange oil (2.40 g, 70% yield).

<sup>1</sup>H NMR (500 MHz, DMSO): δ (ppm) = 8.08-8.05 (m, 2H, ArH), 7.97-7.92 (m, 4H, ArH), 7.67-7.59 (m, 3H, ArH), 4.57 (m, 4H, CH<sub>2</sub>), 3.65 (s, -NH), 3.47 (t, 2H, CH<sub>2</sub>).

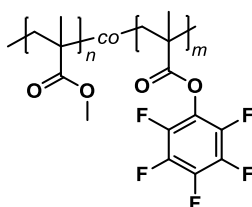
$^{13}\text{C}$  NMR (500 MHz, DMSO):  $\delta$  (ppm) = 170.1 (C=O), 159.7, 157.1, 142.4, 137.9, 134.9, 128.0, 126.6, 47.1 (–CH<sub>2</sub>–), 46.2 (–CH<sub>2</sub>–),

FT-IR (ATR)  $\tilde{\nu}$  (cm<sup>-1</sup>) = 3397, 2933, 1629, 1540, 1296, 858, 690.

HRMS (ESI+)  $m/z$  = 269.1396 [M+H]<sup>+</sup> (calc) / 269.1270 [M+H]<sup>+</sup> (found).

### 5.2.3 Polymer synthesis

#### Poly(methyl methacrylate-*co*-pentafluorophenyl methacrylate) (P<sub>M1</sub>)



The P<sub>M1</sub> samples were subjected to a general free-radical polymerization procedure, with the aim of investigating the outcome of varying the monomer mol% ratio amounts. In order to compare the analytical data, the homopolymers poly(methyl methacrylate) (PMMA) and poly(pentafluorophenyl methacrylate) (P1) were synthesized as well.

**Table 5.1** Expected monomer ratio of M1, monomer masses and yields of the P<sub>M1</sub> series.

Sample	M1 expected (mol%)	$m_{\text{M1}}$ (g)	$m_{\text{MMA}}$ (g)	P <sub>M1</sub> Yield (%)
PMMA	—	—	6.02	98
P1	100	6.01	—	99
P <sub>M1a</sub>	2	0.293	5.71	99
P <sub>M1b</sub>	4	0.569	5.43	98
P <sub>M1c</sub>	6	0.831	5.12	97
P <sub>M1d</sub>	8	1.08	4.92	97
P <sub>M1e</sub>	10	1.32	4.69	98
P <sub>M1f</sub>	12	1.53	4.46	99
P <sub>M1g</sub>	14	1.74	4.25	98

Methyl methacrylate and pentafluorophenyl methacrylate were solubilized in 12 mL of anhydrous 1,4-dioxane under an argon environment, in accordance with the targeted molar

percentage ratio as indicated in Table 5.1. 2,2'-Azobis(2-methylpropionitrile) (25.0 mg) was added, and the reaction mixture was heated at 70 °C and stirred for 6 h. The crude product was dissolved in 10 mL acetone and purified by precipitation in *n*-hexane. The procedure was repeated three times followed by solvent evaporation under reduced pressure. The title polymer sample was obtained as a colorless solid in a quantitative yield (>97%).

**PMMA:**

$^1\text{H NMR}$  (600 MHz, acetone- $d_6$ ):  $\delta$  (ppm) = 3.63 (s,  $-\text{OCH}_3$ ), 1.4-2.1 (br,  $-\text{CH}_2-$  backbone), 0.75-1.4 (br,  $-\text{CH}_3$  backbone).

**P1 (PPFPMA):**

$^1\text{H NMR}$  (600 MHz, acetone- $d_6$ ):  $\delta$  (ppm) = 2.1-2.7 (br,  $\text{CH}_2$  backbone), 1.3-1.8 (br,  $\text{CH}_3$  backbone).

$^{19}\text{F NMR}$  (600 MHz,  $\text{CDCl}_3$ ):  $\delta$  (ppm) = -151.41, -153.05, -159.54, -164.52.

$^{13}\text{C NMR}$  (500 MHz,  $\text{CDCl}_3$ ):  $\delta$  (ppm) = 170.3 (C=O), 141.2 (m, ArC), 138.7 (m, C=C), 137.9 (m, C=C), 60.3 (m,  $-\text{CH}_3$ ), 40.2 (m,  $-\text{CH}_3$ ,  $-\text{CH}_2$ ), 24.3 (m,  $-\text{CH}_2$ ).

**FT-IR (ATR)**  $\tilde{\nu}$  ( $\text{cm}^{-1}$ ) = 1778, 1518, 1054, 991.

**P<sub>M</sub>1:**

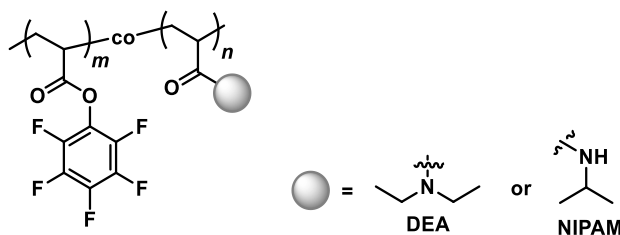
$^1\text{H NMR}$  (500 MHz, acetone- $d_6$ ):  $\delta$  (ppm) = 3.6-3.7 (s,  $\text{OCH}_3$ ), 2.1-2.6 (br,  $\text{CH}_2$  backbone PFPMA), 1.4-2.1 (br,  $\text{CH}_2$  backbone MMA), 0.8-1.9 (br,  $\text{CH}_3$ ).

$^{13}\text{C NMR}$  (500 MHz, acetone- $d_6$ ):  $\delta$  (ppm) = 178.8 (C=O), 177.5 (C=O), 54.4 ( $-\text{C}-$ ), 54.1 ( $-\text{C}-$ ), (52.6 ( $-\text{CH}_2-$ ), 50.5 ( $-\text{OCH}_3$ ), 48.1 ( $-\text{CH}_2-$ ), 17.3 ( $\text{CH}_3$ ), 15.6 ( $-\text{CH}_3$ ).

$^{19}\text{F NMR}$  (600 MHz, acetone- $d_6$ ):  $\delta$  (ppm) = -151.7, -153.1, -161.2, -164.5.

**FT-IR (ATR)**  $\tilde{\nu}$  ( $\text{cm}^{-1}$ ) = 2954, 1783, 1729, 1521, 1251, 1145, 993.

**Poly(*N,N*-diethylacrylamide-*co*-pentafluorophenyl acrylate) (P<sub>D</sub>1a – P<sub>D</sub>1f) and poly(*N*-isopropylacrylamide-*co*-pentafluorophenyl acrylate) (P<sub>N</sub>1a – P<sub>N</sub>1f)**



The P<sub>D</sub>1/P<sub>N</sub>1 samples were subjected to a general free-radical polymerization procedure, with the aim of investigating the outcome of varying the monomer mol% ratio amounts.

Either *N,N*-diethylacrylamide or *N*-isopropylacrylamide and pentafluorophenyl acrylate were solubilized in 20 mL of anhydrous 1,4-dioxane under an argon environment, in accordance with the targeted molar percentage ratio as indicated in Table Table 5.2. 2,2'-Azobis(2-methylpropionitrile) (20.0 mg) was added and the reaction mixture was heated at 70 °C and stirred for 18 h. The crude product was precipitation in *n*-hexane and dissolved in acetone. The procedure was repeated three times followed by solvent evaporation under reduced pressure. The title polymer sample was obtained as a colorless solid in a quantitative yield (>97%).

**Table 5.2.** Expected monomer ratio of **M2**, monomer masses and yields of the **P<sub>D</sub>1** and **P<sub>N</sub>1** series.

Sample	PFPA expected (mol%)	PFPA Weighted portion (g)	DEA/NIPAM Weighted portion (g)	Yield (%)
<b>PDEA</b>	—	—	4.01	99
<b>PD1_a</b>	2	0.227	5.27	99
<b>PD1_b</b>	4	0.442	5.06	98
<b>PD1_c</b>	6	0.651	4.85	97
<b>PD1_d</b>	8	0.851	4.64	98
<b>PD1_e</b>	10	1.04	4.45	98
<b>PD1_f</b>	12	1.22	4.27	99
<b>PNIPAM</b>	—	—	3.99	99
<b>PN1_a</b>	2	0.202	5.30	98
<b>PN1_b</b>	4	0.398	5.10	98
<b>PN1_c</b>	6	0.587	4.91	97
<b>PN1_d</b>	8	0.770	4.73	97
<b>PN1_e</b>	10	0.947	4.55	98
<b>PD1_f</b>	12	1.12	4.38	98

**Poly(*N,N*-diethylacrylamide-co-pentafluorophenyl acrylate) (P<sub>D</sub>1a – P<sub>D</sub>1f) :**

**<sup>1</sup>H NMR** (500 MHz, acetone):  $\delta$  (ppm) = 3.02-3.71 (br, 4H, -CH<sub>2</sub>), 2.27-2.89 (br, 2H, -CH), 1.51-2.21 (br, 4H, -CH<sub>2</sub>), 0.98-1.32 (br, s, 6H, -CH<sub>3</sub>).

**<sup>13</sup>C NMR** (500 MHz, acetone-*d*<sub>6</sub>):  $\delta$  (ppm) = 173.2 (C=O), 166.1 (C=O), 142.1, 140.1, 138.6, 136.9, 136.2, 135.7 (6C, C<sub>Ar</sub>), 40.2 (CH<sub>2</sub>), 40.1 (CH), 39.9 (CH<sub>2</sub>), 36.1 (CH), 35.4 (CH<sub>2</sub> backbone), 35.1 (CH<sub>2</sub> backbone), 13.1 (CH<sub>3</sub>).

**<sup>19</sup>F NMR** (600 MHz, CDCl<sub>3</sub>):  $\delta$  (ppm) = -162,2 (2F), -156,3 (1F), -152,7 (2F).

**FT-IR (ATR)**  $\tilde{\nu}$  (cm<sup>-1</sup>) = 3456, 2975, 2925, 1780, 1616, 1519, 1448, 1280, 1035.

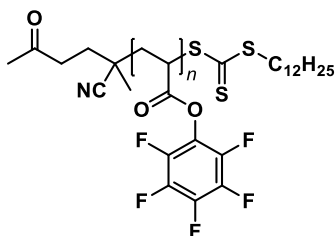
**Poly(*N*-isopropylacrylamide-co-pentafluorophenyl acrylate) (P<sub>N1a</sub> – P<sub>N1f</sub>):**

<sup>1</sup>H NMR (500 MHz, actone):  $\delta$  (ppm) = 7.21 (s, br, 1H, NH), 4.02 (s, –NH–CH), 2.78 (s, 1H, –CH (PFPA), 2.05–2.51 (br, 2H, –CH<sub>2</sub>), 1.43–1.74 (br, 3H, –CH<sub>2</sub>, –CH), 1.19 (br, s, 6H, –CH<sub>3</sub>).

<sup>13</sup>C NMR (500 MHz, aceton-*d*<sub>6</sub>):  $\delta$  (ppm) = 176 (C=O), 171 (C=O), 42.1 (CH<sub>2</sub>), 41.9 (CH), 37.9 (CH<sub>2</sub>), 42.0 (CH), 41.1 (CH), 39.1 (CH<sub>2</sub>), 20.2 (CH<sub>3</sub>).

<sup>19</sup>F NMR (600 MHz, aceton-*d*<sub>6</sub>):  $\delta$  (ppm) = -158, -161, -166.

FT IR (ATR)  $\tilde{\nu}$  (cm<sup>-1</sup>) = 3278, 2973, 2941, 2973, 1776, 1517, 1461, 995.

**Poly(pentafluorophenyl acrylate) (P<sub>RA</sub>) *via* RAFT Polymerization**

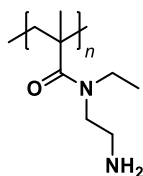
Pentafluorophenyl acrylate (10.2 g, 42.8 mmol), 4-cyano-4-[(dodecyl-sulfanylthiocarbonyl)-sulfanyl]pentanoic acid (84.0 mg, 0.209 mmol) and 2,2'-Azobis(2-methylpropionitrile) (2.70 mg, 16  $\mu$ mol) were added to 60 mL anhydrous 1,3-dioxane in a flask. The mixture was freeze-pump-thaw three times followed by flask filling with argon. The reaction was heated to 75 °C and stirred for 19 h. The crude product was precipitation in *n*-hexane and dissolved in acetone. The procedure was repeated three times followed by solvent evaporation under reduced pressure. The title polymer sample was obtained as a colorless solid (81%).

<sup>1</sup>H NMR (500 MHz, CDCl<sub>3</sub>):  $\delta$  (ppm) = 3.11 (br s), 2.49 (br s), 2.10 (br s).

<sup>13</sup>C NMR (500 MHz, CDCl<sub>3</sub>):  $\delta$  (ppm) = 170.3 (C=O), 141.4 (m, ArC), 138.7 (m, C=C), 137.5 (m, C=C), 60.3 (m, –CH<sub>3</sub>), 40.5 (m, –CH<sub>3</sub>, –CH<sub>2</sub>), 24.9 (m, –CH<sub>2</sub>).

<sup>19</sup>F NMR (600 MHz, CDCl<sub>3</sub>):  $\delta$  (ppm) = -162.2, -157.8, -153.4.

FT-IR (ATR)  $\tilde{\nu}$  (cm<sup>-1</sup>) = 1780, 1512, 1091.

**poly(*N*-(2-aminoethyl)-*N*-ethyl-methacrylamide (P3)**

*N*-ethylethylenediamine (1.50 mL, 14.0 mmol; 10 eq.) was dissolved in MIBK (30 mL; 0.24 mol; 170 eq.). Magnesium sulphate anhydrous (0.910 g; 7.56 mmol; 5.48 eq.) was added and the dispersion was heated while stirring for 21 hours to reflux. Poly(PFPMA) (0.349 g; 1.00 eq.) and triethylamine (2.5 mL; 18 mmol; 13 eq.) dissolved in MIBK (10 mL) were added and heated for additional 48 hours while stirring to reflux. The obtained dispersion was decanted and the slightly orange solution dialysed in acetone. The solvent was removed *via* vacuum and the obtained orange solid was dissolved in 2-propanol (15 mL; 0.20 mol; 140 eq.). Demineralised water (1.5 mL; 83 mmol; 60 eq.) was added and the solution heated to 50 °C while stirring for 21 hours. The solvents were removed *via* vacuum. 0.132 g (61%) of a orange solid was obtained.

$^1\text{H NMR}$  (600 MHz, DMSO- $d_6$ ):  $\delta$  (ppm) = 3.3 -4.3 (br,  $\text{NH}_2$ ), 2.4-2.9 (br,  $\text{CH}_2$ ), 0.6-1.5 (br,  $\text{CH}_3$ ).

$^{19}\text{F NMR}$  (600 MHz, DMSO- $d_6$ ):  $\delta$  (ppm) = -169.69, -170.71, -190.48.

$^{13}\text{C NMR}$  (500 MHz, DMSO- $d_6$ ):  $\delta$  (ppm) = 51.8 ( $-\text{CH}_2-$ ), 50.1 ( $-\text{CH}_2-$ ), 48.5 ( $-\text{CH}_2-$ ), 47.4 ( $-\text{CH}_2-$ ), 35.1 ( $-\text{CH}_3$ ), 18.1 ( $-\text{CH}_3$ )

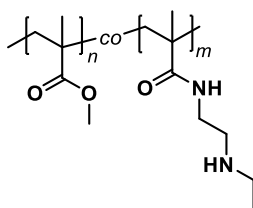
**FT-IR (ATR)**  $\tilde{\nu}$  ( $\text{cm}^{-1}$ ) = 2966, 2930, 1714, 1657, 1456, 1332, 1122, 1005, 977.

## 5.2.4 Post-polymerization modifications

### General procedure of the aminolysis of p(MMA-*co*-PFPMA, $\text{P}_{\text{M1}}$ ), p(NIPAM-*co*-PFPA, $\text{P}_{\text{N2}}$ ) and p(DEA-*co*-PFPA, $\text{P}_{\text{D2}}$ ) with *N*-ethylethylenediamine

All polymer samples were dissolved in a mixture of THF/acetone (4:1 v/v), respectively, and treated with an excess of *N*-ethylethylenediamine (4.0 eq.) and triethylamine (4.0 eq.) as auxiliary base. The reaction solution was heated at 45 °C and stirred. The progress of the PFP ester substitution was monitored by ATR-IR spectroscopy. After achieving full conversion, the crude product was purified by dialysis in acetone ( $\text{MWCO} = 6000 \text{ g mol}^{-1}$ ) for at least 5 d. The solvent was evaporated under reduced pressure. The title compound was obtained as a slightly yellow solid (90-99% yield).

### Poly(*N*-(2-(ethylamino)ethyl)methacrylamide-*co*-methyl methacrylate) ( $\text{P}_{\text{M2}}$ )



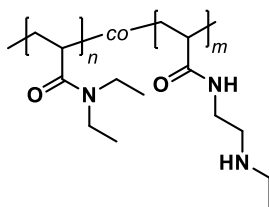
**Reaction time:** 5 d

**$^1\text{H}$  NMR** (500 MHz, acetone- $d_6$ ):  $\delta$  (ppm) = 3.66 (s br,  $-\text{NHCH}_2$ ), 3.53 (s br, 3H,  $-\text{OCH}_3$ ), 3.42 (s br, 2H,  $\text{CH}_2$ ), 2.53-2.85 (m br, 4H,  $\text{CH}_2$ ), 1.75-2.00 (m br), 1.56 (s br), 1.08-1.36 (m br), 0.95 (s br), 0.77 (s br).

**$^{13}\text{C}$  NMR** (500 MHz, acetone- $d_6$ ):  $\delta$  (ppm) = 54.5 ( $-\text{CH}_2-$ ), 51.6 ( $-\text{OCH}_3$ ), 43.7( $-\text{CH}_2-$ ), 43.1 ( $-\text{CH}_2-$ ), 40.1 ( $-\text{NHCH}_2-$ ), 47.3 ( $-\text{CH}_2-$ ), 43.3 ( $-\text{CH}_2-$ ), 27.6 ( $-\text{CH}_3$ ), 18.5 ( $-\text{CH}_3$ ), 16.7 ( $-\text{CH}_3$ )

**FT-IR (ATR)**  $\tilde{\nu}$  ( $\text{cm}^{-1}$ ) = 2956, 1722, 1434, 1236, 1141, 977.

**Poly(*N*-(2-(ethylamino)ethyl)acrylamide-*co*-*N,N*-diethylacrylamide) (P<sub>D2</sub>)**



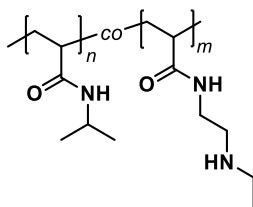
**Reaction time:** 2 d

**$^1\text{H}$  NMR** (500 MHz,  $\text{CDCl}_3$ ):  $\delta$  (ppm) = 3.05-3.70 (br, 6H,  $-\text{CH}_2$ ), 2.21-3.01 (m br, 10 H), 1.57-1.99 (m br, 4H), 1.36 (br, 3H,  $\text{CH}_3$ ) 0.97-1.29 (br, s, 6H,  $-\text{CH}_3$ ).

**$^{13}\text{C}$  NMR** (500 MHz,  $\text{CDCl}_3$ ):  $\delta$  (ppm) = 173.1 (C=O), 172.5 (C=O), 42.2 (CH), 41.4 ( $\text{CH}_2$ ), 41.0 (2C,  $\text{CH}_2$ ), 36.3 ( $\text{CH}_2$  backbone), 36.3 ( $\text{CH}_2$  backbone), 36.1 ( $\text{CH}_3$  backbone), 35.3 ( $\text{CH}_2$  backbone), 14.5 ( $\text{CH}_3$ ), 12.8 ( $\text{CH}_3$ )

**FT-IR (ATR)**  $\tilde{\nu}$  ( $\text{cm}^{-1}$ ) = 3506, 2977, 2929, 1625, 1436, 1268, 1101.

**Poly(*N*-(2-(ethylamino)ethyl)methacrylamide-*co*-*N*-isopropylacrylamide) (P<sub>N2</sub>)**



**Reaction time:** 2 d

**$^1\text{H}$  NMR** (500 MHz, acetone):  $\delta$  (ppm) = 7.39 (s, br, 1H, NH), 4.02-3.97 (s,  $-\text{NH}-\text{CH}_2$ ; 2H, C=ONH $\text{CH}_2$ ), 2.67-2.88 (m br, 4H,  $-\text{CH}_2$ ), 2.48-2.09 (br, 2H,  $-\text{CH}$  backbone), 1.89-1.34 (br, 4H,  $-\text{CH}_2$  backbone), 1.50-1.03 (s, 9H,  $-\text{CH}_3$ ).

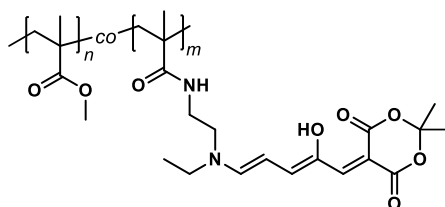
**$^{13}\text{C}$  NMR** (500 MHz,  $\text{CDCl}_3$ ):  $\delta$  (ppm) = 175 (C=O), 171 (C=O), 48.3 ( $\text{CH}_2$ ), 43.1 ( $\text{CH}_2$ ), 42.1 (CH), 41.1 (CH), 39.1 ( $\text{CH}_2$ ), 36.2 ( $\text{CH}_2$  backbone), 35.3 ( $\text{CH}_2$  backbone), 29.3 (CH), 22.1 ( $\text{CH}_3$ ), 14.1 ( $\text{CH}_3$ )

**FT-IR (ATR)**  $\tilde{\nu}$  (cm<sup>-1</sup>) = 3297, 2970, 2932, 1645, 1515, 1452, 1166.

### General synthesis procedure of DASA formation with the precursors S2, S4 and S5

All polymer samples of the **P<sub>M</sub>2/P<sub>D</sub>2/P<sub>N</sub>3** series were dissolved in anhydrous THF, respectively, and treated with an excess of the furan precursor **S2/S4/S5** (5.0 eq.). The reaction mixture was stirred under an argon atmosphere at room temperature. The progress of the DASA formation was monitored using UV-vis spectroscopy.

#### p(MMA-EEDA-DASA) (**P<sub>M</sub>3**)

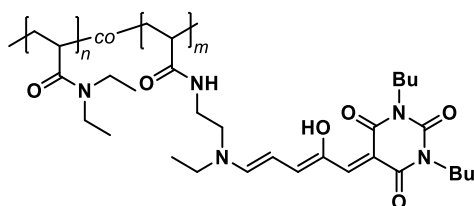


**Reaction time:** 5 d

**<sup>1</sup>H NMR** (500 MHz, CDCl<sub>3</sub>):  $\delta$  (ppm) = 11.4 (s br, 1H, -OH), 7.1-5.9 (m, 4H, C=C), 3.77 (s br, -NHCH<sub>2</sub>), 3.51 (s br, 3H, -OCH<sub>3</sub>), 3.02 (s br, 2H, CH<sub>2</sub>), 2.54-2.81 (m br, 4H, CH<sub>2</sub>), 1.72-2.00 (m br), 1.56 (s br), 1.06-1.46 (m br), 0.94 (s br), 0.77 (s br).

**FT-IR (ATR)**  $\tilde{\nu}$  (cm<sup>-1</sup>) = 2956, 1726, 1708, 1488, 1456, 1253, 1151, 983, 746.

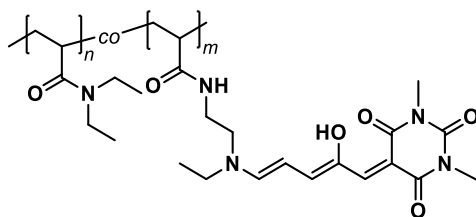
#### p(DEA-EEDA-DASA) (**P<sub>DBu</sub>3**)



**Reaction time:** 5 d

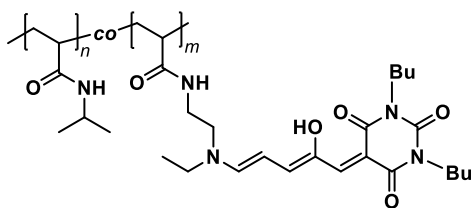
**<sup>1</sup>H NMR** (500 MHz, DMF):  $\delta$  (ppm) = 11.4 (s br, 1H, -OH), 8.21-6.81 (m, 4H, C=C), 4.51 (s br, 2H, CH<sub>2</sub>), 3.92 (m br, 2H, CH<sub>2</sub>), 3.79-3.01 (br, 6H, -CH<sub>2</sub>), 2.51-2.20 (m br), 1.92-1.59 (m br), 1.42-0.91 (m br).

**FT-IR (ATR)**  $\tilde{\nu}$  (cm<sup>-1</sup>) = 3299, 2973, 1712, 1618, 1571, 1488, 1400, 1357, 1004, 981.

**p(DEA-EEDA-DASA) (P<sub>DMe3</sub>)****Reaction time:** 5 d

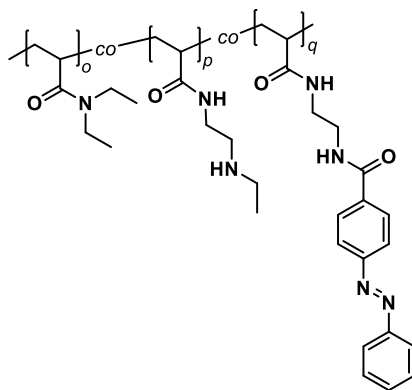
<sup>1</sup>H NMR (500 MHz, DMF):  $\delta$  (ppm) = 11.3 (s br, 1H, -OH), 8.20-6.88 (m, 4H, C=C), 4.50 (s br, 2H, CH<sub>2</sub>), 3.82-3.01 (br, 6H, -CH<sub>2</sub>), 2.51-2.20 (m br), 1.91-1.55 (m br), 1.43-0.90 (m br).

FT-IR (ATR)  $\tilde{\nu}$  (cm<sup>-1</sup>) = 3303, 2973, 1716, 1635, 1571, 1458, 1365, 1000, 786.

**p(NIPAM-EEDA-DASA) (P<sub>N3</sub>)****Reaction time:** 5 d

<sup>1</sup>H NMR (500 MHz, CDCl<sub>3</sub>):  $\delta$  (ppm) = 10.9 (s br, 1H, -OH), 7.11-5.91 (m, 4H, C=C), 4.19 (s br, 2H, NHCH<sub>2</sub>), 3.99 (s br, 1H, NHCH(CH<sub>3</sub>)<sub>2</sub>), 3.71 (br, 2H, -CH<sub>2</sub>), 2.92-2.52 (m br), 2.10-0.81 (m br).

FT IR (ATR)  $\tilde{\nu}$  (cm<sup>-1</sup>) = 3287, 2964, 1770, 1785, 1656, 1410, 1214, 883, 755.

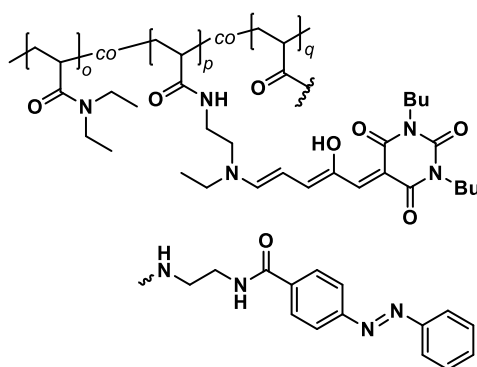
**General post-polymerization procedure of P<sub>Pr</sub> for the synthesis of P1<sub>Azo</sub>**

All polymer samples of **P<sub>PR</sub>** were dissolved in THF, respectively, and treated with different amounts of **S11** (4.0 eq.) and EEDA. Triethylamine (2.0 eq.) was added as auxiliary base. The reaction solution was heated at 45 °C and stirred for a duration of 6 h. An excess of diethylamine (3 eq.) was added and the reaction was stirred for 24 h. The progress of the PFP ester substitution was monitored by ATR-IR spectroscopy. After achieving full conversion, the crude product was purified by dialysis in acetone (MWCO = 1000 g mol<sup>-1</sup>) for 15 d. The solvent was evaporated under reduced pressure. The title compound was obtained as a slightly yellow solid (90-99% yield).

<sup>1</sup>H NMR (500 MHz, acetone-*d*<sub>6</sub>):  $\delta$  (ppm) = 8.23-7.81 (m br, 6H, ArH), 7.48 (s br, 3H, ArH), 3.59-2.89 (m br), 2.87-2.21 (m br), 2.21-1.48 (m br), 1.46-0.81 (m br, 9H, CH<sub>3</sub>).

FT-IR (ATR)  $\tilde{\nu}$  (cm<sup>-1</sup>) = 2971, 2930, 2865, 1718, 1674, 1624, 1494, 1466, 1270, 1066, 978.

#### General post-polymerization procedure of **P1<sub>Azo</sub>** for the synthesis of **P2<sub>Azo</sub>**



All polymer samples of the **P1<sub>Azo</sub>** series were dissolved in anhydrous THF, respectively, and treated with an excess of the furan precursor **S5** (5.0 eq.). The reaction mixture was stirred under an argon atmosphere at room temperature for a duration of 5 d. The progress of the DASA formation was monitored using UV-vis spectroscopy. The crude product was purified by dialysis in dichloromethane (MWCO = 1000 g mol<sup>-1</sup>) for 5 d. The solvent was evaporated under reduced pressure. The title compound was obtained as a slightly purple solid (85-90% yield).

<sup>1</sup>H NMR (500 MHz, CDCl<sub>3</sub>):  $\delta$  (ppm) = 8.36-7.94 (m br, 6H, ArH), 7.60 (s, br, C<sub>H</sub>=CH), 7.49 (s br, 3H, ArH), 7.15 (s, br, C<sub>H</sub>=CH), 6.89 (s, br, C<sub>H</sub>=CH), 6.75 (s, br, C<sub>H</sub>=CH), 4.48 (s, br, NHCH<sub>2</sub>), 3.80-2.81 (m br), 2.85-2.10 (m br), 1.98-1.38 (m br), 1.37-0.85 (m br, 9H, CH<sub>3</sub>).

FT IR (ATR)  $\tilde{\nu}$  (cm<sup>-1</sup>) = 2981, 2935, 1716, 1605, 1513, 1463, 1294, 1161, 1077, 985.

# 6

## References

- (1) H. Staudinger, "Über Polymerisation", *Berichte der deutschen chemischen Gesellschaft (A and B Series)*, **1920**, *53*, 6, 1073–1085.
- (2) C. Priesner; A. J. Ihde, "H. Staudinger, H. Mark und K. H. Meyer: Thesen zur Grosse und Struktur der Makromoleküle: Ursachen und Hintergrunde eines akademischen Disputes", *Weinheim Verlag*, **1980**, *73*, 1, 121–122.
- (3) C. Krüll, "Aufbruch ins Zeitalter der Makromoleküle", *Kultur und Technik*, **1978**, *3*, 44–49.
- (4) PlasticsEurope Deutschland e.V., "Plastics - the facts 2019, Presented at K2019, Düsseldorf, **2019**.
- (5) PlasticsEurope Deutschland e.V., "Plastics - the facts 2016, Presented at K2016, Düsseldorf, **2016**.
- (6) M. L. Tebaldi; R. M. Belardi; F. S. Poletto, "Smart Polymers: Synthetic Strategies, Supramolecular Morphologies, and Drug Loading", **2016**, *32*, 147–164.
- (7) O. Bertrand; J.-F. Gohy, "Photo-responsive polymers: synthesis and applications", *Polym. Chem.*, **2017**, *8*, 1, 52–73.
- (8) R. J. Young; P. A. Lovell, "Introduction to polymers", 3rd ed., *Taylor&Francis Group*, Boca Raton, **2011**.
- (9) E. Saldivar-Guerra; E. Vivaldo-Lima, "Handbook of Polymer Synthesis, Characterization, and Processing", 1st ed., *Wiley*, Hoboken, **2013**.
- (10) M. Szwarc; M. VanBeylen, "Ionic polymerization and living polymers", 1st ed., *Chapman & Hall*, New York, **1993**.
- (11) O. Vogl, "Review and Future of Ionic Polymerization with Special Emphasis on Carbonyl Polymerization", *Journal of Macromolecular Science: Part A - Chemistry*, **1975**, *9*, 5, 663–685.
- (12) G. Moad; D. H. Solomon, "The chemistry of radical polymerization", 2., fully rev. ed., *Elsevier*, Amsterdam, **2006**.
- (13) Handbook of Polymer Synthesis, Characterization, and Processing: *Coordination Polymerization*", 1st ed., Vol. 2013, *Wiley*, **2013**.
- (14) C. C. Price; E. J. Vandenberg, "Coordination Polymerization", 1st ed., Vol. 19, *Springer US*, Boston, **1983**.
- (15) A. D. Jenkins; R. G. Jones; G. Moad, "Terminology for reversible-deactivation radical polymerization previously called "controlled" radical or "living" radical polymerization (IUPAC Recommendations 2010)", *Pure and Applied Chemistry*, **2009**, *82*, 2, 483–491.

- (16) A. D. Jenkins; R. G. Jones; G. Moad, "Terminology for reversible-deactivation radical polymerization previously called "controlled" radical or "living" radical polymerization (IUPAC Recommendations 2010)", *Pure and Applied Chemistry*, **2009**, *82*, 2, 483–491.
- (17) M. K. Mishra; Y. Yagci, "Handbook of vinyl polymers: *Radical polymerization, process, and technology*", 2nd ed., *Taylor & Francis*, Boca Raton, **2010**.
- (18) J. K. Stille, "Step-Growth polymerization", *Journal of Chemical Education*, **1981**, *58*, 11, 862–866.
- (19) W. H. Carothers, "Polymerization", *Chemical Review*, **1931**, *8*, 3, 353–426.
- (20) Su, W.-F., Ed., "Principles of Polymer Design and Synthesis", 1st ed., Lecture Notes in Chemistry, *Springer Berlin Heidelberg*, Berlin, Heidelberg, **2013**.
- (21) M. D. Lechner; K. Gehrke; E. H. Nordmeier, "Synthese von Makromolekülen, Polyreaktionen", 3rd ed., *Birkhäuser*, Basel, 48-166, **2003**.
- (22) K.-M. Schellerer; T. Kufner; O. Mieden; E. Vogel, "Polyvinyl Chloride (PVC)", *Plastics Insights*, **2016**, *10*, 28–32.
- (23) G. Akovali, "Toxicity of building materials: *Plastic materials: polyvinyl chloride (PVC)*", *Woodhead Publishing Limited*, 23-53, **2012**.
- (24) K. Yates, "Packaging Materials: *Polystyrene for food packaging applications*", 1st ed., ILSI Europe Report Series, Vol. 2, *ILSI Europe*, Brussels, **2002**.
- (25) N. H. Ramli Sulong; S. A. S. Mustapa; M. K. Abdul Rashid, "Application of expanded polystyrene (EPS) in buildings and constructions: A review", *J Appl Polym Sci*, **2019**, *45*, 3, 47529.
- (26) U. Ali; K. J. B. A. Karim; N. A. Buang, "A Review of the Properties and Applications of Poly (Methyl Methacrylate) (PMMA)", *Polymer Reviews*, **2015**, *55*, 4, 678–705.
- (27) H. Teng; K. Koike; D. Zhou; Z. Satoh; Y. Koike; Y. Okamoto, "High glass transition temperatures of poly(methyl methacrylate) prepared by free radical initiators", *J. Polym. Sci. A Polym. Chem.*, **2009**, *47*, 1, 315–317.
- (28) S. L. Aggarwal; O. J. Sweeting, "Polyethylene: Preparation, Structure, And Properties", *Chem. Rev.*, **1957**, *57*, 4, 665–742.
- (29) C. Chatgililoglu; A. Studer, "Encyclopedia of radicals in chemistry, biology, and materials: *Radical Polymerization in Industry*", 1st ed., *John Wiley & Sons*, Hoboken, 1-36, **2012**.
- (30) S. Kobayashi; K. Müllen, "Encyclopedia of Polymeric Nanomaterials", 1st ed., *Springer Berlin Heidelberg*, Berlin, Heidelberg, 772-839, **2015**.
- (31) D. Griller; K. U. Ingold, "Persistent carbon-centered radicals", *Acc. Chem. Res.*, **1976**, *9*, 1, 13–19.
- (32) N. Ballard; J. M. Asua, "Radical polymerization of acrylic monomers: An overview", *Progress in Polymer Science*, **2018**, *79*, 40–60.

- (33) V. P. Zubov; M. V. Kumar; M. N. Masterova; V. A. Kabanov, "Reactivity of Allyl Monomers in Radical Polymerization", *Journal of Macromolecular Science: Part A - Chemistry*, **1979**, *13*, 1, 111–131.
- (34) R. O. Ebewele, "Polymer Science and Technology", 1st ed., *Chapman and Hall/CRC*, Boca Raton, **2000**.
- (35) M. Farina, "Chemistry and kinetics of the chain transfer reaction", *Makromolekulare Chemie. Macromolecular Symposia*, **1987**, *10-11*, 1, 255–272.
- (36) J. Chiefari; J. Jeffery; R. T. A. Mayadunne; G. Moad; E. Rizzardo; S. H. Thang, "Chain Transfer to Polymer: A Convenient Route to Macromonomers", *Macromolecules*, **1999**, *32*, 22, 7700–7702.
- (37) G. Moad, "Polymer Science: A Comprehensive Reference", *Polymer*, **2012**, *53*, 3, 59–118.
- (38) B. Klumperman, "Encyclopedia of Polymer Science and Technology: Reversible Deactivation Radical Polymerization", 4th ed., Vol. 7, *Wiley*, Hoboken, **2015**.
- (39) K. Matyjaszewski, "Overview: Fundamentals of Controlled/Living Radical Polymerization", *ACS Symposium Series*, **1998**, *1*, 685, 2–30.
- (40) K. Matyjaszewski, "Comparison and Classification of Controlled/Living Radical Polymerizations", *ACS Symposium Series*, **2000**, *1*, 768, 2–26.
- (41) D. J. Keddie, "A guide to the synthesis of block copolymers using reversible-addition fragmentation chain transfer (RAFT) polymerization", *Chemical Society reviews*, **2014**, *43*, 2, 496–505.
- (42) C. J. Hawker, "Molecular Weight Control by a "Living" Free-Radical Polymerization Process", *J. Am. Chem. Soc.*, **1994**, *116*, 24, 11185–11186.
- (43) M. Kato; M. Kamigaito; M. Sawamoto; T. Higashimura, "Polymerization of Methyl Methacrylate with the Carbon Tetrachloride/Dichlorotris- (triphenylphosphine)ruthenium(II)/Methylaluminum Bis(2,6-di-tert-butylphenoxide) Initiating System: Possibility of Living Radical Polymerization", *Macromolecules*, **1995**, *28*, 5, 1721–1723.
- (44) S. Perrier, "50th Anniversary Perspective : RAFT Polymerization—A User Guide", *Macromolecules*, **2017**, *50*, 19, 7433–7447.
- (45) D. J. Keddie; G. Moad; E. Rizzardo; S. H. Thang, "RAFT Agent Design and Synthesis", *Macromolecules*, **2012**, *45*, 13, 5321–5342.
- (46) G. Moad; E. Rizzardo; S. H. Thang, "Living Radical Polymerization by the RAFT Process—A First Update", *Aust. J. Chem.*, **2006**, *59*, 10, 669.
- (47) J. Jennings; M. Beija; J. T. Kennon; H. Willcock; R. K. O'Reilly; S. Rimmer; S. M. Howdle, "Advantages of Block Copolymer Synthesis by RAFT-Controlled Dispersion Polymerization in Supercritical Carbon Dioxide", *Macromolecules*, **2013**, *46*, 17, 6843–6851.

- (48) A. W. York; S. E. Kirkland; C. L. McCormick, "Advances in the synthesis of amphiphilic block copolymers via RAFT polymerization: stimuli-responsive drug and gene delivery", *Advanced drug delivery reviews*, **2008**, *60*, 9, 1018–1036.
- (49) C. Barner-Kowollik; T. P. Davis; M. H. Stenzel, "Synthesis of Star Polymers using RAFT Polymerization: What is Possible?", *Aust. J. Chem.*, **2006**, *59*, 10, 719.
- (50) C.-Y. Hong; Y.-Z. You; J. Liu; C.-Y. Pan, "Dendrimer-star polymer and block copolymer prepared by reversible addition-fragmentation chain transfer (RAFT) polymerization with dendritic chain transfer agent", *J. Polym. Sci. A Polym. Chem.*, **2005**, *43*, 24, 6379–6393.
- (51) Q. Zheng; C.-Y. Pan, "Synthesis and Characterization of Dendrimer-Star Polymer Using Dithiobenzoate-Terminated Poly(propylene imine) Dendrimer via Reversible Addition-Fragmentation Transfer Polymerization", *Macromolecules*, **2005**, *38*, 16, 6841–6848.
- (52) C. Barner-Kowollik, "Handbook of RAFT polymerization", 1st ed., *Wiley-VCH*, Weinheim, **2008**.
- (53) K. Matyjaszewski; J. Spanswick, "Controlled/living radical polymerization", *Materials Today*, **2005**, *8*, 3, 26–33.
- (54) L. Pilato, "Phenolic resins: 100Years and still going strong", *Reactive and Functional Polymers*, **2013**, *73*, 2, 270–277.
- (55) S. Koltzenburg; M. Maskos; O. Nuyken, "Polymere: Synthese, Eigenschaften und Anwendungen", *Springer Berlin Heidelberg*, Berlin, Heidelberg, **2014**.
- (56) R. Aelion, "Nylon 6 and Related Polymers", *Ind. Eng. Chem.*, **1961**, *53*, 10, 826–828.
- (57) S. C. H. J. Turk; W. P. Kloosterman; D. K. Ninaber; K. P. A. M. Kolen; J. Knutova; E. Suir; M. Schürmann; P. C. Raemakers-Franken; M. Müller; S. M. A. de Wildeman; L. M. Raamsdonk; R. van der Pol; L. Wu; M. F. Temudo; R. A. M. van der Hoeven; M. Akeroyd; R. E. van der Stoel; H. J. Noorman; R. A. L. Bovenberg; A. C. Trefzer, "Metabolic Engineering toward Sustainable Production of Nylon-6", *ACS synthetic biology*, **2016**, *5*, 1, 65–73.
- (58) R. Nisticò, "Polyethylene terephthalate (PET) in the packaging industry", *Polymer Testing*, **2020**, *90*, 106707.
- (59) M. C. Wythers, "Advances in Materials Science Research. Volume 48, Advances in Materials Science Research Ser, *Nova Science Publishers Incorporated*, New York, 132-136, **2021**.
- (60) L. T. Sin; B. S. Tveen, "Plastics and environmental sustainability issues", *Elsevier*, **2023**, *150*, 1–43.
- (61) A. Bossion; K. V. Heifferon; L. Meabe; N. Zivic; D. Taton; J. L. Hedrick; T. E. Long; H. Sardon, "Opportunities for organocatalysis in polymer synthesis via step-growth methods", *Progress in Polymer Science*, **2019**, *90*, 44941, 164–210.

- (62) M. A. Gauthier; M. I. Gibson; H.-A. Klok, "Synthesis of functional polymers by post-polymerization modification", *Angewandte Chemie (International ed. in English)*, **2009**, *48*, 1, 48–58.
- (63) P. Theato, "Synthesis of well-defined polymeric activated esters", *J. Polym. Sci. A Polym. Chem.*, **2008**, *46*, 20, 6677–6687.
- (64) A. Das; P. Theato, "Activated Ester Containing Polymers: Opportunities and Challenges for the Design of Functional Macromolecules", *Chemical reviews*, **2016**, *116*, 3, 1434–1495.
- (65) H. C. Kolb; M. G. Finn; K. B. Sharpless, "Click Chemistry: Diverse Chemical Function from a Few Good Reactions", *Angew. Chem. Int. Ed.*, **2001**, *40*, 11, 2004–2021.
- (66) M. Breugst; H.-U. Reissig, "The Huisgen Reaction: Milestones of the 1,3-Dipolar Cycloaddition", *Angewandte Chemie International Edition*, **2020**, *59*, 30, 12293–12307.
- (67) D. P. Nair; M. Podgórski; S. Chatani; T. Gong; W. Xi; C. R. Fenoli; C. N. Bowman, "The Thiol-Michael Addition Click Reaction: A Powerful and Widely Used Tool in Materials Chemistry", *Chem. Mater.*, **2014**, *26*, 1, 724–744.
- (68) P. Ferruti; A. Bettelli; A. Feré, "High polymers of acrylic and methacrylic esters of N-hydroxysuccinimide as polyacrylamide and polymethacrylamide precursors", *Polymer*, **1972**, *13*, 10, 462–464.
- (69) H. G. Batz; G. Franzmann; H. Ringsdorf, "Model reactions for synthesis of pharmacologically active polymers by way of monomeric and polymeric reactive esters", *Angew. Chem. Int. Ed.*, **1972**, *11*, 12, 1103–1104.
- (70) M. Eberhardt; R. Mruk; R. Zentel; P. Théato, "Synthesis of pentafluorophenyl(meth)acrylate polymers: New precursor polymers for the synthesis of multifunctional materials", *European Polymer Journal*, **2005**, *41*, 7, 1569–1575.
- (71) G. W. Anderson; J. E. Zimmerman; F. M. Callahan, "N-Hydroxysuccinimide Esters in Peptide Synthesis", *J. Am. Chem. Soc.*, **1963**, *85*, 19, 3039.
- (72) T. Tanaka, "Recent Advances in Polymers Bearing Activated Esters for the Synthesis of Glycopolymers by Postpolymerization Modification", *Polymers*, **2024**, *16*, 8, 1100.
- (73) K. A. Günay; P. Theato; H.-A. Klok, "History of Post-Polymerization Modification", **2013**, *7*, 1–44.
- (74) M. Wei; Y. Gao; X. Li; M. J. Serpe, "Stimuli-responsive polymers and their applications", *Polym. Chem.*, **2017**, *8*, 1, 127–143.
- (75) F. D. Jochum; P. Theato, "Temperature- and light-responsive smart polymer materials", *Chemical Society reviews*, **2013**, *42*, 17, 7468–7483.
- (76) M. A. Ward; T. K. Georgiou, "Thermoresponsive Polymers for Biomedical Applications", *Polymers*, **2011**, *3*, 3, 1215–1242.
- (77) E. Cabane; X. Zhang; K. Langowska; C. G. Palivan; W. Meier, "Stimuli-responsive polymers and their applications in nanomedicine", *Biointerphases*, **2012**, *7*, 1-4, 9.

- (78) P. Schattling; F. D. Jochum; P. Theato, "Multi-stimuli responsive polymers – the all-in-one talents", *Polym. Chem.*, **2014**, *5*, 1, 25–36.
- (79) D. Roy; W. L. A. Brooks; B. S. Sumerlin, "New directions in thermoresponsive polymers", *Chemical Society reviews*, **2013**, *42*, 17, 7214–7243.
- (80) Y. Kotsuchibashi, "Recent advances in multi-temperature-responsive polymeric materials", *Polym J*, **2020**, *52*, 7, 681–689.
- (81) A. Gandhi; A. Paul; S. O. Sen; K. K. Sen, "Studies on thermoresponsive polymers: Phase behaviour, drug delivery and biomedical applications", *Asian Journal of Pharmaceutical Sciences*, **2015**, *10*, 2, 99–107.
- (82) M. Karimi; P. Sahandi Zangabad; A. Ghasemi; M. Amiri; M. Bahrami; H. Malekzad; H. Ghahramanzadeh Asl; Z. Mahdieh; M. Bozorgomid; A. Ghasemi; M. R. Rahmani Tajji Boyuk; M. R. Hamblin, "Temperature-Responsive Smart Nanocarriers for Delivery Of Therapeutic Agents: Applications and Recent Advances", *ACS applied materials & interfaces*, **2016**, *8*, 33, 21107–21133.
- (83) C. Pietsch; R. Hoogenboom; U. S. Schubert, "PMMA based soluble polymeric temperature sensors based on UCST transition and solvatochromic dyes", *Polym. Chem.*, **2010**, *1*, 7, 1005–1008.
- (84) H. Zhao; H. An; B. Xi; Y. Yang; J. Qin; Y. Wang; Y. He; X. Wang, "Self-Healing Hydrogels with both LCST and UCST through Cross-Linking Induced Thermo-Response", *Polymers*, **2019**, *11*, 3, 2–17.
- (85) Q. Zhang; C. Weber; U. S. Schubert; R. Hoogenboom, "Thermoresponsive polymers with lower critical solution temperature: from fundamental aspects and measuring techniques to recommended turbidimetry conditions", *Mater. Horiz.*, **2017**, *4*, 2, 109–116.
- (86) C. Weber; R. Hoogenboom; U. S. Schubert, "Temperature responsive bio-compatible polymers based on poly(ethylene oxide) and poly(2-oxazoline)s", *Progress in Polymer Science*, **2012**, *37*, 5, 686–714.
- (87) R. Liu; M. Fraylich; B. R. Saunders, "Thermoresponsive copolymers: from fundamental studies to applications", *Colloid Polym Sci*, **2009**, *287*, 6, 627–643.
- (88) D. J. Phillips; M. I. Gibson, "Towards being genuinely smart: 'isothermally-responsive' polymers as versatile, programmable scaffolds for biologically-adaptable materials", *Polym. Chem.*, **2015**, *6*, 7, 1033–1043.
- (89) G. ten Brinke; F. E. Karasz, "Lower critical solution temperature behavior in polymer blends: compressibility and directional-specific interactions", *Macromolecules*, **1984**, *17*, 4, 815–820.
- (90) F. Liu; M. W. Urban, "Recent advances and challenges in designing stimuli-responsive polymers", *Progress in Polymer Science*, **2010**, *35*, 1-2, 3–23.
- (91) J. Niskanen; H. Tenhu, "How to manipulate the upper critical solution temperature (UCST)?", *Polym. Chem.*, **2017**, *8*, 1, 220–232.

- (92) H. Yamauchi; Y. Maeda, "LCST and UCST behavior of poly(N-isopropylacrylamide) in DMSO/water mixed solvents studied by IR and micro-Raman spectroscopy", *The journal of physical chemistry. B*, **2007**, *111*, 45, 12964–12968.
- (93) S. Saeki; N. Kuwahara; M. Nakata; M. Kaneko, "Upper and lower critical solution temperatures in poly (ethylene glycol) solutions", *Polymer*, **1976**, *17*, 8, 685–689.
- (94) J. Seuring; S. Agarwal, "Polymers with Upper Critical Solution Temperature in Aqueous Solution: Unexpected Properties from Known Building Blocks", *ACS Macro Lett.*, **2013**, *2*, 7, 597–600.
- (95) Z. Xu; W. Liu, "Poly(N-acryloyl glycinamide): a fascinating polymer that exhibits a range of properties from UCST to high-strength hydrogels", *Chemical communications (Cambridge, England)*, **2018**, *54*, 75, 10540–10553.
- (96) H. G. Schild, "Poly(N-isopropylacrylamide): experiment, theory and application", *Progress in Polymer Science*, **1992**, *17*, 2, 163–249.
- (97) K. Jain; R. Vedarajan; M. Watanabe; M. Ishikiriyama; N. Matsumi, "Tunable LCST behavior of poly(N-isopropylacrylamide/ionic liquid) copolymers", *Polym. Chem.*, **2015**, *6*, 38, 6819–6825.
- (98) N. A. Cortez-Lemus; A. Licea-Claverie, "Poly(N-vinylcaprolactam), a comprehensive review on a thermoresponsive polymer becoming popular", *Progress in Polymer Science*, **2016**, *53*, 2, 1–51.
- (99) R. Buscall; T. Corner, "The phase-separation behaviour of aqueous solutions of polyacrylic acid and its partial sodium salts in the presence of sodium chloride", *European Polymer Journal*, **1982**, *18*, 11, 967–974.
- (100) D. Eagland; N. J. Crowther, "Influence of composition and segment distribution upon lower critical demixing of aqueous poly(vinyl alcohol-stat-vinyl acetate) solutions", *European Polymer Journal*, **1991**, *27*, 3, 299–301.
- (101) J. Seuring; F. M. Bayer; K. Huber; S. Agarwal, "Upper Critical Solution Temperature of Poly(N -acryloyl glycinamide) in Water: A Concealed Property", *Macromolecules*, **2012**, *45*, 1, 374–384.
- (102) S. Qiao; H. Wang, "Temperature-responsive polymers: Synthesis, properties, and biomedical applications", *Nano Res.*, **2018**, *11*, 10, 5400–5423.
- (103) T. Kourti, "Turbidimetry in Particle Size Analysis", *Encyclopedia of Analytical Chemistry*, **2006**, *58*, 1–32.
- (104) D. J. MARMER; P. E. HURTUBISE, "NEPHELOMETRIC AND TURBIDIMETRIC IMMUNO-ASSAY", *Acedemic press*, **1996**, *2*, 363–387.
- (105) D.M. Lawler, "Turbidity, Turbidimetry, and Nephelometry", *Encyclopedia of Analytical Science*, **2005**, *179*, 343–351.
- (106) F. A. Jerca; V. V. Jerca; I.-C. Stancu, "Development and Characterization of Photoreponsive Polymers", *Springer International Publishing AG*, **2018**, *5*, 3–47.

- (107) O. Bertrand; J.-F. Gohy, "Photo-responsive polymers: synthesis and applications", *Polym. Chem.*, **2017**, *8*, 1, 52–73.
- (108) M. Irie; Y. Hirano; S. Hashimoto; K. Hayashi, "Photoresponsive polymers. 2. Reversible solution viscosity change of polyamides having azobenzene residues in the main chain", *Macromolecules*, **1981**, *14*, 2, 262–267.
- (109) Y. Zhao, "Light-Responsive Block Copolymer Micelles", *Macromolecules*, **2012**, *45*, 9, 3647–3657.
- (110) K. S. Kumar; V. B. Kumar; P. Paik, "Recent Advancement in Functional Core-Shell Nanoparticles of Polymers: Synthesis, Physical Properties, and Applications in Medical Biotechnology", *Journal of Nanoparticles*, **2013**, *2013*, 10, 1–24.
- (111) S. Kawata; Y. Kawata, "Three-Dimensional Optical Data Storage Using Photochromic Materials", *Chemical reviews*, **2000**, *100*, 5, 1777–1788.
- (112) H. Priya James; R. John; A. Alex; K. R. Anoop, "Smart polymers for the controlled delivery of drugs - a concise overview", *Acta pharmaceutica Sinica. B*, **2014**, *4*, 2, 120–127.
- (113) Y. Zhou; H. Ye; Y. Chen; R. Zhu; L. Yin, "Photoresponsive Drug/Gene Delivery Systems", *Biomacromolecules*, **2018**, *19*, 6, 1840–1857.
- (114) R. M. F. Tomás; M. I. Gibson, "Optimization and Stability of Cell-Polymer Hybrids Obtained by "Clicking" Synthetic Polymers to Metabolically Labeled Cell Surface Glycans", *Biomacromolecules*, **2019**, *20*, 7, 2726–2736.
- (115) L. Li; J. M. Scheiger; P. A. Levkin, "Design and Applications of Photoresponsive Hydrogels", *Advanced materials (Deerfield Beach, Fla.)*, **2019**, *31*, 26, e1807333.
- (116) F. A. Jerca; V. V. Jerca; R. Hoogenboom, "Photoresponsive Polymers on the Move", *Chem*, **2017**, *3*, 4, 533–536.
- (117) F. D. Jochum; P. Theato, "Temperature- and light-responsive smart polymer materials", *Chemical Society reviews*, **2013**, *42*, 17, 7468–7483.
- (118) A. Abdollahi; H. Roghani-Mamaqani; B. Razavi; M. Salami-Kalajahi, "The light-controlling of temperature-responsivity in stimuli-responsive polymers", *Polym. Chem.*, **2019**, *10*, 42, 5686–5720.
- (119) G. W. Breton; X. Vang, "Photodimerization of Anthracene", *J. Chem. Educ.*, **1998**, *75*, 1, 81.
- (120) K. N. Houk; F. Liu; Z. Yang; J. I. Seeman, "Evolution of the Diels-Alder Reaction Mechanism since the 1930s: Woodward, Houk with Woodward, and the Influence of Computational Chemistry on Understanding Cycloadditions", *Angewandte Chemie International Edition*, **2021**, *60*, 23, 12660–12681.
- (121) P. Klán; T. Šolomek; C. G. Bochet; A. Blanc; R. Givens; M. Rubina; V. Popik; A. Kostikov; J. Wirz, "Photoremovable protecting groups in chemistry and biology: reaction mechanisms and efficacy", *Chem. Rev.*, **2013**, *113*, 1, 119–191.

- (122) M. Kondo, "Photomechanical materials driven by photoisomerization or photodimerization", *Polym J*, **2020**, *52*, 9, 1027–1034.
- (123) G. Tillet; B. Boutevin; B. Ameduri, "Chemical reactions of polymer crosslinking and post-crosslinking at room and medium temperature", *Progress in Polymer Science*, **2011**, *36*, 2, 191–217.
- (124) F. Xin; M. Wei; S. Jiang; Y. Gao; J. Nie; Y. Wu; F. Sun, "Design of hydrophilic photocleavage o-nitrobenzyl acrylate-modified nanogels with outstanding biocompatibility prepared by RAFT polymerization for drug carrier", *European Polymer Journal*, **2020**, *122*, 109364.
- (125) H. Zhao; E. S. Sterner; E. B. Coughlin; P. Theato, "o -Nitrobenzyl Alcohol Derivatives: Opportunities in Polymer and Materials Science", *Macromolecules*, **2012**, *45*, 4, 1723–1736.
- (126) M. Gao; D. Kwaria; Y. Norikane; Y. Yue, "Visible-light-switchable azobenzenes: Molecular design, supramolecular systems, and applications", *Natural Sciences*, **2023**, *3*, 1, 479.
- (127) K. Upadhyay; S. Thomas; R. K. Tamrakar; N. Kalarikkal, "Functionalized photo-responsive polymeric system", *Advanced Functional Polymers for Biomedical Application*, **2019**, *42*, 211–233.
- (128) J. Keyvan Rad; Z. Balzade; A. R. Mahdavian, "Spiropyran-based advanced photoswitchable materials: A fascinating pathway to the future stimuli-responsive devices", *Journal of Photochemistry and Photobiology C: Photochemistry Reviews*, **2022**, *51*, 100487.
- (129) L. Kortekaas; W. R. Browne, "The evolution of spiropyran: fundamentals and progress of an extraordinarily versatile photochrome", *Chemical Society reviews*, **2019**, *48*, 12, 3406–3424.
- (130) S. Helmy; S. Oh; F. A. Leibfarth; C. J. Hawker; J. Read de Alaniz, "Design and synthesis of donor-acceptor Stenhouse adducts: a visible light photoswitch derived from furfural", *The Journal of organic chemistry*, **2014**, *79*, 23, 11316–11329.
- (131) J. Abe; H. Yamashita; K. Mutoh, "Photochromism", 1st ed., *Springer*, Berlin, Heidelberg, 1572–1579, **2015**.
- (132) M. Irie, "Photochromism: Memories and Switches-Introduction", *Chemical reviews*, **2000**, *100*, 5, 1683–1684.
- (133) J. García-Amorós; D. Velasco, "Recent advances towards azobenzene-based light-driven real-time information-transmitting materials", *Beilstein journal of organic chemistry*, **2012**, *8*, 1003–1017.
- (134) J. Mei; H. Tian, "Aggregation-Induced Emission (AIE) A Practical Guide Materials Today Aggregation-Induced Emission (AIE) - Chapter 7 Photochromic and thermochromic luminescence in AIE luminogens", 1st ed., Vol. 73, *Elsevier*, 199–251, **2022**.
- (135) K. Nakatani; J. Piard; P. Yu; R. Métivier, "Introduction: Organic Photochromic Molecules, Vol. 73.

- (136) A.-L. Leistner; Z. L. Pianowski, "Smart Photochromic Materials Triggered with Visible Light", *Eur J Org Chem*, **2022**, 2022, 19, 257.
- (137) Z. Ma; J. Wu; Y. Tan; C. Tan, "Azobenzene-Based Conjugated Polymers: Synthesis, Properties, and Biological Applications", *Macromol. Rapid Commun.*, **2024**, 45, 12, e2400048.
- (138) A. Muždalo; P. Saalfrank; J. Vreede; M. Santer, "Cis-to- Trans Isomerization of Azobenzene Derivatives Studied with Transition Path Sampling and Quantum Mechanical/Molecular Mechanical Molecular Dynamics", *Journal of chemical theory and computation*, **2018**, 14, 4, 2042–2051.
- (139) L. Vetráková; V. Ladányi; J. Al Anshori; P. Dvořák; J. Wirz; D. Heger, "The absorption spectrum of cis-azobenzene", *Photochemical & photobiological sciences : Official journal of the European Photochemistry Association and the European Society for Photobiology*, **2017**, 16, 12, 1749–1756.
- (140) M. Zhu; H. Zhou, "Azobenzene-based small molecular photoswitches for protein modulation", *Organic & biomolecular chemistry*, **2018**, 16, 44, 8434–8445.
- (141) A. Goulet-Hanssens; C. J. Barrett, "Photo-control of biological systems with azobenzene polymers", *J. Polym. Sci. Part A: Polym. Chem.*, **2013**, 51, 14, 3058–3070.
- (142) F. Cuétara-Guadarrama; M. Vonlanthen; K. Sorroza-Martínez; I. González-Méndez; E. Rivera, "Photoisomerizable azobenzene dyes incorporated into polymers and dendrimers. Influence of the molecular aggregation on the nonlinear optical properties", *Dyes and Pigments*, **2021**, 194, 109551.
- (143) Z. Wang; K. Müller; M. Valášek; S. Grosjean; S. Bräse; C. Wöll; M. Mayor; L. Heinke, "Series of Photoswitchable Azobenzene-Containing Metal–Organic Frameworks with Variable Adsorption Switching Effect", *J. Phys. Chem. C*, **2018**, 122, 33, 19044–19050.
- (144) M. Clerc; S. Sandlass; O. Rifaie-Graham; J. A. Peterson; N. Bruns; J. Read de Alaniz; L. F. Boesel, "Visible light-responsive materials: the (photo)chemistry and applications of donor-acceptor Stenhouse adducts in polymer science", *Chemical Society reviews*, **2023**, 52, 23, 8245–8294.
- (145) C. A. Reyes; H. J. Lee; C. Karanovic; E. Picazo, "Development and characterization of amino donor-acceptor Stenhouse adducts", *Nature communications*, **2024**, 15, 1, 5533.
- (146) S. Helmy; F. A. Leibfarth; S. Oh; J. E. Poelma; C. J. Hawker; J. Read de Alaniz, "Photoswitching using visible light: a new class of organic photochromic molecules", *Journal of the American Chemical Society*, **2014**, 136, 23, 8169–8172.
- (147) M. M. Lerch; W. Szymański; B. L. Feringa, "The (photo)chemistry of Stenhouse photoswitches: guiding principles and system design", *Chemical Society reviews*, **2018**, 47, 6, 1910–1937.
- (148) O. Nieto Faza; C. Silva López; R. Alvarez; A. R. de Lera, "Theoretical study of the electrocyclic ring closure of hydroxypentadienyl cations", *Chemistry (Weinheim an der Bergstrasse, Germany)*, **2004**, 10, 17, 4324–4333.

- (149) C. Piutti; F. Quartieri, "The Piancatelli rearrangement: new applications for an intriguing reaction", *Molecules (Basel, Switzerland)*, **2013**, *18*, 10, 12290–12312.
- (150) N. Mallo; P. T. Brown; H. Iranmanesh; T. S. C. MacDonald; M. J. Teusner; J. B. Harper; G. E. Ball; J. E. Beves, "Photochromic switching behaviour of donor-acceptor Stenhouse adducts in organic solvents", *Chemical communications (Cambridge, England)*, **2016**, *52*, 93, 13576–13579.
- (151) M. Di Donato; M. M. Lerch; A. Lapini; A. D. Laurent; A. Iagatti; L. Bussotti; S. P. Ihrig; M. Medved'; D. Jacquemin; W. Szymański; W. J. Buma; P. Foggi; B. L. Feringa, "Shedding Light on the Photoisomerization Pathway of Donor-Acceptor Stenhouse Adducts", *J. Am. Chem. Soc.*, **2017**, *139*, 44, 15596–15599.
- (152) M. M. Lerch; M. Medved; A. Lapini; A. D. Laurent; A. Iagatti; L. Bussotti; W. Szymański; W. J. Buma; P. Foggi; M. Di Donato; B. L. Feringa, "Tailoring Photoisomerization Pathways in Donor-Acceptor Stenhouse Adducts: The Role of the Hydroxy Group", *The journal of physical chemistry. A*, **2018**, *122*, 4, 955–964.
- (153) N. Mallo; E. D. Foley; H. Iranmanesh; A. D. W. Kennedy; E. T. Luis; J. Ho; J. B. Harper; J. E. Beves, "Structure-function relationships of donor-acceptor Stenhouse adduct photochromic switches", *Chemical science*, **2018**, *9*, 43, 8242–8252.
- (154) M. M. Lerch; S. J. Wezenberg; W. Szymanski; B. L. Feringa, "Unraveling the Photoswitching Mechanism in Donor-Acceptor Stenhouse Adducts", *J. Am. Chem. Soc.*, **2016**, *138*, 20, 6344–6347.
- (155) A. Balamurugan; H.-i. Lee, "A Visible Light Responsive On–Off Polymeric Photoswitch for the Colorimetric Detection of Nerve Agent Mimics in Solution and in the Vapor Phase", *Macromolecules*, **2016**, *49*, 7, 2568–2574.
- (156) Y. J. Diaz; Z. A. Page; A. S. Knight; N. J. Treat; J. R. Hemmer; C. J. Hawker; J. Read de Alaniz, "A Versatile and Highly Selective Colorimetric Sensor for the Detection of Amines", *Chemistry (Weinheim an der Bergstrasse, Germany)*, **2017**, *23*, 15, 3562–3566.
- (157) B. P. Mason; M. Whittaker; J. Hemmer; S. Arora; A. Harper; S. Alnemrat; A. McEachen; S. Helmy; J. Read de Alaniz; J. P. Hooper, "A temperature-mapping molecular sensor for polyurethane-based elastomers", *Appl. Phys. Lett.*, **2016**, *108*, 4, 41906.
- (158) S. Ulrich; J. R. Hemmer; Z. A. Page; N. D. Dolinski; O. Rifaie-Graham; N. Bruns; C. J. Hawker; L. F. Boesel; J. Read de Alaniz, "Visible Light-Responsive DASA-Polymer Conjugates", *ACS Macro Lett.*, **2017**, *6*, 7, 738–742.
- (159) M. Irie, "Properties and applications of photoresponsive polymers", *Pure and Applied Chemistry*, **1990**, *62*, 8, 1495–1502.
- (160) D. Kungwatchakun; M. Irie, "Photoresponsive polymers. Photocontrol of the phase separation temperature of aqueous solutions of poly-[N-isopropylacrylamide-co-N-(4-phenylazophenyl)acrylamide]", *Makromol. Chem., Rapid Commun.*, **1988**, *9*, 4, 243–246.

- (161) R. Kröger; H. Menzel; M. L. Hallensleben, "Light controlled solubility change of polymers: Copolymers of N, N -dimethylacrylamide and 4-phenylazophenyl acrylate", *Macromol. Chem. Phys.*, **1994**, *195*, 7, 2291–2298.
- (162) F. D. Jochum; P. Theato, "Temperature and light sensitive copolymers containing azobenzene moieties prepared via a polymer analogous reaction", *Polymer*, **2009**, *50*, 14, 3079–3085.
- (163) F. D. Jochum; P. Theato, "Temperature- and Light-Responsive Polyacrylamides Prepared by a Double Polymer Analogous Reaction of Activated Ester Polymers", *Macromolecules*, **2009**, *42*, 16, 5941–5945.
- (164) T. Ueki; Y. Nakamura; A. Yamaguchi; K. Niitsuma; T. P. Lodge; M. Watanabe, "UCST Phase Transition of Azobenzene-Containing Random Copolymer in an Ionic Liquid", *Macromolecules*, **2011**, *44*, 17, 6908–6914.
- (165) Q. Zhang; P. Schattling; P. Theato; R. Hoogenboom, "UV-tunable upper critical solution temperature behavior of azobenzene containing poly(methyl methacrylate) in aqueous ethanol", *European Polymer Journal*, **2015**, *62*, 435–441.
- (166) U. Ali; K. J. B. A. Karim; N. A. Buang, "A Review of the Properties and Applications of Poly (Methyl Methacrylate) (PMMA)", *Polymer Reviews*, **2015**, *55*, 4, 678–705.
- (167) W. Zheng; S.-C. Wong, "Electrical conductivity and dielectric properties of PMMA/expanded graphite composites", *Composites Science and Technology*, **2003**, *63*, 2, 225–235.
- (168) J.-H. Cho; J.-H. Park; J. H. Kim; S.-Y. Lee, "Facile fabrication of nanoporous composite separator membranes for lithium-ion batteries: poly(methyl methacrylate) colloidal particles-embedded nonwoven poly(ethylene terephthalate)", *J. Mater. Chem.*, **2011**, *21*, 22, 8192.
- (169) P. Yang; P. Zhang; C. Shi; L. Chen; J. Dai; J. Zhao, "The functional separator coated with core-shell structured silica-poly(methyl methacrylate) sub-microspheres for lithium-ion batteries", *Journal of Membrane Science*, **2015**, *474*, 148–155.
- (170) H.-S. Hou; K.-L. Lee; C.-H. Wang; T.-H. Hsieh; J.-J. Sun; P.-K. Wei; J.-Y. Cheng, "Simultaneous assessment of cell morphology and adhesion using aluminum nanoslit-based plasmonic biosensing chips", *Scientific reports*, **2019**, *9*, 1, 7204.
- (171) Y.-H. Nien; S.-w. Lin; Y.-N. Hsu, "Preparation and characterization of acrylic bone cement with high drug release", *Materials science & engineering. C, Materials for biological applications*, **2013**, *33*, 2, 974–978.
- (172) R. Hoogenboom; C. R. Becer; C. Guerrero-Sanchez; S. Hoepfner; U. S. Schubert, "Solubility and Thermoresponsiveness of PMMA in Alcohol-Water Solvent Mixtures", *Aust. J. Chem.*, **2010**, *63*, 8, 1173–1178.
- (173) C. Pietsch; R. Hoogenboom; U. S. Schubert, "PMMA based soluble polymeric temperature sensors based on UCST transition and solvatochromic dyes", *Polym. Chem.*, **2010**, *1*, 7, 1005–1008.

- (174) Q. Zhang; P. Schattling; P. Theato; R. Hoogenboom, "Tuning the upper critical solution temperature behavior of poly(methyl methacrylate) in aqueous ethanol by modification of an activated ester comonomer", *Polym. Chem.*, **2012**, *3*, 6, 1418–1426.
- (175) M. Eberhardt; R. Mruk; R. Zentel; P. Théato, "Synthesis of pentafluorophenyl(meth)acrylate polymers: New precursor polymers for the synthesis of multifunctional materials", *European Polymer Journal*, **2005**, *41*, 7, 1569–1575.
- (176) P. Hubbard; W. J. Brittain, "Mechanism of Amine-Catalyzed Ester Formation from an Acid Chloride and Alcohol", *J. Org. Chem.*, **1998**, *63*, 3, 677–683.
- (177) F. Laduron; V. Tamborowski; L. Moens; A. Horváth; D. de Smaele; S. Leurs, "Efficient and Scalable Method for the Selective Alkylation and Acylation of Secondary Amines in the Presence of Primary Amines", *Org. Process Res. Dev.*, **2005**, *9*, 1, 102–104.
- (178) F. Bigi; S. Carloni; L. Ferrari; R. Maggi; A. Mazzacani; G. Sartori, "Clean synthesis in water. Part 2: Uncatalysed condensation reaction of Meldrum's acid and aldehydes", *Tetrahedron Letters*, **2001**, *42*, 31, 5203–5205.
- (179) B. Lovrinčević; I. Jukić; M. Požar, "An Overview on the Dynamics in Aqueous Mixtures of Lower Alcohols, Vol. 71, *Springer, Singapore*, 169–193, **2021**.
- (180) A. Wakisaka; K. Matsuura; M. Uranaga; T. Sekimoto; M. Takahashi, "Azeotropy of alcohol–water mixtures from the viewpoint of cluster-level structures", *Journal of Molecular Liquids*, **2011**, *160*, 2, 103–108.
- (181) C. Boutris; E. G. Chatzi; C. Kiparissides, "Characterization of the LCST behaviour of aqueous poly(N-isopropylacrylamide) solutions by thermal and cloud point techniques", *Polymer*, **1997**, *38*, 10, 2567–2570.
- (182) A. Halperin; M. Kröger; F. Winnik, "Poly(N-isopropylacrylamide) Phase Diagrams: Fifty Years of Research", *Angewandte Chemie International Edition*, **2015**, *54*, 51, 15342–15367.
- (183) X. Fan; S. Gu; L. Wu; L. Yang, "Preparation and characterization of thermoresponsive poly(N-isopropylacrylamide) copolymers with enhanced hydrophilicity", *e-Polymers*, **2020**, *20*, 1, 561–570.
- (184) M. Heskins; J. E. Guillet, "Solution Properties of Poly(N-isopropylacrylamide)", *Journal of Macromolecular Science: Part A - Chemistry*, **1968**, *2*, 8, 1441–1455.
- (185) H. Cicek; A. Tuncel, "Preparation and characterization of thermoresponsive isopropylacrylamide-hydroxyethylmethacrylate copolymer gels", *Journal of Polymer Science Part A: Polymer Chemistry*, **1998**, *36*, 4, 527–541.
- (186) T. Itahara; T. Tsuchida; M. Morimoto, "Solvent-driven swelling and shrinking of poly(NIPAM) gels crosslinked by tris-methacrylated phloroglucinol derivatives", *Polym. Chem.*, **2010**, *1*, 7, 1062–1066.
- (187) Y.-Y. Li; X.-Z. Zhang; H. Cheng; J.-L. Zhu; S.-X. Cheng; R.-X. Zhuo, "Self-Assembled, Thermosensitive PCL-g-P(NIPAAm-co-HEMA) Micelles for Drug Delivery", *Macromol. Rapid Commun.*, **2006**, *27*, 22, 1913–1919.

- (188) M. R. Islam; A. Ahiabu; X. Li; M. J. Serpe, "Poly (N-isopropylacrylamide) microgel-based optical devices for sensing and biosensing", *Sensors (Basel, Switzerland)*, **2014**, *14*, 5, 8984–8995.
- (189) D. Singh; D. Kuckling; V. Choudhary; H.-J. Adler; V. Koul, "Synthesis and characterization of poly(N-isopropylacrylamide) films by photopolymerization", *Polym. Adv. Technol.*, **2006**, *17*, 3, 186–192.
- (190) K. Nagase, "Thermoresponsive interfaces obtained using poly(N-isopropylacrylamide)-based copolymer for bioseparation and tissue engineering applications", *Advances in colloid and interface science*, **2021**, *295*, 102487.
- (191) S. Lanzalaco; E. Armelin, "Poly(N-isopropylacrylamide) and Copolymers: A Review on Recent Progresses in Biomedical Applications", *Gels*, **2017**, *3*, 4, 36.
- (192) G. Masci; L. Giacomelli; V. Crescenzi, "Atom Transfer Radical Polymerization of N-Isopropylacrylamide", *Macromol. Rapid Commun.*, **2004**, *25*, 4, 559–564.
- (193) Z. M.O. Rzaev; S. Dinçer; E. Pişkin, "Functional copolymers of N-isopropylacrylamide for bioengineering applications", *Progress in Polymer Science*, **2007**, *32*, 5, 534–595.
- (194) H. Feil; Y. H. Bae; J. Feijen; S. W. Kim, "Effect of comonomer hydrophilicity and ionization on the lower critical solution temperature of N-isopropylacrylamide copolymers", *Macromolecules*, **1993**, *26*, 10, 2496–2500.
- (195) I. Idziak; D. Avoce; D. Lessard; D. Gravel; X. X. Zhu, "Thermosensitivity of Aqueous Solutions of Poly(N,N -diethylacrylamide)", *Macromolecules*, **1999**, *32*, 4, 1260–1263.
- (196) J. Choi; P. Schattling; F. D. Jochum; J. Pyun; K. Char; P. Theato, "Functionalization and patterning of reactive polymer brushes based on surface reversible addition and fragmentation chain transfer polymerization", *J. Polym. Sci. A Polym. Chem.*, **2012**, *50*, 19, 4010–4018.
- (197) S. R. Jagtap; Y. P. Patil; A. G. Panda; B. M. Bhanage, "Synthesis of 1,3-Disubstituted Symmetrical/Unsymmetrical Ureas via Cs<sub>2</sub>CO<sub>3</sub>-Catalyzed Transamination of Ethylene Carbonate and Primary Amines", *Synthetic Communications*, **2009**, *39*, 12, 2093–2100.
- (198) A. K. Bose; S. Garratt, "A new synthesis of substituted barbituric acids", *Tetrahedron*, **1963**, *19*, 1, 85–89.
- (199) D. A. Pitushkin; V. V. Burmistrov; M. H. A. Saeef; A. A. Vernigora; G. M. Butov, "Synthesis and Properties of 1,3-Disubstituted Ureas and Their Isosteric Analogs Containing Polycyclic Fragments: V. 1-(Bicyclo[2.2.1]heptan-2-yl)-3-R- and 1-(1,7,7-Tricyclo[2.2.1]heptan-2-yl)-3-R-ureas", *Russ J Org Chem*, **2020**, *56*, 11, 1893–1904.
- (200) M. G. Gündüz; S. B. Uğur; F. Güney; C. Özkul; V. S. Krishna; S. Kaya; D. Sriram; Ş. D. Doğan, "1,3-Disubstituted urea derivatives: Synthesis, antimicrobial activity evaluation and in silico studies", *Bioorganic Chemistry*, **2020**, *102*, 104104.

- (201) M. M. Lerch; M. J. Hansen; W. A. Velema; W. Szymanski; B. L. Feringa, "Orthogonal photoswitching in a multifunctional molecular system", *Nature communications*, **2016**, *7*, 12054.
- (202) H. Gaballa; S. Lin; J. Shang; S. Meier; P. Theato, "A synthetic approach toward a pH and sugar-responsive diblock copolymer via post-polymerization modification", *Polym. Chem.*, **2018**, *9*, 24, 3355–3358.
- (203) F.-N. Meng; Z.-Y. Li; Y.-L. Ying; S.-C. Liu; J. Zhang; Y.-T. Long, "Structural stability of the photo-responsive DNA duplexes containing one azobenzene via a confined pore", *Chemical communications (Cambridge, England)*, **2017**, *53*, 68, 9462–9465.
- (204) GESTIS Substance Database. <https://gestis-database.dguv.de/> (accessed 2024-06-19).
- (205) Dokumente. <https://www.sigmaaldrich.com/DE/de/documents-search?tab=sds> (accessed 2024-06-19).
- (206) Globally Harmonized System of Classification and Labelling of Chemicals (GHS Rev. 9, 2021) | UNECE. <https://unece.org/transport/standards/transport/dangerous-goods/ghs-rev9-2021> (accessed 2024-06-19).

## A Additional Supporting Informations

### A.1 NMR spectra

This section provides a list of  $^1\text{H}$  NMR spectra that are either not or not fully included in Chapter 4.

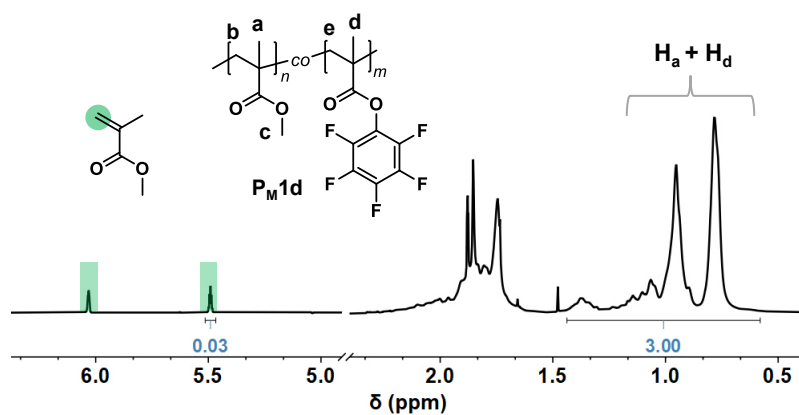


**Figure A.1.** Example of conversion monitoring of the  $\text{P}_{\text{M}1}$  series:  $^1\text{H}$  NMR spectrum ( $\text{CDCl}_3$ ) of the reaction mixture of  $\text{P}_{\text{M}1\text{d}}$  as example for conversion determination. PFPMA monomer peaks are not observed. The integrals lead to quantitative conversion, which was measured after 19 h.

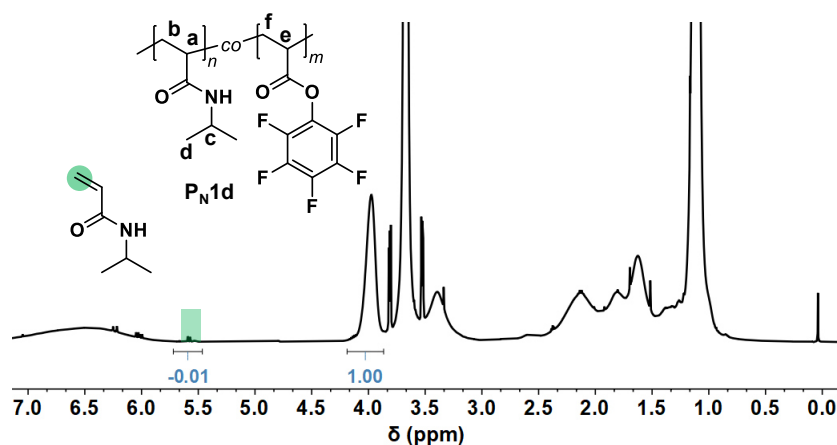


**Figure A.2.** Example of conversion monitoring of the  $\text{P}_{\text{N}3}$  series:  $^1\text{H}$  NMR spectrum ( $\text{acetone-}d_6$ ) of the reaction mixture of  $\text{P}_{\text{N}1\text{d}}$  as example for conversion determination. The integrals lead to quantitative conversion after 20 h.

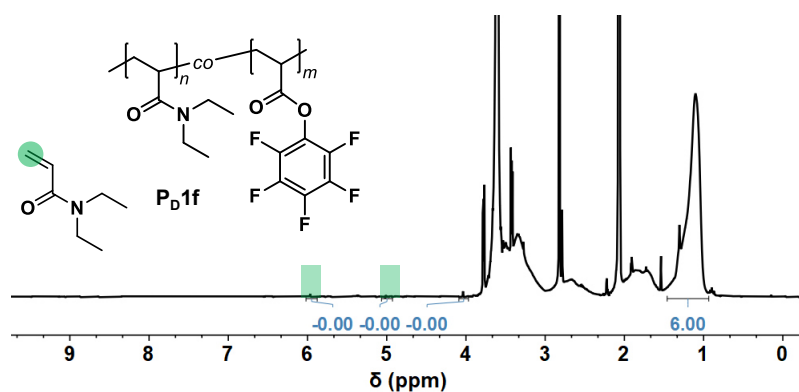


**Figure A.3.** Example of conversion monitoring of the PD3 series:  $^1\text{H}$  NMR spectrum (acetone- $d_6$ ) of the reaction mixture of  $\text{P}_{\text{D}1\text{f}}$  as example for conversion determination. The integrals lead to quantitative conversion after 20 h.

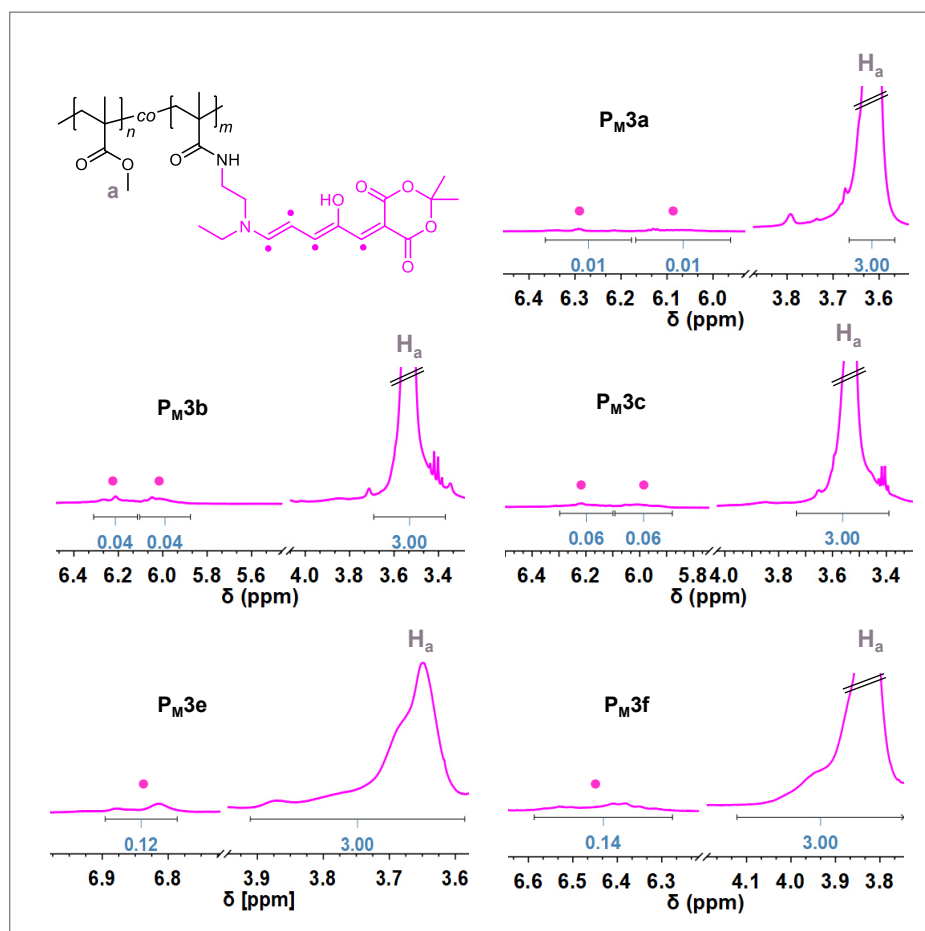


**Figure A.4.** Selected  $^1\text{H}$  NMR regions of the  $\text{P}_{\text{M}3}$  series for DASA content estimation through integrating the peak areas and using Equation (4.3). Samples  $\text{P}_{\text{M}3\text{a}}$ ,  $\text{P}_{\text{M}3\text{b}}$  and  $\text{P}_{\text{M}3\text{c}}$  were measured in  $\text{CDCl}_3$ . Due to poor solubility,  $\text{P}_{\text{M}3\text{d}}$  and  $\text{P}_{\text{M}3\text{e}}$  were measured in  $\text{DMF}-d_7$ .

## A.2 FT-IR spectra

This section provides a list of FT-IR spectra that are either not or not fully (complete wavenumber range) included in Chapter 4.

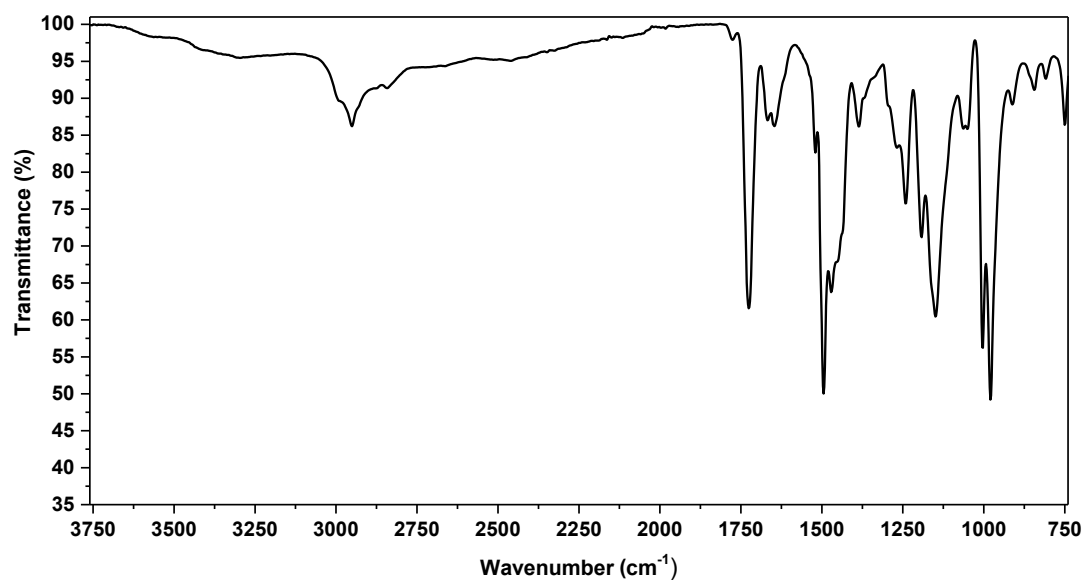


**Figure A.5.** FT-IR spectrum of poly(methyl methacrylate-*co*-pentafluorophenyl methacrylate) (P<sub>M1d</sub>).

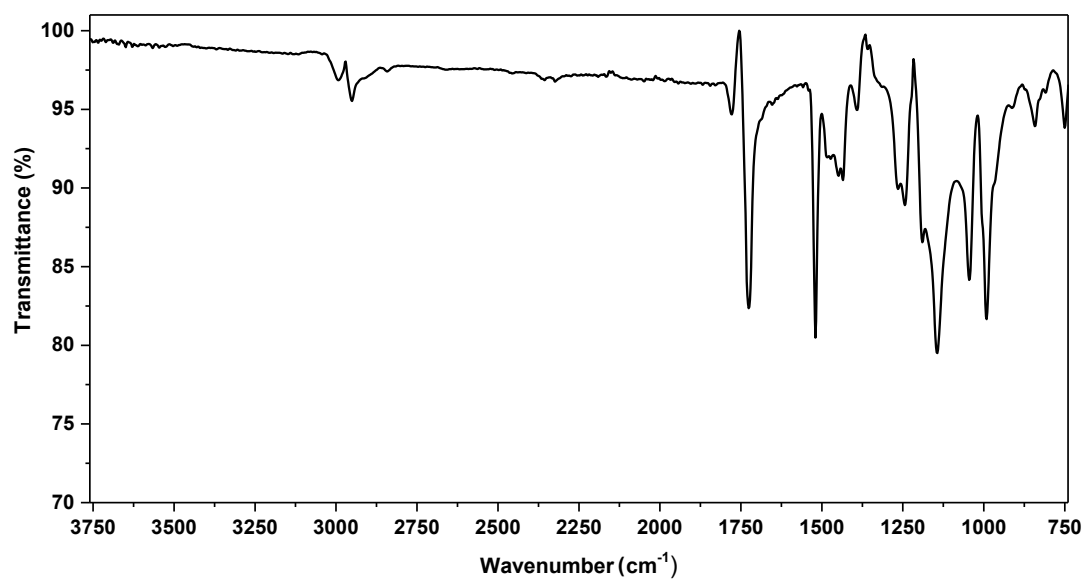


**Figure A.6.** FT-IR spectrum of poly(*N*-(2-(ethylamino)ethyl)-methacrylamide-*co*-MMA) (P<sub>M2e</sub>).

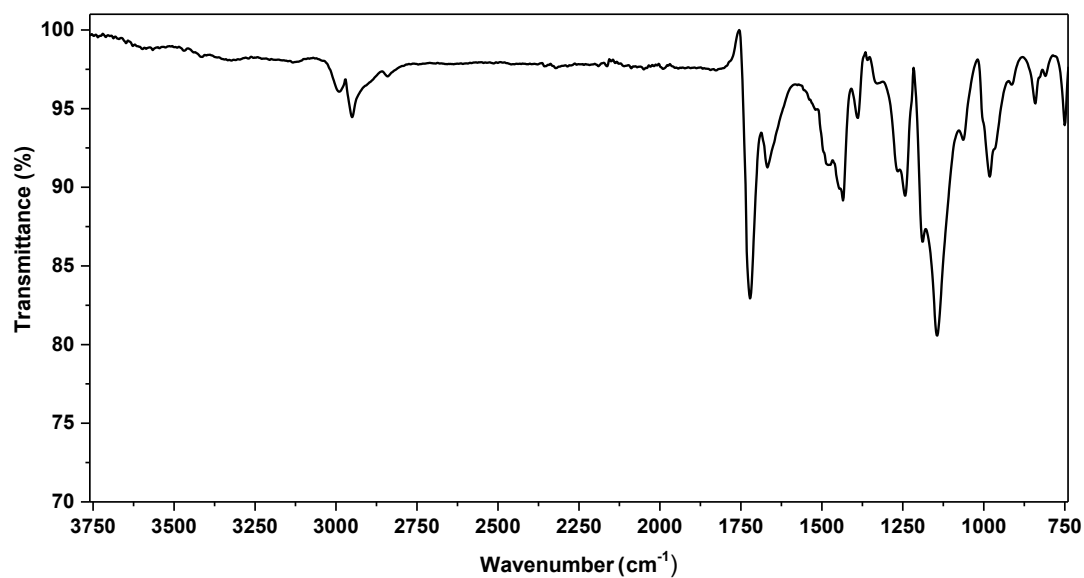


**Figure A.7.** FT-IR spectrum of p(MMA-*co*-EEDA-*co*-DASA) (P<sub>M</sub>3b).

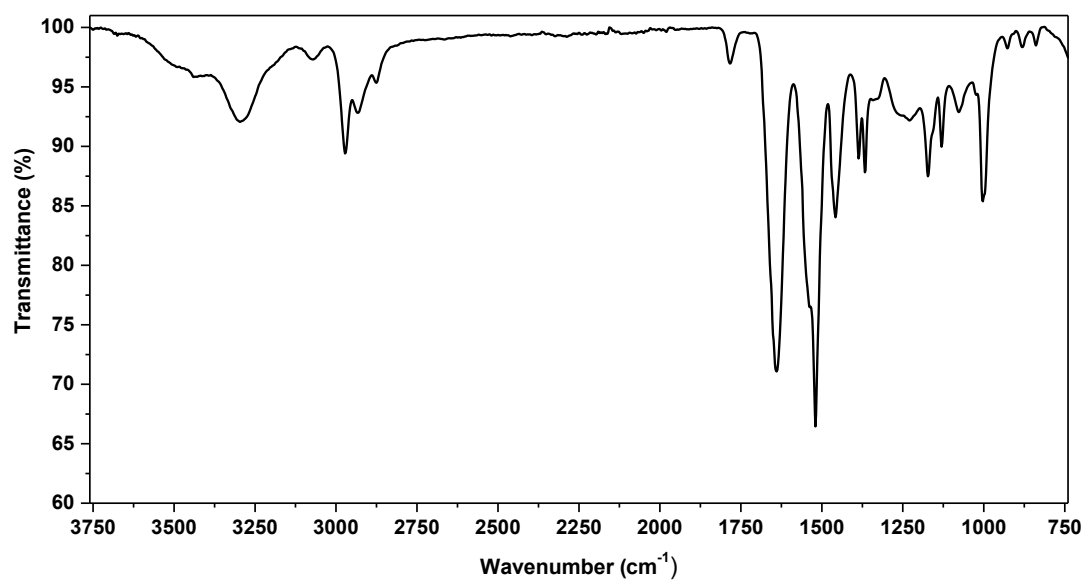


**Figure A.8.** FT-IR spectrum of poly(*N*-isopropylacrylamid-*co*-pentafluorophenyl acrylate) (P<sub>N</sub>1d).

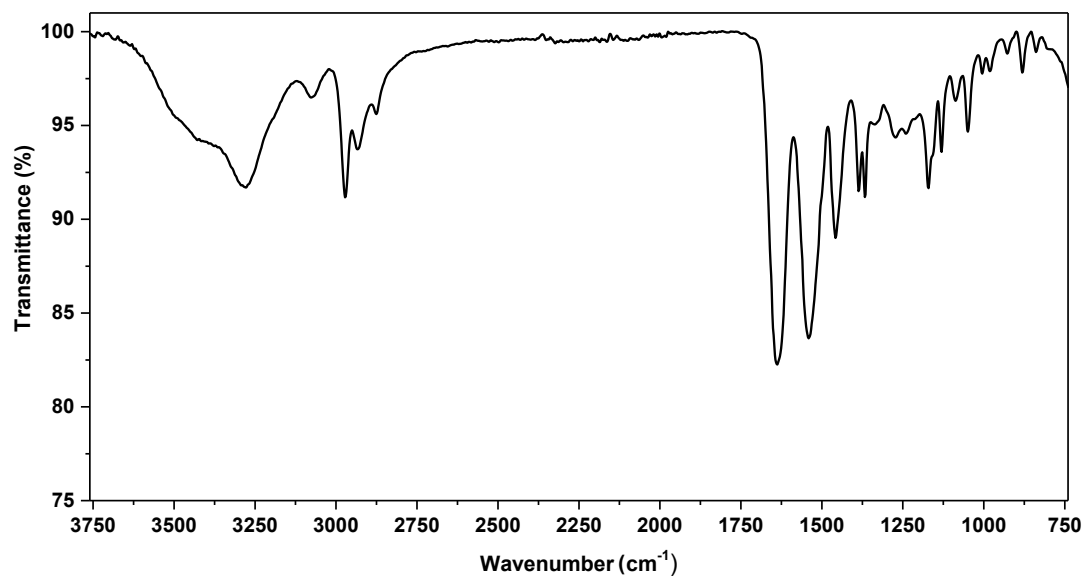


**Figure A.9.** FT-IR spectrum of poly(*N*-(2-(ethylamino)ethyl)-methacrylamide-*co*-NIPAM) (P<sub>N</sub>2d).

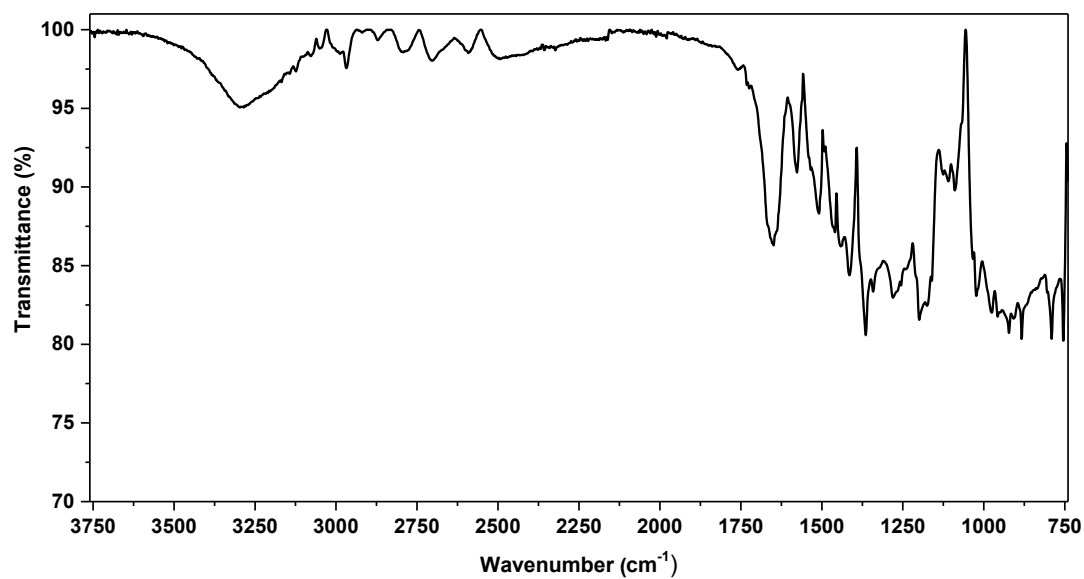


**Figure A.10.** FT-IR spectrum of p(NIPAM-*co*-EEDA-*co*-DASA) (P<sub>N</sub>3c).

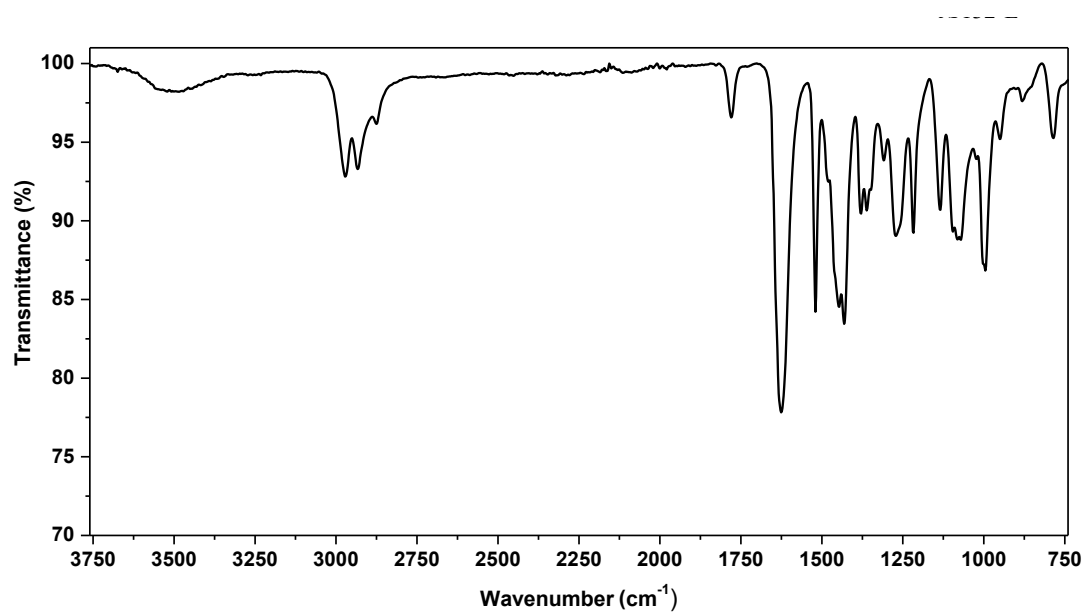


**Figure A.11.** FT-IR spectrum of poly(*N,N*-diethylacrylamid-*co*-pentafluorophenyl methacrylate) (P<sub>D1c</sub>).

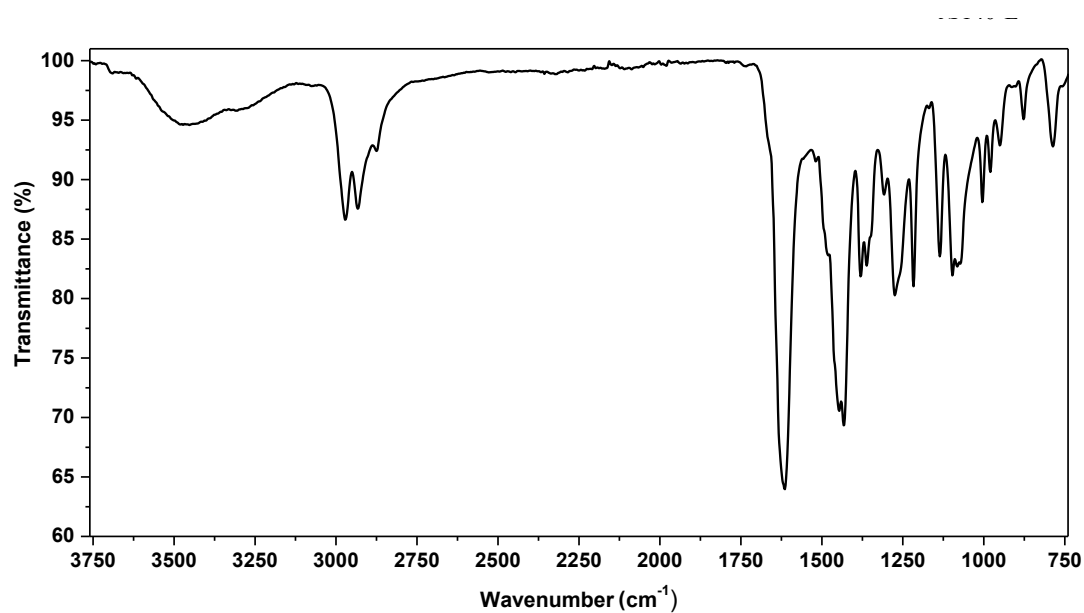


**Figure A.12.** FT-IR spectrum of poly(*N*-(2-(ethylamino)ethyl)-methacrylamide-*co*-DEA) (P<sub>D2d</sub>).

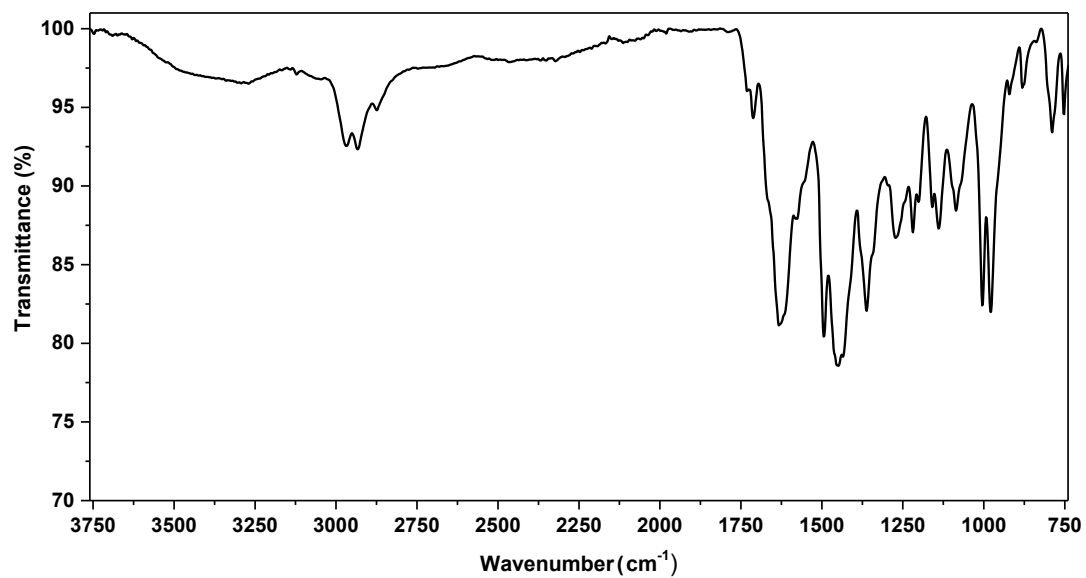


**Figure A.13.** FT-IR spectrum of p(DEA-co-EEDA-co-DASA) (P<sub>DBu</sub>3c)

### A.3 UV-vis linear regression analysis of DASA contents

The calibration series shown in Figure 4.8c was conducted using a stock solution prepared from 32.6 mg (110.4  $\mu\text{mol}$ ) of substance **S3** (with a molecular mass of  $M = 295.3 \text{ g mol}^{-1}$ ) dissolved in 0.5 L (220.7  $\mu\text{mol L}^{-1}$ ) of chloroform. Table A.1 provides a summary of the absorbance values and their matching concentrations of **S3**, as determined by the linear regression fit.

**Table A.1** Concentration of sample **S3** dissolved in chloroform for linear regression fit and the corresponding absorbance.

Concentration $c_{\text{S3}}$ ( $\mu\text{g mL}^{-1}$ )	Absorbance $A$ (a.u.)
11.03	1.324
5.519	0.6772
2.759	0.3370
2.207	0.2669
1.379	0.1752
1.103	0.1387

The DASA contents  $X_{\text{DASA}}$  of the **P<sub>M</sub>3** series were further calculated by using Equation 4.9 with absorbance values of Figure 4.8d and the sample concentrations  $c_{\text{DASA}}$  (Table A.2), which were calculated using Equation 4.8. For the calculation of  $c_{\text{PM3}}$ , the molar masses  $M_{\text{MMA}} = 100.12 \text{ g mol}^{-1}$  and  $M_{\text{DASA}} = 378.43 \text{ g mol}^{-1}$  were used. The UV-vis measurement of each sample occurred from a solution of 7 mg **P<sub>M</sub>3** dissolved in 1000 mL chloroform, which led to the sample concentration  $c_{\text{PM3}}$ .

**Table A.2** Concentration of each **P<sub>M</sub>3** sample series with the corresponding absorbance of the UV-vis spectra, the calculated  $c_{\text{DASA}}$  and the resulting mol%  $X_{\text{DASA}}$  content.

Sample	$c_{\text{PM3}}$ ( $\mu\text{g L}^{-1}$ )	Absorbance $A$ (a.u.)	$c_{\text{DASA}}$ ( $\mu\text{mol l}^{-1}$ )	$X_{\text{DASA}}$ (mol%)
<b>P<sub>M</sub>3a</b>	7000	0.1001	0.7678	1.12
<b>P<sub>M</sub>3b</b>	7000	0.2093	1.681	2.60
<b>P<sub>M</sub>3c</b>	7000	0.3834	3.137	5.13
<b>P<sub>M</sub>3d</b>	7000	0.4759	3.911	6.61
<b>P<sub>M</sub>3e</b>	7000	0.5411	4.456	7.80
<b>P<sub>M</sub>3f</b>	7000	0.6852	5.660	10.5

For the calibration series shown in Figure 4.34c, a stock solution of **S8** was prepared from 41.0 mg dissolved in 500 mL ( $209 \mu\text{mol L}^{-1}$ ) of chloroform (with a molecular mass of  $M = 391.5 \text{ g mol}^{-1}$ ). The absorbance values  $A$  and the corresponding concentrations  $c_{\text{S8}}$  are summarized in Table A.3.

**Table A.3.** Concentration of **S8** dissolved in chloroform for linear regression fit and the corresponding absorbance  $A$ .

Concentration $c_{\text{S8}}$ ( $\mu\text{g mL}^{-1}$ )	Absorbance $A$ (a.u.)
20.92	2.270
10.45	1.270
2.098	0.2678
1.281	0.1703

**Table A.4.** Concentration of each  $\text{P}_{\text{M}3}/\text{P}_{\text{D}3}$  sample series with the corresponding absorbance of the UV-vis spectra, the calculated  $c_{\text{DASA}}$  and the resulting mol%  $X_{\text{DASA}}$  content.

sample	$c$ ( $\text{mg L}^{-1}$ )	Absorbance $A$ (a.u.)	$c_{\text{DASA}}$ ( $\mu\text{mol L}^{-1}$ )	$X_{\text{DASA}}$ (mol%)
<b>P<sub>N</sub>3a</b>	8.00	0.120	0.82	1.04
<b>P<sub>N</sub>3b</b>	7.90	0.254	1.96	3.01
<b>P<sub>N</sub>3c</b>	8.10	0.371	3.05	4.94
<b>P<sub>N</sub>3d</b>	8.00	0.511	4.45	7.90
<b>P<sub>N</sub>3e</b>	8.00	0.675	5.89	11.3
<b>P<sub>N</sub>3f</b>	9.00	0.805	7.10	12.5
<b>P<sub>DBu</sub>3a</b>	8.10	0.104	0.57	0.93
<b>P<sub>DBu</sub>3b</b>	8.00	0.210	1.56	2.65
<b>P<sub>DBu</sub>3c</b>	8.00	0.382	3.15	5.82
<b>P<sub>DBu</sub>3d</b>	8.10	0.483	4.09	7.93
<b>P<sub>DBu</sub>3e</b>	8.00	0.680	4.64	9.30
<b>P<sub>DBu</sub>3f</b>	8.00	0.684	5.97	12.8
<b>P<sub>DMe</sub>3a</b>	7.90	0.130	0.809	1.34
<b>P<sub>DMe</sub>3b</b>	8.00	0.271	2.12	3.71
<b>P<sub>DMe</sub>3c</b>	8.00	0.391	3.24	5.77
<b>P<sub>DMe</sub>3d</b>	8.10	0.478	4.05	7.34
<b>P<sub>DMe</sub>3e</b>	8.00	0.612	5.29	10.2
<b>P<sub>DMe</sub>3f</b>	8.00	0.684	5.97	11.8

The DASA contents  $X_{\text{DASA}}$  of the series **P<sub>DBu3</sub>**/**P<sub>DMe3</sub>** and **P<sub>N3</sub>** were estimated using Equation (4.14). The absorbance values were obtained from the related UV–vis measurements, as illustrated for **P<sub>DBu3</sub>** as an example in Figure 4.34d. These absorbance measurements were utilized to determine the concentrations  $c_{\text{DASA}}$  (Table A.4) with Equation 4.8. The molar mass  $M_{\text{DASA}} = 477.6 \text{ g mol}^{-1}$  was utilized for calculating the copolymers composed of buty-barbituric acid. For the barbituric acid based **P<sub>DMe3</sub>** series, the molar mass was  $M_{\text{DASA}} = 394.47 \text{ g mol}^{-1}$ . For the copolymer sample concentration  $c_{\text{P3M}}$ , the following procedure was used: The molecular masses of  $M_{\text{DEA}} = 127.1 \text{ g mol}^{-1}$  or  $M_{\text{NIPAAm}} = 113.2 \text{ g mol}^{-1}$  were utilized depending on the main polymer structure of the corresponding copolymer sample

## B Safety

This section provides comprehensive information on the safety considerations associated with handling the chemicals used in the experimental work for this thesis.

### B.1 Chemicals

The chemicals utilized in the experimental section of this investigation are enumerated in Table B.1. The GHS danger pictograms, hazard statements, and precautionary statements are in accordance with the classification of substances based on the Global Harmonized System (GHS).<sup>204–206</sup>

**Table B.1.** Used chemicals with respective GHS hazard pictograms, hazard statements and precautionary statements.

Substance	GHS hazard pictogram	Hazard statements	Precautionary statements
Acetic acid		226, 314	210, 233, 240, 280, 303+361+353, 305+351+338
Acetone		225, 319, 336, EUH066	210, 233, 240, 241, 242, 305+351+338
Acryloyl chloride		225, 290, 302, 330, 314	210, 280, 301+312, 303+361+353, 304+340+310, 305+351+338
4-Aminobenzoic acid	—	412	273, 501
3-Aminopropionate hydrochloride	—	—	—
Ammonium chloride	—	—	—
Argon		280	403
2,2'-Azobis(2-methyl-propionitrile)		242, 302 + 332, 412, EUH044	210, 235, 273, 304+340+312, 370+378, 403
Caesium carbonate		315, 319, 335	261, 305+351+338

Substance	GHS hazard pictogram	Hazard statements	Precautionary statements
$\epsilon$ -Caprolactone		319	264, 280, 305+351+338, 337+313
Chloroform- <i>d</i> <sub>1</sub>		302, 315, 319, 331, 336, 351, 361d, 372	202, 301+312, 302+352, 304+340+311, 305+351+338, 308+313
4-Cyano-4-[(dodecylsulfanylthiocarbonyl)-sulfanyl]-pentanoic acid		302	264, 270, 301+312+330, 501
1,3-dibutylpyrimidine-2,4,6(1H,3H,5H)-trione	—	—	—
1,3-Dibutylurea	—	—	—
Dichloromethane		315, 319, 336, 351	202, 261, 264, 302+352, 305+351+338, 308+313
Diethyl ether		224, 302, 336, EUH019, EUH066	210, 233, 240, 241, 242, 243, 261, 264, 270, 271, 280, 301+312, 303+361+353, 304+340, 312, 330, 370+378, 403+233, 403+235, 405, 501
1,3-Dimethylbarbituric acid		302, 318	264, 270, 280, 301+312, 305+351+338, 501
2,2-Dimethyl-1,3-dioxane-4,6-dione	—	—	—
Dimethylsulfoxid- <i>d</i> <sub>6</sub>	—	—	—
1,4-Dioxane		225, 319, 335, 350, EUH019, EUH066	202, 210, 233, 240, 305+351+338, 308+313
Ethyl isocyanate		225, 301, 312 + 332, 315, 317, 319, 334, 335	210, 233, 280, 301+310, 303+361+353, 305+351+338
Ethylacetate		225, 319, 336, EUH066	210, 233, 240, 241, 242, 305+351+338
Ethylene carbonate		302, 319, 373	260, 264, 270, 301+312, 305+351+338, 314

Substance	GHS hazard pictogram	Hazard statements	Precautionary statements
1,2-Ethylenediamine		226, 302 + 332, 311, 314, 317, 334, 412	210, 273, 280, 303+361+353, 304+340+310, 305+351+338
2-Fufuraldehyde		226, 301, 312, 315, 319, 330, 335, 351, 412	210, 273, 280, 303+361+353, 304+340+310, 305+351+338
Hydrochloric acid (1N)		290, 314, 335	234, 261, 271, 280, 303+361+353, 305+351+338
Isopropyl alcohol		225, 302, 319, 336	210, 261, 305+351+338
Magnesium sulfate	—	—	—
Malonyl chloride		226, 314, EUH014	210, 233, 303+361+353, 370+378, 403+235, 501
Methacryloylchloride		225, 302, 330, 314, 317, 412	210, 280, 303+361+353, 310
Methanol		225, 301, 302, 305, 311, 331, 370	P210, P233, P235, P240, P241, P242, P243, P260, P264, P270, P271, P280, P301+P330+P331, 302+352, 303+361+353, 304+340, 305+351+338, 307+311, 310, 311, 312, 337+313, 361, 363, 370
Methyl 3-(3-ethyl-2,4,6-trioxo-tetrahydropyrimidin-1(2H)-yl)propanoate	Presently no categorization based on the GHS.		
Methyl 3-(3-ethylureido)-propanoate	Presently no categorization based on the GHS.		
Methyl 6-hydroxyhexanoate		314	260, 264, 280, 301+330+331, 303+361+353, 304+340, 305+351+338, 310, 321, 363, 405, 501

Substance	GHS hazard pictogram	Hazard statements	Precautionary statements
Methyl isobutyl ketone		225, 319, 332, 336, 351, EUH066	202, 210, 233, 304+340+312, 305+351+338, 308+313
Methyl methacrylate		225, 315, 317, 335	210, 233, 240, 241, 280, 303+361 + 353
<i>N,N</i> -Diethylacrylamide		302, 319	264, 270, 280, 301+312, 305+351+338, 337+313
<i>N,N</i> -Dimethylformamide		226, 312+332, 319, 360D	210, 280, 303+361+353, 304+340+312, 305+351+338, 308+313
<i>n</i> -Butylamine		225, 290, 302, 311+331, 314, 335	210, 280, 301+312, 303+361+353, 304+340+310, 305+351+338
<i>N</i> -Ethylethylenediamine		225, 314, 334	210, 233, 280, 303+361+353, 304+340+310, 305+351+338
<i>n</i> -Hexane		225, 304, 315, 336, 361f, 373, 411	202, 210, 273, 301+310, 303+361+353, 331
<i>N</i> -Isopropylacrylamide		302, 318	264, 270, 280, 301+312, 305+351+338, 501
Nitrobenzene		301 + 311 + 331, 351, 360F, 372, 412	202, 273, 280, 301+310, 302+352+312, 304+340+311
Pentafluorophenol		315, 319 , 335	260, 261, 264, 270, 271, 280, 301+312, 301+330+331, 302+352, 303+361+353, 304+340, 305+351+338, 310, 312, 321, 322, 330, 332+313, 337+313, 362, 363, 403+233, 405, 501

Substance	GHS hazard pictogram	Hazard statements	Precautionary statements
Pentafluorophenyl acrylate		315, 319, 335	261, 264, 271, 280, 302+352, 305+351+338
Pentafluorophenyl methacrylate		227, 315, 319, 335	261, 264, 280, 302+352, 305+351+338, 321, 332+313, 362
Pentafluorophenyl trifluoroacetate	 	226, 315, 319, 335	210, 233, 240, 241, 303+361+353, 305+351+338
Perfluorophenyl ( <i>E</i> )-4-(phenyldiazenyl)benzoate	Presently no categorization based on the GHS.		
Petrolether 40-60	   	225, 304, 315, 336, 411	210, 240, 273, 301+310, 331, 403+235
Poly(methyl methacrylate- <i>co</i> -pentafluorophenyl methacrylate)	Presently no categorization based on the GHS.		
Poly(methyl methacrylate- <i>co</i> -pentafluorophenyl methacrylate)	Presently no categorization based on the GHS.		
Poly( <i>N</i> -(2-(ethylamino)ethyl)acrylamide- <i>co</i> - <i>N,N</i> -diethylacrylamide)	Presently no categorization based on the GHS.		
Poly( <i>N</i> -(2-(ethylamino)ethyl)methacrylamide- <i>co</i> -methyl methacrylate)	Presently no categorization based on the GHS.		
Poly( <i>N</i> -(2-(ethylamino)ethyl)methacrylamide- <i>co</i> - <i>N</i> -isopropylacrylamide)	Presently no categorization based on the GHS.		
Poly( <i>N</i> -(2-aminoethyl)- <i>N</i> -ethylmethacrylamide)	Presently no categorization based on the GHS.		
Poly( <i>N,N</i> -diethylacrylamide- <i>co</i> -pentafluorophenyl acrylate)	Presently no categorization based on the GHS.		
Poly( <i>N</i> -isopropylacrylamide- <i>co</i> -pentafluorophenyl acrylate)	Presently no categorization based on the GHS.		
Poly(pentafluorophenyl acrylate)	—	—	—

Substance	GHS hazard pictogram	Hazard statements	Precautionary statements
Polymethylacrylate	—	—	—
Polymethylmethacrylate	—	—	—
Silica gel	—	—	—
Sodium bicarbonate	—	—	—
Sodium sulfat	—	—	—
Sulfuric acid (96%)		290, 314	234, 280, 301+330+331, 303+361+353, 304+340+310, 305+351+338
Tetrahydrofuran	  	225, 302, 319, 335, 336, 351, EUH019	202, 210, 233, 301+312, 305+351+338, 308+313
Triethylamine	  	225, 302, 312, 314, 332	210, 280, 301+312, 303+361+353, 304+340+311, 305+351+338+310
Water	—	—	—

## B.2 CMR substances

The list of all carcinogenic, mutagenic, and reprotoxic (CMR) compounds utilized in the development of this work, along with their respective quantities, can be obtained from Table B.2.

Table B.2. Utilized CMR substances with category (1A or 1B), amount and number of experiments.

<b>CAS-Nr.</b>	<b>Substance and Category</b>	<b>Procedure and utilized amount</b>	<b>Number of experiments</b>
4472-41-7	<i>N,N</i> -Dimethylformamide- <i>d</i> <sub>7</sub> , 1B	NMR solvent, 0.7 mL	40
123-91-1	1,4-Dioxane, 1B	Solvent for polymerizations, 10 mL	50
98-95-3	Nitrobenzene, 1B	( <i>E</i> )-4-(Phenyldi-azeny)-ben- zoic acid synthesis, 10 g	2

## C Danksagung

An erster Stelle möchte ich mich bei Herrn Prof. Dr. Théato für die Aufnahme in seine Arbeitsgruppe und die damit verbundene Möglichkeit meine Doktorarbeit durchführen zu können bedanken. Die internationale Atmosphäre hat mich stets wissenschaftlich inspiriert und darüber hinaus meinen kulturellen Horizont erweitert. Ein weiterer besonderer Dank gilt Prof. Dr. Luinstra für die Anfertigung des Zweitgutachtens und seine stets offene Art während konstruktiver Gespräche.

Ein herzlicher Dank gilt auch allen Mitarbeitern der Technischen und Makromolekularen Chemie der Universität Hamburg. Besonders hervorheben möchte ich hier Dr. Scheliga, der mich tatkräftig mit Fachwissen bei analytischen Messmethoden unterstützte. Zudem bedanke ich mich herzlich bei Ilona Inselmann für ihre labortechnische Zuarbeit und bei Kathleen Pruntsch, die immer ein offenes Ohr hatte und mir mit ihrer hilfsbereiten Art meinen Alltag erleichtert hat. Dr. Dennis Brillowski danke ich für die schöne Zeit im Labor. Weiterhin möchte ich mich bei Christina Khenkhar bedanken, die gern ihren Kaffee mit mir teilte und mir stets ein Lächeln ins Gesicht gezaubert hat. Bei allen ehemaligen Mitgliedern der Arbeitsgruppe in Hamburg: Anidita, Denis, Fenja, Heba, Jiaojiao, Lindsey, Michi, Tim, Sven, Wenwen, Xia, Xinjang Zengwen und Ziaoziao möchte ich mich für die gute Zusammenarbeit und Hilfsbereitschaft bedanken. Ich habe durch euch viel gelernt und durfte inspirierende Momente erleben. Auf diesem Wege möchte ich mich auch bei allen Auszubildenen und Studierenden bedanken, die im Zuge ihrer Praktika einen Beitrag zu dieser Arbeit geleistet haben.

Mein Dank gilt des Weiteren auch ganz besonders Freunden außerhalb des wissenschaftlichen Umfeldes: Britta, Eric, Dirk, Florian, Jan, Nicole, René, Ria. Ihr seid wundervoll! Besonders hervorheben möchte ich an dieser Stelle Felix und Tobias: Mit euren (erbarmungslos) ehrlichen Meinungen habt ihr mich gefordert, geformt und mir die Kraft gegeben, die mich unendlich unterstützt hat. Vom ganzen Herzen bedanken möchte ich mich vor allem auch bei Marco und Sven. Ohne eure bedingungslose Hilfe, wäre diese Arbeit nicht möglich gewesen.

Der größte Dank geht an meine Familie und im besonderen Maße an meine liebevollen Eltern. Danke, dass ich bei euch immer sein darf, wie ich bin und ihr keinen meiner Wege infrage gestellt habt.

## D Erklärung zur Identität der digitalen und schriftlichen Fassungen

Ich versichere, dass dieses Exemplar der Dissertation und das in elektronischer Form eingereichte Dissertationsexemplar (über den Docata-Upload) und das im Studienbüro bzw. Promotionsbüro Chemie der MIN Fakultät zur Archivierung eingereichte gedruckte und gebundene Exemplar der Dissertationsschrift identisch sind.

Hamburg, 20. September 2024



---

Julia Steicke

## E Eidesstattliche Versicherung

Hiermit versichere ich an Eides statt, die vorliegende Dissertationsschrift selbst verfasst und keine anderen als die angegebenen Quellen und Hilfsmittel benutzt zu haben. Sofern im Zuge der Erstellung der vorliegenden Dissertationsschrift generative Künstliche Intelligenz (gKI) basierte elektronische Hilfsmittel verwendet wurden, versichere ich, dass meine eigene Leistung im Vordergrund stand und dass eine vollständige Dokumentation aller verwendeten Hilfsmittel gemäß der Guten wissenschaftlichen Praxis vorliegt. Ich trage die Verantwortung für eventuell durch die KI generierte fehlerhafte oder verzerrte Inhalte, fehlerhafte Referenzen, Verstöße gegen das Datenschutz- und Urheberrecht oder Plagiate.

Hamburg, 20. September 2024



---

Julia Steicke